Discrete time quantum walks : from synthetic gauge fields to spontaneous equilibration

Giuseppe Di Molfetta

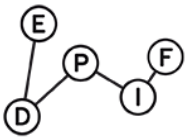

Université Pierre et Marie Curie

École Doctorale Physique en Île de France (ED 564)

Laboratoire d'Étude du Rayonnement et de la Matière en Astrophysique et Atmosphères (LERMA)

Discrete time quantum walks:
from synthetic gauge fields to spontaneous equilibration

Par Di Molfetta Giuseppe
Thèse de Doctorat en Physique Théorique

Directeur: Fabrice Debbasch (LERMA - UPMC)
Co-directeur : Marc Brachet (LPS ENS, CNRS)

Présentée et soutenue publiquement le 28/07/2015
à l'Université Pierre et Marie Curie, devant un jury composé de :

M. Jean-Michel Raimond	Professeur	Examinateur
M. Dieter Meschede	Professor	Rapporteur
M. Pablo Arrighi	Professor	Rapporteur
M. Yutaka Shikano	Professeur	Examinateur
M. Fabrice Debbasch	Maître de Conférence	Directeur de thèse
M. Marc Brachet	Directeur de Recherche	(Invité) Co-directeur de thèse

Remerciements

J'ai commencé ma thèse en septembre 2012 au Laboratoire d'Études du Rayonnement et de la Matière en Astrophysique et Atmosphères (LERMA) de l'Observatoire de Paris, dont je tiens à remercier l'ex-directeur Michel PÉRAULT et l'actuel directeur Darek LIS pour leur accueil au sein de leur unité. Je remercie également Maryvonne GERIN pour m'avoir accueilli dans son èquipe du LRA à l'Ecole Normale Supérieure où j'ai passé mes deux premières années de these, et Chantal STEHLE pour avoir fait de même à Jussieu pendant ma dernière année.

Cette thèse a été dirigée par Fabrice DEBBASCH, que j'ai rencontré pendant mon premier stage de M1 à l'Université Pierre Marie Curie. Avec lui, j'ai découvert le sujet de ce doctorat et j'ai échangé sur une infinité de sujets scientifique. Je le remercie pour la confiance et le soutien dont il a fait preuve pendant tout mon travail, jusqu'aux derniers jours de rédaction du manuscrit. Ce qu'il ma donné de plus précieux, c'est son grand enthousiasme pour la science, la recherche et la découverte, que je garderai dans mon futur professionnel. Je voudrais également remercier Marc-Etienne BRACHET pour m'avoir co-encadré pendant ces trois ans. Notamment, je lui suis reconnaissant pour sa patience, son expertise scientifique et la transmission d'une partie de son énorme connaissance. À lui va aussi ma gratitude sa profonde humanité.

Je voudrais également remercier Martine BEN AMAR pour m'avoir accueilli dans le Master de Physique des systèmes complexes et Jean-Bernard ZUBER pour sa disponibilité pendant mes premiers mois de permanence à Paris. J'exprime ma plus profonde reconnaissance à Pablo ARRIGHI et Dieter MESCHEDE qui m'ont fait l'honneur d'accepter d'être rapporteurs de la prèsente thèse (thank you Prof. P. ARRIGHI and Prof. D. MESCHEDE to have accepted to be the examiners of this thesis). J'associe à ces remerciements les autres membres de jury: Jean-Michel RAIMOND et Yutaka SHIKANO. En particulier je remercie J.-M. RAIMOND pour l'intérêt qu'il a montré envers les résultats que j'ai obtenu lors de mon premier stage.
Je suis aussi reconnaissant envers Y. SHIKANO pour son accueil au sein de son unité à Okazaki. Mon séjour au Japon, qui a été la plus belle et intense expérience professionnelle pendant mon doctorat, aurait été très difficile sans la disponibilité et la sympathie de Naoko KONDO, Mayuko KATO et tous les autres membres du IMS. Je remercie parement Beatrice GUIBAL du LERMA pour avoir géré toutes mes questions administratives. Pendant ces trois années de travail, j'ai eu l'occasion de profiter de la grande expertise de Giorgio KRSTULOVIC, Stéphan FAUVE, Fabio SCIARRINO, Stéphane ATTAL, Carlo DI FRANCO, Christopher CEDZICH, Fumiaki MATSUOKA, Yu-Xiang ZHANG et Tatsuaki WADA. Je les remercie pour leurs nombreux et précieux conseils. Je remercie aussi, pour leur esprit convivial et la patience d'avoir partagé le bureau avec moi, Marco PADOVANI, Lionel de SA et Uddhab CHAULAGAIN. En particulier Pablo ARNAULT pour son humilité et son vrai enthousiasme pour la physique.

Merci aussi à mes frères de l'école Nam Anh qui m'ont aidé à tracer ma route, et à tous les amis qui m'ont soutenu et fait sourire sur ce chemin parfois difficile.
Une remerciement spécial va à ma famille, notamment ma mère qui n'a jamais arrêté de croire en moi et de m'encourager.
Je dédie cette thèse à Vera qui m'a enseigné à *écouter* avec amour.

Caminante, son tus huellas
el camino y nada mas;
Caminante, no hay camino,
se hace camino al andar. (A.M.)

Discrete Time Quantum Walks: From synthetic gauge fields to spontaneous equilibration.

ABSTRACT

Keywords: Discrete Time Quantum Walks, Quantum Simulations, Synthetic Gauge Fields
Quantum Decoherence, Quantum Gauge Lattice, Thermalization.

Problems too demanding for classical computers can be approached promisingly with quantum simulators, which operate using one controllable quantum system in order to investigate the behavior and properties of a less accessible one. Over the past few years, significant progress has been made in a number of experimental and theoretical fields. Quantum Walks (QWs) are simple and sophisticated discrete space and time dynamical systems and it has been shown that in the continuous limit different emergent quantum fields can be simulated. In this thesis we will draw on QWs to further explore various areas of interest in Physics. More specifically our analysis will branch out into three main directions: (i) the connection between QWs and quantum field theory, with particular attention to bridging the quantum coin of QWs with the geometrical properties of gauge field theories; (ii) the study of QWs' classical limit and of the transient semi-classical dynamics, especially in relation with field theories; (iii) the spontaneous equilibration and thermalization in some nonlinear QWs-like models. Every step of this thesis will be validated by specific analytical results and numerical implementations.

Marches quantiques à temps discret : des champs de jauge de synthèse à l'équilibration spontanée

RÉSUMÉ

Les simulateurs quantiques, qui utilisent un système quantique contrôlable pour étudier le comportement et les propriétés d'un autre système quantique, moins accessible, sont une ressource prometteuse. Dans les dernières années, des progrès significatifs ont été faits dans de nombreux domaines expérimentaux et théoriques. Les marches quantiques à temps discret sont des systèmes simples et sophistiqués. En particulier, il a été montré qu'à la limite continue, ces marches peuvent simuler certaines théories de champs. Dans ce travail de thèse, lesdites marches sont utilisées pour explorer certains sujets d'intérêt physique, qui s'articulent autour de trois axes : (i) la connexion entre les propriétés géométriques de la marche et celles de divers champs de jauge ; (ii) la limite classique et la limite quasi-quantique, en relation surtout avec les théories de champs ; (iii) l'équilibration spontanée pour certains modèles non linéaires de marches quantiques. Chaque résultat est appuyé par une étude numérique et analytique.

Mots-clés: Marches quantiques à temps discret, Simulation quantique, Champs de jauge de synthèse, Décohérence quantique, Théories de jauge sur réseau, Thermalisation.

Contents

List of Figures v

INTRODUCTION 1

I Quantum walks: from synthetic gauge fields... 7

1 HOMOGENEOUS QUANTUM WALKS 9
1.1 Quantum walks . . . 9
1.1.1 Introduction . . . 9
1.1.2 From Classical to Quantum random walks . . . 10
1.1.3 General Setup of a Discrete Time Quantum Walks . . . 11
1.1.4 Qualitative description . . . 13
1.1.5 Quantitative description . . . 16
1.2 Connections between Quantum Walks and Relativistic Wave Equations . . . 17
1.2.1 Quantum walks and Feynman's Checkerboard . . . 17
1.2.2 Homogeneous DTQWs and Weyl equation . . . 19
1.2.3 Publication: "Massless Dirac Equation from Fibonacci Discrete-Time Quantum Walk" . . . 20

2 INHOMOGENEOUS QUANTUM WALKS AND CONTINUOUS LIMITS 35
2.1 Inhomogeneous Quantum Walks as synthetic gauge fields simulators . . . 35
2.1.1 Quantum Simulation . . . 35
2.1.2 What is a synthetic gauge field? . . . 36
2.1.3 From Inhomogeneous Quantum Walks to synthetic gauge fields . . . 37
2.2 A synthetic gravitational gauge field . . . 39
2.2.1 Simulating the effects of a gravitational gauge field . . . 39
2.2.2 Curved spacetime and chiral field theory: an introduction . . . 39
2.2.3 A formal general setup . . . 40
2.2.4 Dirac equation in curved spacetime in (1+1) dimensions . . . 44
2.2.5 Publication: "Quantum walks as massless Dirac fermions in curved spacetime" . . . 44
2.3 A synthetic electric gauge field . . . 51
2.3.1 Publication: "Quantum Walks in artificial electric and gravitational gauge fields." . . . 51

3 QUANTUM WALKS, DECOHERENCE AND RANDOM SYNTHETIC GAUGE FIELD 69
3.1 Quantum Decoherence: An introduction . . . 69
3.2 Quantum Walks and decoherence . . . 70
3.2.1 An overview . . . 70
3.2.2 A qualitative picture . . . 72
3.2.3 Projections cause spin and spatial decoherence . . . 74
3.3 Publication : "Discrete-time Quantum Walks in random artificial Gauge Fields." 75

II ... to spontaneous equilibration. 97

4 THERMALIZATION AND QUANTUM WALKS 99
4.1 Absolute equilibrium in conservative systems . . . 99
4.1.1 A general introduction . . . 99
4.1.2 Thermalization and absolute equilibria in Galerkin truncated PDEs . . . 100
4.1.3 From microcanonical to grand canonical ensemble . . . 101
4.2 Nonlinear QW-like models and thermalization . . . 102
4.2.1 Thermalization in closed quantum systems . . . 102
4.2.2 QWs on N-cycle and limiting distribution . . . 103
4.2.3 A Nonlinear Quantum Walk-like model on N-cycle . . . 104
4.3 Publication: "Nonlinear Optical Galton Board: thermalization and continuous limit" . . . 105

III Conclusions and Perspectives 119

5 CONCLUSIONS AND PERSPECTIVES 121
5.1 Conclusions . . . 121
5.2 Perspectives . . . 122

6 ACADEMIC PUBLISHING AND SCIENTIFIC COMMUNICATIONS 125
6.1 Academic publishing . . . 125
6.1.1 Submitted . . . 125
6.1.2 Published . . . 125
6.1.3 Scientific Projects . . . 126
6.2 Awards and Fellowship . . . 126
6.3 Workshop . . . 126

Appendices 127

Appendix A NUMERICAL METHODS 129
A.1 Spectral Methods . . . 129
A.1.1 Fundamentals . . . 129
A.2 Convergence in spectral methods . . . 130
A.3 Approximate a PDE by spectral method . . . 130
A.3.1 Galerkin method . . . 131
A.3.2 Pseudo-spectral method . . . 131
A.3.3 De-aliasing . . . 132
A.3.4 Time-stepping . . . 132
A.4 Discrete Fourier Transform . . . 133

Appendix B TRUNCATED EULER-VOIGT-α EQUATION AND THERMALIZATION 135
B.1 Absolute equilibria in truncated Euler equation . . . 135
B.2 Eddy-damped quasi-normal Markovian theory (EDQNM) . . . 136
B.3 Self-truncation . . . 136

B.4 Publication A1: "Self-truncation and scaling in Euler-Voigt-α and related fluid models" 137

List of Figures

1.1 Spread of probability density of a Hadamard walk on n grid points with asymmetric initial state $\Psi_0 = \sum_m \psi_{0,m}\ (c^L|b_L\rangle + e^{i\phi}c^R|b_R\rangle)$ T where (i) $c_L = 1, c_R = 1, \phi = 0$ or (ii) $c_L = 1, c_R = -1, \phi = 0$ and symmetric initial state $c_L = 1, c_R = 1, \phi = \pi/2$. The spatial component is given by $\psi_0 = \sum_m \delta_{0,m}$ 14

1.2 Square root of variance of a Hadamard Walk with symmetric initial state and localized position in the origin. The slope is $(1 - \frac{1}{\sqrt{2}})^{1/2}$. 15

1.3 Spread of probability density of the DTQW with symmetric initial state and different values of θ, for $\alpha = -\pi/2$, $\xi = \pi/2$ and $\zeta = \pi/2$. 15

1.4 Value of K_θ for a given θ. 16

1.5 Feynman's Checkerboard representation in the discrete space time lattice (x, t). . 18

2.1 Distortion in a vector field in the transport from a point i to a point j of the curved spacetime. 42

3.1 Variation of entropy of measurement (or entanglement) $(S_r)_j$ VS time for different values of θ. Inside the figure: the variation of entropy VS θ for a given number of steps. 74

4.1 Classical Galton Board. 106

4.2 (Left) The optical ring cavity for the implementation of the Optical Galton Board. The EOMs are the electro-optical modulators and the BS is the beam splitter. The solid gray rectangle is the partially reflecting mirror serving as input and output port and the black ones are the fully reflecting mirror of the cavity.(Adapted from Knight et al. [10]) (Right) On the top the probability distribution of a classical Galton board, and on the bottom the density profile of frequencies in the wave-mechanical case within the Landau-Zener crossings. Φ_1 is a control parameter proportional to time. (Adapted from Bouwmeester et al. [4]) 106

INTRODUCTION

Quantum simulation has recently established itself as an area of study in quantum physics that merges fundamental and applied questions. Such an interaction results in a more operational understanding of some aspects of quantum mechanics in terms of nature description. The idea to simulate the dynamics of a quantum system by a quantum device was first introduced by Richard Feynman in a seminal article in 1982 [19] and developed in different frameworks, from quantum optics to condensed matter physics.
A way to describe quantum systems and their dynamics within a computational perspective is given by the large class of Quantum Cellular Automata (QCA), that is a grid of quantum autonomous systems, interacting through local rules [44, 37, 8, 7, 38]. Over the last years, many definitions and models of QCA have been proposed. For instance, Schumacher and Werner [37] proposed a class of reversible QCA, where the evolution of the QCA is given by local unitary operations that act on the neighborhood of a given cell, and it is further updated by a single cell unitary operation. This is in accordance with the expected microscopic fully quantum dynamics. However in recent years an agreement has been achieved and many definitions have been proven to be equivalent by Arrighi and Grattage [6].

This class of quantum systems displays a wide range of complex phenomena and it has been extensively used for the comprehension of Quantum Field Theory (QFT). Bialynicki-Birula [9] first underlines the connection between QCA and QFT. Then Meyer [29] showed that QCA mostly correspond to lattice gas models and are closely related to the Dirac equation; in addition to this, again Meyer and Shakeel [30], have recently proved that QCA with no particle interpretation exist and that they propagate information.

Quantum Walks (QWs) are a special case of reversible QCA , but in the sigle particle sector. Differently from QCA, they describe the unitary dynamics of one quantum particle. They have been introduced independently by Grossing and Zeilinger [22] and Y. Aharonov et al. [3] and then extended systematically on graphs by D. Aharonov et al. [2]. QWs have been, later, fully mathematically examined by Konno [27].

Quite surprisingly, this simple one-particle quantum automaton is an excellent tool for modeling a large spectrum of physical phenomena and it is interesting both for fundamental quantum physics and for physical applications. Already in the formal introduction by Y. Aharonov, QWs appear as models of coherent quantum transport. Therefore it is not astonishing that Feynman and Hibbs [18] provided a model of QCA, the "Feynman Checkerboard", resembling QW, as path discretization of the Dirac propagator.

Let us remark that all these historical landmarks concern the so-called Discrete-Time Quantum Walk (DTQW), that is an automaton living in discrete time and discrete space. Whilst a continuous-time version of QW (CTQW) - living in continuous time and discrete space - has been introduced independently in the literature, we will not deal with it in the present work. Just let us keep in mind that, even though both models are mathematically defined in a different way, Strauch [42] has connected CTQW and DTQW, putting in evidence striking similarities

in the continuous limit.

Nowadays QWs can be realized experimentally with a large spectrum of physical objects and setups. A first natural way to physically implement a QW is in optical networks. For instance, Knight et al. [26] realized experimentally the first optical implementation of a QW in an optical ring cavity, as a modified experimental setup of the optical linear quincunx described by Bouwmeester et al. [10], the Optical Galton Board.

A second way to implement QWs is the Nuclear Magnetic Resonance (NMR), proposed by Ryan et al. [33] for a DTQW, subsequent to the work of Du et al. [15]. This method consists in manipulating and coupling spin orientations, in constituting quantum logic gates and in performing unitary operations on the nuclei quantum state in the magnetic field.

Other possible implementations can be realized in Quantum Electrodynamics (QED). In effect, the physical scheme proposed by Y. Aharonov in its seminal paper [3] has inspired Agarwal and Pathak [1] to realize a DTQW in this framework. They implemented it by injecting a single Rydberg atom into an optical cavity and by driving it by a strong external field. The effective Hamiltonian introduced in their article reproduces perfectly the Aharonov's scheme. A more recent implementation of QW in cavity QED is due to Sanders et al. [34].

Other techniques range from quantum optics (Zhang et al. [45], [46]), to ion traps (Travaglione and Milburn [43]), and to neutral atom traps (Chandrashekar [12],Eckert et al. [17], Dür et al. [16]). In particular, quite useful for the implementation of QWs on cycle is the interacting quantum dots architecture presented by Solenov and Fedichkin [40] in a solid state framework.

Recent developments, however, have shown an increasing interest for two or more correlated QWs, due to the large class of emergent quantum phenomena (Peruzzo et al. [32], Sansoni et al. [35], Schreiber et al. [36] and more recently Defienne et al. [14]). However, this thesis is dedicated to the study of the single-particle dynamics and we will not take into account multi-particle systems.

As for the physical implementations, the potential applications of QWs are too numerous to be listed here. They spread from search algorithms [13] and graph isomorphism [4, 21] to modeling and simulating quantum dynamics [36] and classical system [41]. We can redirect the reader to Lovett et al. [28] for an introductory review on the quantum walk algorithm. Concerning modeling quantum dynamics we can recall some remarkable applications in condensed matter. For instance, in topological insulators realization [25, 24], for spintronic applications [23], and for quantum transport on 2-dimensional layer, as in graphene-like materials [20].

This thesis is specifically devoted to only one of the various DTQWs' applications: quantum simulation of quantum systems dynamics. In particular, let us remind the reader that, rather than a monograph, this manuscript appears as a collection of our main publications with an accurate introductory section to each of them. All our works deal with QWs propagating in one spatial dimension.

The thesis is organized in three main parts and four chapters. In the first part, the Chapter (1) is devoted to introduce DTQWs and report their main features, largely explored in the recent literature. In particular, we present the method to perform the continuous limit and its re-

lated sufficient conditions. Moreover, we formally prove that not all families of homogeneous DTQWs (HDTQWs) admit such conditions. In Chapter (2), we extend the same analysis to the inhomogeneous DTQWs (IDTQWs) and we introduce the idea of synthetic gauge field. Above all, we prove that some special families of IDTQWs mimic the propagation in curved $(1+1)$-spacetime of a Dirac fermion, coupled to a gauge electric potential. Let us recall that similar results have been recently obtained by our group in a $(1+2)$ spacetime dimension (Arnault and Debbasch [5]). We conclude the first part with Chapter (3), introducing a randomized version of the IDTQW. We analytically provide detailed calculations demonstrating the loss of coherence and the emergent classical diffusive behavior of the walk.

In the second part and last chapter, Chapter (4), our analysis concerns the very new problem of equilibration in QWs. Generally, equilibration is the process through which a system, under a given dynamics, reaches a steady state. By thermalization we mean that this steady state can be interpreted as a thermal state at a given temperature.
Thermalization is observed typically in nonlinear systems, but all QWs describe the motion of a single particle and are linear by definition. Moreover nonlinear QW-like implementations have been considered in different contexts. In the context of optics, the so-called Optical Galton Boards (OGB) [11] have been generalized to include nonlinear Kerr effects by Navarrete-Benlloch et al. [31] or in Shikano et al. [39], who proposed a DTQW with feed-forward quantum coin displaying high nonlinearities. In those models very complex and rich behaviors have been observed. The aim of this last chapter, and our main contribution, is to observe and characterize thermalization phenomena in a spatially-periodic version of the Nonlinear OGB.

Bibliography

[1] G. S. Agarwal and P. K. Pathak. Quantum random walk of the field in an externally driven cavity. *Physical Review A*, 72(3):033815, 2005.

[2] D. Aharonov, A. Ambainis, J. Kempe, and U. Vazirani. Quantum walks on graphs. In *Proceedings of the thirty-third annual ACM symposium on Theory of computing*, pages 50–59. ACM, 2001.

[3] Y. Aharonov, L. Davidovich, and N. Zagury. Quantum random walks. *Phys. Rev. A*, 48:1687, 1993.

[4] A. Ambainis. Quantum walks and their algorithmic applications. *International Journal of Quantum Information*, 1(04):507–518, 2003.

[5] P. Arnault and F. Debbasch. Landau levels for discrete-time quantum walks in artificial magnetic fields. *arXiv preprint*, 1412.4337, 2014.

[6] P. Arrighi and J. Grattage. Partitioned quantum cellular automata are intrinsically universal. *Natural Computing*, 11:13, 2012.

[7] P. Arrighi and J. Grattage. Partitioned quantum cellular automata are intrinsically universal. *Natural Computing*, 11(1):13–22, 2012.

[8] P. Arrighi, V. Nesme, and R. Werner. One-dimensional quantum cellular automata over finite, unbounded configurations. In *Language and Automata Theory and Applications*, pages 64–75. Springer, 2008.

[9] I. Bialynicki-Birula. Weyl, dirac, and maxwell equations on a lattice as unitary cellular automata. *Physical Review D*, 49(12):6920, 1994.

[10] D. Bouwmeester, I. Marzoli, G. P. Karman, W. Schleich, and J. Woerdman. Optical galton board. *Physical Review A*, 61(1):013410, 1999.

[11] D. Bouwmeester, I. Marzoli, G. P. Karman, W. Schleich, and J. P. Woerdman. Optical Galton board. *Phys. Rev. A*, 61:013410, Dec 1999. doi: 10.1103/PhysRevA.61.013410. URL http://link.aps.org/doi/10.1103/PhysRevA.61.013410.

[12] C. Chandrashekar. Implementing the one-dimensional quantum (hadamard) walk using a bose-einstein condensate. *Physical Review A*, 74(3):032307, 2006.

[13] A. M. Childs, R. Cleve, E. Deotto, E. Farhi, S. Gutmann, and D. A. Spielman. Exponential algorithmic speedup by a quantum walk. In *Proceedings of the thirty-fifth annual ACM symposium on Theory of computing*, pages 59–68. ACM, 2003.

[14] H. Defienne, M. Barbieri, I. A. Walmsley, B. J. Smith, and S. Gigan. Control of two-photon quantum walk in a complex multimode system by wavefront shaping. *arXiv preprint arXiv:1504.03178*, 2015.

[15] J. Du, H. Li, X. Xu, M. Shi, J. Wu, X. Zhou, and R. Han. Experimental implementation of the quantum random-walk algorithm. *Physical Review A*, 67(4):042316, 2003.

[16] W. Dür, R. Raussendorf, V. M. Kendon, and H.-J. Briegel. Quantum walks in optical lattices. *Physical Review A*, 66(5):052319, 2002.

[17] K. Eckert, J. Mompart, G. Birkl, and M. Lewenstein. One-and two-dimensional quantum walks in arrays of optical traps. *Physical Review A*, 72(1):012327, 2005.

[18] R. Feynman and A. Hibbs. Quantum mechanics and path integrals. *International Series in Pure and Applied Physics. McGraw-Hill Book Company*, 1965.

[19] R. P. Feynman. Simulating physics with computers. *International journal of theoretical physics*, 21 (6):467–488, 1982.

[20] I. Foulger, S. Gnutzmann, and G. Tanner. Quantum walks and quantum search on graphene lattices. *arXiv preprint arXiv:1501.07543*, 2015.

[21] J. K. Gamble, M. Friesen, D. Zhou, R. Joynt, and S. Coppersmith. Two-particle quantum walks applied to the graph isomorphism problem. *Physical Review A*, 81(5):052313, 2010.

[22] G. Grossing and A. Zeilinger. Quantum cellular automata. *Complex Systems*, 2(2):197–208, 1988.

[23] O. Kálmán, T. Kiss, and P. Földi. Quantum walk on the line with quantum rings. *Physical Review B*, 80(3):035327, 2009.

[24] T. Kitagawa, M. S. Rudner, E. Berg, and E. Demler. Exploring topological phases with quantum walks. *Physical Review A*, 82(3):033429, 2010.

[25] T. Kitagawa, M. A. Broome, A. Fedrizzi, M. S. Rudner, E. Berg, I. Kassal, A. Aspuru-Guzik, E. Demler, and A. G. White. Observation of topologically protected bound states in photonic quantum walks. *Nature communications*, 3:882, 2012.

[26] P. Knight, E. Roldn, and J. Sipe. Quantum walk on the line as an interference phenomenon. *Phys. Rev. A*, 68:020301, 2003.

[27] N. Konno. Quantum random walks in one dimension. *Quantum Information Processing*, 1(5): 345–354, 2002.

[28] N. B. Lovett, S. Cooper, M. Everitt, M. Trevers, and V. Kendon. Universal quantum computation using the discrete-time quantum walk. *Physical Review A*, 81(4):042330, 2010.

[29] D. A. Meyer. From quantum cellular automata to quantum lattice gases. *Journal of Statistical Physics*, 85(5-6):551–574, 1996.

[30] D. A. Meyer and A. Shakeel. Quantum cellular automata without particles. *arXiv preprint arXiv:1506.01639*, 2015.

[31] C. Navarrete-Benlloch, A. Perez, and E. Roldan. Nonlinear optical galton board. *Phys. Rev. A*, 75:062333, Jun 2007. doi: 10.1103/PhysRevA.75.062333. URL http://link.aps.org/doi/10.1103/PhysRevA.75.062333.

[32] A. Peruzzo, M. Lobino, J. C. Matthews, N. Matsuda, A. Politi, K. Poulios, X.-Q. Zhou, Y. Lahini, N. Ismail, K. Wörhoff, et al. Quantum walks of correlated photons. *Science*, 329(5998):1500–1503, 2010.

[33] C. Ryan, M. Laforest, J. Boileau, and R. Laflamme. Experimental implementation of a discrete-time quantum random walk on an nmr quantum-information processor. *Physical Review A*, 72(6): 062317, 2005.

[34] B. C. Sanders, S. D. Bartlett, B. Tregenna, and P. L. Knight. Quantum quincunx in cavity quantum electrodynamics. *Physical Review A*, 67(4):042305, 2003.

[35] L. Sansoni, F. Sciarrino, G. Vallone, P. Mataloni, A. Crespi, R. Ramponi, and R. Osellame. Two-particle bosonic-fermionic quantum walk via integrated photonics. *Physical review letters*, 108(1): 010502, 2012.

[36] A. Schreiber, A. Gábris, P. P. Rohde, K. Laiho, M. Štefaňák, V. Potoček, C. Hamilton, I. Jex, and C. Silberhorn. A 2d quantum walk simulation of two-particle dynamics. *Science*, 336(6077):55–58, 2012.

[37] B. Schumacher and R. F. Werner. Reversible quantum cellular automata. *arXiv preprint quant-ph/0405174*, 2004.

[38] A. Shakeel, D. A. Meyer, and P. J. Love. History dependent quantum random walks as quantum lattice gas automata. *Journal of Mathematical Physics*, 55(12):122204, 2014.

[39] Y. Shikano, T. Wada, and J. Horikawa. Discrete-time quantum walk with feed-forward quantum coin. *Scientific reports*, 4, 2014.

[40] D. Solenov and L. Fedichkin. Continuous-time quantum walks on a cycle graph. *arXiv preprint quant-ph/0506096*, 2005.

[41] R. Somma, S. Boixo, H. Barnum, and E. Knill. Quantum simulations of classical annealing processes. *Physical review letters*, 101(13):130504, 2008.

[42] F. Strauch. Connecting the discrete- and continuous-time quantum walks. *Phys. Rev. A*, 74:030301, 2006.

[43] B. C. Travaglione and G. J. Milburn. Implementing the quantum random walk. *Physical Review A*, 65(3):032310, 2002.

[44] J. Watrous. On one-dimensional quantum cellular automata. In *Foundations of Computer Science, 1995. Proceedings., 36th Annual Symposium on*, pages 528–537. IEEE, 1995.

[45] P. Zhang, X.-F. Ren, X.-B. Zou, B.-H. Liu, Y.-F. Huang, and G.-C. Guo. Demonstration of one-dimensional quantum random walks using orbital angular momentum of photons. *Physical Review A*, 75(5):052310, 2007.

[46] P. Zhang, B.-H. Liu, R.-F. Liu, H.-R. Li, F.-L. Li, and G.-C. Guo. Implementation of one-dimensional quantum walks on spin-orbital angular momentum space of photons. *Physical Review A*, 81(5): 052322, 2010.

Part I

Quantum walks: from synthetic gauge fields...

CHAPTER 1

HOMOGENEOUS QUANTUM WALKS

Summary

1.1 Quantum walks 9
1.1.1 Introduction 9
1.1.2 From Classical to Quantum random walks 10
1.1.3 General Setup of a Discrete Time Quantum Walks 11
1.1.4 Qualitative description 13
1.1.5 Quantitative description 16
1.1.5.1 Fourier methods for the Hadamard walk 16
1.2 Connections between Quantum Walks and Relativistic Wave Equations 17
1.2.1 Quantum walks and Feynman's Checkerboard 17
1.2.2 Homogeneous DTQWs and Weyl equation 19
1.2.3 Publication: "Massless Dirac Equation from Fibonacci Discrete-Time Quantum Walk" 20

1.1 Quantum walks

1.1.1 Introduction

Classical random walks (CRWs) are employed to model phenomena as chemical reactions [15, 26, 46], genetic sequence location [45, 28, 33], optimal search strategies [29, 4, 36], diffusion and mobility in materials [25, 13, 44], exchange rate forecasts in economical sciences [30, 6, 24] and information spreading in complex networks [35, 34, 41]. Furthermore, they can successfully implement efficient algorithms, for example they can solve differential equations [3, 20], optimization [4, 5] and clustering problems [38, 48]. Random walks spread to every domain of science for more than a century and are still an important source for researchers nowadays.

Even though in the second half of last century the interest in a quantum analogous to the classical stochastic process led to further investigation of quantum mechanics and quantum information, since the 1960s, numerous scientists [42, 21, 17, 14, 12, 1, 23, 37] have extended the Brownian motion and stochastic calculus to particles which exhibited quantum effects. Schwinger was the first to demonstrate the importance of coherence effects in the evolution of a Brownian quantum particle. Just few years later, Fjeldso et al. [11] proposed the first discrete model with the intention of recovering a quantum version of the CRW. This first example represented a quantum planar rotor on a lattice which dynamics can be approximated by a

random walk. Another important milestone was the work of Gudder [19] who studied systematically quantum Markov processes and established formally a connection with Feymann path integral formalism.

Interestingly some years later, Godoy and Fujita [16] and Grossing and Zeilinger [18] had independently the same intuition of developing a quantum analogous to the CRW in discrete time and discrete space. Godoy proposed a one-dimensional Markovian quantum walk displaying a diffusive behavior and Grossing and Zeilinger [18] formalized the first model of unitary Quantum Walk (QW), which dynamics was fully propagative. Let us remark that, although the latter was defined as a QCA this model is completely equivalent to the one proposed later by Aharonov et al. [2].

Thanks to its features, especially the unitarity, QWs were immediately considered a new and efficient tools for solving, in a wider range of applications, technical problems in a more convenient way than classical random walks.

1.1.2 From Classical to Quantum random walks

In explicating the main differences between DTQW and its classical counterpart, we briefly recall the definition of a discrete time random walk (DTRW) on an unrestricted line. Let us imagine a man moving along a line, taking, at random, steps to the left and to the right with equal probability. The step are of unit length so that his position can take on only the value n, where $n \in \mathbb{Z}$. We want to know with what probability he reaches, at a given point, a distance n from the origin after a given elapsed time. The traditional way to solve this problem is to allow the walker to take steps at time N ($N \in \mathbb{N}$) at which time he must jump either left or right, with equal probability. The DTRW can be written:

$$P(n, N+1 \mid n', N') = \frac{1}{2}[P(n+1, N \mid n', N') + P(n-1, N \mid n', N')] \tag{1.1}$$

where $P(n, N \mid n', N')$ is the probability to find the particle at time N at position n, if at time N' it was at n'. Once solved this equation and fixing one initial condition, the probability distribution is known as the Bernoulli distribution. It gives the probability of a total of n heads in tossing an unbiased coin N times:

$$P(n, N \mid 0, 0) = \left(\frac{1}{2}\right)^N N! \left[\left(\frac{N-n}{2}\right)! \left(\frac{N+n}{2}\right)!\right]^{-1} \tag{1.2}$$

Therefore, a DTRW, on a line, is defined in terms of classical particle's probabilities, and it may show a very rich and complex dynamics (Revesz [39]). Notably the square root of variance σ_{CW} is proportional to $\sqrt{n}$.

Now, if we imagine the particle to be quantum and completely isolated, we should conclude that there is at least one fundamental difference from the classical case: a quantum analogous of CRW is described by complex amplitudes and not by probabilities. Moreover, the quantum nature of the particle implicates the existence of entanglement states, *i.e.* non factorizable states, that have no analogous in classical physics. The presence of internal quantum states is another striking difference, and we will see, for instance, that it will recover a fundamental role in the definition of QW.

Now, let us introduce more properly the theoretical background for the DTQW.

1.1.3 General Setup of a Discrete Time Quantum Walks

Let $\mathcal{K}$ be a finite dimensional Hilbert space and let $\mathcal{H} = \mathcal{K} \otimes \mathbb{Z}^d$. The Hilbert space $\mathcal{H}$ is that of a QW in $\mathbb{Z}^d$ with k=dim($\mathcal{K}$) internal degrees of freedom. The space $\mathcal{K}$ is called the coin space and we denote the canonical basis of $\mathcal{K}$ by $\{|b_\tau\rangle\}_{\tau\in K=\{1,\dots,k\}}$. The projectors on the basis of $\{|b_\tau\rangle\}$ are noted by $\mathcal{P}_\tau = |b_\tau\rangle\langle b_\tau|$. We shall indicate the canonical basis of $\mathbb{Z}^d$ by $\{|m\rangle\}_{m\in\mathbb{Z}^d}$ so that any vector $\Psi \in \mathcal{H}$ can be written as:

$$\Psi = \sum_{m\in\mathbb{Z}^d} \Psi_m |m\rangle, \tag{1.3}$$

where

$$\Psi_m = \sum_{\tau\in K} \psi_m^\tau |b_\tau\rangle \in \mathcal{K}, \tag{1.4}$$

and $||\Psi_m||_2 < \infty$ where $||\cdot||_2 = (\sum_{m\in\mathbb{Z}^d} |\cdot|^2)^{\frac{1}{2}}$. We specify, in the following, the elements of the corresponding orthonormal composite basis of $\mathcal{H}$ by $|b_\tau, m\rangle = |b_\tau\rangle \otimes |m\rangle \in \mathcal{H}$. Let us now introduce the shift operator $\mathcal{T}$ defined by:

$$\mathcal{T} = \sum_{m\in\mathbb{Z}^d} \sum_{\tau\in K} P_\tau \otimes |m + S(\tau)\rangle\langle m|. \tag{1.5}$$

The walker at the site m with internal degree of freedom b_τ, represented by the vector $|b_\tau, m\rangle$, is just sent by $\mathcal{T}$ to one of the neighboring sites depending on τ determined by the shift function $S : K \to \mathbb{Z}^d$. The action of $\mathcal{T}$ is given as follows:

$$\mathcal{T}|b_\tau, m\rangle = |b_\tau, m + S(\tau)\rangle. \tag{1.6}$$

Consider now $\mathcal{B}(\mathcal{K})$ the set of complex valued matrices acting on $\mathcal{K}$ and consider the map:

$$\mathcal{B}(\mathcal{K}) : \psi \to \mathcal{B}(\mathcal{K})[\Psi]. \tag{1.7}$$

The one step evolution of the quantum walk is given by the map $\mathcal{U} : \mathcal{H} \to \mathcal{H}$

$$\Psi = \sum_{m\in\mathbb{Z}^d} \Psi_m |m\rangle \to \mathcal{U}[\Psi] = \mathcal{T}\mathcal{B}(\mathcal{K})[\Psi]. \tag{1.8}$$

In order to recover a one space dimensional QW with two internal state, we simply choose d=1 and $\mathcal{K} = \mathbb{C}^2$, whose basis we signal by $\{b_\tau\}_{\tau\in K}$ and $K = \{+1, -1\}$. The shift function corresponds to:

$$S : \{+1, -1\} \to \mathbb{Z}, \tag{1.9}$$

where $S(\pm 1) = \pm 1$.

We then choose the quantum coin B as an element of $U(2)$:

$$B_{\alpha,\theta,\xi,\zeta} = e^{i\alpha} \begin{pmatrix} e^{i\xi}\cos\theta & e^{i\zeta}\sin\theta \\ -e^{-i\zeta}\sin\theta & e^{-i\xi}\cos\theta \end{pmatrix} \tag{1.10}$$

where the set of the four parameters $(\alpha, \theta, \xi, \zeta)$ lives in $\mathbb{R}^4$. Note that $B_{\alpha,\theta,\xi,\zeta} \in SU(2)$ if $\alpha = k\pi$, $k \in \mathbb{Z}$.

Symmetries and properties of the above quantum coin have been widely investigated by Chandrashekar et al. [9]. Let us observe for $\theta = \pi/4$, $\alpha = -\xi = \pi/2$ and $\zeta = \pi/2$, the above

quantum coin recover the so called Hadamard coin, B_H defined as below:

$$B_H = \frac{1}{\sqrt{2}}\begin{pmatrix} 1 & 1 \\ 1 & -1 \end{pmatrix} \tag{1.11}$$

Also note that the global phase $\exp(i\alpha)$ does not play any role in homogeneous walks and notably in the time evolution of the probability density. However, it will play an important role in the next chapter when the quantum coin will depend on time and space points of the lattice.

Let us introduce the notation $\Psi_j = \mathcal{U}\cdot ... \cdot \mathcal{U}[\Psi_0]$, where $\Psi_0 = \sum_m \psi_{0,m}\ (c^L|b_L\rangle + c^R|b_R\rangle)$[1], where $\psi_{0,m}$ is a complex regular function, at least twice differentiable, and so that $||\psi_{0,m}||_2 < \infty$. The couple of constants $(c^L, c^R) \in \mathbb{C}^2$.
The finite difference equations after 1-fold iteration of the map $\mathcal{U}$, for each amplitude $\psi^L_{j,m} = \langle b_L, m|\Psi_j$ and $\psi^R_{j,m} = \langle b_R, m|\Psi_j$ are given by:

$$\psi^L_{j+1,m} = e^{i\alpha}(\cos(\theta)e^{i\xi}\psi^L_{j,m-1} + \sin(\theta)e^{i\zeta}\psi^R_{j,m-1}) \tag{1.12}$$

$$\psi^R_{j+1,m} = e^{i\alpha}(-\sin(\theta)e^{-i\zeta}\psi^L_{j,m+1} + \cos(\theta)e^{-i\xi}\psi^R_{j,m+1}) \tag{1.13}$$

The above equations usually define in the literature DTQW evolution. Nonetheless, there are other remarkable definitions of DTQW. For instance, let us recall the *embedded QW* Chandrashekar [8], a generic quantum walk model that uses a quantum coin embedded in the unitary shift operator $\mathcal{T}$, where an additional degree of freedom is added. Let us state $\mathcal{K} = \mathcal{K}_1 \otimes \mathcal{K}_2$ where $\mathcal{K}_1$ is the usual internal coin space and $\mathcal{K}_2$ is an external coin space. The main role of the $\mathcal{T}$ is to move the particle in the superposition of position space at each time step, eliminating the need for a separate coin toss operation after every unitary step.

Another model definition is introduced in some of the publications included in this thesis, which simply consists in inverting the shift operator $\mathcal{T}$ and the action of the quantum coin B:

$$\Psi = \sum_{m\in\mathbb{Z}^d} \Psi_m|m\rangle \rightarrow \mathcal{U}[\Psi] = \mathcal{B}(\mathcal{K})\mathcal{T}[\Psi] \tag{1.14}$$

Then the amplitude, coding the probability of the particle to go towards the left $\psi^L_{j,m}$ and towards the right $\psi^R_{j,m}$ after one time step, is:

$$\psi^L_{j+1,m} = e^{i\alpha}(\cos(\theta)e^{i\xi}\psi^L_{j,m-1} + \sin(\theta)e^{i\zeta}\psi^R_{j,m+1}) \tag{1.15}$$

$$\psi^R_{j+1,m} = e^{i\alpha}(-\sin(\theta)e^{-i\zeta}\psi^L_{j,m-1} + \cos(\theta)e^{-i\xi}\psi^R_{j,m+1}) \tag{1.16}$$

Observe that this definition of the walk is totally equivalent to the usual standard definition in case of homogeneous and static quantum coin and symmetric density time evolution.

Let us conclude with a comment on the formalism which will be useful in the following chapters. Suppose we want to represent the entire history of a quantum walk observed through a stroboscope of period n. For all $(n, j) \in \mathbb{N}^2$, the collection

$$W^n_j = (\Psi_{k,m})_{k=nj, m\in\mathbb{Z}}. \tag{1.17}$$

This collection represents the state of the quantum walk at *time* $k = nj$. For any given n, the

[1] More generally $\Psi_0 = \sum_m \psi_{0,m}\ (c^L|b_L\rangle + e^{i\phi}c^R|b_R\rangle$ where $e^{i\phi}$ is a complex phase which can be tuned to modify the symmetry of the initial condition.

collection

$$S^n = (W_j^n)_{j\in\mathbb{Z}}, \tag{1.18}$$

where the final state observed through a stroboscope of period n. The evolution equations for S^n are those linking W_{j+1}^n to W_j^n for all j. These can be deduced from the original evolution (1.12, 1.13) or (1.15, 1.16) from the walk, which also coincides with the evolution equations of S^1.

1.1.4 Qualitative description

A general qualitative description of quantum walk dynamics has been largely reported by Venegas-Andraca [47]. We recall here the main features of a DTQW moving on unrestricted line. For simplicity let us consider here the simplest version of the DTQW, the Hadamard walk. The discrete time equations read:

$$\psi_{j+1,m}^L = \frac{1}{\sqrt{2}}(\psi_{j,m-1}^L + \psi_{j,m-1}^R) \tag{1.19}$$

$$\psi_{j+1,m}^R = \frac{1}{\sqrt{2}}(\psi_{j,m+1}^L - \psi_{j,m+1}^R) \tag{1.20}$$

where the quantum coin is the Hadamard Coin (or Hadamard gate), B_H has been defined in (1.11).

The Hadamard walk has been extensively studied and it is known that the final distribution depends on the initial state of the particle. For instance, let us acknowledge an initial condition as $\Psi_0 = \sum_m \psi_{0,m}\,(c^L|b_L\rangle + e^{i\phi}c^R|b_R\rangle)$, where $\psi_{0,m}$ is normally distributed and centered about $m = 0$ and $\phi \in \mathbb{R}$. From Fig. 1.1 we can notice that (i) the probability distribution is significantly different from the DTRW's one, which is Gaussian; (ii) the unitary operator treats differently the initial condition if (a) $c_L = 1, c_R = 1, \phi = 0$ or (b) $c_L = 1, c_R = -1, \phi = 0$. Between the two cases, there is a phase difference and the asymmetry arises from the constructive interference on one side, and from the destructive interference on the other side of the position space. In order to obtain a symmetric final state we can prepare a symmetric superposition state, as for example:

$$\Psi_0 = \sum_m \frac{\psi_{0,m}}{2}(|b_L\rangle + i|b_R\rangle). \tag{1.21}$$

where $c_L = 1, c_R = 1, \phi = \frac{\pi}{2}$.

Let us remark that for a Hadamard walk on the line, it is proved by Venegas-Andraca [47] that after N steps, the probability distribution is spread on the interval $[-\frac{N}{\sqrt{2}}, \frac{N}{\sqrt{2}}]$ and decreases quickly outside this region, as we can see in Fig. 1.1.

The approximation of the root of the variance, for a large number of steps, varies as following:

$$\sigma_j \propto \sqrt{1 - \frac{1}{\sqrt{2}}}\,j. \tag{1.22}$$

Let us now examine the $U(2)$ quantum coin as in Eq. (1.10). It is possible to disregard the role of the particle's initial state, in order to obtain a symmetric amplitude distribution, just tuning the three parameters (θ, ξ, ζ). In fact, let us consider $P_\pm$ encoding the probability to find the particle in position $m = 1$ and in position $m = -1$. Starting from a symmetric initial state

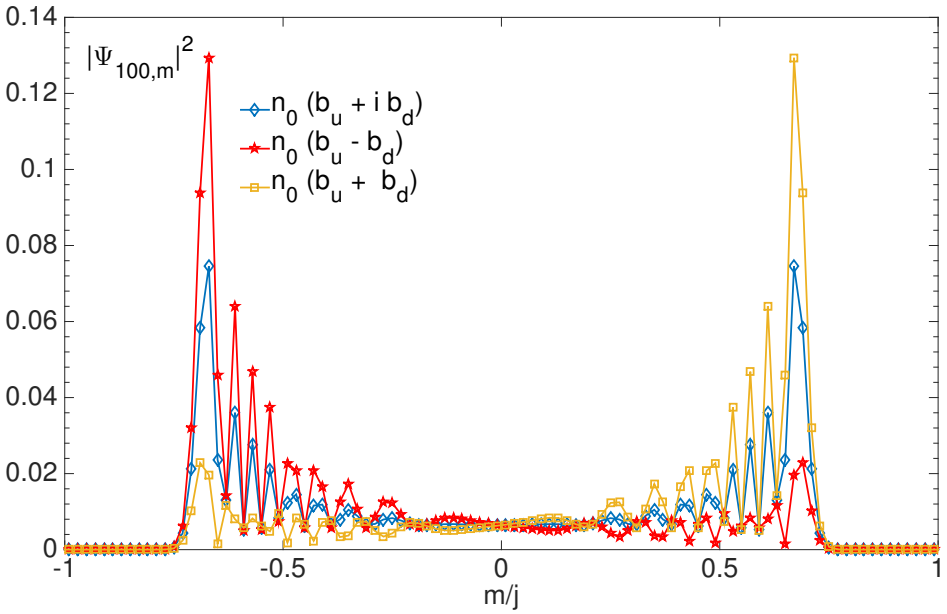

Figure 1.1: *Spread of probability density of a Hadamard walk on n grid points with asymmetric initial state* $\Psi_0 = \sum_m \psi_{0,m}\ (c^L|b_L\rangle + e^{i\phi}c^R|b_R\rangle)$ *T where (i)* $c_L = 1, c_R = 1, \phi = 0$ *or (ii)* $c_L = 1, c_R = -1, \phi = 0$ *and symmetric initial state* $c_L = 1, c_R = 1, \phi = \pi/2$. *The spatial component is given by* $\psi_0 = \sum_m \delta_{0,m}$

Ψ_0, with $c_L = 1, c_R = 1, \phi = 0$, obeying to the Eqs.(1.12, 1.13), the probabilities $P_\pm$ read:

$$P_{\mp}^{QW} = (1 \pm \sin(2\theta)\cos(\zeta - \xi)) \tag{1.23}$$

This probability distribution will be equal and lead to a left-right symmetry in position if $\zeta - \xi = (2k+1)\frac{\pi}{2}$, $k \in \mathbb{N}$ [2]. Otherwise the parameters ξ and ζ will introduce bias in the spatial probability distribution from the very first step.
Concerning again the variance of the walk, the three Euler angles do not change qualitatively the dynamics in respect to the Hadamard case, which always remains ballistic. However, now the root of the variance σ is a function of all the three Euler angles:

$$\sigma \propto K_{\theta,\xi,\zeta}\, j. \tag{1.24}$$

A simple case can be shown taking into account, for instance, all the angles equal to zero except θ and $K_\theta \propto \sqrt{1-\sin\theta}$ [7]. Observe in Fig.1.4 that the value of K_θ decreases as θ increases. In particular in the limit of $\theta = \pi/2$ the walker does not spread, but it is localized around the origin, therefore $K_\theta = 0$. Conversely, if $\theta = k\pi$, $k \in \mathbb{Z}$, the particle spreads with $K_\theta = 1$. Intermediate values of the variance are dominated by the interference effects, and the probability distribution spreads, after N steps, over the interval (- $N\cos\theta$, $N\cos\theta$). As in the Hadamard walk, the probability distribution decreases rapidly beyond $|N\cos\theta|$.

[2] Note that in case of Eqs.(1.15, 1.16), the probability to find the particle in position $m = \mp 1$ starting from a symmetric initial state, reads $P_\mp = (1 \mp \sin(2\theta)\cos(\zeta + \xi))$. This probability distribution will be equal and lead to a left-right symmetry in position if $\zeta + \xi = (2k+1)\frac{\pi}{2}$, $k \in \mathbb{N}$.

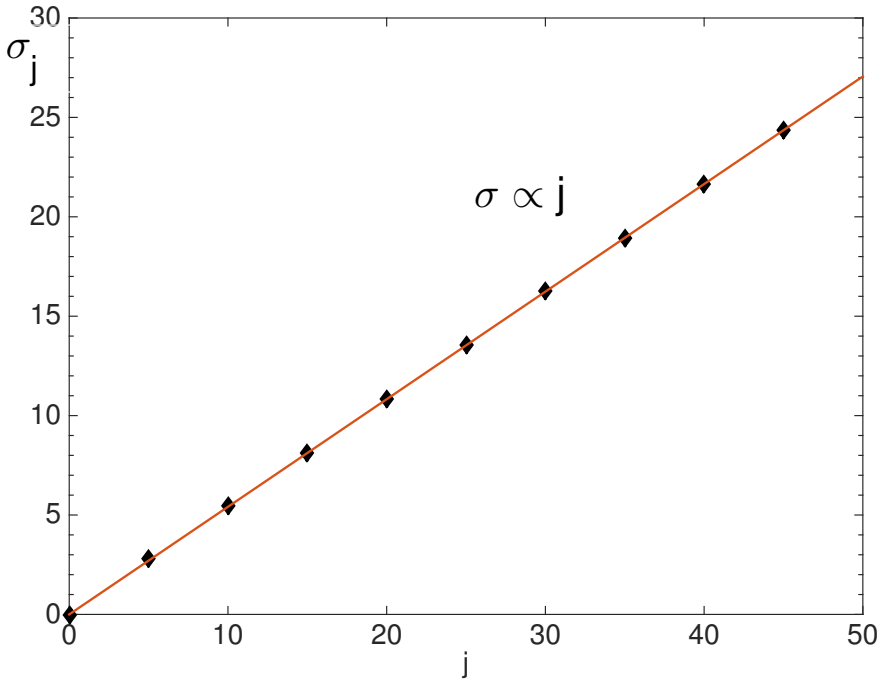

Figure 1.2: *Square root of variance of a Hadamard Walk with symmetric initial state and localized position in the origin. The slope is* $(1-\frac{1}{\sqrt{2}})^{1/2}$.

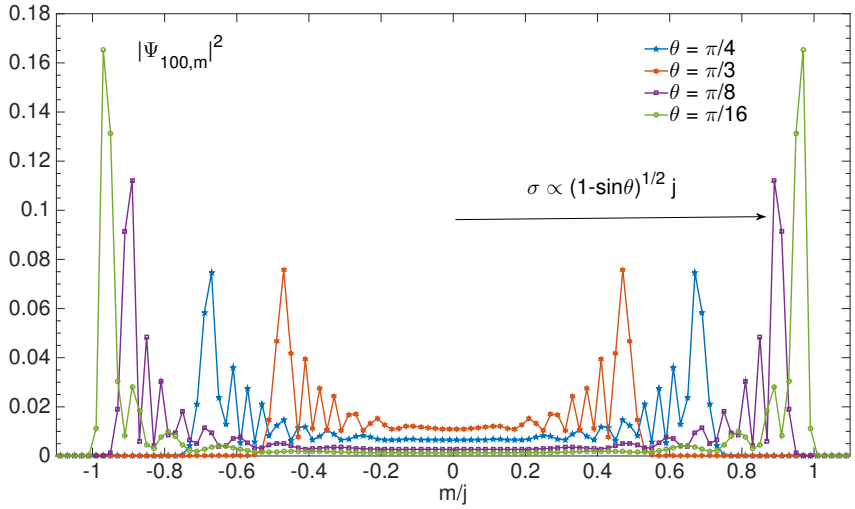

Figure 1.3: *Spread of probability density of the DTQW with symmetric initial state and different values of* θ, *for* $\alpha = -\pi/2$, $\xi = \pi/2$ *and* $\zeta = \pi/2$.

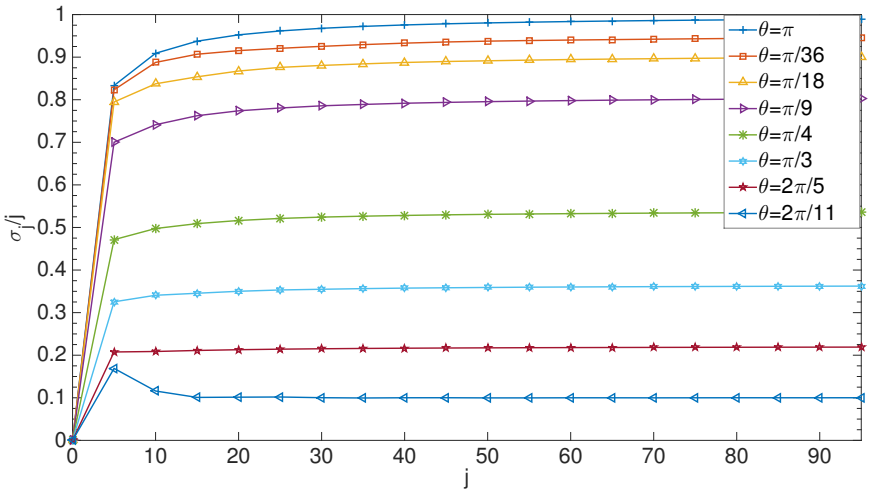

Figure 1.4: *Value of K_θ for a given θ.*

1.1.5 Quantitative description

1.1.5.1 Fourier methods for the Hadamard walk

The analytical description of QWs dynamics has represented over the last few years an important field of investigation. Two methods have been extensively used: (i) the Fourier method and (ii) the combinatorial approach. In the former, the QW dynamics is studied in Fourier space in order to get a closed-form of the coin amplitude equations and, therefore, computing statistical properties of the walker. It was first introduced by Nayak and Vishwanath [32] and later by Kosik [27]. In the combinatorial approach, we shall compute the amplitude for a particular position m component by summing up the amplitudes of all the paths which begin in the given initial condition and up in the same position m. This approach is also called discrete path integral approach and was developed mainly by Machida and Konno [31].

Here, we briefly recall the first method for the family of QWs obeying to Eqs. (1.12) and (1.13). Note that this could easily be extended to Eqs. (1.15) and (1.16). The closed-form of the coin amplitude is straightforward if we consider Eqs. (1.12) and (1.13) in Fourier space. Then let us look at $\hat{\Psi}_{j,k} = \sum_m \Psi_{j,m} e^{ikm}$ Fourier transformed state of $\Psi_{j,m}$. The finite difference equations read:

$$\begin{pmatrix} \hat{\psi}^L_{j+1,k} \\ \hat{\psi}^R_{j+1,k} \end{pmatrix} = e^{i\alpha} \begin{pmatrix} e^{i(\xi-k)}\cos\theta & e^{i(\zeta-k)}\sin\theta \\ -e^{-i(\zeta-k)}\sin\theta & e^{-i(\xi-k)}\cos\theta \end{pmatrix} \begin{pmatrix} \hat{\psi}^L_{j,k} \\ \hat{\psi}^R_{j,k} \end{pmatrix} \tag{1.25}$$

or more compactly $\hat{\Psi}_{j+1,k} = U_k \hat{\Psi}_{j,k}$, where U_k is the Fourier transform of the unitary operator driving the walk and it is local. In order to compute the solution after N steps, we need to compute $(U_k)^N$ and this is easily accomplished if we diagonalize the unitary matrix associated with the operator U_k. A unitary matrix is always diagonalizable as a consequence of the spectral theorem. Therefore U_k is diagonalizable:

$$V_k = \mathcal{O}^{-1} U_k \mathcal{O} \tag{1.26}$$

where $\mathcal{O}$ are unitary matrix and V_k is diagonal. The eigenvalues $\lambda_1 = (V_k)_{11}$ and $\lambda_2 = (V_k)_{22}$ are

real. Moreover, the power U_k^N is simply given by $U_k = \mathcal{O}(V_k)^N\mathcal{O}^{-1}$ or by:

$$U_k^N = \mathcal{O}\begin{pmatrix} {\lambda_1}^N & 0 \\ 0 & {\lambda_2}^N \end{pmatrix}\mathcal{O}^{-1} \tag{1.27}$$

To compute the solution, let us take into account as initial condition $\hat{\Psi}_{0,k} = \sum_m \Psi_{0,m}e^{ikm}$, where $\Psi_{0,m} = \delta_{m,0}|b_L\rangle$. Computations of the exact expression for the Fourier-transformed amplitudes $\hat{\psi}^L$ and $\hat{\psi}^R$ are straightforwards. For instance, we report the solution for the amplitudes obeying to a Hadamard walk, that is for $B_H = B_{-\pi/2,\pi/4,\pi/2,\pi/2}$:

$$\psi^L_{j,m} = \left(\frac{1}{2\pi}\int_{-\pi}^{\pi}\frac{-ie^{ik}}{2\sqrt{1+\cos^2 k}}(e^{-i(\omega_k j - km)})dk\right) \tag{1.28}$$

$$\psi^R_{j,m} = \left(\frac{1}{2\pi}\int_{-\pi}^{\pi}1+\frac{\cos(k)}{\sqrt{1+\cos^2 k}}(e^{-i(\omega_k j - km)})dk\right) \tag{1.29}$$

where ω_k =$\sin^{-1}(\frac{\sin(k)}{\sqrt{2}})$ and $\omega_k \in [-\frac{\pi}{2},\frac{\pi}{2}]$. As we can see, the amplitudes for even m at odd j vanish and the same for the odd n at even j. Having an analytical expression of Ψ_j allows the study of the asymptotical behavior of the probability distribution $|\Psi_{j,m}|^2$. Results of this study are extensively treated in [47], and confirm the previous qualitative description. We summarize here two important conclusions: (i) both amplitudes ψ^L and ψ^R are almost uniformly spread over the region $[-j/\sqrt{2}, j/\sqrt{2}]$, in general over $[-jK_{\theta,\xi,\zeta}, jK_{\theta,\xi,\zeta}]$, and they decay rapidly to zero outside the region; (ii) the position probability distribution spreads as a function of j, in contrast to the standard deviation of an unrestricted CRW on a line, which is of order $O(\sqrt{j})$.

1.2 Connections between Quantum Walks and Relativistic Wave Equations

1.2.1 Quantum walks and Feynman's Checkerboard

In Feynman's picture, a particle zig-zags at the speed-of-light across a spacetime lattice, flipping its chirality from left to right with an infinitesimal probability each time-step. The resulting dynamics, in the continuum limit, is the Dirac equation, with the flipping rate determined by the mass of the particle. (Strauch [43])

The Feynman's Checkerboard was first introduced in its original version by Feynman and Hibbs [10] as a simple path integral representation for the retarded Dirac propagator in 1+1 dimensions. In this model the particle's motion is restricted to be either forward (right) or backward (left) at the velocity of light. Feynman's path integral results from a particular finite differencing of the massive Dirac equation in (1+1):

$$(\frac{\partial}{\partial_t} \pm \frac{\partial}{\partial_x})\psi^{L,R} = iM\psi^{R,L}. \tag{1.30}$$

where M is the real and constant mass of the fermion.
On a square spacetime lattice $(m, j) \in (\mathbb{Z}\times\mathbb{N})$ as in Fig.(1.5) with a mesh size ϵ, the real variables (x, t) are discretized so that $t_j = \epsilon j$ and $x_m = \epsilon m$. The finite difference equations, as prosed by

Feynman, read:

$$\psi^L_{j,m} = \psi^L_{j-1,m-1} + i\tilde{M}\psi^R_{j-1,m+1} \tag{1.31}$$

$$\psi^R_{j,m} = \psi^R_{j-1,m+1} + i\tilde{M}\psi^L_{j-1,m-1} \tag{1.32}$$

where $\tilde{M} = \epsilon M$. These equations may be interpreted as following: the probability amplitude for a particle to be at (j,m) moving toward the right, is equal to the amplitude encountered at $(j-1,m+1)$ moving toward the right plus $i\epsilon M$ times the amplitude encountered at $(j-1,m-1)$ moving toward the left. Instead the probability amplitude for a particle to be at (j,m) moving toward the left, is equal to the amplitude encountered at $(j-1,m-1)$ moving toward the left plus $i\epsilon M$ times the amplitude encountered at $(j-1,m+1)$ moving toward the right. Iterating

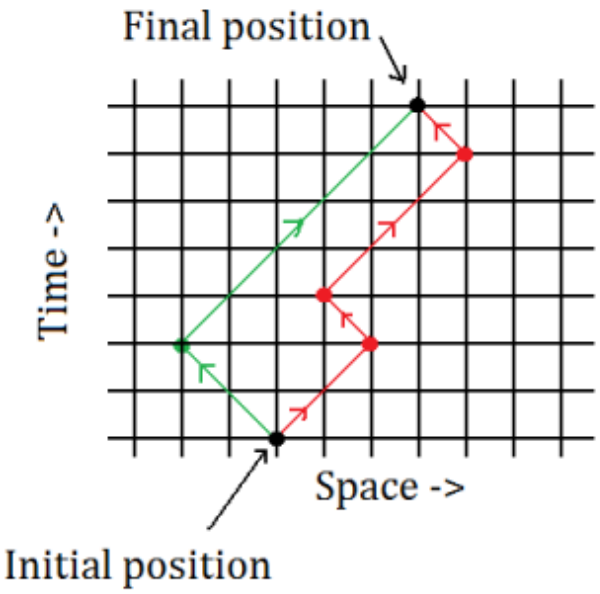

Figure 1.5: *Feynman's Checkerboard representation in the discrete space time lattice (x,t).*

the finite difference Eqs. (1.32), $\psi^{L,R}$ may be expressed as a sum over paths leading to (j,m). The retarded propagator $K_{j,m}$ is, therefore, the sum of number of paths, with N steps, leaving the point m' in direction χ' and end at point m" in direction χ and switching direction B times. Thus $K_{j,m}$ can be expressed as:

$$K_{\chi\chi'} = \sum_B (\Phi_{\chi\chi'})_{j,m;B} (i\epsilon M)^B \tag{1.33}$$

The convergence of Eq. (1.33) to the exact continuum propagator in the limit $\epsilon \to 0$ is demonstrated by Jacobson and Schulman [22].

We can recognize that the probabilities (1.23) of a homogenous QW are related with what Feynman found for the Dirac particle of mass M. In fact, imposing $\theta = \frac{\epsilon M}{2}$, the probability distribution reads:

$$P^{QW}_{\pm} \approx (1 \pm \epsilon M). \tag{1.34}$$

The relationship between the Feynman's Checkerboard and QWs is even more clear if we consider the discrete path integral approach introduced in modeling quantum walks, for instance,

by Machida and Konno [31]. Thus, we dedicate the next section and the next chapter to understand the nature of this connection.

1.2.2 Homogeneous DTQWs and Weyl equation

Differently to what Feynman did, in this section we want to investigate the formal continuous limit of DTQWs with homogeneous and static quantum coin operator $B_{\alpha,\xi,\zeta,\theta}$.
In order to investigate the continuous limit we first introduce a time step Δt and a space step Δx. We then introduce for any quantity a appearing in Eq. (1.15) and (1.16), a function $\tilde{a}$ defined on $\mathbb{R}^+ \times \mathbb{R}$ such that the number $a_{j,m}$ is the value taken by $\tilde{a}$ at the spacetime point $(t_j = j\Delta t, x_m = m\Delta x)$. We then suppose $\Psi(t_j, x_m)$ to be at least C^2 and that its characteristic length Λ to be much larger than the lattice parameter Δx. Let us consider here the equations (1.15) and (1.16):

$$\begin{pmatrix} \psi^L(t_j + \Delta t, x_m) \\ \psi^R(t_j + \Delta t, x_m) \end{pmatrix} = B_{\alpha,\xi,\zeta,\theta} \begin{pmatrix} \psi^L(t_j, x_m - \Delta x) \\ \psi^R(t_j, x_m + \Delta x) \end{pmatrix} \tag{1.35}$$

If the formal continuous limit exists, it will be obtained formally: (i) expanding each terms of the equations in Δt and Δx at fixed t_j and x_m and finally (ii) moving Δt and Δx to zero.

Let us now introduce a time-scale $\tau \in \mathbb{R}$ and a length-scale $\lambda \in \mathbb{R}$ and an $\epsilon \in \mathbb{R}$ so that $\tau\epsilon \ll 1$ and $\lambda\epsilon \ll 1$. Define $\Delta t = \tau\epsilon$ and $\Delta x = \lambda\epsilon^\delta$, where δ is a strictly positive real number, which traces the fact that Δt and Δx may tend to zero differently. The Taylor expansion of each spacetime dependent function in (1.35), up to order $O(\epsilon^2)$, reads:

$$\begin{aligned} \Psi^{L,R}(t_j + \Delta t_j, x_m) &= \Psi^{L,R}(t_j, x_m) + \tau\epsilon\partial_t \Psi^{L,R}(t_j, x_m) + O(\epsilon^2) \\ \Psi^{L,R}(t_j, x_m \pm \Delta x) &= \Psi^{L,R}(t_j, x_m) \pm \lambda\epsilon^\delta \partial_x \Psi^{L,R}(t_j, x_m) + O(\epsilon^{2\delta}) \end{aligned} \tag{1.36}$$

The Eq. (1.35) then leads us to:

$$\begin{pmatrix} \psi^L(t_j, x_m) \\ \psi^R(t_j, x_m) \end{pmatrix} + \tau\epsilon\partial_t \begin{pmatrix} \psi^L(t_j, x_m) \\ \psi^R(t_j, x_m) \end{pmatrix} + O(\epsilon^2) = B_{\alpha,\xi,\zeta,\theta}(1 + \lambda\epsilon^\delta \partial_x + O(\epsilon^{2\delta})) \begin{pmatrix} \psi^L(t_j, x_m) \\ \psi^R(t_j, x_m) \end{pmatrix} \tag{1.37}$$

Note that, in order to cancel the zeroth order contribution out, we have to impose that $B_{\alpha,\xi,\zeta,\theta}$ tends to the identity matrix $\mathcal{I}_2$ of dimension 2×2. Therefore the following equations must be satisfied:

$$\begin{aligned} e^{i(\alpha+\xi)} \cos\theta &= 1 \\ e^{i(\alpha-\xi)} \cos\theta &= 1 \\ e^{i(\zeta+\alpha)} \sin\theta &= 0 \end{aligned} \tag{1.38}$$

The above relations imply $\theta = k\pi$, $\alpha = (k + k^+ + k^-)\pi$, $\xi = (k_+ - k_-)\pi$, $(k, k_-, k_+) \in \mathbb{Z}^3$. The angle ζ does not enter this constraint and is therefore an arbitrary real value.
Finally, letting ϵ to zero, the Eqs. (1.37) admits formally two continuous limits: (i) one for $\delta > 1$. In this case there is no propagation and the particle is localized at the initial condition; (ii) the most interesting case is for $\delta = 1$ because all contributions are then of equal importance.

Let us now regard $T = t/\tau, X = x/\lambda$, the equations of motion for the continuous limit of S^1_ϵ in this simple homogeneous case read:

$$(\frac{\partial}{\partial_T} - \frac{\partial}{\partial_X})\psi^L = 0 \tag{1.39}$$

$$(\frac{\partial}{\partial_T}+\frac{\partial}{\partial_X})\psi^R=0 \tag{1.40}$$

Taken together, these two coupled first-order PDEs forms a system of relativistic wave equations describing massless spin-1/2 particles, otherwise known as Weyl equations. Let us remember that, in flat two-dimensional spacetime, the Clifford algebra can be represented by matrices acting on two-component spinors. This algebra admits two independent generators γ_0 and γ_1 , which can be represented by matrices obeying to the usual anti-commutation relation $\{\gamma^a,\gamma^b\}=2\eta^{ab}\mathcal{I}$, where η is the Minkowski metric and $\mathcal{I}$ is the Identity matrix. Consider the (non unique) representation $\gamma^0=\sigma_1$ and $\gamma^1=-\sigma_1\sigma_3=i\sigma_2$, where σ_1,σ_2 and σ_3 are the three Pauli matrices:

$$\sigma_1=\begin{bmatrix}0&1\\1&0\end{bmatrix},\ \sigma_2=\begin{bmatrix}0&-i\\i&0\end{bmatrix},\ \sigma_3=\begin{bmatrix}1&0\\0&-1\end{bmatrix}. \tag{1.41}$$

The Eqs. (1.39,1.40) can be recast in the following compact form:

$$i\gamma_\mu\partial^\mu\Psi=0 \tag{1.42}$$

where $\partial^0=\frac{\partial}{\partial_T}$, $\partial^1=\frac{\partial}{\partial_X}$.

1.2.3 Publication: "Massless Dirac Equation from Fibonacci Discrete-Time Quantum Walk"

This publication is a joint effort between the collaboration of the JSPS fellow Di Molfetta with the Shikano group, and the internship of two undergraduate Australian students, Lauchlan Honter and Ben Luo, from The University of Western Australia. We present two modified versions of the aperiodic quantum walk introduced by Ribeiro et al. [40], as a simple but non trivial case of the continuous limit with a homogeneous and periodic unitary step operator.

We introduce two models of DTQWs. The first, labeled FDTQW-I, is a generalized Hadamard coin $B(\theta_j)=B_j$ following the infinite Fibonacci sequence, as below:

$$B_{j+1}=B_jB_{j-1} \tag{1.43}$$

where $B_0=B(\alpha)$ and $B_1=B(\beta)B(\alpha)$. We found that this sequence when applied to the coin operator is six-steps periodic. The formal continuous limit of the stroboscope of period six coincides with a ballistic equation that recover the Weyl equation in two spacetime dimension.

In the second case, FDTQW-II, the Fibonacci sequence is followed by the QW's step operator $\mathcal{U}=\mathcal{T}B$:

$$\mathcal{U}_{j+1}=\mathcal{U}_j\mathcal{U}_{j-1} \tag{1.44}$$

where $\mathcal{U}_0=\mathcal{T}B(\alpha)$ and $\mathcal{U}_1=\mathcal{T}B(\beta)\mathcal{T}B(\alpha)$. In this case the sequence is no longer periodic but aperiodic as Ribeiro et al. [40] proved in his paper. In particular they showed that this model displays a sub ballistic behavior. What we prove is that if we truncate the Fibonacci sequence in FDTQW-II the behavior is no longer sub-balistic and display a standard propagative behavior. There still remains a problem concerning the type of transition occurring when the periodicity FDTQW-II increases towards infinity, and the mechanism by which the dynamical behavior of the periodic extension changes into that of the infinite sequence [40].

Quantum Stud.: Math. Found.
DOI 10.1007/s40509-015-0038-6

CHAPMAN UNIVERSITY | INSTITUTE FOR QUANTUM STUDIES

REGULAR PAPER

Massless Dirac equation from Fibonacci discrete-time quantum walk

Giuseppe Di Molfetta · Lauchlan Honter · Ben B. Luo · Tatsuaki Wada · Yutaka Shikano

Received: 1 February 2015 / Accepted: 14 March 2015

Abstract Discrete-time quantum walks can be regarded as quantum dynamical simulators since they can simulate spatially discretized Schrödinger, massive Dirac, and Klein–Gordon equations. Here, two different types of Fibonacci discrete-time quantum walks are studied analytically. The first is the Fibonacci coin sequence with a generalized Hadamard coin and demonstrates six-step periodic dynamics. The other model is assumed to have three- or six-step periodic dynamics with the Fibonacci sequence. We analytically show that these models have ballistic transportation properties and continuous limits identical to those of the massless Dirac equation with coin basis change.

Keywords Quantum Walk · Massless Dirac equation · Quantum Simulation

G. Di Molfetta, L. Honter, and B. B. Luo are equally contributed to this work.

G. Di Molfetta · L. Honter · B. B. Luo · Y. Shikano
Research Center of Integrative Molecular Systems (CIMoS), Institute for Molecular Science, Natural Institutes of Natural Sciences, 38 Nishigo-Naka, Myodaiji, Okazaki, Aichi 444-8585, Japan

G. Di Molfetta
LERMA, Observatoire de Paris, PSL Research University, CNRS, Sorbonne Universités, UPMC Univ. Paris 6, UMR 8112, F-75014 Paris, France
e-mail: giuseppe.dimolfetta@ens.fr

L. Honter · B. B. Luo
School of Physics, The University of Western Australia, 35 Stirling Hwy, Crawley, Perth, WA 6009, Australia

T. Wada
Department of Electrical and Electronic Engineering, Ibaraki University, 12-4-1 Nakanarusawa, Hitachi, Ibaraki 316-8511, Japan

Y. Shikano ( )
Institute for Quantum Studies, Chapman University, 1 University Dr., Orange, CA 92866, USA
e-mail: yshikano@ims.ac.jp

Published online: 03 April 2015

1 Introduction

Discrete-time quantum walks (DTQWs) are defined as quantum-mechanical analogues of classical random walks. The concept of DTQWs was first considered by Feynman [1] and then introduced in greater generality by Refs. [2–4]. They have been realized experimentally in Refs. [5–20] and are important in many fields, from fundamental quantum physics [15,21–23] to quantum algorithm [24–26] and condensed matter physics [27–37]. Previously, it has been shown that several DTQWs on a line admit a continuous limit identical to the propagation equations of a massive Dirac fermion [39–43] and those of massless Dirac fermion equations [21,39]. Furthermore, the relationship between DTQWs and artificial electric and gravitational fields has been shown [21,44]. Thus, DTQWs can be regarded as quantum dynamical simulators [39,40]. Additionally, it is well known that the classical random walk leads to a diffusive behavior characterized by the time evolution of the standard deviation, with $\sigma(t) \sim t^{1/2}$, while the standard DTQW leads to ballistic behavior, as $\sigma(t) \sim t$. Further, the standard DTQW can be considerably enriched by generalizing the quantum coin operator and arranging it along different sequences. It has already been shown that quasi-periodic coin sequences induced by the Fibonacci sequence lead to sub-ballistic behavior, whereas random sequences lead to diffusive spreading [48–50]. Here, we consider two different Fibonacci DTQWs with periodic coin sequences. The first model (FDTQW-I) considers a time-dependent quantum coin following the Fibonacci sequence, while the second model (FDTQW-II) considers a modified version of the unitary operator first defined in Ref. [48], where the Fibonacci sequence is applied to the step operator. We show numerically and analytically that the continuous limit of these models reduces to a massless Dirac equation in $(1+1)$ dimensions.

2 Discrete-time quantum walk with Fibonacci sequence coin

Let us consider the two-dimensional spin state $\Psi_{m,j} \in \mathbb{C}^2$, spanned by the orthonormal basis (b_u, b_d), and defined by its discrete one-dimensional position $m \in \mathbb{Z}$ and discrete time $j \in \mathbb{N}_0$. The standard DTQW's time evolution is given by the application of the quantum coin operator (QCO) $\hat{C}$ on $\Psi_{m,j} = u_{m,j} b_u + d_{m,j} b_d = \begin{pmatrix} u_{m,j} \\ d_{m,j} \end{pmatrix}$, followed by the chiral-dependent translation operator $\hat{T}$, which is defined as:

$$\begin{pmatrix} u_{m-1,j} \\ d_{m+1,j} \end{pmatrix} = \hat{T} \begin{pmatrix} u_{m,j} \\ d_{m,j} \end{pmatrix}. \tag{1}$$

Here, we introduce the simplest quantum coin, the generalized Hadamard coin, which is expressed as:

$$\hat{C}(\theta) = \begin{pmatrix} \cos(\theta) & \sin(\theta) \\ \sin(\theta) & -\cos(\theta) \end{pmatrix}, \tag{2}$$

where $\theta \in [0, 2\pi]$. The one-step discrete time evolution is then given by:

$$\begin{pmatrix} u_{m,j+1} \\ d_{m,j+1} \end{pmatrix} = \hat{T}\hat{C}(\theta) \begin{pmatrix} u_{m,j} \\ d_{m,j} \end{pmatrix}. \tag{3}$$

First, we consider FDTQW-I, which is the simplest case as only the QCO is defined as a Fibonacci series. Here,

$$\hat{U}_j = \hat{T}\hat{C}_j\,, \qquad j \in \mathbb{N}_0\,, \qquad \hat{C}_{j+1} = \hat{C}_j \hat{C}_{j-1}\,, \tag{4}$$

with the initial conditions

$$\hat{C}_0 = \hat{C}(\alpha)\,, \qquad \hat{C}_1 = \hat{C}(\alpha)\hat{C}(\beta), \tag{5}$$

where j is the time step. On considering the DTQW acted upon by the Fibonacci coin series, we analytically find that the time evolution of the coin is cyclic with period 6. These coin operators then reduce to,

$$
\begin{aligned}
\hat{C}_0 &= \begin{pmatrix} \cos(\alpha) & \sin(\alpha) \\ \sin(\alpha) & -\cos(\alpha) \end{pmatrix}, \\
\hat{C}_1 &= \begin{pmatrix} \cos(\alpha-\beta) & -\sin(\alpha-\beta) \\ \sin(\alpha-\beta) & \cos(\alpha-\beta) \end{pmatrix}, \\
\hat{C}_2 &= \begin{pmatrix} \cos(2\alpha-\beta) & \sin(2\alpha-\beta) \\ \sin(2\alpha-\beta) & -\cos(2\alpha-\beta) \end{pmatrix}, \\
\hat{C}_3 &= \begin{pmatrix} \cos(\alpha) & \sin(\alpha) \\ \sin(\alpha) & -\cos(\alpha) \end{pmatrix}, \\
\hat{C}_4 &= \begin{pmatrix} \cos(\alpha-\beta) & \sin(\alpha-\beta) \\ -\sin(\alpha-\beta) & \cos(\alpha-\beta) \end{pmatrix}, \\
\hat{C}_5 &= \begin{pmatrix} \cos(\beta) & \sin(\beta) \\ \sin(\beta) & -\cos(\beta) \end{pmatrix}.
\end{aligned} \tag{6}
$$

Here, the collection $W_j^n = (\Psi_{m,k})_{m\in\mathbb{Z},k=nj}$ is defined for $j \in \mathbb{N}$ and $n \in \{0, 1, 2, 3, 4, 5\}$, and represents the state of the walk at time $k = nj$. For any given n we define $S^n = (W_j^n)_{j\in\mathbb{Z}}$, where S^n represents the entire history of the walk observed through a stroboscope of period n. Successive application of the 6 unitary operators to an initial state then gives the stroboscopic recursion equations for S^6. The discrete-step equations for S^6 read

$$
u_{m,j+6} = \sum_{k=-3}^{3} \big(A_{2k}(\alpha,\beta)u_{m+2k,j} + B_{2k}(\alpha,\beta)d_{m+2k,j}\big), \tag{7}
$$

$$
d_{m,j+6} = \sum_{k=-3}^{3} \big(B_{-2k}(-\alpha,-\beta)u_{m+2k,j} + A_{-2k}(-\alpha,-\beta)d_{m+2k,j}\big). \tag{8}
$$

Here, the index $k \in \{-6, -4, -2, 0, 2, 4, 6\}$ and the coefficients $A_k, B_k \in \mathbb{R}$ are explicitly given as

$$
\begin{aligned}
A_{-6} &= c_\alpha^2 c_\beta c_{\alpha-\beta}^2 c_{2\alpha-\beta} \\
A_{-4} &= -\frac{1}{4} c_\alpha c_{\alpha-\beta}^2 (c_{\alpha-2\beta} + 3c_{3\alpha-2\beta} - 5c_\alpha + c_{3\alpha}) \\
A_{-2} &= \frac{1}{16}(-6c_{2(\alpha-\beta)} + 4c_{4(\alpha-\beta)} - c_{2(\alpha+\beta)} - c_{2(\alpha-2\beta)} \\
&\quad + 2c_{4\alpha-2\beta} - c_{6\alpha-2\beta} + c_{6\alpha-4\beta} - 2c_{4\alpha} - 2c_{2\beta} + 6) \\
A_{\,0} &= \frac{1}{4} c_{\alpha-\beta}^2 (-6c_{2(\alpha-\beta)} + c_{4\alpha-2\beta} - 2c_{2\alpha} + c_{4\alpha} + c_{2\beta} + 5) \\
A_{\,2} &= \frac{1}{8} c_{\alpha-\beta}^2 (6c_{2(\alpha-\beta)} - 3c_{4\alpha-2\beta} - 2c_{2\alpha} + c_{4\alpha} + c_{2\beta} - 3) \\
A_{\,4} &= \frac{1}{2} s_{2\alpha} s_\beta c_{\alpha-\beta}^2 c_{2\alpha-\beta} \\
A_{\,6} &= 0
\end{aligned} \tag{9}
$$

$$
\begin{aligned}
B_{-6} &= \frac{1}{2} s_{2\alpha} c_\beta c_{\alpha-\beta}^2 c_{2\alpha-\beta} \\
B_{-4} &= \frac{1}{8}\big(s_{2\alpha} s_\beta (s_\beta - s_{4\alpha-3\beta}) + c_\beta (3s_{2\alpha-\beta} - s_{4\alpha-\beta} + \\
&\quad 3s_{4\alpha-3\beta} - s_{6\alpha-3\beta})\big) \\
B_{-2} &= \frac{1}{8}\Big((c_{2\alpha} - 3)s_{4\alpha-4\beta} - 2s_{4\alpha} c_{\alpha-\beta}^2\Big)
\end{aligned} \tag{10}
$$

$$
\begin{aligned}
B_0 &= \frac{1}{16}\big(- s_{2\alpha-4\beta} + 4s_{4\alpha-4\beta} + s_{6\alpha-4\beta} + 2c_\alpha(s_{\alpha+2\beta} - \\
&\quad s_{\alpha-2\beta} - 3s_{3\alpha-2\beta} + s_{5\alpha-2\beta}) - 2s_{2\alpha} + 2s_{4\alpha}\big) \\
B_2 &= -\frac{1}{16}c_\alpha(s_{3\alpha-4\beta} + 3s_{5\alpha-4\beta} + 8s_\alpha^3 c_{2\alpha-2\beta} + 4s_\alpha - 2s_{3\alpha}) \\
B_4 &= -c_\alpha^2 s_\beta c_{\alpha-\beta}^2 c_{2\alpha-\beta} \\
B_6 &= 0
\end{aligned}
$$

with $c_\theta := \cos(\theta)$ and $s_\theta := \sin(\theta)$.

Let us define the time and space variables, $t_j = j\Delta t$ and $x_m = m\Delta x$, where Δt and Δx are the time and space steps, respectively. As Δt and Δx tend to zero, this allows us to take a Taylor expansion of the recursion relations for the DTQW and, hence, derive a pair of partial differential equations (PDEs). To take the continuous limit, we define

$$
\begin{aligned}
\Delta t &= \epsilon\,, \\
\Delta x &= \epsilon^\gamma\,,
\end{aligned}
\tag{11}
$$

where ϵ is an infinitesimal and $\gamma > 0$ is a scaling parameter. The difference between the two expressions is to account for the fact that Δt and Δx may tend to 0 differently. Then, taking a Taylor expansion about ϵ up to the leading orders of Eqs. (7) and (8), we obtain the following

$$u(x,t) + 6\epsilon\partial_t u(x,t) = u(x,t) + \epsilon^\gamma\,(p_1\partial_x u(x,t) + p_2\partial_x d(x,t)) + O(\epsilon^2), \tag{12}$$

$$d(x,t) + 6\epsilon\partial_t d(x,t) = d(x,t) + \epsilon^\gamma\,(p_2\partial_x u(x,t) - p_1\partial_x d(x,t)) + O(\epsilon^2), \tag{13}$$

where

$$p_1 = \sum_{k=-3}^{3}\frac{2k}{6}A_{2k}(\alpha,\beta) = -\frac{1}{6}(c_{4\alpha-2\beta} + 2c_{2\alpha} + c_{2\beta} + 2), \tag{14}$$

$$p_2 = \sum_{k=-3}^{3}\frac{2k}{6}B_{2k}(\alpha,\beta) = -\frac{2}{3}(s_{2\alpha}c_{\alpha-\beta}^2). \tag{15}$$

Choosing scaling of $\gamma = 1$ and then taking the limit as $\epsilon \to 0$, we obtain the following pair of PDEs:

$$
\begin{aligned}
\partial_t u(x,t) &= p_1\partial_x d(x,t) + p_2\partial_x u(x,t), \\
\partial_t d(x,t) &= p_2\partial_x d(x,t) - p_1\partial_x u(x,t).
\end{aligned}
\tag{16}
$$

This set of equations can be then be recast, such that

$$\mathbb{I}\partial_t\Psi + P\partial_x\Psi = 0\,, \quad P = \begin{pmatrix} p_1 & p_2 \\ p_2 & -p_1 \end{pmatrix}, \tag{17}$$

where $\mathbb{I}$ is the 2×2 identity matrix. To diagonalize the operator acting on Ψ, we perform a change of basis from (b_u,b_d) to the new basis, ($\overline{b_u}$, $\overline{b_d}$), with $\overline{\Psi} = \overline{u}\overline{b}_u + \overline{d}\overline{b}_d$. The new basis components are

$$\overline{b_u} = \frac{1}{Z}\left(\frac{p_2}{\omega - p_1}b_u + b_d\right), \tag{18}$$

$$\overline{b_d} = \frac{1}{Z}\left(-\frac{p_2}{\omega + p_1}b_u + b_d\right), \tag{19}$$

with $\omega = \sqrt{p_1^2 + p_2^2}$ and Z a normalized constant. Hence, Eq. (17) in the new basis reads

$$\mathbb{I}\partial_t \overline{\Psi} + v(\alpha, \beta)\sigma_z \partial_x \overline{\Psi} = 0, \tag{20}$$

where

$$v_1(\alpha, \beta) = \frac{\sqrt{8c_\alpha^2 c_{2\alpha-2\beta} + c_{4\alpha-4\beta} + 4c_{2\alpha} + 5}}{3\sqrt{2}}, \tag{21}$$

can be seen as the propagation velocity of the continuous limit distribution and σ_z is the third Pauli matrix. We may also evaluate the standard deviation σ_j of the probability distribution depicted in Fig. 1 as a function of time, by considering the exponent $\eta(\alpha, \beta)$ in $\sigma_j \sim j^{\eta(\alpha,\beta)}$. For the FDTQW-I case, we observe ballistic behavior for general (α, β), that is, $\eta(\alpha, \beta) = 1$.

Now consider Eq. (20) in the covariant form, which is expressed as:

$$i(\gamma^0 \partial_0 + \gamma^1 \partial_1)\overline{\Psi} = 0, \tag{22}$$

where $\gamma^0 = \sigma_x$ and $\gamma^1 = -i\sigma_y$ are the usual gamma matrices, $\partial_0 = \partial_s$, $\partial_1 = \partial_{\tilde{x}}$, and the rescaled coordinate $\tilde{x} = x/v_1(\alpha, \beta)$. This equation can now be interpreted as the massless Dirac equation in the 1+1 space-time dimension. In Fig. 2, we observe the density profile of the FDTQW-I case at a time step of $j = 800$, with a symmetric Gaussian initial condition that is sufficiently regular and large with respect to the lattice interval Δx. A truly ballistic propagation can be noted, as the continuous limit suggests. This result confirms that FDTQW-I can be used to simulate massless Dirac dynamics.

3 Discrete-time quantum walk with Fibonacci sequence quantum walk operator

The FDTQW-II previously defined in Refs. [48,51] can be expressed in the most general case as a unitary evolution, and the unitary evolution operator can then be defined using the following Fibonacci sequence

$$\hat{U}_j = \hat{U}_{j-1}\hat{U}_{j-2}, \tag{23}$$

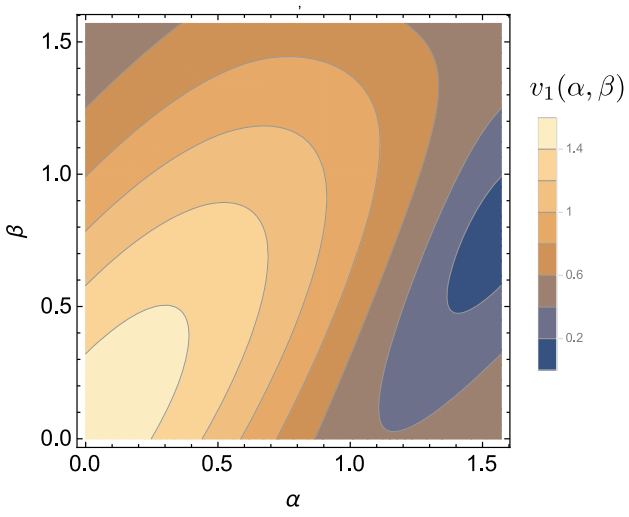

Fig. 1 Velocity contour plot for the Fibonacci sequence on the QCO, with α and $\beta \in [0, \frac{\pi}{2}]$

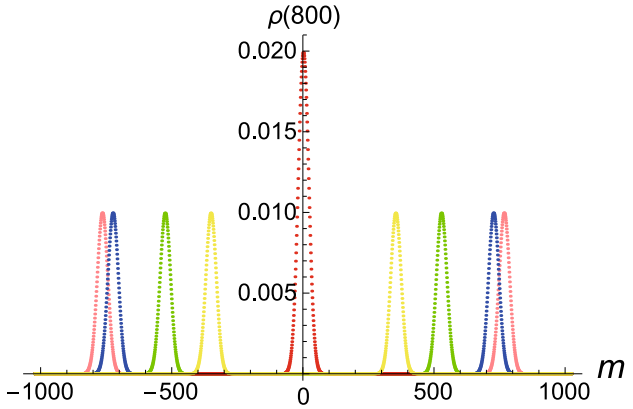

Fig. 2 Density profile of FDTQW-I at time step, $j = 800$, $\rho(j) = \mid \Psi_{m,j} \mid^2$, versus space step, m. The resolution (i.e. ϵ value) is $n = 2^{11}$. The *dashed red line* indicates $\alpha = \pi/2$ and $\beta = \pi/4$; the *dashed yellow line* is for $\alpha = \pi/3$ and $\beta = \pi/6$; the *dashed green line* represents $\alpha = \pi/4$ and $\beta = \pi/8$; the *dashed blue line* indicates $\alpha = \pi/8$ and $\beta = \pi/16$; and the *dashed pink line* represents $\alpha = \pi/12$ and $\beta = \pi/24$. The initial condition is $\Psi(0, x) = \sqrt{N_0(x)}(b_u + Ib_d)$, where $N_0(x)$ is a Gaussian function of width $20\Delta x$ and $\Delta x = 2\,\pi/n$

with the initial conditions

$$\hat{U}_0 = \hat{T}\hat{C}(\alpha), \qquad \hat{U}_1 = \hat{T}\hat{C}(\alpha)\hat{T}\hat{C}(\beta). \tag{24}$$

Since each step operator contains increasing numbers of translation operators, the boundary size increases at an exponential rate. To account for this, we now parametrize time using the number of translation operators that have thus far been applied. It can then be noted that this DTQW has a quasi-periodic coin sequence. Thus, we define a new parameter for time r, such that $s_r = r\Delta t$, where $r = \sum_{n=0}^{j-1} F(n)$ and $F(n)$ is the Fibonacci sequence with initial conditions, $F(0) = 1$ and $F(1) = 2$. This means how many translation operators a quantum walker is operated. This allows us to easily study the continuous limits of Eq. (3) for the operator expressed in Eq. (23). For the continuous limit to exist, we first require that $\Psi(s_r + \tau\Delta t) \to \Psi(s_r)$. It can be shown that this is true only when $\tau \in 6\mathbb{N}_0$, that is, when τ is any positive integer multiple of 6, as the sequence of unitary operators then reduces to the identity operator. We assume the simplest periodic case, for which $\tau = 6$, and the discrete-time equations read

$$u_{m,r+6} = \sum_{k=-3}^{3} \big(A_{2k}(\alpha, \beta)u_{m+2k,r} + B_{2k}(\alpha, \beta)d_{m+2k,r}\big), \tag{25}$$

$$d_{m,r+6} = \sum_{k=-3}^{3} \big(B_{-2k}(-\alpha, -\beta)u_{m+2k,r} + A_{-2k}(-\alpha, -\beta)d_{m+2k,r}\big), \tag{26}$$

where $A_k \in \mathbb{R}$ and $B_k \in \mathbb{R}$ are

$$\begin{aligned}
A_{-6} &= c_\alpha^4 c_\beta^2 \\
A_{-4} &= c_\alpha^2 s_\alpha (c_\beta^2 s_\alpha + 2c_\alpha s_{2\beta}) \\
A_{-2} &= -\frac{1}{8} s_{2\alpha}\big(-2s_{2\alpha} + s_{2(\alpha-\beta)} + 5s_{2(\alpha+\beta)}\big) \\
A_{\,0} &= -\frac{1}{8}\big(3 + c_{4\alpha} - (1 + 3c_{4\alpha})c_{2\beta} - 16c_\alpha s_\alpha^3 s_{2\beta}\big) \\
A_{\,2} &= c_\beta^2 s_\alpha^4 - 2c_\alpha^3 c_\beta s_\alpha s_\beta + c_\alpha s_\alpha^3 s_{2\beta} \\
A_{\,4} &= c_\alpha^2 c_\beta^2 s_\alpha^2 \\
A_{\,6} &= 0
\end{aligned} \tag{27}$$

$$
\begin{aligned}
B_{-6} &= c_\alpha^3 c_\beta^2 s_\alpha \\
B_{-4} &= c_\alpha c_\beta \left(s_\alpha^3 c_\beta + c_\alpha (1 - 2c_{2\alpha}) s_\beta\right) \\
B_{-2} &= \frac{1}{8}\left(s_{4\alpha}(3c_{2\beta} - 1) - 4s_\alpha^2 (2c_{2\alpha} + 1) s_{2\beta}\right) \\
B_{\,0} &= \frac{1}{8}\left(4s_\alpha^2 (2c_{2\alpha} + 1) s_{2\beta} + s_{4\alpha}(1 - 3c_{2\beta})\right) \\
B_{\,2} &= c_\alpha c_\beta \left(c_\alpha (2c_{2\alpha} - 1) s_\beta - s_\alpha^3 c_\beta\right) \\
B_{\,4} &= -s_\alpha c_\alpha^3 c_\beta^2 \\
B_{\,6} &= 0.
\end{aligned}
\tag{28}
$$

Taking the continuous limit of S^6 about ϵ (as in the previous section) and noting that the zeroth order terms cancel, we arrive at the first order term expressions for this system

$$
\begin{aligned}
\partial_s u(x,s) &= p_1' \partial_x d(x,s) + p_2' \partial_x u(x,s), \\
\partial_s d(x,s) &= p_2' \partial_x d(x,s) - p_1' \partial_x u(x,s),
\end{aligned}
\tag{29}
$$

and

$$
p_1' = \sum_{k=-3}^{3} \frac{2k}{6} A_{2k}(\alpha,\beta) = -\frac{1}{3}(c_{2\alpha-\beta}^2 + 2c_\beta c_{2\alpha-\beta}) \tag{30}
$$

$$
p_2' = \sum_{k=-3}^{3} \frac{2k}{6} B_{2k}(\alpha,\beta) = \frac{1}{3} s_{2\alpha-\beta}(c_{2\alpha-\beta} + 2c_\beta). \tag{31}
$$

As in the previous case, we can rewrite these equations in matrix form, such that,

$$
\begin{aligned}
&\partial_s \Psi + P' \partial_x \Psi = 0, \\
&P' = \begin{pmatrix} p_1' & p_2' \\ p_2' & -p_1' \end{pmatrix},
\end{aligned}
\tag{32}
$$

Again, we diagonalize the differential operator acting on Ψ, which spans Ψ itself on the new basis, $(\overline{b_u'}, \overline{b_d'})$. The new basis components read

$$
\overline{b_u'} = \frac{1}{Z'}\left(\frac{p_2'}{\omega' - p_1'} b_u + b_d\right), \tag{33}
$$

$$
\overline{b_d'} = \frac{1}{Z'}\left(-\frac{p_2'}{\omega' + p_1'} b_u + b_d\right), \tag{34}
$$

with $\omega' = \sqrt{{p_1'}^2 + {p_2'}^2}$ and Z' a normalized constant. Eq. (32), expressed in terms of $\overline{\Psi}$, then becomes

$$
\partial_s \overline{\Psi} + v(\alpha,\beta)\sigma_z \partial_x \overline{\Psi} = 0, \qquad v_2(\alpha,\beta) = \tfrac{1}{3}\left|c_{2\alpha-\beta} + 2c_\beta\right|. \tag{35}
$$

This PDE implies ballistic propagation of the quantum walker for fixed α and β. Similar results are obtained when other periodic sequences of finite length are considered, with each result yielding a similar differential equation, albeit with varying functions for v, as seen in Fig. 3. As in the previous section, the latter equation can be reformulated in the following covariant form:

$$
i(\gamma^0 \partial_0 + \gamma^1 \partial_1)\overline{\Psi} = 0, \tag{36}
$$

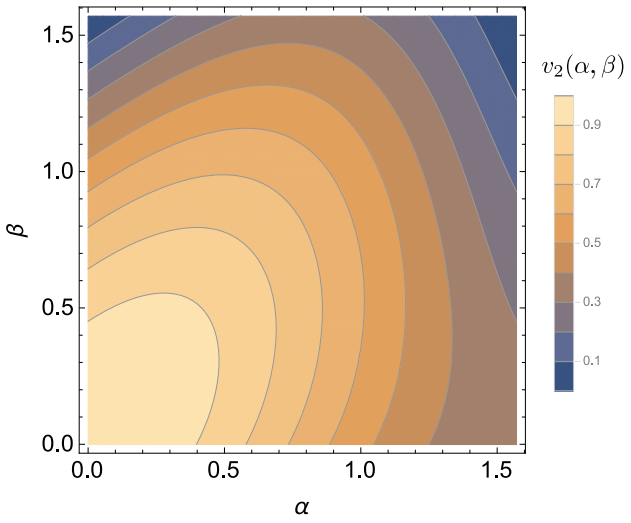

Fig. 3 Contour plot for velocity in the case in which Fibonacci sequence is on the step operator for the three periodic Fibonacci sequence

where $\gamma^0 = \sigma_x$, $\gamma^1 = -i\sigma_y$, $\partial_0 = \partial_s$, $\partial_1 = \partial_{\tilde{x}}$, while the rescaled coordinate is now $\tilde{x} = x/v_2(\alpha, \beta)$. In this rescaled time-space, the velocity is 1 and the FDTQW-II can again be interpreted as a massless Dirac equation in the $(1 + 1)$ dimension.

4 Conclusion

By taking the continuous limit, we have characterized the propagation behavior of the DTQWs based on both the Fibonacci sequence of the coin operators and the periodic extension of these sequences. Our analysis shows that both of these quantum walks are ballistic and that the continuous limits can reduce to the $(1 + 1)$-dimensional massless Dirac equation. There still remain several unexplored topics, however. For example, we have not examined the continuous limit on the infinite sequence of step operators, as originally defined in Ref. [48]. The propagation properties of this model were numerically analyzed in [48, Fig.3]. According to Ref. [48], this walk is either ballistic or sub-ballistic depending on the initial values of α and β. Other unknown aspects include the type of transition that occurs when τ increases towards infinity, and the mechanism by which the behavior of the periodic extension changes into that of the infinite sequence.

Acknowledgments The authors acknowledge useful discussion with Fabrice Debbasch and Jingbo Wang. G.D.M. expresses thanks to the JSPS summer program (SP14203) for financial support, while L.H. and B.L. thank the Department of Education of the Australian Government for financial support through the AsiaBound Grants Program. T.W. thanks the JSPS KAKENHI 25400188 and IMS Joint Study Program for financial support, while Y.S. thanks the DAIKO Foundation, also for financial support.

References

1. Feynman, R.P., Hibbs, A.R.: Quantum mechanics and path integrals. McGraw-Hill Book Company (1965)
2. Aharonov, Y., Davidovich, L., Zagury, N.: Quantum random walks. Phys. Rev. A **48**, 1687 (1993)
3. Meyer, D.A.: From quantum cellular automata to quantum lattice gases. J. Stat. Phys. **85**, 551 (1996)
4. Gudder, S.P.: Quantum Probability. Academic Press, Quantum probability (1988)
5. Cardano, F., Massa, F., Qassim, H., Karimi, E., Slussarenko, S., Paparo, D., de Lisio, C., Sciarrino, F., Santamato, E., Boyd, R.W., Marrucci, L.: Quantum walks and quantum simulation of wavepacket dynamics with twisted photons. arXiv:1407.5424
6. Broome, M.A., Fedrizzi, A., Lanyon, B.P., Kassal, I., Aspuru-Guzik, A., White, A.G.: Discrete Single-Photon Quantum Walks with Tunable Decoherence. Phys. Rev. Lett. **104**, 153602 (2010)
7. Kitagawa, T., Broome, M.A., Fedrizzi, A., Rudner, M.S., Berg, E., Kassal, I., Aspuru-Guzik, A., Demler, E., White, A.G.: Observation of topologically protected bound states in photonic quantum walks. Nat. Commun. **3**, 882 (2012)
8. Schreiber, A., Gabris, A., Rohde, P.P., Laiho, K., Stefanak, M., Potocek, V., Hamilton, C., Jex, I., Silberhorn, C.: A 2D quantum walk simulation of two-particle dynamics. Science **336**, 55 (2012)

9. Schmitz, H., Matjeschk, R., Schneider, C., Glueckert, J., Enderlein, M., Huber, T., Schaetz, T.: Quantum Walk of a Trapped Ion in Phase Space. Phys. Rev. Lett. **103**, 090504 (2009)
10. Zähringer, F., Kirchmair, G., Gerritsma, R., Solano, E., Blatt, R., Roos, C.F.: Realization of a Quantum Walk with One and Two Trapped Ions. Phys. Rev. Lett. **104**, 100503 (2010)
11. Schreiber, A., Cassemiro, K.N., Potocek, V., Gabris, A., Mosley, P.J., Andersson, E., Jex, I., Silberhorn, C.: Photons Walking the Line: A Quantum Walk with Adjustable Coin Operations. Phys. Rev. Lett. **104**, 050502 (2010)
12. Karski, M., Forster, L., Choi, J.M., Steffen, A., Alt, W., Meschede, D., Widera, A.: Quantum walk in position space with single optically trapped atoms. Science **325**, 174 (2009)
13. Sansoni, L., Sciarrino, F., Vallone, G., Mataloni, P., Crespi, A., Ramponi, R., Osellame, R.: Two-Particle Bosonic-Fermionic Quantum Walk via Integrated Photonics. Phys. Rev. Lett. **108**, 010502 (2012)
14. Sanders, B.C., Bartlett, S.D., Tregenna, B., Knight, P.L.: Quantum quincunx in cavity quantum electrodynamics. Phys. Rev. A **67**, 042305 (2003)
15. Perets, H.B., Lahini, Y., Pozzi, F., Sorel, M., Morandotti, R., Silberberg, Y.: Realization of Quantum Walks with Negligible Decoherence in Waveguide Lattices. Phys. Rev. Lett. **100**, 170506 (2008)
16. Crespi, A., Osellame, R., Ramponi, R., Giovannetti, V., Fazio, R., Sansoni, L., De Nicola, F., Sciarrino, F., Mataloni, P.: Anderson localization of entangled photons in an integrated quantum walk. Nat. Photonics **7**, 322 (2013)
17. Jeong, Y.C., Di Franco, C., Lim, H.T., Kim, M.S., Kim, Y.H.: Experimental realization of a delayed-choice quantum walk. Nat. Commun. **4**, 2471 (2013)
18. Fukuhara, T., Schaus, P., Endres, M., Hild, S., Cheneau, M., Bloch, I., Gross, C.: Microscopic observation of magnon bound states and their dynamics. Nature **502**, 76 (2013)
19. Xue, P., Qin, H., Tang, B., Sanders, B.C.: Observation of quasiperiodic dynamics in a one-dimensional quantum walk of single photons in space. N. J. Phys. **16**, 53009 (2014)
20. Manouchehri, K., Wang, J.B.: Physical implementation of quantum walks. Springer, Berlin (2014)
21. Di Molfetta, G., Brachet, M., Debbasch, F.: Quantum walks in artificial electric and gravitational fields. Phys. A **397**, 157 (2014)
22. Shikano, Y., Chisaki, K., Segawa, E., Konno, N.: Emergence of randomness and arrow of time in quantum walks. Phys. Rev. A **81**, 062129 (2010)
23. Chandrashekar, C.M., Laflamme, R.: Quantum phase transition using quantum walks in an optical lattice. Phys. Rev. A **78**, 022314 (2008)
24. Ambainis, A.: Quantum Walk Algorithm for Element Distinctness. SIAM J. Comput. **37**, 210 (2007)
25. Magniez, F., Nayak, A., Roland, J., Santha, M.: Search via Quantum Walk. SIAM J. Comput. **40**, 142 (2006)
26. Dheeraj, M.N., Brun, T.A.: Continuous Limit of Discrete Quantum Walks. arXiv:1501.06950
27. Bose, S.: Quantum Communication through an Unmodulated Spin Chain. Phys. Rev. Lett. **91**, 207901 (2003)
28. Aslangul, C.: Quantum dynamics of a particle with a spin-dependent velocity. J. Phys. A Math. Gen. **38**, 1 (2005)
29. Oka, T., Konno, N., Arita, R., Aoki, H.: Breakdown of an Electric-Field Driven System: A Mapping to a Quantum Walk. Phys. Rev. Lett. **94**, 100602 (2005)
30. Bose, S.: Quantum communication through spin chain dynamics: an introductory overview. Contemp. Phys. **48**, 13 (2007)
31. Kitagawa, T., Rudner, M.S., Berg, E., Demler, E.: Exploring topological phases with quantum walks. Phys. Rev. A **82**, 033429 (2010)
32. Gönülol, G., Aydıner, R., Shikano, Y., Müstecaphoglu, Ö.E.: Survival probability in a one-dimensional quantum walk on a trapped lattice. New J. Phys. **13**, 033037 (2011)
33. Gönülol, G., Aydıner, R., Shikano, Y., Müstecaphoglu, Ö.E.: Survival Probability in a Quantum Walk on a One-Dimensional Lattice with Partially Absorbing Traps. J. Comput. Theor. Nanosci. **10**, 1596–1600 (2013)
34. Shikano, Y., Katsura, H.: Localization and fractality in inhomogeneous quantum walks with self-duality. Phys. Rev. E **82**, 03112 (2010)
35. Shikano, Y., Katsura, H.: Notes on Inhomogeneous Quantum Walks. AIP Conf. Proc. **1363**, 151–154 (2011)
36. Obuse, T., Kawakami, N.: Topological phases and delocalization of quantum walks in random environments. Phys. Rev. B **84**, 195139 (2011)
37. Asbóth, J.K., Obuse, H.: Bulk-boundary correspondence for chiral symmetric quantum walks. Phys. Rev. B **88**, 121406(R) (2013)
38. Strauch, F.W.: Relativistic effects and rigorous limits for discrete- and continuous-time quantum walks. J. Math. Phys. **48**, 082102 (2007)
39. Bracken, A.J., Ellinas, D., Smyrnakis, I.: Free-Dirac-particle evolution as a quantum random walk. Phys. Rev. A **75**, 022322 (2007)
40. Chisaki, K., Konno, N., Segawa, E., Shikano, Y.: Crossovers induced by discrete-time quantum walks. Quant. Inf. Comp. **11**, 741 (2011)
41. Sato, F., Katori, M.: Dirac equation with an ultraviolet cutoff and a quantum walk. Phys. Rev. A **81**, 012314 (2010)
42. Chandrashekar, C.M., Banerjee, S., Srikanth, R.: Relationship between quantum walks and relativistic quantum mechanics. Phys. Rev. A **81**, 062340 (2010)
43. Di Molfetta, G., Debbasch, F.: Discrete-time quantum walks: continuous limit and symmetries. J. Math. Phys. **53**, 123302 (2011)
44. Di Molfetta, G., Brachet, M., Debbasch, F.: Quantum walks as massless Dirac fermions in curved space-time. Phys. Rev. A **88**, 042301 (2013)
45. Shikano, Y.: From Discrete Time Quantum Walk to Continuous Time Quantum Walk in Limit Distribution. J. Comput. Theor. Nanosci. **10**, 1558 (2013)

Quantum Stud.: Math. Found.
DOI 10.1007/s40509-015-0042-x

CHAPMAN UNIVERSITY | INSTITUTE FOR QUANTUM STUDIES

PUBLISHER'S ERRATUM

Erratum to: Massless Dirac equation from Fibonacci discrete-time quantum walk

Giuseppe Di Molfetta · Lauchlan Honter · Ben B. Luo · Tatsuaki Wada · Yutaka Shikano

Erratum to: Quantum Stud.: Math. Found.
DOI 10.1007/s40509-015-0038-6

On finalizing the publication process of the original article, we had the following mistakes and make the corrections.

1. In page 2 line 5, we had the mistake on the citation as follows: the original manuscript "of a massive Dirac fermion [39–43]" should be changed to "of a massive Dirac fermion [38–43]".
2. In page 2 line 7, we had the mistake on the citation as follows: the original manuscript "can be regarded as quantum dynamical simulators [39, 40]" should be changed to "can be regarded as quantum dynamical simulators [40, 45]".
3. In page 10, we had the mistake on the double citation. References [46, 47] are exactly same to those of Refs. [49, 50] [1,2], respectively. Since we did not cite Refs. [46, 47] in the original manuscript, we delete these.

The online version of the original article can be found under doi:10.1007/s40509-015-0038-6.

G. Di Molfetta · L. Honter · B. B. Luo · Y. Shikano
Research Center of Integrative Molecular Systems (CIMoS), Institute for Molecular Science,
Natural Institutes of Natural Sciences, 38 Nishigo-Naka, Myodaiji, Okazaki, Aichi 444-8585, Japan

G. Di Molfetta
LERMA, Observatoire de Paris, PSL Research University, CNRS, Sorbonne Universités,
UPMC Univ. Paris 6, UMR 8112, 75014 Paris, France
e-mail: giuseppe.dimolfetta@ens.fr

L. Honter · B. B. Luo
School of Physics, The University of Western Australia, 35 Stirling Hwy, Crawley, Perth, WA 6009, Australia

T. Wada
Department of Electrical and Electronic Engineering, Ibaraki University,
12-4-1 Nakanarusawa, Hitachi, Ibaraki 316-8511, Japan

Y. Shikano ( )
Institute for Quantum Studies, Chapman University, 1 University Dr., Orange, CA 92866, USA
e-mail: yshikano@ims.ac.jp

Published online: 14 May 2015

References

1. Rohde, P.P., Brennen, G.K., Gilchrist, A.G.: Quantum walks with memory provided by recycled coins and a memory of the coin-flip history. Phys. Rev. A **87**, 052302 (2013)
2. Shikano, Y., Wada, T., Horikawa, J.: Discrete-time quantum walk with feed-forward quantum coin. Sci. Rep. **4**, 4427 (2014)

Bibliography

[1] L. Accardi, Y. G. Lu, I. Volovich, et al. *Quantum theory and its stochastic limit*, volume 6. Springer Berlin, 2002.

[2] Y. Aharonov, L. Davidovich, and N. Zagury. Quantum random walks. *Phys. Rev. A*, 48:1687, 1993.

[3] J. B. Anderson. A random-walk simulation of the schrödinger equation: H+ 3. *The Journal of Chemical Physics*, 63(4):1499–1503, 1975.

[4] F. Bartumeus, M. G. E. da Luz, G. Viswanathan, and J. Catalan. Animal search strategies: a quantitative random-walk analysis. *Ecology*, 86(11):3078–3087, 2005.

[5] I. O. Bohachevsky, M. E. Johnson, and M. L. Stein. Generalized simulated annealing for function optimization. *Technometrics*, 28(3):209–217, 1986.

[6] J. Y. Campbell, A. W.-C. Lo, A. C. MacKinlay, et al. *The econometrics of financial markets*, volume 2. princeton University press Princeton, NJ, 1997.

[7] C. Chandrashekar. Discrete-time quantum walk-dynamics and applications. *arXiv preprint arXiv:1001.5326*, 2010.

[8] C. M. Chandrashekar. Generic quantum walk using a coin-embedded shift operator. *Phys. Rev. A*, 78:052309, Nov 2008. doi: 10.1103/PhysRevA.78.052309. URL http://link.aps.org/doi/10.1103/PhysRevA.78.052309.

[9] C. M. Chandrashekar, R. Srikanth, and S. Banerjee. Symmetries and noise in quantum walk. *Phys. Rev. A*, 76:022316, Aug 2007. doi: 10.1103/PhysRevA.76.022316. URL http://link.aps.org/doi/10.1103/PhysRevA.76.022316.

[10] R. Feynman and A. Hibbs. Quantum mechanics and path integrals. *International Series in Pure and Applied Physics. McGraw-Hill Book Company*, 1965.

[11] N. Fjeldso, J. Midtdal, and F. Ravndal. Random walks of a quantum particle on a circle. *Journal of Physics A: Mathematical and General*, 21(7):1633, 1988. URL http://stacks.iop.org/0305-4470/21/i=7/a=027.

[12] C. Flindt, T. Novotnỳ, A. Braggio, M. Sassetti, and A.-P. Jauho. Counting statistics of non-markovian quantum stochastic processes. *Physical review letters*, 100(15):150601, 2008.

[13] H.-J. Galla, W. Hartmann, U. Theilen, and E. Sackmann. On two-dimensional passive random walk in lipid bilayers and fluid pathways in biomembranes. *The Journal of membrane biology*, 48 (3):215–236, 1979.

[14] C. W. Gardiner et al. *Handbook of stochastic methods*, volume 4. Springer Berlin, 1985.

[15] D. T. Gillespie. Exact stochastic simulation of coupled chemical reactions. *The journal of physical chemistry*, 81(25):2340–2361, 1977.

[16] S. Godoy and S. Fujita. A quantum random walk model for tunneling diffusion in a 1d lattice. a quantum correction to fick's law. *The Journal of Chemical Physics*, 97(7):5148–5154, 1992. doi: http://dx.doi.org/10.1063/1.463812. URL http://scitation.aip.org/content/aip/journal/jcp/97/7/10.1063/1.463812.

[17] H. Grabert and P. Talkner. Quantum brownian motion. *Physical Review Letters*, 50(18):1335, 1983.

[18] G. Grossing and A. Zeilinger. Quantum cellular automata. *Complex Systems*, 2(2):197–208, 1988.

[19] S. Gudder. Quantum stochastic processes. *Foundations of Physics*, 20(11):1345–1363, 1990. ISSN 0015-9018. doi: 10.1007/BF01883490. URL http://dx.doi.org/10.1007/BF01883490.

[20] D. J. Higham. An algorithmic introduction to numerical simulation of stochastic differential equations. *SIAM review*, 43(3):525–546, 2001.

[21] G. Iche and P. Nozieres. Quantum brownian motion of a heavy particle: An adiabatic expansion. *Physica A: Statistical Mechanics and its Applications*, 91(3):485–506, 1978.

[22] T. Jacobson and L. S. Schulman. Quantum stochastic: the passage from a relativistic to a non-relativistic path integral. *Journal of Physics A: Mathematical and General*, 17(2):375, 1984. URL http://stacks.iop.org/0305-4470/17/i=2/a=023.

[23] M. R. James, H. Nurdin, I. R. Petersen, et al. Control of linear quantum stochastic systems. *Automatic Control, IEEE Transactions on*, 53(8):1787–1803, 2008.

[24] L. Kilian and M. P. Taylor. Why is it so difficult to beat the random walk forecast of exchange rates? *Journal of International Economics*, 60(1):85–107, 2003.

[25] R. Kirchheim and U. Stolz. Modelling tracer diffusion and mobility of interstitials in disordered materials. *Journal of non-crystalline solids*, 70(3):323–341, 1985.

[26] V. Komkov and V. Dannon. Random walk simulation of chemical reactions represented by nonlinear reaction-diffusion equations. *ZAMM-Journal of Applied Mathematics and Mechanics/Zeitschrift für Angewandte Mathematik und Mechanik*, 71(3):135–150, 1991.

[27] J. Kosik. Two models of quantum random walk. *Central European Journal of Physics*, 1(4):556–573, 2003. ISSN 1895-1082. doi: 10.2478/BF02475903. URL http://dx.doi.org/10.2478/BF02475903.

[28] K. Lange and E. Sobel. A random walk method for computing genetic location scores. *American journal of human genetics*, 49(6):1320, 1991.

[29] Q. Lv, P. Cao, E. Cohen, K. Li, and S. Shenker. Search and replication in unstructured peer-to-peer networks. In *Proceedings of the 16th international conference on Supercomputing*, pages 84–95. ACM, 2002.

[30] R. MacDonald and M. P. Taylor. The monetary model of the exchange rate: long-run relationships, short-run dynamics and how to beat a random walk. *Journal of international Money and finance*, 13(3):276–290, 1994.

[31] T. Machida and N. Konno. Limit theorem for a time-dependent coined quantum walk on the line. -, 2:226–235, 2010. doi: 10.1007/978-4-431-53868-4_26. URL http://dx.doi.org/10.1007/978-4-431-53868-4_26.

[32] A. Nayak and A. Vishwanath. Quantum walk on the line. *arXiv preprint quant-ph/0010117*, 2000.

[33] J. E. Neigel and J. C. Avise. Application of a random walk model to geographic distributions of animal mitochondrial dna variation. *Genetics*, 135(4):1209–1220, 1993.

[34] M. E. Newman. A measure of betweenness centrality based on random walks. *Social networks*, 27 (1):39–54, 2005.

[35] J. D. Noh and H. Rieger. Random walks on complex networks. *Physical review letters*, 92(11): 118701, 2004.

[36] G. Oshanin, H. Wio, K. Lindenberg, and S. Burlatsky. Intermittent random walks for an optimal search strategy: one-dimensional case. *Journal of Physics: Condensed Matter*, 19(6):065142, 2007.

[37] K. R. Parthasarathy. *An introduction to quantum stochastic calculus*. Springer Science & Business Media, 2012.

[38] R. Rammal and G. Toulouse. Random walks on fractal structures and percolation clusters. *Journal de Physique Lettres*, 44(1):13–22, 1983.

[39] P. Revesz. *Random walk in random and non-random environments*. World Scientific Publishing Company Incorporated, 2005.

[40] P. Ribeiro, P. Milman, and R. Mosseri. Aperiodic quantum random walks. *Phys. Rev. Lett.*, 93: 190503, Nov 2004. doi: 10.1103/PhysRevLett.93.190503. URL http://link.aps.org/doi/10.1103/PhysRevLett.93.190503.

[41] M. Rosvall and C. T. Bergstrom. Maps of random walks on complex networks reveal community structure. *Proceedings of the National Academy of Sciences*, 105(4):1118–1123, 2008.

[42] J. Schwinger. Brownian motion of a quantum oscillator. *Journal of Mathematical Physics*, 2(3): 407–432, 1961. doi: http://dx.doi.org/10.1063/1.1703727. URL http://scitation.aip.org/content/aip/journal/jmp/2/3/10.1063/1.1703727.

[43] F. Strauch. Connecting the discrete- and continuous-time quantum walks. *Phys. Rev. A*, 74:030301, 2006.

[44] J. Tunaley. Asymptotic solutions of the continuous-time random walk model of diffusion. *Journal of Statistical Physics*, 11(5):397–408, 1974.

[45] G. van den Engh, R. Sachs, and B. J. Trask. Estimating genomic distance from dna sequence location in cell nuclei by a random walk model. *Science*, 257(5075):1410–1412, 1992.

[46] N. G. Van Kampen. *Stochastic processes in physics and chemistry*, volume 1. Elsevier, 1992.

[47] S. E. Venegas-Andraca. Quantum walks: a comprehensive review. *Quantum Information Processing*, 11(5):1015–1106, 2012.

[48] L. Yen, D. Vanvyve, F. Wouters, F. Fouss, M. Verleysen, M. Saerens, et al. clustering using a random walk based distance measure. In *ESANN*, pages 317–324, 2005.

CHAPTER 2

INHOMOGENEOUS QUANTUM WALKS AND CONTINUOUS LIMITS

Summary

2.1 Inhomogeneous Quantum Walks as synthetic gauge fields simulators 35
2.1.1 Quantum Simulation 35
2.1.2 What is a synthetic gauge field? 36
2.1.3 From Inhomogeneous Quantum Walks to synthetic gauge fields 37
2.1.3.1 Spacetime dependent quantum coin 38
2.2 A synthetic gravitational gauge field 39
2.2.1 Simulating the effects of a gravitational gauge field 39
2.2.2 Curved spacetime and chiral field theory: an introduction 39
2.2.3 A formal general setup 40
2.2.3.1 Mathematical Framework 40
2.2.3.2 Affine connection and Spin connection 41
2.2.3.3 Lorentz invariance in curved spacetime 43
2.2.4 Dirac equation in curved spacetime in (1+1) dimensions 44
2.2.5 Publication: "Quantum walks as massless Dirac fermions in curved spacetime" 44
2.3 A synthetic electric gauge field 51
2.3.1 Publication: "Quantum Walks in artificial electric and gravitational gauge fields." 51

2.1 Inhomogeneous Quantum Walks as synthetic gauge fields simulators

2.1.1 Quantum Simulation

Non-human animals can be reductively explained as automata. (Descartes, De homines, 1662)
Let the computer itself be built of quantum mechanical elements which obey quantum mechanical laws" (Feynman, 1982)

Since the first ideas on simulating quantum mechanics were formulated, it emerged that the simulation of the quantum system dynamics was a very challenging matter. This problem was unsolved until Feynman [20] [21] envisaged a solution: simulate quantum mechanics

through an other quantum device. Unfortunately even though he foresaw this idea, he did not know how to realize it.

Nowadays, quantum computers (i.e. *an ensemble of well-defined qubits that can be initialized, measured and on which universal quantum gates can be performed* Georgescu et al. [23]) are a reality and quantum computing and information are very active research fields. More important though is that we now acknowledge the possibility of implementing quantum simulation without an all-purpose, perfect quantum computer. Indeed, simpler quantum systems that are able to mimic the evolution of other quantum systems can be used for this task. In general, quantum simulations can be used to investigate physical problems that are either not solvable on classical computers or experimentally challenging and, in particular, they are useful to test new theoretical models. Applications can range from condensed matter physics [12, 43, 40, 38] to high energy physics [24, 48, 11], from cosmology [39, 26, 2] to atom [25, 54], to quantum chemistry [32, 18] and, last but not least, to open quantum systems [34, 53] and quantum chaos [55, 27].

2.1.2 What is a synthetic gauge field?

Eichinvarianz (Hermann Weyl, 1929)

To introduce the idea of gauge invariance and gauge field, let us introduce a closed system described by the action:

$$S = \int_{t_1}^{t_2} dt \int d^3\mathbf{x}\, \mathcal{L}(\psi(\mathbf{x}), \partial_\mu \psi(\mathbf{x})), \tag{2.1}$$

where $\mathcal{L}(\psi(x), \partial_\mu \psi(x))$ is the Lagrangian density and $\psi(x)$ is a complex, differentiable field. The equation of motion follows from Hamilton's principle of least action. In other words, the action should be stationary:

$$\delta S = \delta \int_{t_1}^{t_2} dt \int d^3\mathbf{x} \mathcal{L}(\psi(\mathbf{x}), \partial_\mu \psi(\mathbf{x})) = \mathbf{0}. \tag{2.2}$$

As usual, the fields ψ have to vanish at points t_1 and t_2. As consequence of the least action principle, we derive the Euler-Lagrange equations, which allow us to write down the equations of motion for the fields $\psi(x)$:

$$\frac{\partial \mathcal{L}}{\partial \psi(x)} = \partial_\mu \frac{\partial \mathcal{L}}{\partial(\partial_\mu \psi(x))} \tag{2.3}$$

Now consider to multiply the $\psi(x)$ by a global phase $e^{i\theta}$, where θ is a real constant. We can easily verify that such a transformation leave tshe Lagrangian density unaffected:

$$\delta \mathcal{L} = 0. \tag{2.4}$$

Evidently, if the Lagrangian density is unchanged under a global phase transformation, the equation of motions are invariant too. Let us now make a more systematic investigation of phase invariance. Consider an inhomogeneous phase $e^{i\theta(x)}$ and the transformation:

$$\psi(x) \to \psi(x)' = e^{i\theta(x)} \psi(x). \tag{2.5}$$

As consequence of this local phase rotations on the field, all terms depending on the derivative

of the field transform as below:

$$\partial_\mu \psi(x)' \rightarrow e^{i\theta(x)}(\partial_\mu \psi(x) + i(\partial_\mu \theta(x))\psi(x)) \tag{2.6}$$

It is clear that the Lagrangian density, and therefore the equations of motion, are no more invariant under local phase rotation. However, the invariance can be restored if we replace everywhere ∂_μ by

$$D_\mu = (\partial_\mu + i A_\mu), \tag{2.7}$$

where A_μ is introduced to take into account the non-homogeneity of the local phase rotation. Let us call the new derivative (2.7) the *gauge-covariant* derivative and the field A_μ, the *electromagnetic gauge field*. In fact, the Eq. (2.7) together with the Eq. (2.6) demands that $A_\mu(x)$, in order to preserve global gauge invariance, transforms as:

$$A_\mu(x) \rightarrow A'_\mu(x) \equiv A_\mu(x) - \partial_\mu \theta(x). \tag{2.8}$$

Therefore,

$$D_\mu \psi(x) \rightarrow e^{i\theta(x)} D_\mu \psi(x). \tag{2.9}$$

For instance, if we explicitly introduce the Lagrangian density for a Dirac field:

$$\mathcal{L}_0 = \overline{\psi}(i\gamma^\mu \partial_\mu - m)\psi, \tag{2.10}$$

and we substitute ∂_μ by D_μ, the gauge invariant Lagrangian density reads:

$$\mathcal{L} = \overline{\psi}(i\gamma^\mu D_\mu - m)\psi = \mathcal{L}_0 - A_\mu \overline{\psi}\gamma^\mu \psi. \tag{2.11}$$

The last term is known as the electromagnetic current and come from the only requirement of the global gauge invariance. Historically, Weyl [56] was the first to introduce the idea of gauge invariance as a geometrical principle to formalize the electromagnetism. Let us finally elucidate that a gauge field is usually called *synthetic* when it is defined as the result of the *effective* dynamics of the system. We will prove in the following sections that the effective dynamics of the IDTQWs coincides with the quantum propagation of a Dirac fermion in gauge fields, such as the electric or the gravitational field.

2.1.3 From Inhomogeneous Quantum Walks to synthetic gauge fields

The inhomogeneous QWs are usually characterized by a spatial dependence of the coin. Here we extend this definition to a dependence on each spacetime point of the lattice. Over the past decade many theoretical and experimental researches have been addressed to this particular family of walks.

Time dependent quantum coins have been introduced by Ribeiro et al. [46]. They defined a walk with several biased step operators applied aperiodically, and Banuls et al. [5] proposed a model with a time dependent coin as a control mechanism over a possible phase arising during the walk (as for example a consequence of an additional interaction). Albertini and D'Alessandro [1],[15] extended the analysis to a d-dimensional lattice and to the cycle. Recently Montero [41] unveiled some unexplored invariance in quantum walks with time-dependent coin.

Space dependent quantum coins have been first introduced by Linden and Sharam [35]

who investigated a spatial inhomogeneous quantum walk, where the coin operator depended periodically on the position; Shikano and Katsura [49] numerically and analytically showed the energy spectrum of such walks and Konno et al. [31], [30] have investigated the localization problems and the limit measures. Cedzich et al. [14] studied propagation and spectral properties of a QW in an electric field introduced as a space dependent phase in the quantum coin.

One of the main contribution of this thesis is to show that inhomogeneous QWs can be used to provide the gauge invariance with respect to certain gauge transformations, and therefore code for the corresponding gauge field, much in the same way as explained in the previous subsection for the continuum. In the continuum limit, the QW gauge field tend toward the Dirac equation gauge fields; as we will show for both the electric and the gravitational field in subsection 2.2.5 and as well as their attached papers.

2.1.3.1 Spacetime dependent quantum coin

The QWs defined here belong to a family larger than the ones introduced in Chapter (1), where the quantum coin is homogeneous in spacetime. In the inhomogeneous case, Eqs. (1.15) and (1.16) are transcribed in the following system of finite difference equations:

$$\begin{pmatrix} \psi^L_{j+1,m} \\ \psi^R_{j+1,m} \end{pmatrix} = B_{j,m} \begin{pmatrix} \psi^L_{j,m-1} \\ \psi^R_{j,m+1} \end{pmatrix} \tag{2.12}$$

The quantum coin $B_{j,m}$ belongs to $U(2)$ and is given by:

$$B(\alpha_{j,m},\theta_{j,m},\xi_{j,m},\zeta_{j,m}) = e^{i\alpha_{j,m}} \begin{pmatrix} e^{i\xi_{j,m}}\cos\theta_{j,m} & e^{i\zeta_{j,m}}\sin\theta_{j,m} \\ -e^{-i\zeta_{j,m}}\sin\theta_{j,m} & e^{-i\xi_{j,m}}\cos\theta_{j,m} \end{pmatrix} \tag{2.13}$$

As in equations (1.15) (1.16) and (1.12) (1.13) the probability $\Pi_j = \sum_m |\Psi_{j,m}|^2$ is finite and can be normalized to 1. It does not depend on j because of the unitarity of the dynamics.
To investigate the continuous limit of a general stroboscopic equation S^n, exactly as in sec. (1.2.2), we introduce a time step Δt and a space step Δx, scaling with ϵ:

$$\Delta x = \epsilon^\delta \lambda \tag{2.14}$$

$$\Delta t = \epsilon \tau \tag{2.15}$$

Now we should take into account the time and space dependency of the quantum coin and investigate formally the continuous limit of the walks, we should split each scalar field a in its homogeneous part a_0 and in its non-homogenous part $\overline{a}$. In particular we consider that the spacetime dependent component of the field scales as $O(\epsilon)$:

$$a = a_0 + \epsilon^\omega \overline{a}(t_j, x_m) \tag{2.16}$$

The exponent ω is a real and strictly positive number and is in general different from δ.

Note that in the Eq. (2.16), the spacetime dependency of the perturbation $\overline{a}(t_j, x_m)$ permits to identify uniquely a family of QWs admitting a continuous limit, because the homogenous and the inhomogeneous part are in general always distinguishable.

Furthermore, the inhomogeneities $\alpha(t_j, x_m)$, $\theta(t_j, x_m)$, $\xi(t_j, x_m)$ and $\zeta(t_j, x_m)$, upcoming in subsection 2.2.5 and as well as their attached papers, are linked to the emergent electric and gravitational fields . The proof of the existence of these two emergent gauge fields will be the main goal of the following sections. Let us first and foremost introduce to the reader one of them: the synthetic gravitational field.

2.2 A synthetic gravitational gauge field

2.2.1 Simulating the effects of a gravitational gauge field

How to create synthetic gravity is a question often related to the reproduction of the gravitational force. This physical and engineering question can pertain both to zero-gravity environments and to the Earth. This task can be accomplished by several methods: for example by mechanical procedures [47], or by producing electric [28] and magnetic [29] forces. However, in this section, *synthetic gravitational field* has a quite different meaning and refers to mimicking the effect of gravity on the spacetime curvature of a specific particle motion. As we know, curved spacetime is not accessible in the labs, what we can look for is an *analogue* curved spacetime.

An interesting challenge is represented, for instance, by the simulation and study of QFTs in curved spacetime. Cold atoms have become a very useful tool for simulating gauge fields. Zohar et al. [58] and Boada et al. [7] were the first to prove that using ultra-cold atoms in optical lattices makes possible to mimic various types of statics and dynamical curved spacetime through simple manipulation of the optical setup.

Here we propose a new idea of simulators that reproduces the propagation of massless particle with two internal states on a curved $(1+1)$ spacetime. In particular, the correction to the spinor propagation due to the gravitational deformation of the spacetime, is not *real*, but emerge as a geometric property of the QW. However, before we introduce the model, let us define several important elements of general relativity and curved field theory.

2.2.2 Curved spacetime and chiral field theory: an introduction

In the pre-relativistic context the framework of scientific researchers was the flat space of Euclidean geometry, grounded on the five Euclid's postulates. In 1827, in the *Disquitiones generales circa superficies curvas*, Gauss distinguished for the first time the inner or intrinsic properties of a surface from the outer or extrinsic ones. The former is measured by an observer living on the surface. The latter is derived from embedding the surface in a higher-dimensional space.

According to Gauss, the most fundamental inner property of a surface was the shortest path between two points. He realized, for instance, that a distance measured over a conic surface was the same as that one measured over a cylinder. These two surfaces, in fact, share the same intrinsic properties and in particular, their metric is flat. We cannot say the same for a sphere, as a sphere cannot be mapped onto a plane without distortions. However, since a cylinder or a cone are round in radial direction, we might be led to think they are curved surfaces.

This is due to the fact that we consider them as 2-dimensional surfaces in a 3-dimensional space, and we intuitively compare the curvature of the lines, which are on the surfaces, with straight lines in the flat 3-dimensional space.

The interplay between the inner and the outer properties of surfaces is one of the key point of the Einstein's theory of general relativity. To be more clear we need first to introduce the formalism and the main assumptions of the theory. Then we will be prepared to define properly the Dirac equation in curved spacetime.

2.2.3 A formal general setup

"*Riemannian geometry is characterized by the facts that the infinitesimal neighborhood of every point P has a Euclidian metric, and that the magnitudes of two line elements that belong to the infinitesimal neighborhoods of two finitely distant points P and Q are comparable. However, the concept of parallelism of these two line elements is missing; for finite regions the concept of direction does not exist. The theory put forward in the following is characterized by the introduction, in addition to the Riemann metric, of a direction, or of equality of direction, or of parallelism for finite distances. Correspondingly, new invariants and tensors will appear in addition to those of Riemann geometry.* (Einstein [19] ,1928)

With no extra constructs, and by simply using the only intuitive idea of parallelism, Einstein introduced, as reported in the above cited manuscript, for the first time the concept of *connection* and *curvature* in field theory. This later entailed the formulation of a new theory called the *vierbein* field theory that has permitted to derive a gauge field theory approach to general relativity [57]. In particular, we will employ this approach to derive Dirac equation in curved spacetime.

To that end, let us first introduce the standard mathematical framework to treat the curved spacetime and the sufficient ingredients, with a particular attention to the notion of spin connection and Lorentz invariance. All we introduce in the following introductory section can be find in any standard textbook on curved QFT and we address the reader in particular for detailed computations to Boulanger et al. [8], Brill and Wheeler [9] or Birrell and Davies [6] for a general discussion on chiral matter in curved spacetime or for a synthetic but rigorous approach Yepez [57]. Moreover, en elegant differential approach is proposed by Lasenby et al. [33].

2.2.3.1 Mathematical Framework

Let us consider a Lorentzian manifold (M, g), where M is a pseudo-Riemannian manifold and g is a Lorentzian metric, that is g relates at each point $p \in M$ a Lorentzian scalar product g_p on the tangent space T_p. The differential basis is given by the partial derivatives of the coordinates at p:

$$\hat{\mathbf{e}}_{(\mu)} = \partial_{(\mu)}, \tag{2.17}$$

where the hat denote the unit vector, related to the basis vector $\hat{\mathbf{e}}$. The subscript (μ) denotes a component of the basis vector, that serves as the coordinate system representation. All vectors

$A \in T_p$ can be spanned on this basis and read:

$$A = A^{\mu}\hat{\mathbf{e}}_{(\mu)}. \tag{2.18}$$

The cotangent basis is defined by the *dual* space of the T_p, and the differential basis is:

$$\hat{\mathbf{e}}^{(\mu)} = \mathbf{dx}^{(\mu)}. \tag{2.19}$$

Let us call the dual space T_p^*. All vectors in this space have components:

$$A = A_{\mu}\hat{\mathbf{e}}^{(\mu)} = g_{\mu\nu}A^{\nu}\hat{\mathbf{e}}^{(\mu)}. \tag{2.20}$$

Now let us bring in a non-coordinate unit vector basis, an orthonormal basis that is independent from the coordinates. In a (1+3)-dimensional spacetime the basis is composed by four linear independent elements and let us call it *tetrads* (*group of four* from Greek). Alternatively in (1+1)-spacetime we call in the following this orthonormal basis *dyads*, and we denote each component by $\hat{\mathbf{e}}_{(a)}$.

$$\hat{\mathbf{e}}_{(a)} \cdot \hat{\mathbf{e}}_{(b)} = \eta_{ab}, \tag{2.21}$$

where η_{ab} is the Minkowski metric of flat spacetime. The non-coordinate unit vector bases spans all coordinate basis with a given local curvature (depending on x):

$$\hat{\mathbf{e}}_{(\mu)} = e^{a}_{\mu}(x)\hat{\mathbf{e}}_{(a)}. \tag{2.22}$$

The matrix $e^{a}_{\mu}(x)$ is invertible and named *vierbein field*. These fields has to be at least C^1 and are defined such that:

$$g_{\mu\nu}(x)e^{\mu}_{a}(x)e^{\nu}_{b}(x) = \eta_{ab}. \tag{2.23}$$

or equivalently

$$g_{\mu\nu}(x) = e^{a}_{\mu}(x)e^{b}_{\nu}(x)\eta_{ab}. \tag{2.24}$$

Now, let us notice that the *triads* are not uniquely determined, in fact under a local Lorentz transformation:

$$\hat{\mathbf{e}}_{(a)} \rightarrow \hat{\mathbf{e}}_{(a')} = \Lambda^{a}_{a'}(x)\hat{\mathbf{e}}_{(a)}, \tag{2.25}$$

where $\Lambda^{a}_{a'}(x)$ is the position dependent transformation, so that:

$$\Lambda^{a}_{a'}(x)\Lambda^{b}_{b'}(x)\eta_{ab} = \eta_{a'b'}. \tag{2.26}$$

2.2.3.2 Affine connection and Spin connection

To introduce the notion of connection, let us describe the Fig. 2.1. Consider two spacetime points $x^{\alpha} \equiv A$ and $x^{\alpha} + \delta x^{\alpha} \equiv B$ and denote by $X^{\alpha}(x)$ a vector at point A. If we perform a translation of $\delta X^{\alpha}(x)$ in spacetime, the transformed vector, at point B, $(X^{\alpha}(x))'$, is given by $X^{\alpha}(x) + \delta X^{\alpha}(x)$. In general, the pseudo-Riemann manifold possesses a non-vanishing curvature and, thus, we should consider a distortion effect in respect to the vector $X^{\alpha} + \overline{\delta}X^{\alpha}$ as in a flat spacetime. From the Fig. 2.1 we can geometrically observe that the curvature of the manifold is measured by the quantity $[X^{\alpha} + \delta X^{\alpha}] - [X^{\alpha} + \overline{\delta}X^{\alpha}] = \delta X^{\alpha} - \overline{\delta}X^{\alpha}$. The affine connection represents the discrepancy between the variation $\overline{\delta}X^{\alpha}$ and the vector δX^{α}. It represents a multiplicative factor between X^{β} itself and the finite displacement δx^{γ}. Let us denote this factor by $\Gamma^{\alpha}_{\beta\gamma}X^{\beta}$.

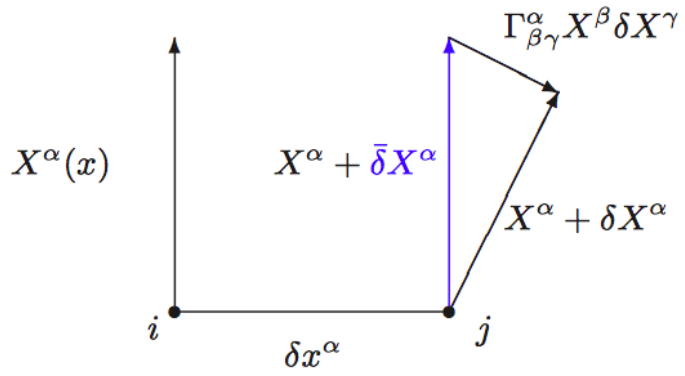

Figure 2.1: *Distortion in a vector field in the transport from a point i to a point j of the curved spacetime.*

Now let us include the following finite difference:

$$\nabla_{\gamma}X^{\alpha}(x) \equiv \frac{1}{\delta x^{\gamma}}(X^{\alpha}(x+\delta x) - [X^{\alpha}(x) + \overline{\delta}X^{\alpha}(x)]) \tag{2.27}$$

and comment that, if the curvature is zero, or $\overline{\delta}X^{\alpha}(x) = \delta X^{\alpha}(x)$, the above expression coincides, in the continuous limit, with the standard partial derivative at point x.
Otherwise, it is possible to demonstrate [57] that the above definition transcribe in the following covariant derivative:

$$\nabla_{\gamma}X^{\alpha} = \partial_{\gamma}X^{\alpha} + \Gamma^{\alpha}_{\beta\gamma}X^{\beta} \tag{2.28}$$

In other terms, in coordinate-based differential geometry, the covariant derivative of a tensor is given by its partial derivative plus a correction terms, one for each index, involving an affine connection contracted with the tensor.

Exactly for the same principle, in the non-coordinate based differential geometry, the *spin connection* takes the place of the affine connection. For each index we get a correction factor, conventionally positive for upper index, negative for lower index:

$$\nabla_{\gamma}X^{a}_{b} = \partial_{\mu}X^{a}_{b} + \omega^{a}_{\mu\ c}X^{c}_{b} - \omega^{c}_{\mu\ b}X^{a}_{c}. \tag{2.29}$$

Let us acknowledge that, using the *vierbein* matrices, we can write the affine connections in terms of spin connections and vice versa:

$$\Gamma^{\nu}_{\mu\lambda} = e^{\nu}_{a}\partial_{\mu}e^{a}_{\lambda} + e^{\nu}_{a}e^{b}_{\lambda}\omega^{a}_{\mu\ b} \qquad \omega^{a}_{\mu\ b} = e^{a}_{\nu}e^{\lambda}_{b}\Gamma^{\nu}_{\mu\lambda} - e^{\lambda}_{b}\partial_{\mu}e^{a}_{\lambda}. \tag{2.30}$$

Another essential ingredient is *the tetrad postulate*. It states that the covariant derivative of the *vierbein field* exists and vanishes, or in other words, the *vierbein field* is invariant under parallel transport:

$$\nabla_{\mu}e^{a}_{\nu} = 0. \tag{2.31}$$

An important consequence of this postulate, called *metric compatibility*, is that the metric

tensor $g_{\nu\lambda}$ itself is also invariant under parallel transport:

$$\nabla_\mu g_{\nu\lambda} = 0. \tag{2.32}$$

Let us now introduce the last ingredient, that is the relation between the affine connection and the metric tensor. Permute the indices in the latter equation as follows:

$$\nabla_\rho g_{\mu\nu} = \partial_\rho g_{\mu\nu} - \Gamma^\lambda_{\rho\mu} g_{\lambda\nu} - \Gamma^\lambda_{\rho\nu} g_{\mu\lambda} = 0, \tag{2.33}$$

$$\nabla_\mu g_{\mu\rho} = \partial_\mu g_{\nu\rho} - \Gamma^\lambda_{\mu\nu} g_{\lambda\rho} - \Gamma^\lambda_{\mu\rho} g_{\nu\lambda} = 0, \tag{2.34}$$

$$\nabla_\nu g_{\rho\mu} = \partial_\nu g_{\rho\mu} - \Gamma^\lambda_{\nu\rho} g_{\lambda\mu} - \Gamma^\lambda_{\nu\mu} g_{\rho\lambda} = 0, \tag{2.35}$$

Take (2.33)-(2.34)-(2.35), multiply by $g^{\sigma\rho}$ and contract the indices σ and μ, the affine connections read:

$$\Gamma^\mu_{\mu\nu} = \frac{1}{2} g^{\mu\rho} \partial_\nu g_{\rho\mu}. \tag{2.36}$$

The latter equation can be transcribed in:

$$\Gamma^\mu_{\mu\nu} = \frac{1}{2} Tr(g^{\lambda\rho} \partial_\nu g_{\rho\mu}) = \frac{1}{\sqrt{-g}} \partial_\nu \sqrt{-g} \tag{2.37}$$

where $g \equiv -Det(g_{\rho\mu})$. Observe that from the above relation, given the Eqs. (2.30), we can derive simply the relation between the metric tensor and the spin connection.

2.2.3.3 Lorentz invariance in curved spacetime

To formalize a relativistic curved field theory demands the Dirac equation to be Lorentz invariant. In flat space, the Lorentz transformation acts in general on the physical space and on the spinor states. Notably the Dirac gamma matrices transform under an internal Lorentz unitary transformation $U(\Lambda)$ as follows:

$$U(\Lambda)^{-1} \gamma^\mu U(\Lambda) = \Lambda^\mu_\sigma \gamma^\sigma. \tag{2.38}$$

and therefore the Dirac equation changes as follows:

$$[i\gamma^\mu \partial_\mu - m]\psi(x) \to U(\Lambda)[i\gamma^\mu \partial_\mu - m]\psi(\Lambda^{-1}x). \tag{2.39}$$

We redirect the reader to Peskin and Schroeder [45] for a detailed demonstration of the Lorentz invariance of Dirac equation in flat space. In curved spacetime we should take into account the correction due to the curvature of the space. Let us call it Γ_μ. Following [57] Gamma matrices transform under Lorentz transformations as follows:

$$\Lambda^\mu_\sigma \gamma^\sigma (\Lambda^{-1})^\nu_\mu = \gamma^\nu \tag{2.40}$$

and the Dirac equation in curved space:

$$\gamma^\mu(\partial_\mu + \Gamma_\mu)\psi(x) \to \Lambda^\mu_\lambda e^\lambda_a \gamma^a (\Lambda^{-1})^\nu_\mu (\partial_\mu + \Gamma'_\mu) U(\Lambda)\psi(U(\Lambda)^{-1}x) \tag{2.41}$$

where $\gamma^\mu = e^\mu_a \gamma^a$. A tedious computation of the RHS of the above transformation, leads us to the condition, to be respected in order to preserve the Lorentz invariance:

$$\Gamma'_\nu = U(\Lambda)\Gamma_\nu U(\Lambda)^{-1} - \partial_\nu(U(\Lambda))U(\Lambda)^{-1} \tag{2.42}$$

Finally the Dirac equation in curved spacetime reads:

$$i\gamma^a e_a^\mu(x)\mathcal{D}_\mu\psi - m\psi = 0 \tag{2.43}$$

where the covariant derivative

$$\mathcal{D}_\mu = \partial_\mu + \Gamma_\mu \tag{2.44}$$

where Γ_μ transforms according to Eq. (2.42). The last step is to determine explicitly the covariant derivative and notably the form of the correction Γ_μ. To do this, we should demand the spinor field to be invariant under Lorentz transformations. The correction to the spinor field is found to be:

$$\Gamma_\alpha = \frac{1}{2}e_k^\beta(\partial_\alpha e_{\beta h})S^{hk}. \tag{2.45}$$

Yepez [57].

Let us remark that all we presented in this section is casted purely in terms of QW by Arrighi et al. [3].

2.2.4 Dirac equation in curved spacetime in (1+1) dimensions

We have now all the elements to derive the Dirac equation in a curved spacetime of arbitrary dimension. The $(1+1)$ dimensional case is straightforward[1]. The problem in fact simplify greatly. The product $\gamma^a e_a^\mu(x)\mathcal{D}_\mu$ in Eq. (2.43) transcribes in:

$$\frac{1}{2}\gamma^a\frac{1}{\sqrt{-g}}\partial_\mu(\sqrt{-g}e_a^\mu) \tag{2.46}$$

thus the Dirac equation can be written as follows:

$$[i\gamma^a e_a^\mu\partial_\mu + \frac{i}{2}\gamma^a\frac{1}{\sqrt{-g}}\partial_\mu(\sqrt{-g}e_a^\mu) - m]\psi = 0. \tag{2.47}$$

Observe that we have derived the Dirac equation from considerations of invariance with respect to Lorentz transformations, in analogous way the electromagnetism is derived from a gauge invariance principle.

2.2.5 Publication: "Quantum walks as massless Dirac fermions in curved spacetime"

The intent of this publication is to show how a particular family of IDTQWs can mimic a massless fermion propagating in a curved metric. In order to show a specific case, a spherically symmetric solution to Einstein equation in vacuum such as the Schwarzschild metric, which represents a Schwarzschild black hole, has been chosen. This kind of black hole is no charged and its angular momentum associated to its mass is zero. Observe, finally that, even though we model the motion of a particle in a curved $(1+1)-$spacetime, we do not mimic two dimensional gravity. We notably study the case of a particle confined on the radial dimension of a $(3+1)$-spherical metric. Because the particle is massless, it follows the geodesics for all times and consequently it can be described by a $(1+1)$-curved Dirac equation. However, gravity in $(1+1)$ has been investigated for instance by Brown et al. [10] and Morsink and Mann [42], [36]. Despite its simplicity, this theory also has a number of striking classical and semi-classical

[1] Let us notice that Dirac equation in (1+1) curved spacetime has been derived by Sinha and Roychoudhury [51], Morsink and Mann [42], Carter and McLenaghan [13], Birrell and Davies [6], Fulling [22], Parker [44]

features, including a well-defined Newtonian limit ([37]), FRW cosmologies, gravitational collapse, cosmological solutions and gravitational waves (Sikkema and Mann [50]).

Di Molfetta et al. [17], [16] investigated systematically the continuous limit of the QW's stroboscopic equation S^2 and they formally recovered the $(1+1)$-Dirac equation in curved spacetime. The curvature of spacetime in continuous limit is linked (through the metrics g) to the quantum coin of the walk, B_{jm}, in discrete spacetime.

Albeit recents, these results have immediately inspired others to investigate the matter further. For instance Arrighi et al. [4] recovered the massive Dirac equation in curved $(1+1)$-spacetime, performing the continuous limit by a new method. They introduced in the standard definition of the QW time evolution operator, three extra unitary operations: encoding, grouping and decoding. These operations allowed the authors to build a map between usual QWs and usual QWs of increased dimension, called *paired QWs*. The continuous limit is consequently taken on the latter.

Furthermore, the continuous limit of Paired QW also offers a new potential perspective: it can be seen as an emergent property of spacetime grouping. For instance, seeing QWs as a specific case of QCA , we can change the local interactions betweens the cells and the spatial distributions of the cells, i.e., the QCA interaction graph, to obtain different emergent dynamics in the grouping operations. This can lead us to connect the geometrical aspects of the interaction graph with the geometrical properties of gauge QFT, in a similar fashion to the gravitational field connected to the curvature of the spacetime. In this way, through the geometrical aspects of its interaction graph as such, gauge fields are naturally built into the very fabric of the associated QCA, and by changing the QCA structure we change the quantum field theory that has been described. This can a be a new potential possibility to explore in the future. Let finally remark that, in consequence to we said in this paragraph, the model proposed by Arrighi et al. can recover our model, by choosing a specific spacetime grouping or a QCA interaction graph.

Another approach was recently introduced by S.Succi et al. [52], who explored the connection between Dirac equation, QWs and Quantum lattice Boltzmann (QLB). However, their method is even more different from what has been described before. They showed that the discretization of the Dirac equation in flat and curved spacetime, through lattice Boltzmann numerical schemes, can be recast in the QW formalism.

Quantum walks as massless Dirac fermions in curved space-time

Giuseppe Di Molfetta,[1] M. Brachet,[2] and Fabrice Debbasch[1]
[1]*LERMA, UMR 8112, UPMC and Observatoire de Paris, 61 Avenue de l'Observatoire 75014 Paris, France*
[2]*CNRS, Laboratoire de Physique Statistique Ecole Normale Supérieure, 75231 Paris Cedex 05, France*
(Received 23 December 2012; revised manuscript received 13 April 2013; published 1 October 2013)

A particular family of time- and space-dependent discrete-time quantum walks (QWs) is considered in one-dimensional physical space. The continuous limit of these walks is defined through a procedure discussed here and computed in full detail. In this limit, the walks coincide with the propagation of a massless Dirac fermion in an arbitrary gravitational field. A QW mimicking the radial propagation of a fermion outside and inside the event horizon of a Schwarzschild black hole is explicitly constructed and simulated numerically. Thus, the family of QWs considered in our manuscript provides an analog system to study experimentally coherent quantum propagation in curved spacetime.

DOI: 10.1103/PhysRevA.88.042301 PACS number(s): 03.67.−a, 03.65.−w

The first quantum walk (QW) was built by Feynman [1] as a possible discretization of the standard, massive Dirac dynamics in flat spacetime. General discrete-time QWs have then been introduced in the physics literature by Refs. [2,3] and the continuous-time version first appeared in Ref. [4]. QWs are the simplest formal analogs of classical random walks and are important in many fields, ranging from fundamental quantum physics [5,6] to quantum algorithmics [7,8], solid-state physics [9–12], and biophysics [13,14].

QWs have been realized experimentally; for example, as transport of trapped ions [15,16], of photons in wave guide lattices [6] or optical networks [17] and of atoms in optical lattices [18]. QW experiments of two photons [19] have recently been performed, with the possibility of simulating Bose or Fermi statistics [20], and cavity QED QWs have also been proposed [21].

Following Feynman's idea, several authors have studied the continuous limit of general QWs. Most publications [22–29] only envisage QWs with constant coefficients. The continuous limit of QWs with time- and space-dependent coefficients has been considered only recently, in Refs. [30–32]. These references present several families of QWs, in both $(1+1)$ or $(1+2)$ spacetime dimensions, whose continuous limit is described by a flat spacetime Dirac equation with a generalized mass term and electromagnetic coupling. The electromagnetic field is generated by the spacetime dependence of the angles defining the walks and thus vanishes if these angles are constant.

The other gauge field which couples naturally to a Dirac spinor is evidently gravity. Yet, QWs whose continuous limit are described by Dirac equations in curved spacetime have remained elusive. This article considers a particular family of discrete-time QWs with nonconstant angles in $(1+1)$ spacetime dimensions and associates to this family a continuous limit which is described by a massless Dirac equation in curved spacetime. This family was not investigated in Refs. [30–32] and the limit procedure used in these references cannot be applied to the family discussed here. The result presented in this article opens the way to possible laboratory experiments simulating coherent quantum propagation in relativistic gravitational fields. It also establishes a connection between general relativity and all the aforementioned fields where QWs are useful.

We consider QWs defined over discrete time and discrete one-dimensional (1D) space, driven by time- and space-dependent quantum coins acting on a two-dimensional (2D) Hilbert space $\mathcal{H}$. The walks are defined by the following finite difference equations, valid for all $(j,m) \in \mathbb{N} \times \mathbb{Z}$:

$$\begin{bmatrix} \psi^L_{j+1,m} \\ \psi^R_{j+1,m} \end{bmatrix} = B\left(\theta_{j,m}\right) \begin{bmatrix} \psi^L_{j,m+1} \\ \psi^R_{j,m-1} \end{bmatrix}, \tag{1}$$

where

$$B(\theta) = \begin{bmatrix} -\cos\theta & i\sin\theta \\ -i\sin\theta & +\cos\theta \end{bmatrix}. \tag{2}$$

The index j labels instants and the index m labels spatial points. For each instant j and each spatial point m, the wave function $\Psi_{jm} = \psi^L_{jm} b_L + \psi^R_{jm} b_R$ has two components ψ^L_{jm} and ψ^R_{jm} on the spin basis (b_L, b_R) and these code for the probability amplitudes of the particle jumping towards the left or towards the right. Note that the spin basis is interpreted as being independent of j and m. The total probability $\pi_j = \sum_m (|\psi^L_{j,m}|^2 + |\psi^R_{j,m}|^2)$ is independent of j; i.e., conserved by the walk. The set of angles $\{\theta_{j,m}, (j,m) \in \mathbb{N} \times \mathbb{Z}\}$ defines the walks and is arbitrary.

Consider now, for all $(n,j) \in \mathbb{N}^2$, the collection $W^n_j = (\Psi_{k,m})_{k=nj, m\in\mathbb{Z}}$. This collection represents the state of the QW at "time" $k = nj$. For any given n, the collection $S^n = (W^n_j)_{j\in\mathbb{N}}$ thus represents the entire history of the QW observed through a stroboscope of "period" n. The evolution equations for S^n are those linking W^n_{j+1} to W^n_j for all j. These can be deduced from the original evolution equations (1) of the walk, which also coincide with the evolution equations of S^1. In particular, the evolution equations of S^2 read

$$\begin{aligned} \psi^L_{j+2,m} &= c_{j+1,m}\left(c_{j,m+1}\psi^L_{j,m+2} - i s_{j,m+1}\psi^R_{j,m}\right) \\ &\quad + s_{j+1,m}\left(s_{j,m-1}\psi^L_{j,m} + i c_{j,m-1}\psi^R_{j,m-2}\right), \end{aligned} \tag{3}$$

$$\begin{aligned} \psi^R_{j+2,m} &= s_{j+1,m}\left(i c_{j,m+1}\psi^L_{j,m+2} + s_{j,m+1}\psi^R_{j,m}\right) \\ &\quad - c_{j+1,m}\left(i s_{j,m-1}\psi^L_{j,m} - c_{j,m-1}\psi^R_{j,m-2}\right), \end{aligned} \tag{4}$$

where $c_{jm} = \cos(\theta_{jm})$ and $s_{jm} = \sin(\theta_{jm})$.

To investigate the continuous limit of S^n, we first introduce a time step Δt and a space step Δx. We then consider

that Ψ_{jm} and θ_{jm} are the values taken by a two-component wave function Ψ and by a function θ at the spacetime point $(t_j = j\Delta t, x_m = m\Delta x)$. We finally suppose that Ψ and θ are at least twice differentiable with respect to both space and time variables for all sufficiently small values of Δt and Δx. The formal continuous limit of S^n is defined as the couple of differential equations obtained from the discrete-time evolution equations defining S^n by letting both Δt and Δx tend to zero. Let us therefore introduce a time-scale $\mathcal{T}$, a length-scale $\mathcal{L}$, an infinitesimal ϵ and write $\Delta t = \epsilon\mathcal{T}$ and $\Delta x = \epsilon\mathcal{L}$. The continuous limit of S^n can then be investigated by Taylor expanding in powers of ϵ the discrete equations defining S^n. For the limit to exist, all zeroth-order terms must identically cancel each other and the differential equation describing the limit is then obtained by equating to zero the nonidentically vanishing, lowest-order contribution. Consider first S^1, which is identical to the original walk. It is rather obvious that zeroth-order terms cancel each other only if the operator B defining the walk tends to unity as ϵ tends to 0 (see Ref. [30] for a detailed discussion of this point). The operator B defining the family of walks considered in this article does not depend on ϵ and is different from unity for all values of θ. Thus, S^1 does not admit a continuous limit for the family of walks defined by Eq. (1). But S^2, on the other hand, does. Indeed, a straightforward computation delivers the following equation obeyed by the wave function Ψ:

$$\Psi_T + (\cos\theta)P\Psi_X = Q\Psi, \tag{5}$$

where the operators P and Q are represented, in the base (b_L, b_R), by the matrices

$$P = \begin{pmatrix} -\cos\theta & i\sin\theta \\ -i\sin\theta & \cos\theta \end{pmatrix} \tag{6}$$

and

$$Q = \begin{pmatrix} -\theta_X \frac{\sin 2\theta}{2} & \frac{i}{2}[\theta_T - \theta_X(\cos 2\theta)] \\ \frac{i}{2}[\theta_T + \theta_X(\cos 2\theta)] & \theta_X \frac{\sin 2\theta}{2} \end{pmatrix}. \tag{7}$$

In Eqs. (5) and (7), the subscript T (X) indicates a derivative with respect to the dimensionless variable $T = t/\mathcal{T}$ $(X = x/\mathcal{L})$.

The operator P is self-adjoint and its eigenvalues are -1 and $+1$. Two eigenvectors associated with these eigenvalues are

$$b_- = i\left(\cos\frac{\theta}{2}\right)b_L - \left(\sin\frac{\theta}{2}\right)b_R, \tag{8}$$

$$b_+ = i\left(\sin\frac{\theta}{2}\right)b_L + \left(\cos\frac{\theta}{2}\right)b_R. \tag{9}$$

The family (b_-, b_+) forms an orthonormal basis of the two-dimensional-spin Hilbert space. Let us now rewrite Eq. (5) in components, but in this new orthonormal basis. A tedious but straightforward computation leads to

$$\begin{aligned} \psi_T^- - (\cos\theta)\psi_X^- + \frac{\theta_X}{2}(\sin\theta)\psi^- = 0, \\ \psi_T^+ + (\cos\theta)\psi_X^+ - \frac{\theta_X}{2}(\sin\theta)\psi^+ = 0, \end{aligned} \tag{10}$$

where ψ^- and ψ^+ are the components of Ψ in the new basis. This form of the equations makes it easy to check that the continuous dynamics conserves the total probability $\pi(T) = \int dX|\Psi(T,X)|^2 = \int dX[|\psi^-(T,X)|^2 + |\psi^+(T,X)|^2]$, as it should.

Suppose now, to make the discussion definite, that $\cos\theta$ is strictly positive and introduce in spacetime $\{(T,X)\}$ the Lorentzian, possibly curved metric G defined by its covariant components $(G_{\mu\nu}) = \mathrm{diag}(1, -1/\cos^2\theta)$, where $(\mu,\nu) \in \{T,X\}^2$. This metric defines the canonical, scalar "volume" element $\mathcal{D}_G X = \sqrt{-G}dX = dX/\cos\theta$ in physical 1D X space, where G is the determinant of the metric components $G_{\mu\nu}$. Dirac spinors are normalized to unity with respect to $\mathcal{D}_G X$, whereas Ψ is normalized to unity with respect to dX. We thus introduce $\Phi = \Psi\sqrt{\cos\theta}$ and rewrite the equations of motion (10) in terms of Φ. We obtain

$$\gamma^a\left[e_a^\mu\partial_\mu\Phi + \frac{1}{2}\frac{1}{\sqrt{-G}}\partial_\mu\left(\sqrt{-G}e_a^\mu\right)\Phi\right] = 0, \tag{11}$$

where $\mu \in \{T,X\}$, $a \in \{0,1\}$. The usual 2D gamma matrices are

$$\gamma^0 = \begin{pmatrix} 0 & 1 \\ 1 & 0 \end{pmatrix}, \quad \gamma^1 = \begin{pmatrix} 0 & 1 \\ -1 & 0 \end{pmatrix}, \tag{12}$$

and the e_a^μ are the components of the diad (orthonormal basis) $e_0 = e_T$ and $e_1 = (\cos\theta)e_X$ on the original coordinate basis (e_T, e_X). Equation (11) is the standard [33] equation of motion for a massless Dirac spinor in $(1+1)$-dimensional spacetime with metric G. The spin basis is (b_-, b_+).

This result shows that QWs can be used to model quantum transport in any 2D gravitational field. Indeed, any 2D Lorentzian metric can be put under the above diagonal form by a suitable choice of coordinates. The single angle $\theta(t,x)$ is thus enough to describe any 2D gravitational field. Let us stress, however, that gravity is very different in 2D and in 4D since, in particular, all 2D spacetimes are conformally flat [34]. But Eq. (11) can also be used to model quantum transport in higher-dimensional spacetimes by QWs on the line. As an example, we now construct a QW on the line which mimics the radial motion of a Dirac spinor in a spherically symmetric 4D black hole.

A Schwarzschild black hole is a spherically symmetric solution of Einstein equation *in vacuo*. The corresponding 4D metric reads, in dimensionless Lemaître coordinates (τ,ρ,θ,ϕ) [35],

$$ds^2 = d\tau^2 - \frac{r_g}{r}d\rho^2 - r^2 d\Omega, \tag{13}$$

where $r(\tau,\rho) = r_g^{1/3}[\frac{3}{2}(\rho-\tau)]^{2/3}$, $d\Omega = d\theta^2 + (\sin^2\theta)d\phi^2$. The event horizon is located at $r = r_g$, i.e., $\rho = \tau + (2/3)r_g$, and the singularity is located at $r = 0$, i.e., $\rho = \tau$. The exterior of the black hole is the domain $r > r_g$.The range of variations for the Lemaître coordinates is $\tau \geqslant 0$, $\rho \geqslant \tau$ [i.e., $r(\tau,\rho) \geqslant 0$], $0 \leqslant \theta \leqslant \pi$, $0 \leqslant \phi < 2\pi$.

Because of the spherical symmetry, a point mass which starts its motion radially will go on moving radially. Radial motion can be studied by introducing the 2D metric g, also singular at $r = 0$, with covariant components $g_{\tau\tau} = 1$, $g_{\rho\rho} = -r_g/r$, $g_{\tau\rho} = g_{\rho\tau} = 0$. The null geodesics of g are defined by $d\tau = \pm[r_g/r(\tau,\rho)]^{1/2}d\rho$. Note that the 2D projection of the horizon on the (τ,ρ) plane coincides with a null geodesics of g.

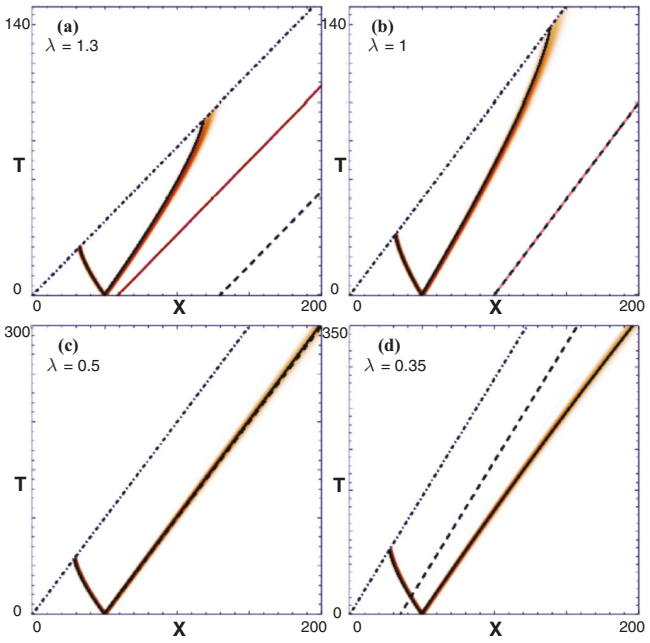

FIG. 1. (Color online) Density of the QW vs null geodesics (solid curves) of the 2D Schwarzschild metric for various values of λ [see text and Eq. (14)]. The singularity is represented by the dotted and dashed line on the left and the horizon (which is a null geodesic) is represented by the dashed line. (a), (b) The two branches of the QW which starts inside the horizon end up on the singularity. The (red) solid line represents the limit of the definition domain $\mathcal{D}$ of the QW. (c) One branch of a QW which starts on the horizon stays on the horizon while the other branch ends up on the singularity. (d) One branch of the QW which starts outside the horizon propagates away from the black hole, and the other branch ends up on the singularity.

We now identify the dimensionless time T with the time coordinate τ and the dimensionless space variable X with $\lambda\rho$, where λ is an arbitrary strictly positive real number (see Fig. 1). The "radius" r can then be expressed as a function of T and X:

$$r(T,X) = \left[\frac{3}{2}\left(\frac{X}{\lambda} - T\right)\right]^{2/3} r_g^{1/3}, \tag{14}$$

and the components of g in the coordinate basis associated with T and X are $g_{TT} = 1$, $g_{XX} = -r_g/(\lambda^2 r)$, $g_{TX} = g_{XT} = 0$. Note that the condition $\rho \geqslant \tau$ transcribes into $X \geqslant \lambda T$.

Let $\mathcal{D}$ be the domain where $-g_{XX} \geqslant 1$. This domain is characterized, in (T,X) coordinates, by the condition $X \leqslant \lambda T + \frac{2}{3\lambda^2} r_g$. In $\mathcal{D}$ the metric g can be identified with the metric G. This identification defines a angle θ which depends on T and X by

$$(\cos\theta)(T,X) = \lambda\sqrt{\frac{r(T,X)}{r_g}} \tag{15}$$

and, by extension, a QW in $\mathcal{D}$.

The condition defining $\mathcal{D}$ can be rewritten as $r \leqslant r_g/\lambda^2$. The domain $\mathcal{D}$ thus includes, for all λ, the singularity located at $r = 0$. For $\lambda > 1$, $r_g/\lambda^2 < r_g$ and $\mathcal{D}$ is then entirely located inside the horizon. For $\lambda = 1$, $\mathcal{D}$ coincides with the interior of the horizon, and $\mathcal{D}$ extends outside the horizon for $\lambda < 1$.

The spatial density $|\Psi(T,X)|^2$ of the walk defined by Eqs. (1), (2), and (15) is plotted in Fig. 1. All graphs have been obtained with $r_g = 150$ and $\epsilon = 0.5$. The initial condition is $\Psi(0,X) = \sqrt{n_0(X)}(b_L + i b_R)$ with an initial Gaussian density n_0 of variance $\Delta X_0 = 2.5$ centered on $X_0 = 50.5$. In Figs. 1(a) and 1(b) (in which the right limit of $\mathcal{D}$ coincides with the horizon), both branches of the QW starts their evolution inside the horizon and end up on the singularity. In Fig. 1(c) the QW starts exactly on the horizon; the right branch follows it while the left branch ends up on the singularity. In Fig. 1(d) the QW starts outside the horizon; its right branch propagates away from the horizon while the left branch still ends up on the singularity.

Figure 1 clearly shows that the QW closely follows null geodesics of the metric, i.e., it behaves as a massless fermion in the gravitational field of the black hole. The agreement between the geodesics and the density profile of the walk is all the more remarkable given that all graphs correspond to $\epsilon = 0.5$, which lies well outside of the continuous limit $\epsilon \ll 1$ envisaged above. Note, however, that the right branch of the QW lags slightly behind the null geodesic when approaching the $r = 0$ singularity [see top of Fig. 1(b)]. The numerical results thus suggest that the main result of this article can somehow be extended beyond the continuous limit. This interesting point will be investigated in future presentations.

In summary, we have considered a particular family of one-dimensional QWs which does not admit a continuous limit by the procedure used in Refs. [30–32]. The procedure used here keeps one time step out of two, and gives a continuous limit to walks from this family. We have computed this limit and proven that it coincides with the propagation of a massless Dirac fermion in an arbitrary gravitational field. Note, however, that Fig. 1, where all time steps are retained, shows that the density clearly follows, at all times, the null geodesic predicted by the continuous limit. We have also constructed explicitly a QW which mimics the propagation of a fermion outside and inside the event horizon of a Schwarzschild black hole and illustrated this construction by numerical simulations.

Let us now discuss the above results. Keeping only one time step of the QW out of two to build a continuous limit might appear unnatural and might even look like a purely mathematical trick. Let us explain now in detail why this is not so. Consider first, as an instructive example, the sequence of numbers u_j defined by $u_0 = 1$ and

$$u_{j+1} = \sigma \exp(i\omega\mathcal{T}) u_j, \tag{16}$$

for $j \in \mathbb{N}$; here, ω is an arbitrary real number, $\mathcal{T}$ is a time-scale and $\sigma = \pm 1$ and does not depend on j. A direct computation shows that $u_j = \sigma^j \exp(i\omega t_j)$ with $t_j = j\mathcal{T}$. Suppose $\sigma = +1$. The sequence u_j is then a simple circular function of the time t_j. On the contrary, if $\sigma = -1$, the sequence u_j is then a circular function of the time t_j combined with an extra phase shift of π at every time step. The sequence u_j admits a continuous limit if $\sigma = +1$. But, it does not if $\sigma = -1$, because of this extra phase shift. In particular, if $\sigma = -1$, the oscillating behavior of the sequence u_j cannot be recovered by simply taking the continuous limit of the evolution equation (16). The best way to recover this oscillating behavior is then to consider the new sequence v_k built out of u_j by keeping only one time

step out of two. Indeed, this new sequence obeys the discrete evolution equation $v_{k+1} = \exp(2i\omega\mathcal{T})v_k$. This equation admits a continuous limit, described by the ordinary differential equation $\frac{dv}{dt} = 2i\omega v$, which clearly reveals the oscillating behavior in v and, thus, in u. Naturally, all information on the extra phase shift of π is lost in this procedure. Note, however, that this extra phase shift does not influence the sequence of the squared moduli $|u_j|^2$.

Let us now compare the preceding example with the QWs examined in Refs. [30–32] and in this article. The spinor Ψ plays a role similar to u and the evolution equation of the walk [Eq. (1) for the QWs considered in this article] has the same status as Eq. (16). The QWs studied in Refs. [30–32] are equivalent to the sequence u_j obtained with $\sigma = +1$. They thus admit a standard continuous limit, which is fully described in these earlier publications. This limit coincides with the propagation in flat spacetime of a Dirac fermion possibly coupled to an electric field. On the other hand, the QWs defined by Eqs. (1) and (2) correspond to the sequence u_j with $\sigma = -1$ and they do not admit a continuous limit. But the derived walks built by keeping only one time step out of two of the original QWs do admit a continuous limit because the squared matrix $\mathcal{B}^2 = 1$, just as $(-1)^2 = 1$. Keeping one time step out of two is thus not a contrived, unphysical procedure. On the contrary, it is dictated by the very definition of the QWs we study in this article and it is the only one which delivers a continuous limit for these walks. The obtained continuous limit coincides with the physically interesting situation of a massless Dirac fermion propagating in curved spacetime. Since the retained limit procedure is itself dictated by the QWs studied in this article, the geometry appearing in their continuous limit is an intrinsic property of the walks themselves.

The explicit construction of a QW mimicking propagation in and around a black hole shows that it is possible, at least in principle, to simulate by laboratory experiments the propagation of quantum systems in interesting relativistic gravitational fields.

The work presented in this article should naturally be extended in several directions. One should first investigate systematically all QWs on the line defined with a quantum coin acting on a 2D Hilbert space and, for each family of walks, try and determine if and how a continuous limit can be obtained. One should also extend the main result of this article to QWs defined on physical space of higher dimension and/or defined by quantum coins acting on a higher-dimensional Hilbert space. A particular goal would be to obtain walks whose limits are described by a Dirac fermion coupled to both a gravitational and an electromagnetic field.

As noted earlier, the geometry appearing in the continuous limit of the QWs studied in this article is an intrinsic property of these walks and is not to be confused with the geometry the "real", "physical" spacetime which might be used to realize the walk experimentally. Another extension of this work would therefore be to consider walks defined on curved physical spaces (graphs) and to investigate how the geometry of the underlying space (graph) couples to the intrinsic geometry of the walk. This is not a purely academic problem, since QWs can model photon transport in networks of algae, which may have a nontrivial geometry.

The main result of this article also suggests that concepts from general relativity and differential geometry may play a key role in understanding the behavior of QWs on graphs and their use in quantum algorithmics. This role should also be investigated thoroughly.

[1] S. S. Schweber, Rev. Mod. Phys. **58**, 449 (1986).
[2] Y. Aharonov, L. Davidovich, and N. Zagury, Phys. Rev. A **48**, 1687 (1993).
[3] D. A. Meyer, J. Stat. Phys. **85**, 551 (1996).
[4] E. Farhi and S. Gutmann, Phys. Rev. A **58**, 915 (1998).
[5] D. Giulini, E. Joos, C. Kiefer, J. Kupsch, I.-O. Stamatescu, and H. D. Zeh, *Decoherence and the Appearance of a Classical World in Quantum Theory* (Springer-Verlag, Berlin, 1996).
[6] H. B. Perets, Y. Lahini, F. Pozzi, M. Sorel, R. Morandotti, and Y. Silberberg, Phys. Rev. Lett. **100**, 170506 (2008).
[7] A. Ambainis, SIAM J. Comput. **37**, 210 (2007).
[8] F. Magniez, A. Nayak, J. Roland, and M. Santha, *Search via Quantum Walk*, in Proceedings of the Thirty-Ninth Annual ACM Symposium on Theory of Computing (ACM, New York, 2007).
[9] S. Bose, Phys. Rev. Lett. **91**, 207901 (2003).
[10] C. Aslangul, J. Phys. A: Math. Gen. **38**, 1 (2005).
[11] D. Burgarth, Ph.D. thesis, University College London, 2006.
[12] S. Bose, Contemp. Phys. **48**, 13 (2007).
[13] G. S. Engel, T. R. Calhoun, R. L. Read, T.-K. Ahn, T. Manal, Y.-C. Cheng, R. E. Blankenship, and G. R. Fleming, Nature (London) **446**, 782 (2007).
[14] E. Collini, C. Y. Wong, K. E. Wilk, P. M. G. Curmi, P. Brumer, and G. D. Scholes, Nature (Longon) **463**, 644 (2010).
[15] H. Schmitz, R. Matjeschk, C. Schneider, J. Glueckert, M. Enderlein, T. Huber, and T. Schaetz, Phys. Rev. Lett. **103**, 090504 (2009).
[16] F. Zähringer, G. Kirchmair, R. Gerritsma, E. Solano, R. Blatt, and C. F. Roos, Phys. Rev. Lett. **104**, 100503 (2010).
[17] A. Schreiber, K. N. Cassemiro, V. Potoček, A. Gábris, P. J. Mosley, E. Andersson, I. Jex, and C. Silberhorn, Phys. Rev. Lett. **104**, 050502 (2010).
[18] M. Karski *et al.*, Science **325**, 174 (2009).
[19] A. Peruzzo *et al.*, Science **329**, 1500 (2010).
[20] L. Sansoni, F. Sciarrino, G. Vallone, P. Mataloni, A. Crespi, R. Ramponi, and R. Osellame, Phys. Rev. Lett. **108**, 010502 (2012).
[21] B. C. Sanders, S. D. Bartlett, B. Tregenna, and P. L. Knight, Phys. Rev. A **67**, 042305 (2003).
[22] R. P. Feynman and A. R. Hibbs, *Quantum Mechanics and Path Integrals*, International Series in Pure and Applied Physics (McGraw-Hill Book Company, New York, 1965).
[23] P. L. Knight, E. Roldàn, and J. E. Sipe, Phys. Rev. A **68**, 020301 (2003).
[24] Ph. Blanchard and M.-O. Hongler, Phys. Rev. Lett. **92**, 120601 (2004).

[25] F. W. Strauch, Phys. Rev. A **73**, 054302 (2006).
[26] F. W. Strauch, Phys. Rev. A **74**, 030301 (2006).
[27] F. W. Strauch, J. Math. Phys. **48**, 082102 (2007).
[28] A. J. Bracken, D. Ellinas, and I. Smyrnakis, Phys. Rev. A **75**, 022322 (2007).
[29] C. M. Chandrasekhar, S. Banerjee, and R. Srikanth, Phys. Rev. A **81**, 062340 (2010).
[30] G. Di Molfetta and F. Debbasch, J. Math. Phys. **53**, 123302 (2012).
[31] F. Debbasch, G. Di Molfetta, D. Espaze, and V. Foulonneau, Phys. Scr. T **151**, 014044 (2012).
[32] F. Debbasch and G. Di Molfetta, J. Comput. Theor. Nanosci. **10**, 1621 (2013).
[33] A. Sinha and R. Roychoudhury, Int. J. Theor. Phys. **33**, 1511 (1994).
[34] R. Wald, *Gravitation* (University of Chicago Press, Chicago, 1984).
[35] G. Lemaître, Ann. Soc. Sc. Bruxelles A **5**, 51 (1933).

2.3 A synthetic electric gauge field

2.3.1 Publication: "Quantum Walks in artificial electric and gravitational gauge fields."

The following publication represents an extension of the previous one. In the previous section we have seen that QWs can model fermion transport on a curved spacetime and that the gravitational field was characterized, in the continuous limit, by the metric $G(t,x) = \left(1, -\cos^{-2}\theta(t,x)\right)$ where $\theta(t,x)$ is a spacetime dependent parameter of the quantum coin defined in (2.13) and the other parameters are constant.

Furthermore, in the following publication, we explore all the parameters' space of the quantum coin. The walk is therefore characterized by three time- and space-dependent Euler angles (θ,ξ,ζ) and by a global, also time- and space-dependent phase α.

Exploring systematically the QW's stroboscopic equation S^1 and S^2, we prove that this class of QWs exhibits an exact discrete $U(1)$ gauge invariance. Let us consider the local phase transformation

$$\Psi_{jm} \to \Psi_{jm} e^{i\phi_{jm}}, \tag{2.48}$$

where $\{\phi_{jm}, (j,m) \in \mathbb{N}\times\mathbb{Z}\}$.

The finite difference equations of the QWs are left invariant if we replace the parameter of the coin $\{\alpha_{j,m}, \xi_{j,m}, \zeta_{j,m}, \theta_{j,m}\}$ by:

$$\begin{aligned} \alpha_{j,m} &\to \alpha_{j,m} + \frac{\sigma_{j,m}}{2} \\ \xi_{j,m} &\to \xi_{j,m} + \delta_{j,m} \\ \zeta_{j,m} &\to \zeta_{j,m} - \delta_{j,m} \\ \theta_{j,m} &\to \theta_{j,m} \end{aligned} \tag{2.49}$$

where

$$\sigma_{j,m} = \phi_{j,m+1} + \phi_{j,m-1} - 2\phi_{j+1,m} \tag{2.50}$$

$$\delta_{j,m} = \frac{\phi_{j,m+1} - \phi_{j,m-1}}{2}. \tag{2.51}$$

Observe that this discrete gauge invariance transcribes, in the continuous limit, into the standard continuous $U(1)$ gauge invariance of electromagnetism presented in sec. (2.1.2). The electric field generated by the gauge potential in the continuous limit:

$$A(t,x) = (V(t,x), A(t,x)) = \left(\bar{\alpha}(t,x), -\bar{\xi}(t,x)\right), \tag{2.52}$$

is, therefore, closely related to the $U(1)$ discrete gauge invariance of the QW.

Physica A 397 (2014) 157–168

Contents lists available at ScienceDirect

Physica A

journal homepage: www.elsevier.com/locate/physa

Quantum walks in artificial electric and gravitational fields

Giuseppe Di Molfetta [a], Marc Brachet [b], Fabrice Debbasch [a,*]

[a] LERMA, UMR 8112, UPMC and Observatoire de Paris, 61 Avenue de l'Observatoire 75014 Paris, France
[b] Laboratoire de Physique Statistique, Ecole Normale Superieure, UPMC Université Paris 06, Université Paris Diderot, CNRS, 24 rue Lhomond, 75005 Paris, France

HIGHLIGHTS

- The continuous limit of quantum walks on the line is investigated systematically through a new method.
- In all cases but one, the continuous limit coincides with the propagation of a Dirac fermion.
- Inhomogeneities in the walk transcribe as artificial electric and gravitational fields.
- New, state of the art simulations of a quantum walk propagating in an artificial electric field.
- New, state of the art simulations of a quantum walk propagating in and around an artificial black hole.

ARTICLE INFO

Article history:
Received 20 August 2013
Received in revised form 19 November 2013
Available online 9 December 2013

Keywords:
Quantum walks
Artficial gauge fields
Low dimensional physics
Quantum optics

ABSTRACT

The continuous limit of quantum walks (QWs) on the line is revisited through a new, recently developed method. In all cases but one, the limit coincides with the dynamics of a Dirac fermion coupled to an artificial electric and/or relativistic gravitational field. All results are carefully discussed and illustrated by numerical simulations. Possible experimental realizations are also addressed.

1. Introduction

QWs are simple formal analogues of classical random walks. They were first considered by Feynman [1] as possible discretizations of the free Dirac dynamics in flat space–time. They have been introduced in the physics literature by Refs. [2,3] and the continuous-time version first appeared in Ref. [4]. They have been realized experimentally in Refs. [5–12] and are important in many fields, ranging from fundamental quantum physics [12,13] to quantum algorithmics [14,15], solid state physics [16–19] and biophysics [20,21]. Following Feynman's idea, several authors have studied the continuous limit of various QWs. The first publications [22–24,1,25–28] only addressed QWs with constant coefficients and recent work has extended the discussion to QWs with time- and space-dependent coefficients [29–32], in both $(1+1)$ and $(1+2)$ space–time dimensions. In particular, a new method was developed in Refs. [29–32] to investigate the continuous limit of QWs with nonconstant coefficients. This method delivers interesting results, not only for standard QWs, but also for 'derived' QWs obtained from original QWs by keeping only one time-step out of two [32]. So far, this new method has only been applied to particular families of walks. This article presents the systematic application of this method to all QWs in $(1+1)$ space–time dimensions. The main conclusions are: (i) all families of walks do not admit a continuous limit (ii) when the limit exists, it

* Corresponding author. Tel.: +33 144277286; fax: +33 144277287.
E-mail address: fabrice.debbasch@gmail.com (F. Debbasch).

0378-4371/$ – see front matter © 2013 Elsevier B.V. All rights reserved.
http://dx.doi.org/10.1016/j.physa.2013.11.036

coincides, in all cases but one, with the dynamics of a Dirac fermion coupled to an artificial electric field and/or relativistic gravitational field. These theoretical conclusions are illustrated by numerical simulations. Connections with previous results as well as other topics like transport in graphene are discussed and possible experimental realizations are also mentioned.

2. Fundamentals

We consider quantum walks defined over discrete time and discrete one-dimensional space, driven by time- and space-dependent quantum coins acting on a two-dimensional Hilbert space $\mathcal{H}$. The walks are defined by the following finite difference equations, valid for all $(j, m) \in \mathbb{N} \times \mathbb{Z}$:

$$\begin{bmatrix} \psi^L_{j+1,m} \\ \psi^R_{j+1,m} \end{bmatrix} = B\left(\theta_{j,m}, \xi_{j,m}, \zeta_{j,m}, \alpha_{j,m}\right) \begin{bmatrix} \psi^L_{j,m+1} \\ \psi^R_{j,m-1} \end{bmatrix}, \tag{1}$$

where

$$B(\theta, \xi, \zeta, \alpha) = \mathrm{e}^{\mathrm{i}\alpha} \begin{bmatrix} \mathrm{e}^{\mathrm{i}\xi} \cos\theta & \mathrm{e}^{\mathrm{i}\zeta} \sin\theta \\ -\mathrm{e}^{-\mathrm{i}\zeta} \sin\theta & \mathrm{e}^{-\mathrm{i}\xi} \cos\theta \end{bmatrix}. \tag{2}$$

This operator is in $U(2)$, and is in $SU(2)$ only for $\alpha = p\pi,\ p \in \mathbb{Z}$, and θ, ξ and ζ are then called the three Euler angles of B. The index j labels instants and the index m labels spatial points. The two functions ψ^L and ψ^R can be interpreted as the components of a wave function Ψ on a certain orthonormal basis (b_L, b_R) independent of j and m. These two components code for the probability amplitudes of the particle jumping towards the left or towards the right. The total probability $\pi_j = \sum_m \left(|\psi^L_{j,m}|^2 + |\psi^R_{j,m}|^2\right)$ is independent of j, that is, it is conserved by the walk. The set of angles $\left\{\theta_{j,m}, \xi_{j,m}, \zeta_{j,m}, \alpha_{j,m}, (j, m) \in \mathbb{N} \times \mathbb{Z}\right\}$ defines the walks and is at this stage arbitrary.

Consider now, for all $(n, j) \in \mathbb{N}^2$, the collection $W^n_j = (\Psi_{k,m})_{k=nj,\ m\in\mathbb{Z}}$. This collection represents the state of the quantum walk at 'time' $k = nj$. For any given n, the collection $S^n = (W^n_j)_{j\in\mathbb{Z}}$ thus represents the entire history quantum walk observed through a stroboscope of 'period' n. The evolution equations for S^n are those linking W^n_{j+1} to W^n_j for all j. These can be deduced from the original evolution Eqs. (1) and (2) of the walk, which also coincide with the evolution equations of S^1. For example, the evolution equations of S^2 read

$$\begin{aligned} \psi^L_{j+2,m} &= A^L_{j,m}\psi^L_{j,m+2} + B^L_{j,m}\psi^L_{j,m} + C^L_{j,m}\psi^R_{j,m} + D^L_{j,m}\psi^R_{j,m-2} \\ \psi^R_{j+2,m} &= A^R_{j,m}\psi^L_{j,m+2} + B^R_{j,m}\psi^L_{j,m} + C^R_{j,m}\psi^R_{j,m} + D^R_{j,m}\psi^R_{j,m-2}, \end{aligned} \tag{3}$$

where

$$\begin{aligned} A^L_{j,m} &= c_{j+1,m}\, c_{j,m+1}\, \mathrm{e}^{\mathrm{i}(\alpha_{j+1,m}+\xi_{j+1,m}+\alpha_{j,m+1}+\xi_{j,m+1})} \\ B^L_{j,m} &= -s_{j+1,m}\, s_{j,m-1}\, \mathrm{e}^{\mathrm{i}(\alpha_{j+1,m}+\zeta_{j+1,m}+\alpha_{j,m-1}-\zeta_{j,m-1})} \\ C^L_{j,m} &= c_{j+1,m}\, s_{j,m+1}\, \mathrm{e}^{\mathrm{i}(\alpha_{j+1,m}+\xi_{j+1,m}+\alpha_{j,m+1}+\zeta_{j,m+1})} \\ D^L_{j,m} &= s_{j+1,m}\, c_{j,m-1}\, \mathrm{e}^{\mathrm{i}(\alpha_{j+1,m}+\zeta_{j+1,m}+\alpha_{j,m-1}-\xi_{j,m-1})}, \end{aligned} \tag{4}$$

$$\begin{aligned} A^R_{j,m} &= -s_{j+1,m}\, c_{j,m+1}\, \mathrm{e}^{\mathrm{i}(\alpha_{j+1,m}-\zeta_{j+1,m}+\alpha_{j,m+1}+\xi_{j,m+1})} \\ B^R_{j,m} &= -s_{j,m-1}\, c_{j+1,m}\, \mathrm{e}^{\mathrm{i}(\alpha_{j+1,m}-\xi_{j+1,m}+\alpha_{j,m-1}-\zeta_{j,m-1})} \\ C^R_{j,m} &= -s_{j+1,m}\, s_{j,m+1}\, \mathrm{e}^{\mathrm{i}(\alpha_{j+1,m}-\zeta_{j+1,m}+\alpha_{j,m+1}+\zeta_{j,m+1})} \\ D^R_{j,m} &= c_{j,m-1}\, c_{j+1,m}\, \mathrm{e}^{\mathrm{i}(\alpha_{j+1,m}-\xi_{j+1,m}+\alpha_{j,m-1}-\xi_{j,m-1})}, \end{aligned} \tag{5}$$

with $c_{jm} = \cos(\theta_{j,m})$ and $s_{jm} = \sin(\theta_{j,m})$.

The QWs defined by (1) admit a remarkable exact $U(1)$ gauge invariance. Consider indeed an arbitrary set of numbers $\{\phi_{jm}, (j, m) \in \mathbb{N} \times \mathbb{Z}\}$, and write $\Psi_{jm} = \Psi'_{jm} \exp(\mathrm{i}\phi_{jm})$. A straightforward computation shows that Ψ' obeys

$$\begin{bmatrix} \psi'^L_{j+1,m} \\ \psi'^R_{j+1,m} \end{bmatrix} = B\left(\theta'_{j,m}, \xi'_{j,m}, \zeta'_{j,m}, \alpha'_{j,m}\right) \begin{bmatrix} \psi'^L_{j,m+1} \\ \psi'^R_{j,m-1} \end{bmatrix}, \tag{6}$$

with

$$\begin{aligned} \alpha'_{j,m} &= \alpha_{j,m} + \frac{\sigma_{j,m}}{2} \\ \xi'_{j,m} &= \xi_{j,m} + \delta_{j,m} \\ \zeta'_{j,m} &= \zeta_{j,m} - \delta_{j,m} \\ \theta'_{j,m} &= \theta_{j,m} \end{aligned} \tag{7}$$

and

$$\sigma_{j,m} = \phi_{j,m+1} + \phi_{j,m-1} - 2\phi_{j+1,m} \tag{8}$$

$$\delta_{j,m} = \frac{\phi_{j,m+1} - \phi_{j,m-1}}{2}. \tag{9}$$

It can also be shown that the S^2-type QWs admit the same discrete invariance. As detailed in Sections 4 and 5, this discrete gauge invariance transcribes in the continuous limit into the standard continuous $U(1)$ gauge invariance of Maxwell electromagnetism.

To investigate the continuous limit of a collection S^n, we first introduce a time step Δt and a space step Δx. We then consider that Ψ_{jm}, θ_{jm}, ξ_{jm}, ζ_{jm} and α_{jm} are the values taken by a two-component wave function Ψ and by four functions θ, ξ, ζ and α at the space–time point $(t_j = j\Delta t, x_m = m\Delta x)$. Thus, Eq. (1) transcribes into

$$\begin{bmatrix} \psi^L(t_j + \Delta t, x_m) \\ \psi^R(t_j + \Delta t, x_m) \end{bmatrix} = B\left(\theta(t_j, x_m), \xi(t_j, x_m), \zeta(t_j, x_m), \alpha(t_j, x_m)\right) \begin{bmatrix} \psi^L(t_j, x_m + \Delta x) \\ \psi^R(t_j, x_m - \Delta x) \end{bmatrix}. \tag{10}$$

We finally suppose that Ψ and θ are at least twice differentiable with respect to both space and time variables for all sufficiently small values of Δt and Δx. The formal continuous limit of S^n is defined as the couple of partial differential equations (PDEs) obtained from the discrete-time evolution equations defining S^n by letting both Δt and Δx tend to zero.

3. How to determine the continuous limit

Let us introduce a time scale $\mathcal{T}$, a length-scale $\mathcal{L}$, an infinitesimal ϵ and write

$$\begin{aligned} \Delta t &= \epsilon \mathcal{T} \\ \Delta x &= \epsilon^\delta \mathcal{L}, \end{aligned} \tag{11}$$

where $\delta > 0$ allows Δt and Δx to tend to zero differently. We also allow the angles defining the walk to depend on ϵ and characterize the ϵ-dependence of these angles near $\epsilon = 0$ by the following scaling laws:

$$\begin{aligned} \theta_\epsilon(t, x) &= \theta_0(t, x) + \bar{\theta}(t, x)\epsilon^\omega \\ \xi_\epsilon(t, x) &= \xi_0(t, x) + \bar{\xi}(t, x)\epsilon^\beta \\ \zeta_\epsilon(t, x) &= \zeta_0(t, x) + \bar{\zeta}(t, x)\epsilon^\gamma \\ \alpha_\epsilon(t, x) &= \alpha_0(t, x) + \bar{\alpha}(t, x)\epsilon^\eta, \end{aligned} \tag{12}$$

where the four exponents ω, β, γ and η are all positive. We also suppose that all functions are at least C^2 in t and x. The above relations define 1-jets of quantum walks. We finally denote by $\mathcal{B}_\epsilon(t, x)$ the matrix $B(\theta_\epsilon(t, x), \xi_\epsilon(t, x), \zeta_\epsilon(t, x), \alpha_\epsilon(t, x))$.

Expand now the original discrete equations obeyed by a jet S^n_ϵ around $\epsilon = 0$. A necessary and sufficient condition for the expansion to be self-consistent at order 0 in ϵ is that $\mathcal{B}^n_0(t, x) = 1$ for all t and x (note from Eq. (1) that this condition is self-evident for $n = 1$). This transcribes into a constraint for the zeroth-order angles θ_0, ξ_0, ζ_0, α_0.

Suppose this constraint is satisfied. The differential equations defining the continuous limit are obtained from the expansion by stating that the next lowest order contribution in ϵ identically vanishes. If one excepts zeroth-order terms, the terms of lowest order in the expansion scale as ϵ, ϵ^δ, ϵ^ω, ϵ^β, ϵ^γ, ϵ^η (see for example the similar expansions performed on particular simple quantum walks and presented in Refs. [30,31]). The richest and most interesting scaling is thus $\delta = \omega = \beta = \gamma = \eta = 1$, because this makes all the above terms of the same order and, thus, delivers a differential equation with a maximum number of contributions. This scaling will be retained in the remainder of this article.

Note that Eqs. (11) and (12) have actually very different meanings. Indeed, (11) states that the relative variations of Ψ between $j + 1$, m and j, $m \pm 1$ should be small, while (12) states that the angles defining the walk do not deviate much from their zeroth-order values.

We will now present in detail the continuous limit of the jets S^n_ϵ for both $n = 1$ and $n = 2$.

4. Limit of S^1_ϵ

4.1. Zeroth-order values of the angles

The constraint on the zeroth-order angles reads

$$\begin{aligned} &\sin\theta_0 = 0 \\ &e^{i(\alpha_0+\xi_0)}\cos\theta_0 = 1 \\ &e^{i(\alpha_0-\xi_0)}\cos\theta_0 = 1. \end{aligned} \tag{13}$$

The above relations imply $\theta_0 = k\pi$, $\alpha_0 = (k + k_+ + k_-)\pi$, $\xi_0 = (k_+ - k_-)\pi$, $(k, k_+, k_-) \in \mathbb{Z}^3$. The angle ζ_0 does not enter this constraint and is therefore an arbitrary function of t and x. For a given value of ϵ, there is thus no meaningful distinction between ζ_0 and ζ. We will therefore from here on denote ζ_0 by ζ in all equations, if only to simplify the notation.

4.2. Equations of motion

Let now $T = t/\mathcal{T}$, $X = x/\mathcal{L}$, $x^{\pm} = (T \pm X)/2$ and $\partial_{\pm} = \partial_{x^{\pm}} = \partial_T \pm \partial_X$. The variables $x^{\pm}$ are null coordinates in the flat $2D$ space–time. With these notations, the equations of motion for the continuous limit of S^1_ϵ read

$$\begin{aligned}
&\partial_- \psi^L - \mathrm{i}(\bar{\alpha} + \bar{\xi})\psi^L = +\bar{\theta}\mathrm{e}^{\mathrm{i}(\theta_0+\alpha_0+\zeta)}\psi^R \\
&\partial_+ \psi^R - \mathrm{i}(\bar{\alpha} - \bar{\xi})\psi^R = -\bar{\theta}\mathrm{e}^{\mathrm{i}(\theta_0+\alpha_0-\zeta)}\psi^L,
\end{aligned} \tag{14}$$

where θ_0 and α_0 are arbitrary multiples of π (see the constraint above) and ζ is an arbitrary real function of T and X.

Taken together, these two coupled first-order PDEs form a Dirac equation in $(1+1)$ dimensions. Let us recall that, in flat two-dimensional space–times, the Clifford algebra can be represented by 2×2 matrices acting on two-component spinors. This algebra admits two independent generators γ^0 and γ^1, which can be represented by 2×2 matrices obeying the usual anti-commutation relation

$$\{\gamma^a, \gamma^b\} = 2\eta^{ab}\mathbb{1}, \tag{15}$$

where η is the Minkowski metric and $\mathbb{1}$ is the identity (unit) matrix. Consider the representation $\gamma^0 = \sigma_1$ and $\gamma^1 = -\sigma_1\sigma_3 = \mathrm{i}\sigma_2$, where σ_1, σ_2 and σ_3 are the three Pauli matrices:

$$\sigma_1 = \begin{bmatrix} 0 & 1 \\ 1 & 0 \end{bmatrix}, \qquad \sigma_2 = \begin{bmatrix} 0 & -\mathrm{i} \\ \mathrm{i} & 0 \end{bmatrix}, \qquad \sigma_3 = \begin{bmatrix} 1 & 0 \\ 0 & -1 \end{bmatrix}. \tag{16}$$

Eq. (14) can be recast in the following compact form:

$$(\mathrm{i}\gamma^0 D_0 + \mathrm{i}\gamma^1 D_1 - \mathcal{M})\Psi = 0, \tag{17}$$

where $D_\mu = \partial_\mu - \mathrm{i}A_\mu$, $\partial_0 = \partial_T$, $\partial_1 = \partial_X$, $A_0 = \bar{\alpha}$, $A_1 = -\bar{\xi}$, $\mathcal{M} = \mathrm{diag}\,(m^-, m^+)$ and $m^{\mp} = \pm\mathrm{i}\,\bar{\theta}\exp\{\mathrm{i}(\theta_0 + \alpha_0 \pm \zeta)\}$.

This equation describes the propagation in flat space–time of a Dirac spinor coupled to the Maxwell potential A (the corresponding electric field is $E_X = \partial_T\bar{\xi} - \partial_X\bar{\alpha}$). The discrete gauge invariance presented in Section 2 degenerates accordingly into the standard local $U(1)$ invariance associated with electromagnetism. Indeed, suppose that the numbers ϕ_{jm} (see Section 2) are the values taken by a function ϕ at space–time points $(t_j = j\Delta t, x_m = m\Delta x)$. Expanding Eqs. (7) and (9) at first order in ϵ delivers

$$\begin{aligned}
\alpha' &= \alpha - \epsilon\,\frac{\partial\phi}{\partial T} \\
\xi' &= \xi + \epsilon\,\frac{\partial\phi}{\partial X} \\
\zeta' &= \zeta - \epsilon\,\frac{\partial\phi}{\partial X} \\
\theta' &= \theta.
\end{aligned} \tag{18}$$

The first two equations imply

$$\begin{aligned}
A'_0 &= \frac{1}{\epsilon}\left(\alpha' - \alpha_0\right) = \frac{1}{\epsilon}\left(\alpha - \epsilon\,\frac{\partial\phi}{\partial T} - \alpha_0\right) = A_0 - \frac{\partial\phi}{\partial T} \\
A'_1 &= \frac{1}{\epsilon}\left(\xi_0 - \xi'\right) = \frac{1}{\epsilon}\left(\xi_0 - \epsilon\,\frac{\partial\phi}{\partial X} - \xi\right) = A_X - \frac{\partial\phi}{\partial X},
\end{aligned} \tag{19}$$

which are simply the standard gauge transformation for the potential A. The fourth relation implies that the mass tensor $\mathcal{M}$ is gauge invariant. Since the continuous limit equation of motion (14) depends only on ζ_0 (as opposed to ζ), the third equation is not relevant to the continuous limit investigated in this section.

The angles θ_0 and α_0 are both multiples of π. Both masses are therefore complex conjugates of each other. They are real, and therefore identical, if ζ_0 is an uneven multiple of $\pi/2$. They are both real and positive, equal to $|\bar{\theta}|$, if $\zeta_0 = \theta_0 + \alpha_0 + \bar{\sigma} + (2p+1)\pi/2$, where $\exp(\mathrm{i}\bar{\sigma}) = \mathrm{sgn}\,\bar{\theta}$ is the sign of $\bar{\theta}$ and p is an arbitrary integer. Note that, even in this case, the mass may depend on both T and X.

5. Limit of S^2_ϵ

5.1. Zeroth-order values of the angles

The constraint on the zeroth-order angles now reads

$$\begin{aligned}
&\cos\xi_0 \sin(2\theta_0) = 0 \\
&\mathrm{e}^{2\mathrm{i}\alpha_0}\left(\mathrm{e}^{2\mathrm{i}\xi_0}\cos^2\theta_0 - \sin^2\theta_0\right) = 1 \\
&\mathrm{e}^{2\mathrm{i}\alpha_0}\left(\mathrm{e}^{-2\mathrm{i}\xi_0}\cos^2\theta_0 - \sin^2\theta_0\right) = 1.
\end{aligned} \tag{20}$$

As for $n = 1$, ζ_0 does enter this constraint; it is therefore an arbitrary function of t and x, which we denote simply by ζ (see the discussion at the end of Section 4.1).

The first relation implies that $\cos\xi_0 = 0$ (case 1) or $\sin 2\theta_0 = 0$ (case 2). The first case corresponds to $\xi_0 = (2k+1)\pi/2$, $k \in \mathbb{Z}$. The second and third relations then transcribe into the single constraint $\alpha_0 = (2k'+1)\pi/2$, with $k' \in \mathbb{Z}$. Note that θ_0 can then be an arbitrary function of t and x, as ζ_0. This function will be simply denoted by θ, just as ζ denotes ζ_0.

In contrast, the second case corresponds to $\theta_0 = k\pi/2,\ k \in \mathbb{Z}$. If $k = 2p+1,\ p \in \mathbb{Z}$ (case 2.1), the last two constraint relations deliver $\alpha_0 = (2k'+1)\pi/2$, with $k' \in \mathbb{Z}$. The angle ξ_0 is then arbitrary and will be denoted simply by ξ. If $k = 2p$ (case 2.2), the last two constraint relations deliver $\alpha_0 = k'\pi/2$, $\xi_0 = \alpha_0 + k''\pi$, $(k',\ k'') \in \mathbb{Z}^2$.

Cases 1, 2.1 and 2.2 partly overlap. Indeed, jets obeying $\theta_0 = k\pi,\ \xi_0 = (2k+1)\pi/2$ and $\alpha_0 = (2k'+1)\pi/2$ can be field under both case 1 and case 2. These are the only jets which can be field under both cases.

Let us now give the equations of motion of the continuous limit in cases 1, 2.1 and 2.2.

5.2. Equations of motion: case 1

$$\begin{aligned}
&2\left(\partial_T - (\cos^2\theta)\partial_X\right)\psi^L - 2\mathrm{i}\left(\bar\alpha + (\cos^2\theta)\bar\xi\right)\psi^L - \mathrm{e}^{+\mathrm{i}(\zeta-\xi_0)}(\sin 2\theta)\partial_X\psi^R \\
&\quad = \left(-(\sin 2\theta)(\partial_X\theta) + \mathrm{i}(\sin^2\theta)(\partial_+\zeta)\right)\psi^L \\
&\qquad + \mathrm{e}^{+\mathrm{i}(\xi_0+\zeta)}\left(\mathrm{i}(\partial_-\zeta)\frac{\sin 2\theta}{2} - \mathrm{i}\bar\xi(\sin 2\theta) + (\partial_T\theta) - (\partial_X\theta)(\cos 2\theta)\right)\psi^R
\end{aligned} \tag{21}$$

and

$$\begin{aligned}
&2\left(\partial_T + (\cos^2\theta)\partial_X\right)\psi^R - 2\mathrm{i}\left(\bar\alpha - (\cos^2\theta)\bar\xi\right)\psi^R - \mathrm{e}^{-\mathrm{i}(\zeta-\xi_0)}(\sin 2\theta)\partial_X\psi^L \\
&\quad = \left(+(\sin 2\theta)(\partial_X\theta) - \mathrm{i}(\sin^2\theta)(\partial_-\zeta)\right)\psi^R \\
&\qquad + \mathrm{e}^{-\mathrm{i}(\xi_0+\zeta)}\left(\mathrm{i}(\partial_+\zeta)\frac{\sin 2\theta}{2} - \mathrm{i}\bar\xi(\sin 2\theta) - (\partial_T\theta) - (\partial_X\theta)(\cos 2\theta)\right)\psi^L.
\end{aligned} \tag{22}$$

These equations can be put into the more compact form

$$\partial_T\Psi + (\cos\theta)P\partial_X\Psi = Q\Psi, \tag{23}$$

where $\Psi = \psi^L b_L + \psi^R b_R$,

$$P = \begin{pmatrix} -\cos\theta & -\mathrm{e}^{+\mathrm{i}(\zeta-\xi_0)}\sin\theta \\ -\mathrm{e}^{-\mathrm{i}(\zeta-\xi_0)}\sin\theta & \cos\theta \end{pmatrix} \tag{24}$$

and

$$Q = \begin{pmatrix} Q_L^L & Q_R^L \\ Q_L^R & Q_R^R \end{pmatrix} \tag{25}$$

with

$$\begin{aligned}
Q_L^L &= \mathrm{i}\left(\bar\alpha + (\cos^2\theta)\bar\xi\right) - \frac{\sin 2\theta}{2}(\partial_X\theta) + \frac{\mathrm{i}}{2}(\sin^2\theta)(\partial_+\zeta) \\
Q_R^R &= \mathrm{i}\left(\bar\alpha - (\cos^2\theta)\bar\xi\right) + \frac{\sin 2\theta}{2}(\partial_X\theta) - \frac{\mathrm{i}}{2}(\sin^2\theta)(\partial_-\zeta) \\
Q_R^L &= \frac{\mathrm{e}^{+\mathrm{i}(\xi_0+\zeta)}}{2}\left(\mathrm{i}(\partial_-\zeta)\frac{\sin 2\theta}{2} - \mathrm{i}\bar\xi(\sin 2\theta) + (\partial_T\theta) - (\partial_X\theta)(\cos 2\theta)\right) \\
Q_L^R &= \frac{\mathrm{e}^{-\mathrm{i}(\xi_0+\zeta)}}{2}\left(\mathrm{i}(\partial_+\zeta)\frac{\sin 2\theta}{2} - \mathrm{i}\bar\xi(\sin 2\theta) - (\partial_T\theta) - (\partial_X\theta)(\cos 2\theta)\right).
\end{aligned} \tag{26}$$

The operator P is self-adjoint and its eigenvalues are -1 and $+1$. Two eigenvectors associated with these eigenvalues are

$$b_- = \left(\cos\frac{\theta}{2}\right)b_L + \mathrm{e}^{\mathrm{i}(-\zeta+\xi_0)}\left(\sin\frac{\theta}{2}\right)b_R, \tag{27}$$

$$b_+ = \left(\sin\frac{\theta}{2}\right)\mathrm{e}^{\mathrm{i}(\zeta+\xi_0)}b_L + \left(\cos\frac{\theta}{2}\right)b_R. \tag{28}$$

The family (b_-, b_+) forms an orthonormal basis of the two-dimensional spin Hilbert space, alternate to the original basis (b_L, b_R). Let $\Psi = \psi^- b_- + \psi^+ b_+$. Eq. (23) transcribes into

$$\begin{aligned}
&\partial_T \psi^- - (\cos\theta)\partial_X \psi^- - \mathrm{i}\bar{\alpha}\psi^- - \mathrm{i}\cos\theta\bar{\xi}\psi^- + \frac{\mathrm{i}}{2}((\cos\theta - 1)\partial_+\zeta)\psi^- + \frac{\partial_X\theta}{2}(\sin\theta)\,\psi^- = 0\\
&\partial_T \psi^+ + (\cos\theta)\partial_X \psi^+ - \mathrm{i}\bar{\alpha}\psi^+ + \mathrm{i}\cos\theta\bar{\xi}\psi^+ - \frac{\mathrm{i}}{2}((\cos\theta - 1)\partial_-\zeta)\psi^+ - \frac{\partial_X\theta}{2}(\sin\theta)\,\psi^+ = 0.
\end{aligned} \tag{29}$$

Suppose now, to make the discussion definite, that $\cos\theta$ is strictly positive and introduce in space–time $\{(T, X)\}$ the Lorentzian, possibly curved metric G defined by its covariant components

$$(G_{\mu\nu}) = \begin{pmatrix} 1 & 0 \\ 0 & -\dfrac{1}{\cos^2\theta} \end{pmatrix}, \tag{30}$$

where $(\mu, \nu) \in \{T, X\}^2$. This metric defines the canonical, scalar 'volume' element $\mathcal{D}_G X = \sqrt{-G}\,\mathrm{d}X = \mathrm{d}X/\cos\theta$ in physical 1D X-space, where G is the determinant of the metric components $G_{\mu\nu}$. Dirac spinors are normalized to unity with respect to $\mathcal{D}_G X$, whereas Ψ is normalized to unity with respect to $\mathrm{d}X$. We thus introduce $\Phi = \Psi\sqrt{\cos\theta}$ and rewrite the equations of motion (29) in terms of Φ. We obtain

$$\gamma^a \left[e_a^\mu D_\mu \Phi + \frac{1}{2}\frac{1}{\sqrt{-G}}\,\partial_\mu\left(\sqrt{-G}e_a^\mu\right)\Phi \right] = 0, \tag{31}$$

where $\mu \in \{T, X\}$, $a \in \{0, 1\}$ and $D_\mu = \partial_\mu - \mathrm{i}A_\mu$ with

$$A_T = \bar{\alpha} + \frac{1 - \cos\theta}{2}\,\partial_X\zeta \tag{32}$$

and

$$A_X = -\bar{\xi} - \frac{1 - \cos\theta}{2\cos\theta}\,\partial_T\zeta. \tag{33}$$

The usual $2D$ gamma matrices are

$$\gamma^0 = \begin{pmatrix} 0 & 1 \\ 1 & 0 \end{pmatrix}, \qquad \gamma^1 = \begin{pmatrix} 0 & 1 \\ -1 & 0 \end{pmatrix}, \tag{34}$$

and the e_a^μ are the components of the dyad (orthonormal basis) $e_0 = e_T$ and $e_1 = \cos\theta\, e_X$ on the original coordinate basis (e_T, e_X). Eq. (31) is the standard [33] equation of motion for a massless Dirac spinor propagating in $(1 + 1)$-dimensional space–time under the combined influence of the gravitational field G and the electric field E deriving from A. Since the Dirac field is massless, its components are not coupled and evolve independently of each other. Each component follows a null geodesic of the gravitational field, and the electric field only modifies the energy along a given geodesic. Numerical simulations of a QW propagating radially in the gravitational field of a Schwarzschild black hole are presented in Section 6.3.

Let us conclude this section by commenting briefly on how the discrete gauge invariance presented in Section 2 transcribes in the present context. The continuous limit equation (18) is of course valid. Combining these with (32), (33) and keeping only the lowest order terms in ϵ leads to the standard gauge transformation $A_0' = A_0 - \partial\phi/\partial T$ and $A_1' = A_1 - \partial\phi/\partial X$. Just as it was the case in Section 4, the transformation law for ζ does not contribute to the continuous gauge transformation, but it is not for the same reason. In Section 4, the potential A itself does not depend on ζ. Here, the potential A does depend on ζ, but the gauge transformation for ζ generates terms of order ϵ in the gauge transformation for A, and these terms vanish as ϵ tends to zero. In the present context, the final, fourth equation in (18) reflects the fact that the gravitational field does not depend on the choice of gauge for the phase of the spinor Ψ.

5.3. Equations of motion: case 2.1

The equations of motion of the continuous limit read

$$\begin{aligned}
&2\partial_T \psi^L - 2\mathrm{i}\bar{\alpha}\psi^L = +\mathrm{i}(\partial_+\zeta)\psi^L + 2\bar{\theta}\mathrm{e}^{+\mathrm{i}\zeta}(\cos\xi)\,\psi^R\\
&2\partial_T \psi^R - 2\mathrm{i}\bar{\alpha}\psi^R = -\mathrm{i}(\partial_-\zeta)\psi^R - 2\bar{\theta}\mathrm{e}^{-\mathrm{i}\zeta}(\cos\xi)\,\psi^L,
\end{aligned} \tag{35}$$

where ξ and ζ are arbitrary functions of T and X. These equations are not PDEs, but *ordinary* differential equations (ODEs) in $\psi^\pm$. Thus, there is for example no propagation in this case. Technically, this comes from the fact that θ_0 is here constrained to be an uneven multiple of $\pi/2$.

5.4. Equations of motion: case 2.2

The equations of motion read

$$2\partial_- \psi^L - 2\mathrm{i}\left(\bar{\alpha} + \bar{\xi}\right)\psi^L = +2\bar{\theta}\mathrm{e}^{\mathrm{i}(2\alpha_0+\zeta)}(\cos\xi_0)\psi^R$$
$$2\partial_+ \psi^R - 2\mathrm{i}\left(\bar{\alpha} - \bar{\xi}\right)\psi^R = -2\bar{\theta}\mathrm{e}^{\mathrm{i}(2\alpha_0-\zeta)}(\cos\xi_0)\psi^L, \tag{36}$$

where α_0 is a multiple of $\pi/2$, $\xi_0 - \alpha_0$ is multiple of π and ζ is an arbitrary function of T and X. Eq. (36) can be recast in the following compact form:

$$(\mathrm{i}\gamma^0 D_0 + \mathrm{i}\gamma^1 D_1 - \mathcal{M})\Psi = 0 \tag{37}$$

where $D_\mu = \partial_\mu - \mathrm{i}A_\mu$, $\partial_0 = \partial_T$, $\partial_1 = \partial_X$, $A_0 = \bar{\alpha}$, $A_1 = -\bar{\xi}$, $\mathcal{M} = \mathrm{diag}\,(m^-, m^+)$ and $m^\mp = \pm\mathrm{i}\,\bar{\theta}\exp\{\mathrm{i}(2\alpha_0 \pm \zeta)\}\,(\cos\xi_0)$. This equation describes the propagation in flat space–time of a Dirac spinor Ψ coupled to the potential A and with a mass tensor $\mathcal{M}$.

6. Numerical simulations

6.1. Basics

In order to ascertain the validity of the continuous limits that were derived above, we wish to compare numerical solutions of the QW defined by the finite difference Eqs. (1) and (2) with the corresponding Dirac-type PDEs defined by Eqs. (31) and (17).

While the numerical integration of the QW finite difference equations poses no particular problem, controlling the error on numerical solutions of PDEs is a more involved matter. This hurdle can be avoided in the special case where the mass terms cancels, because one can then compare the numerical solutions of the QW finite difference equations with the numerical solutions of the ODEs defining the *characteristics* of the massless Dirac PDE (see Section 6.3).

We have chosen to use Fourier pseudo-spectral methods [34], for their precision and ease of implementation. We therefore restrict ourselves to 2π-periodic boundary conditions. A generic field $\psi(x)$ is thus evaluated on the n collocation points $x_j = 2\pi j/n$, with $j = 0, n-1$ as $\psi_j = \psi(x_j)$. The discrete Fourier transforms are standardly defined as

$$\psi(x_j) = \sum_{k=-n/2}^{n/2-1} \exp(\mathrm{i}kx_j)\hat{\psi}_k$$
$$\hat{\psi}_k = \frac{1}{n}\sum_{j=0}^{n-1} \psi(x_j)\exp(-\mathrm{i}kx_j). \tag{38}$$

These sums can be evaluated in only $n\log(n)$ operations by using Fast Fourier Transforms (FFTs). Spatial derivatives of fields are evaluated in spectral space by multiplying by i k and products are evaluated in physical space.

The original QW Eqs. (1) and (2) can also be simply cast in this setting, as the translation operator $\psi_j \to \psi_{j\pm1}$ is represented in Fourier space by $\hat{\psi}_k \to \hat{\psi}_k \exp(\pm\mathrm{i}\,k2\pi/n)$. In this setting, the continuous limit is automatically taken when n is increased.

6.2. QWs in constant a uniform electric field

As explained in Section 2, the QWs and the Dirac equation exhibit a $U(1)$ gauge invariance. All choices of gauge thus correspond to the same physics. Within a pseudo-spectral code, the right gauge to work with a $1D$ constant uniform electric field E is $A_0 = 0$, $A_1 = -E\,T$; in particular, the other 'natural choice' $A_0 = -E\,X$, A_1 breaks the spatial periodicity condition. In all QW simulations, the retained choice of gauge has been implemented by choosing the following numerical values:

$$\alpha(T, X) = 0$$
$$\xi(T, X) = 1.1\,T$$
$$\zeta(T, X) = \frac{\pi}{2}$$
$$\theta(T, X) = 0.24.$$

We used initial data consisting of Gaussian wave packets of positive energy solutions to the free Dirac equation. The Gaussian widths σ_X are such that they are well resolved within the used resolutions so that spectral convergence is ensured.

As discussed above (see end of Section 6.1) the QW and its Dirac continuous limit can be jointly simulated within the same pseudo-spectral algorithm. This allows for a very simple, direct evaluation of the discrepancy between the QW and the corresponding solution of the Dirac equation. This discrepancy can be measured by the relative difference δN_{rel} between the density of the QW and the density of the solution of the Dirac equation.

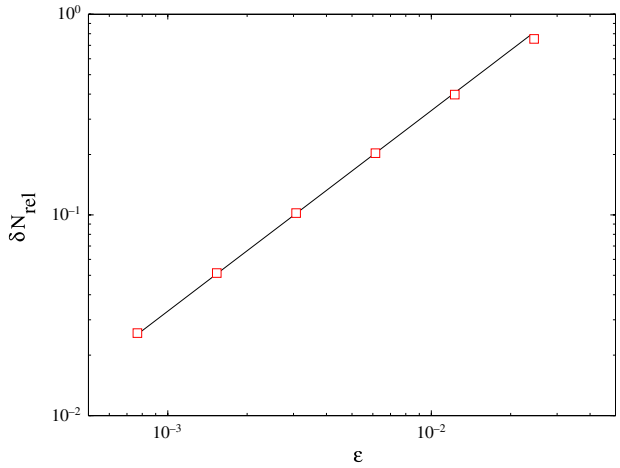

Fig. 1. Relative difference between the density of the QW and the density of the solution of the Dirac equation $\delta N_{\text{rel}} = \sqrt{< (N_{QW} - N_D)^2 >} / < (N_D) >$ plotted at $T = 100$ versus $\epsilon = \Delta X$ in Log–Log representation. We have plotted the relative difference in the same conditions as in Fig. 2(a) but for five different resolutions (i.e. value of ϵ): from the left $n = 2^8, 2^9, 2^{10}, 2^{11}, 2^{12}, 2^{13}$. The solid black line represents the expected ϵ^1 scaling.

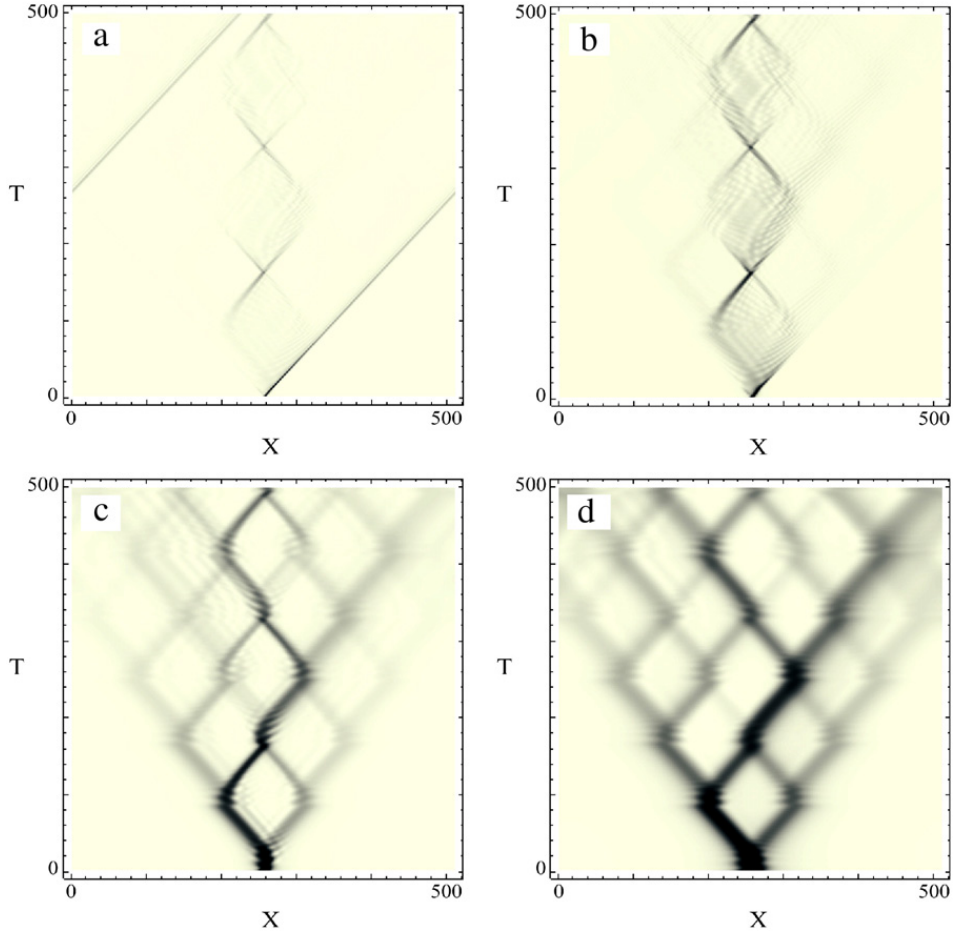

Fig. 2. Quantum simulation of Eqs. (1) and (2) representing a Dirac particle in a constant and static electric background (see Section 4.2 and Eq. (39)). The initial condition is a Gaussian wave packet of positive energy solutions with width $\sigma_X = 0.005$ in (a), 0.01 in (b), 0.03 in (c), 0.08 in (d) and resolution $n = 2^9$.

Fig. 1 shows that such a typical relative difference scales as ϵ, as expected. Indeed, for a single time-step, the discrepancy is theoretically of order ϵ^2. Thus, after a *fixed time* $T = O(\epsilon^{-1})$, the discrepancy is of order $\epsilon^{-1}\epsilon^2 = \epsilon$.

This result confirms that QWs can be used to simulate Dirac dynamics in constant electric field, as was done for example in Refs. [35,36]. Both QW and Dirac dynamics are very rich, as exemplified by Fig. 2, which compare with Fig. 2 of Ref. [35] and Fig. 3 of Ref. [36].

Note that, as σ_X increases, the spatial dispersion of the wave packet also increases which makes the time evolution of the density more complex. The solution which is initially a positive energy planar wave starts to oscillate between positive and negative modes under the action of the constant electric field displaying high-frequency Zitterbewegung in Fig. 2(c)–(d). Offering new results of the Dirac dynamics in the presence of an electric field is not the purpose of this article. Let us conclude this section by offering instead a brief historical overview of the very large literature already existing on the topic.

In 1929, Klein studied a relativistic scalar particle moving in an external step function potential. He found a paradox that, in the case of a strong potential, the reflected flux is larger than the incident flux although the total flux is conserved [37]. Sauter studied this problem for a Dirac spin 1/2 particle by considering a potential corresponding to a electric field with constant value E_0 on a given interval. He found an expression for the transmission coefficient of the wave through the electric potential barrier from the negative energy state to positive energy states [38]. This remarkable phenomenon was related, in 1936, to positron–electron pair creations by Heisenberg and his student Hans Euler [39].

Of course, in order to deal with anti-particles a massive reinterpretation of the Dirac equation theory is necessary [40], leading to modern field theory and quantum electrodynamics. The modern formula for pair creation in a constant external electric field was delivered, in 1951, by Schwinger [41]. It involves the same dominant exponential term $\exp(-\pi \frac{m_e^2 c^3}{\hbar e E})$ that was derived, 20 years before, by Sauter. A detailed review of these historical developments is given in the first sections of Ref. [42].

6.3. QWs in Schwarzschild black hole

A Schwarzschild black hole is a spherically symmetric solution of the Einstein equation in vacuo. The corresponding 4*D* metric reads, in dimensionless Lemaître coordinates $(\tau, \rho, \theta, \phi)$ [43]:

$$\mathrm{d}s^2 = \mathrm{d}\tau^2 - \frac{r_g}{r}\,\mathrm{d}\rho^2 - r^2\mathrm{d}\Omega, \tag{39}$$

where $r(\tau, \rho) = r_g^{1/3}\left[\frac{3}{2}(\rho - \tau)\right]^{2/3}$, $\mathrm{d}\Omega = \mathrm{d}\theta^2 + (\sin^2\theta)\mathrm{d}\phi^2$. The event horizon is located at $r = r_g$, that is, $\rho = \tau + (2/3)r_g$, and the singularity is located at $r = 0$ *i.e.* $\rho = \tau$. The exterior of the black hole is the domain $r > r_g$. The range of variations for the Lemaître coordinates is $\tau \geq 0$, $\rho \geq \tau$, that is, $r(\tau, \rho) \geq 0$), $0 \leq \theta \leq \pi$, $0 \leq \phi < 2\pi$.

Because of the spherical symmetry, a point mass which starts its motion radially will go on moving radially. Radial motion can be studied by introducing the 2*D* metric g, also singular at $r = 0$, with covariant components $g_{\tau\tau} = 1, g_{\rho\rho} = -r_g/r, g_{\tau\rho} = g_{\rho\tau} = 0$. The null geodesics of g are defined by $\mathrm{d}\tau = \pm\left(r_g/r(\tau, \rho)\right)^{1/2}\mathrm{d}\rho$. Note that the 2*D* projection of the horizon on the (τ, ρ)-plane coincides with a null geodesics of g.

We now identify the dimensionless time T with the time coordinate τ and the dimensionless space variable X with $\lambda\rho$, where λ is an arbitrary strictly positive real number (see Fig. 3). The 'radius' r can then be expressed as a function of T and X:

$$r(T, X) = \left[\frac{3}{2}\left(\frac{X}{\lambda} - T\right)\right]^{2/3} r_g^{1/3}, \tag{40}$$

and the components of g in the coordinate basis associated to T and X are $g_{TT} = 1, g_{XX} = -r_g/(\lambda^2 r), g_{TX} = g_{XT} = 0$. Note that the condition $\rho \geq \tau$ transcribes into $X \geq \lambda T$.

Let $\mathcal{D}$ be the domain where $-g_{XX} \geq 1$. This domain is characterized, in (T, X) coordinates, by the condition

$$X \leq \lambda T + \frac{2}{3\lambda^2}\, r_g. \tag{41}$$

In $\mathcal{D}$ the metric g can be identified with the metric G (see Eq. (30)). This identification defines an angle θ which depends on T and X by

$$(\cos\theta)(T, X) = \lambda\sqrt{\frac{r(T, X)}{r_g}}. \tag{42}$$

A QW in $\mathcal{D}$ can be defined by complementing this choice of *theta* by a choice of the other three angles. All simulations were done with

$$\begin{aligned} \alpha(T, X) &= 0 \\ \xi(T, X) &= \pi \\ \zeta(T, X) &= \frac{\pi}{2}. \end{aligned} \tag{43}$$

This QW has already been considered in Ref. [32].

The condition defining $\mathcal{D}$ can be rewritten as $r \leq r_g/\lambda^2$, The domain $\mathcal{D}$ thus includes, for all λ, the singularity located at $r = 0$. For $\lambda > 1$, $r_g/\lambda^2 < r_g$ and $\mathcal{D}$ is then entirely located inside the horizon. For $\lambda = 1$, $\mathcal{D}$ coincides with the interior of the horizon, and $\mathcal{D}$ extends outside the horizon for $\lambda < 1$.

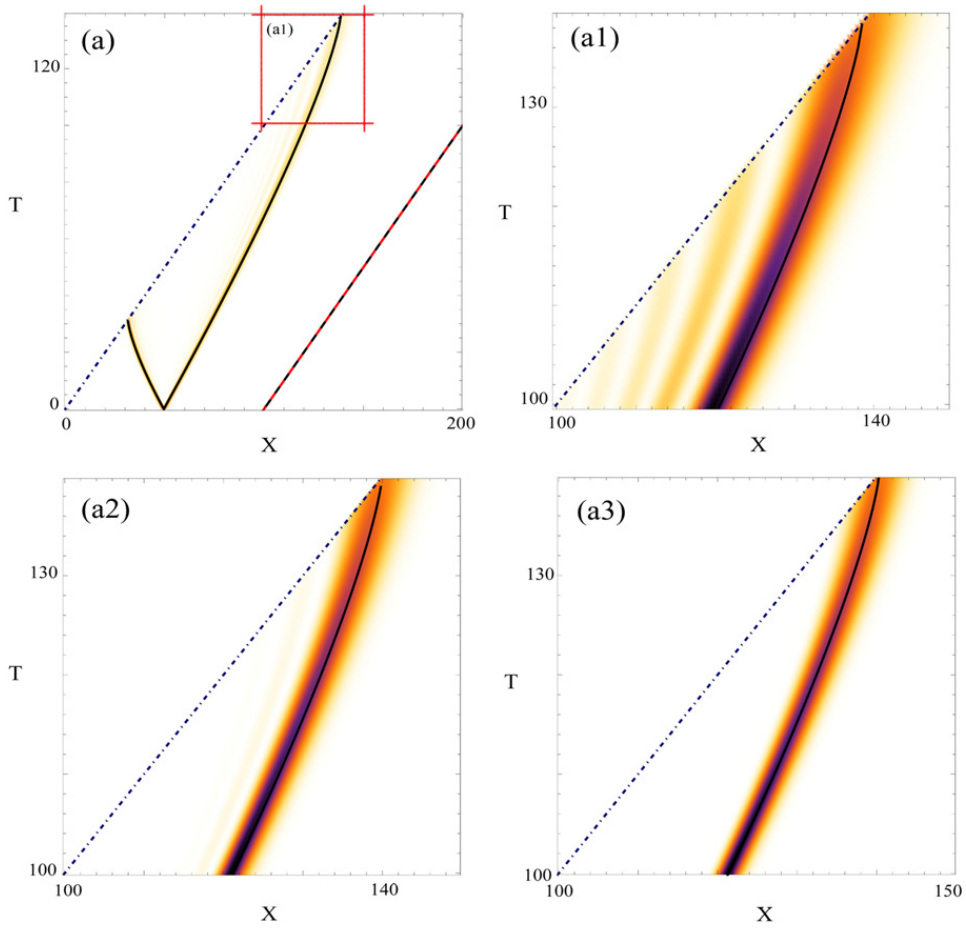

Fig. 3. (Color online) Time evolution density of the QW vs. null geodesics (solid curves) of the 2D Schwarzschild metric with $\lambda = 1$. The initial condition is $\Psi(0, X) = \sqrt{N_0}(X)(b_L + Ib_R)$ with an initial Gaussian density N_0 of $\sigma_X = 0.5$ centered on $X_0 = 50.5$. The singularity is represented by the dotted and dashed line on the left and the horizon (which is a null geodesic) is represented by the dashed line. The two branches of the QW which starts inside the horizon end up on the singularity. The (red) solid line represents the limit of the definition domain $\mathcal{D}$ of the QW. In (a1) note that the right branch of the QW lags slightly behind the null geodesic when approaching the $r = 0$ singularity. The agreement between the geodesics and the density profile of the walk gets better as we increase the resolution of the simulation: 200 gridpoints in (a1), 800 in (a2) and 1600 in (a3).

Ref. [32] offers plots of the spatial density $|\Psi(T, X)|^2$ for several initial conditions. These plots confirm that the QW follows to a great accuracy the radial null geodesics of the Schwarzschild metric, except perhaps as the QW approaches the singularity. This phenomenon is explored in detail by Fig. 3. The plots reveal the existence of interesting 'interferences' near the singularity (see (a1) and (a2)), which seem to disappear as ϵ tends to zero.

7. Conclusion

We have revisited the continuous limit of discrete time QWs on the line, keeping every step or only one step out of two. We have identified all families of walks which admit a continuous limit and obtained the associated PDEs. In all cases but one, the PDE describes the propagation of a Dirac fermion coupled to an electric field and, possibly, to a general relativistic gravitational field. We have also illustrated these conclusions by new numerical simulations.

Let us now briefly discuss the above results.

As mentioned in the introduction, all above literal computations are based on a new method first introduced in Refs. [30–32,29]. New to this article is all the material presented in Section 5. The Dirac equation obtained in Section 4 has already been presented in Refs. [30–32,29], but without the important discussion of the $U(1)$ gauge invariance. The discrete gauge invariance presented in Section 2 is also new. Let us mention in this context that QWs coupled to a uniform and constant electric field have also been considered theoretically and experimentally in Refs. [44,45]. These so-called 'electric walks' are particular cases of the walks considered in Refs. [30–32,29] and in Section 4 of the present article. In Ref. [44], the constant and uniform electric field is put by hand on the equations of motion of the walks. In contrast, the approach developed in the present article makes it clear that the electric field is simply a manifestation of the time-and space-dependence of the angles defining the walks. This approach also allows for a straightforward generalization to nonconstant and/or nonuniform electric fields (Sections 4 and 5), and to gravitational fields 5. The electric and gravitational fields coupled top the QWs thus clearly appear as synthetic gauge fields [46].

Experiments with time- and space-dependent coins are now possible thanks to at least two recently developed techniques [47,48]. For example, one can use integrated waveguide circuits [47] where the quantum coin and step operator at a given point and time corresponds to a precise beamsplitter that can be individually set. These techniques could be used to implement experiments where arbitrary electric and/or gravitational fields are simulated by properly choosing the time- and space-dependence of the angles α, ξ and θ.

The work presented in this article should be extended in several directions. One should first determine how the new method works, and what it delivers, when one keeps only one step out of n for arbitrary $n > 2$. Extensions to higher dimensional space and/or to higher dimensional Hilbert space are also desirable. In particular, the fact that some QWs on the line can be interpreted as the propagation of charged massless Dirac fermions suggests that QWs could be useful in modeling charge transport in graphene [49,50], both natural and artificial [51,52]. Let us note that the inherent discreteness would give QWs a strong computational advantage over the more traditional models based on PDEs. Finally, determining systematically the continuous limit of nonlinear QWs [53] and of walks in random media [54] should also prove interesting.

References

[1] R.P. Feynman, A.R. Hibbs, Quantum Mechanics and Path Integrals, in: International Series in Pure and Applied Physics, McGraw-Hill Book Company, 1965.
[2] Y. Aharonov, L. Davidovich, N. Zagury, Quantum random walks, Phys. Rev. A 48 (1993) 1687.
[3] D.A. Meyer, From quantum cellular automata to quantum lattice gases, J. Stat. Phys. 85 (1996).
[4] E. Farhi, S. Gutmann, Quantum computation and decision trees, Phys. Rev. A 58 (1998) 915.
[5] H. Schmitz, R. Matjeschk, Ch. Schneider, J. Glueckert, M. Enderlein, T. Huber, T. Schaetz, Quantum walk of a trapped ion in phase space, Phys. Rev. Lett. 103 (9) (2009) 090504.
[6] F. Zähringer, G. Kirchmair, R. Gerritsma, E. Solano, R. Blatt, C.F. Roos, Realization of a quantum walk with one and two trapped ions, Phys. Rev. Lett. 104 (2010) 100503.
[7] A. Schreiber, K.N. Cassemiro, A. Gábris, V. Potoček, P.J. Mosley, E. Andersson, I. Jex, Ch. Silberhorn, Photons walking the line, Phys. Rev. Lett. 104 (5) (2010) 050502.
[8] Michal Karski, Leonid Förster, Jai-Min Cho, Andreas Steffen, Wolfgang Alt, Dieter Meschede, Artur Widera, Quantum walk in position space with single optically trapped atoms, Science 325 (5937) (2009) 174–177.
[9] Alberto Peruzzo, Mirko Lobino, Jonathan C.F. Matthews, Nobuyuki Matsuda, Alberto Politi, Konstantinos Poulios, Xiao-Qi Zhou, Yoav Lahini, Nur Ismail, Kerstin Wörhoff, Yaron Bromberg, Yaron Silberberg, Mark G. Thompson, Jeremy L. OBrien, Quantum walks of correlated photons, Science 329 (5998) (2010) 1500–1503.
[10] L. Sansoni, F. Sciarrino, G. Vallone, P. Mataloni, A. Crespi, R. Ramponi, R. Osellame, Two-particle bosonic-fermionic quantum walk via 3D integrated photonics, Phys. Rev. Lett. 108 (1) (2012) 010502.
[11] B.C. Sanders, S.D. Bartlett, B. Tregenna, P.L. Knight, Two-particle bosonic-fermionic quantum walk via 3D integrated photonics, Phys. Rev. A 67 (2003) 042305.
[12] B. Perets, Y. Lahini, F. Pozzi, M. Sorel, R. Morandotti, Y. Silberberg, Realization of quantum walks with negligible decoherence in waveguide lattices, Phys. Rev. Lett. 100 (2008) 170506.
[13] D. Giulini, E. Joos, C. Kiefer, J. Kupsch, I.-O. Stamatescu, H.D. Zeh, Decoherence and the Appearance of a Classical World in Quantum Theory, Springer-Verlag, Berlin, 1996.
[14] A. Ambainis, Quantum walk algorithm for element distinctness, SIAM J. Comput. 37 (2007) 210–239.
[15] F. Magniez, J. Roland, A. Nayak, M. Santha, Search via quantum walk, in: SIAM Journal on Computing—Proceedings of the Thirty-Ninth Annual ACM Symposium on Theory of Computing, ACM, New York, 2007.
[16] C. Aslangul, Quantum dynamics of a particle with a spin-dependent velocity, J. Phys. A 38 (2005) 1–16.
[17] S. Bose, Quantum communication through an unmodulated spin chain, Phys. Rev. Lett. 91 (2003) 207901.
[18] D. Burgarth, Quantum state transfer with spin chains, University College London, Ph.D. Thesis, 2006.
[19] S. Bose, Quantum communication through spin chain dynamics: an introductory overview, Contemp. Phys. 48 (1) (2007) 13–30.
[20] E. Collini, C.Y. Wong, K.E. Wilk, P.M.G. Curmi, P. Brumer, G.D. Scholes, Coherently wired light-harvesting in photosynthetic marine algae at ambient temperature, Nature 463 (2010) 644.
[21] G.S. Engel, T.R. Calhoun, R.L. Read, T.-K. Ahn, T. Manal, Y.-C. Cheng, R.E. Blankenship, G.R. Fleming, Evidence for wavelike energy transfer through quantum coherence in photosynthetic systems, Nature 446 (2007) 782.
[22] A.J. Bracken, D. Ellinas, I. Smymakis, Free-dirac-particle evolution as a quantum random walk, Phys. Rev. A 75 (2007) 022322.
[23] Ph. Blanchard, M.-O. Hongler, Quantum random walks and piecewise deterministic evolutions, Phys. Rev. Lett. 92 (2004) 120601-1–120601-4.
[24] C.M. Chandrasekhar, S. Banerjee, R. Srikanth, Relationship between quantum walks and relativistic quantum mechanics, Phys. Rev. A 81 (2010) 062340.
[25] P.L. Knight, E. Roldàn, J.E. Sipe, Quantum walk on the line as an interference phenomenon, Phys. Rev. A 68 (2003) 020301.
[26] F.W. Strauch, Relativistic quantum walks, Phys. Rev. A 73 (2006) 054302.
[27] F.W. Strauch, Relativistic effects and rigorous limits for discrete-time and continuous-time quantum walks, J. Math. Phys. 48 (2007) 082102.
[28] F.W. Strauch, Connecting the discrete- and continuous-time quantum walks, Phys. Rev. A 74 (2006) 030301.
[29] F. Debbasch, G. Di Molfetta, D. Espaze, V. Foulonneau, Propagation in quantum walks and relativistic diffusions, Phys. Scr. 151 (2012) 014044.
[30] G. Di Molfetta, F. Debbasch, Discrete-time quantum walks: continuous limit and symmetries, J. Math. Phys. 53 (2012) 123302.
[31] G. Di Molfetta, F. Debbasch, Discrete-time quantum walks: continuous limit in $1+1$ and $1+2$ dimension, J. Comput. Theor. Nanosci. 10 (7) (2012) 1621–1625.
[32] G. Di Molfetta, F. Debbasch, M. Brachet, Quantum walks as massless dirac fermions in curved space, Phys. Rev. A 88 (2013).
[33] A. Sinha, R. Roychoudhury, Dirac equation in (1 + 1)-dimensional curved space–time, Int. J. Theor. Phys. 33 (1994) 1511–1522.
[34] D. Gottlieb, S.A. Orszag, Numerical Analysis of Spectral Methods, SIAM, Philadelphia, 1977.
[35] D. Witthaut, Quantum walks and quantum simulations with Bloch-oscillating spinor atoms, Phys. Rev. A 82 (2010) 033602.
[36] S. Longhi, Bloch–zener quantum walk, J. Phys. B: At. Mol. Opt. Phys. 45 (2010) 225504.
[37] O. Klein, Die reflexion von elektronen an einem potentialsprung nach der relativistischen dynamik von Dirac, Z. Phys. 53 (3–4) (1929) 157–165.
[38] Fritz Sauter, Über das verhalten eines elektrons im homogenen elektrischen feld nach der relativistischen theorie Diracs, Z. Phys. 69 (11–12) (1931) 742–764.
[39] W. Heisenberg, H. Euler, Folgerungen aus der diracschen theorie des positrons, Z. Phys. 98 (11–12) (1936) 714–732.
[40] J.D. Bjorken, S.D. Drell, Relativistic Quantum Mechanics, in: International Series in Pure and Applied Physics, McGraw-Hill, 1964.
[41] Julian Schwinger, On gauge invariance and vacuum polarization, Phys. Rev. 82 (1951) 664–679.
[42] Remo Ruffini, Gregory Vereshchagin, She-Sheng Xue, Electron–positron pairs in physics and astrophysics: from heavy nuclei to black holes, Phys. Rep. 487 (1–4) (2010) 1–140.
[43] G. Lemaître, L'univers en expansion, Ann. Soc. Sci. Brux. A 53 (1933) 51–85.

[44] M. Genske, W. Alt, A. Steffen, A.H. Werner, R.F. Werner, D. Meschede, A. Alberti, Electric quantum walks with individual atoms, Phys. Rev. Lett. 110 (2013) 190601.
[45] C. Cedzich, T. Rybár, A.H. Werner, A. Alberti, M. Genske, R.F. Werner, Propagation of quantum walks in electric fields, Phys. Rev. Lett. 111 (2013) 160601.
[46] J. Dalibard, F. Gerbier, G. Juzeliūnas, P. Öhberg, Artificial gauge potential for neutral atoms, Rev. Modern Phys. 83 (2010) 1523.
[47] A. Crespi, R. Osellame, R. Ramponi, V. Giovannetti, R. Fazio, L. Sansoni, F. De Nicola, F. Sciarrino, P. Mataloni, Anderson localization of entangled photons in an integrated quantum walk, Nat. Photonics 7 (2013) 322–328.
[48] A. Schreiber, A. Gábris, P.P. Rohde, K. Laiho, M. Štefaňák, V. Potocek, C. Hamilton, I. Jex, C. Silberhorn, A 2D quantum walk simulation of two-particle dynamics, Science 336 (2012) 55.
[49] K.S. Novoselov, A.K. Geim, S.V. Morozov, D. Jiang, M.I. Katsnelson, I.V. Grigorieva, S.V. Dubonos, A.A. Firsov, Two-dimensional gas of massless dirac fermions in graphene, Nature 438 (2005) 197–200.
[50] D.C. Elias, R.V. Gorbachev, A.S. Mayorov, S.V. Morozov, A.A. Zhukov, P. Blake, L.A. Ponomarenko, I.V. Grigorieva, K.S. Novoselov, F. Guinea, A.K. Geim, Dirac cones reshaped by interaction effects in suspended graphene, Nature 7 (2011) 701–704.
[51] M. Polini, F. Guinea, M. Lewenstein, H.C. Manoharan, V. Pelligrini, Artificial honeycomb lattices for electrons, atoms and photons, Nat. Nanotechnol. 8 (2013) 625–633.
[52] T. Uehlinger, G. Jotzu, M. Messer, D. Greif, W. Hofstetter, U. Bissbort, T. Esslinger, Artificial graphene with tunable interactions, Phys. Rev. Lett. 111 (2013) 185307.
[53] C. Navarrete-Benlloch, A. Perez, Eugenio Roldan, Nonlinear optical galton board, Phys. Rev. A 75 (2010) 062333.
[54] C.M. Chandrashekar, Th. Busch, Quantum percolation and anderson transition point for transport of a two-state particle, 2013. ArXiv Preprint arXiv:1303.7013.

Bibliography

[1] F. Albertini and D. D'Alessandro. Analysis of quantum walks with time-varying coin on d-dimensional lattices. *Journal of Mathematical Physics*, 50(12):122106, 2009. doi: http://dx.doi.org/10.1063/1.3271109. URL http://scitation.aip.org/content/aip/journal/jmp/50/12/10.1063/1.3271109.

[2] P. M. Alsing, J. P. Dowling, and G. Milburn. Ion trap simulations of quantum fields in an expanding universe. *Physical review letters*, 94(22):220401, 2005.

[3] P. Arrighi, S. Facchini, and M. Forets. Discrete lorentz covariance for quantum walks and quantum cellular automata. *New Journal of Physics*, 16(9):093007, 2014.

[4] P. Arrighi, S. Facchini, and M. Forets. Quantum walks in curved spacetime. *arXiv preprint*, 1505.07023, 2015.

[5] M. C. Banuls, C. Navarrete, A. Perez, E. Roldan, and J. C. Soriano. Quantum walk with a time-dependent coin. *Phys. Rev. A*, 73:062304, Jun 2006. doi: 10.1103/PhysRevA.73.062304. URL http://link.aps.org/doi/10.1103/PhysRevA.73.062304.

[6] N. D. Birrell and P. C. W. Davies. *Quantum fields in curved space*. Number 7. Cambridge university press, 1984.

[7] O. Boada, A. Celi, J. Latorre, and M. Lewenstein. Dirac equation for cold atoms in artificial curved spacetimes. *New Journal of Physics*, 13(3):035002, 2011.

[8] N. Boulanger, P. Spindel, and F. Buisseret. Bound states of dirac particles in gravitational fields. *Physical Review D*, 74(12):125014, 2006.

[9] D. R. Brill and J. A. Wheeler. Interaction of neutrinos and gravitational fields. *Reviews of Modern Physics*, 29(3):465, 1957.

[10] J. D. Brown, M. Henneaux, and C. Teitelboim. Black holes in two spacetime dimensions. *Phys. Rev. D*, 33:319–323, Jan 1986. doi: 10.1103/PhysRevD.33.319. URL http://link.aps.org/doi/10.1103/PhysRevD.33.319.

[11] T. Byrnes and Y. Yamamoto. Simulating lattice gauge theories on a quantum computer. *Physical Review A*, 73(2):022328, 2006.

[12] J. Cai, A. Retzker, F. Jelezko, and M. B. Plenio. A large-scale quantum simulator on a diamond surface at room temperature. *Nature Physics*, 9(3):168–173, 2013.

[13] B. Carter and R. McLenaghan. Generalized total angular momentum operator for the dirac equation in curved space-time. *Physical Review D*, 19(4):1093, 1979.

[14] C. Cedzich, T. Rybar, A. H. Werner, A. Alberti, M. Genske, and R. F. Werner. Propagation of quantum walks in electric fields. *Phys. Rev. Lett.*, 111:160601, Oct 2013. doi: 10.1103/PhysRevLett.111.160601. URL http://link.aps.org/doi/10.1103/PhysRevLett.111.160601.

[15] D. D'Alessandro, G. Parlangeli, and F. Albertini. Non-stationary quantum walks on the cycle. *Journal of Physics A: Mathematical and Theoretical*, 40(48):14447, 2007. URL http://stacks.iop.org/1751-8121/40/i=48/a=010.

[16] G. Di Molfetta, F. Debbasch, and M. Brachet. Quantum walks as massless dirac fermions in curved space. *Phys. Rev. A*, 88, 2013.

[17] G. Di Molfetta, F. Debbasch, and F. Brachet. Quantum walks in artificial electric and gravitational fields. *Phys. A*, 397, 2014.

[18] J. Du, N. Xu, X. Peng, P. Wang, S. Wu, and D. Lu. Nmr implementation of a molecular hydrogen quantum simulation with adiabatic state preparation. *Physical review letters*, 104(3):030502, 2010.

[19] A. Einstein. Riemannian geometry with maintaining the notion of distant parallelism. *Session Report of the Prussian Academy of Sciences*, pages 217–221, 1928.

[20] R. P. Feynman. Simulating physics with computers. *International journal of theoretical physics*, 21 (6):467–488, 1982.

[21] R. P. Feynman. Quantum mechanical computers. *Foundations of physics*, 16(6):507–531, 1986.

[22] S. A. Fulling. *Aspects of quantum field theory in curved spacetime*, volume 17. Cambridge university press, 1989.

[23] I. Georgescu, S. Ashhab, and F. Nori. Quantum simulation. *Reviews of Modern Physics*, 86(1):153, 2014.

[24] R. Gerritsma, B. Lanyon, G. Kirchmair, F. Zähringer, C. Hempel, J. Casanova, J. J. García-Ripoll, E. Solano, R. Blatt, and C. F. Roos. Quantum simulation of the klein paradox with trapped ions. *Physical review letters*, 106(6):060503, 2011.

[25] M. Grajcar, S. Van der Ploeg, A. Izmalkov, E. Il?ichev, H.-G. Meyer, A. Fedorov, A. Shnirman, and G. Schön. Sisyphus cooling and amplification by a superconducting qubit. *Nature physics*, 4(8): 612–616, 2008.

[26] B. Horstmann, B. Reznik, S. Fagnocchi, and J. I. Cirac. Hawking radiation from an acoustic black hole on an ion ring. *Physical review letters*, 104(25):250403, 2010.

[27] J. C. Howell and J. A. Yeazell. Linear optics simulations of the quantum baker?s map. *Physical Review A*, 61(1):012304, 1999.

[28] B. Ivanov. Electrically induced gravity in two dimensions. *Physics Letters A*, 210(4–5):255 – 257, 1996. ISSN 0375-9601. doi: http://dx.doi.org/10.1016/0375-9601(95)00918-3. URL http://www.sciencedirect.com/science/article/pii/0375960195009183.

[29] B. Ivanov. Gravitational effects in a spherical solenoid. *Modern Physics Letters A*, 12(05):285–294, 1997.

[30] N. Konno. Localization of an inhomogeneous discrete-time quantum walk on the line. *Quantum Information Processing*, 9(3):405–418, 2010. ISSN 1570-0755. doi: 10.1007/s11128-009-0147-4. URL http://dx.doi.org/10.1007/s11128-009-0147-4.

[31] N. Konno, T. Luczak, and E. Segawa. Limit measures of inhomogeneous discrete-time quantum walks in one dimension. *Quantum Information Processing*, 12(1):33–53, 2013. ISSN 1570-0755. doi: 10.1007/s11128-011-0353-8. URL http://dx.doi.org/10.1007/s11128-011-0353-8.

[32] B. P. Lanyon, J. D. Whitfield, G. Gillett, M. E. Goggin, M. P. Almeida, I. Kassal, J. D. Biamonte, M. Mohseni, B. J. Powell, M. Barbieri, et al. Towards quantum chemistry on a quantum computer. *Nature Chemistry*, 2(2):106–111, 2010.

[33] A. Lasenby, C. Doran, and S. Gull. Gravity, gauge theories and geometric algebra. *Philosophical Transactions of the Royal Society of London A: Mathematical, Physical and Engineering Sciences*, 356(1737):487–582, 1998.

[34] J. Li, M. Silveri, K. Kumar, J.-M. Pirkkalainen, A. Vepsäläinen, W. Chien, J. Tuorila, M. Sillanpää, P. Hakonen, E. Thuneberg, et al. Motional averaging in a superconducting qubit. *Nature communications*, 4:1420, 2013.

[35] N. Linden and J. Sharam. Inhomogeneous quantum walks. *Phys. Rev. A*, 80:052327, Nov 2009. doi: 10.1103/PhysRevA.80.052327. URL http://link.aps.org/doi/10.1103/PhysRevA.80.052327.

[36] R. B. Mann and S. F. Ross. Gravitation and cosmology in (1+1)-dimensional dilaton gravity. *Phys. Rev. D*, 47:3312–3318, Apr 1993. doi: 10.1103/PhysRevD.47.3312. URL http://link.aps.org/doi/10.1103/PhysRevD.47.3312.

[37] R. B. Mann, S. M. Morsink, A. E. Sikkema, and T. G. Steele. Semiclassical gravity in 1+1 dimensions. *Phys. Rev. D*, 43:3948–3957, Jun 1991. doi: 10.1103/PhysRevD.43.3948. URL http://link.aps.org/doi/10.1103/PhysRevD.43.3948.

[38] F. Mei, V. M. Stojanović, I. Siddiqi, and L. Tian. Analog superconducting quantum simulator for holstein polarons. *Physical Review B*, 88(22):224502, 2013.

[39] N. C. Menicucci, S. J. Olson, and G. J. Milburn. Simulating quantum effects of cosmological expansion using a static ion trap. *New Journal of Physics*, 12(9):095019, 2010.

[40] A. Mezzacapo, J. Casanova, L. Lamata, and E. Solano. Digital quantum simulation of the holstein model in trapped ions. *Physical review letters*, 109(20):200501, 2012.

[41] M. Montero. Invariance in quantum walks with time-dependent coin operators. *Phys. Rev. A*, 90:062312, Dec 2014. doi: 10.1103/PhysRevA.90.062312. URL http://link.aps.org/doi/10.1103/PhysRevA.90.062312.

[42] S. M. Morsink and R. B. Mann. Black hole radiation of dirac particles in 1+1 dimensions. *Classical and Quantum Gravity*, 8(12):2257, 1991. URL http://stacks.iop.org/0264-9381/8/i=12/a=010.

[43] C. Negrevergne, R. Somma, G. Ortiz, E. Knill, and R. Laflamme. Liquid-state nmr simulations of quantum many-body problems. *Physical Review A*, 71(3):032344, 2005.

[44] L. Parker. One-electron atom in curved space-time. *Physical Review Letters*, 44(23):1559, 1980.

[45] M. E. Peskin and D. V. Schroeder. *An introduction to quantum field theory*. Westview, 1995.

[46] P. Ribeiro, P. Milman, and R. Mosseri. Aperiodic quantum random walks. *Phys. Rev. Lett.*, 93:190503, Nov 2004. doi: 10.1103/PhysRevLett.93.190503. URL http://link.aps.org/doi/10.1103/PhysRevLett.93.190503.

[47] H. Sandler. Artificial gravity. *Acta Astronautica*, 35(4-5):363 – 372, 1995. ISSN 0094-5765. doi: http://dx.doi.org/10.1016/0094-5765(95)98737-T. URL http://www.sciencedirect.com/science/article/pii/009457659598737T. Countermeasures: Extending Manned Spaceflight.

[48] F. L. Semião and M. Paternostro. Quantum circuits for spin and flavor degrees of freedom of quarks forming nucleons. *Quantum Information Processing*, 11(1):67–75, 2012.

[49] Y. Shikano and H. Katsura. Localization and fractality in inhomogeneous quantum walks with self-duality. *Phys. Rev. E*, 82:031122, Sep 2010. doi: 10.1103/PhysRevE.82.031122. URL http://link.aps.org/doi/10.1103/PhysRevE.82.031122.

[50] A. E. Sikkema and R. B. Mann. Gravitation and cosmology in (1+1) dimensions. *Classical and Quantum Gravity*, 8(1):219, 1991. URL http://stacks.iop.org/0264-9381/8/i=1/a=022.

[51] A. Sinha and R. Roychoudhury. Dirac equation in (1+1)-dimensional curved space-time. *International Journal of Theoretical Physics*, 33(7):1511–1522, 1994. ISSN 0020-7748. doi: 10.1007/BF00670693. URL http://dx.doi.org/10.1007/BF00670693.

[52] S.Succi, F. Fillion-Gourdeau, and S. Palpacelli. Quantum lattice boltzmann is a quantum walk. *arXiv preprint*, 1504.03158, 2015.

[53] C. Tseng, S. Somaroo, Y. Sharf, E. Knill, R. Laflamme, T. F. Havel, and D. G. Cory. Quantum simulation with natural decoherence. *Physical Review A*, 62(3):032309, 2000.

[54] A. Wallraff, D. I. Schuster, A. Blais, L. Frunzio, R.-S. Huang, J. Majer, S. Kumar, S. M. Girvin, and R. J. Schoelkopf. Strong coupling of a single photon to a superconducting qubit using circuit quantum electrodynamics. *Nature*, 431(7005):162–167, 2004.

[55] Y. S. Weinstein, S. Lloyd, J. Emerson, and D. G. Cory. Experimental implementation of the quantum baker?s map. *Physical review letters*, 89(15):157902, 2002.

[56] H. Weyl. Gravitation and electricity. *Sitzungsber. Konigl. Preuss. Akad. Wiss.*, 26:465–480, 1918.

[57] J. Yepez. Einstein's vierbein field theory of curved space. *arXiv preprint arXiv:1106.2037*, 2011.

[58] E. Zohar, J. I. Cirac, and B. Reznik. Quantum simulations of gauge theories with ultracold atoms: Local gauge invariance from angular-momentum conservation. *Physical Review A*, 88(2):023617, 2013.

CHAPTER 3

QUANTUM WALKS, DECOHERENCE AND RANDOM SYNTHETIC GAUGE FIELD

Summary

3.1 Quantum Decoherence: An introduction 69
3.2 Quantum Walks and decoherence 70
3.2.1 An overview 70
3.2.2 A qualitative picture 72
3.2.3 Projections cause spin and spatial decoherence 74
3.3 Publication : "Discrete-time Quantum Walks in random artificial Gauge Fields." 75

3.1 Quantum Decoherence: An introduction

There is no room for a real collapse in the purely unitary models of measurements (Neumann, 1932)

The study of quantum decoherence, a milestone of quantum theory, is a relatively young subject. The *Copenhagen interpretation* has been predominant in the first half of 20th century based on a strict distinction between the classical *macroscopic* world and the *microscopic* quantum realm [30]. The border between those two worlds has been unclear for a long time in that period and the debate about the nature of transition from one to the other pertained more to the philosophical domain than to the physical or mathematical one. The main problem concerned the duality inherent in the quantum theory's axioms. According to them there are two ways for the state of a quantum system to change: unitary evolution, which is *deterministic* and reversible, and measurement, which is *probabilisitic* and not reversible. Each of them obeys to two different dynamical laws, and the discontinuity in-between is marked by a sudden collapse of the wave function on one of the eigenstates of the system. All this led people to suspect that quantum theory was not complete [7].

The interaction between a single quantum system and both the classical environment and the frontier quantum/classical physics is still an hard puzzling problem. In a seminal paper Schrödinger [35] illustrated this mechanism through the paradox of an imaginary cat which exists in a superposition of dead and alive states. He coined the term *Verschränkung* (the entanglement) as the result of the interaction between the macroscopic apparatus and the microscopic system. In contemporary physics, decoherence is still based on this latter idea. The physical system S is entangled with the environment $\mathcal{E}$ that encode the informon about

some "monitored" states of S. The *cat states* are defined as the superposition of these states. Schrödinger's *cat states* and quantum decoherence have been widely investigated in several theoretical and experimental seminal works [27, 39, 33, 15, 10].

The first mathematical treatment of quantum decoherence has been proposed by von Neumann [28], who postulated that the measurement bring about the quantum system into a statistical mixture in some "preferred" basis, corresponding to the eigenvalues of the measured observable. Once the system is in this "mixture", the information about the system can be described by classical probability.
The foundations of the theoretical contemporary approach were laid by H.D. Zeh and W. H. Zurek. Between 1970s and 1980s they contributed to build a complete theory on the emergence of classicality in the framework of open quantum systems ([38]).

Following [42], the idea that the openness of quantum systems might have anything to do with the transition from quantum to classical was ignored for a very long time. Even though Gottfried [17] anticipated some later developments and Zeh [40, 41] ventured saying that it was not possible to isolate a macroscopic quantum system, the understanding of "how the environment distills the classical essence from quantum systems" [42] has been reached much more recently.

The decoherence mechanism has been widely investigated in recent years, and within the outline of physical systems it has been the focus of various experimental setups. However, far to be simply a fundamental problem, decoherence represents today the key obstacle to the realization of quantum computers [24]. In order to minimize the effects of decoherence on a *qubit*, we should minimize the interaction of these systems with the environment, while keeping it sufficiently open to permit quantum operations. In order to prolong the characteristic time of decoherence, quantum physics researchers have developed several techniques and schemes, such as the active quantum error correction [25, 14] or the environment engineering [37, 11]. Furthermore, new controllable quantum systems have been built to better understand decoherence and quantum entanglement. Among these new actors, we should cite QA and among them the QWs. Let us recall that the interest upon these new quantum systems is twofold: (i) they are versatile tools to reproduce a wide variety of quantum complex dynamics and (ii) they play today a fundamental role in the development of quantum computing.

3.2 Quantum Walks and decoherence

3.2.1 An overview

We have seen in the first two chapters that QWs belong to a very rich and complex class of coherent quantum dynamics with a wide variety of applications in quantum computing, quantum transports and quantum simulations. Now let us affirme that QWs dynamics are unitary and completely reversible, and that they show ballistic behaviors. However, the loss of quantum coherence due to a breakdown of unitarity, turns into diffusive behaviors or in some particular cases into anomalous diffusion [32]. Non unitarity may be caused by a byproduct of some other operations (such as a measurement/projection operation) or by the unwanted interaction with the environment.

Aharonov et al. [1] were the first to prove that performing orthogonal projections on spin state causes a breakdown of unitarity in QWs dynamics, and to observe that the system behaved asymptotically as a classical system. In particular, he derived asymptotically the expression of the second moment computed on the spatial probability distribution and showed that in contrast to unitary quantum walks, quantum random walks exhibit asymptotically diffusive spreading. After him, a vast literature has numerically and theoretically shown that QWs, in case of loss of quantum coherence, behave asymptotically like classical random walks [21]. However, even when displaying the same spreading behavior asymptotically, the dynamic mechanisms underlying quantum decoherence in QWs may be various. For this reason the variance of the walk can be used as an immediate method to characterize dynamical properties of a decoherent QWs, but it is totally useless to discriminate the different mechanisms of decoherence. Nonetheless, a detailed study on the time evolution of the density profile of decoherent QWs has been developed by Dür et al. [16].

Over the last few years, some important physical implementations have led us to a deeper understanding of decoherent QWs. Karski et al. [20] realized a QW with a single laser-cooled cesium atoms trapped in the potential wells of a 1D optical lattice. Here the coherence of the system was gradually suppressed by coupling internal and external degrees of freedom by diabatic transport. Broome et al. [8] introduced in a single-photon QWs dynamics a controlled amount of decoherence. In the coherent case photons propagated through six calcite beam-displacers perfectly aligned and the tunable decoherence was introduced by an intentional misalignment of QW steps, which introduced a dephasing in the evolution operator of the system. The suppression of interference induced the QWs to fully loose coherence and to behave classically. In another experience, Schreiber et al. [34] introduced decoherence by activating tunable fluctuations in the vertical and horizontal polarization of a coherent diode laser reproducing the QWs unitary dynamics. In such a way they randomize the coin state of the system causing transition to diffusion behavior. The earliest experimental analysis on the different decoherence mechanisms was proposed by Alberti et al. [4]. They proposed how Markovian and non Markovian decoherence act on coin and position state space, and came up with new methods to discriminate between spin and spatial decoherence models by implementing a Hadamard QW in neutral atoms experiment.

Let us observe that the reason to introduce intentionally decoherence in unitary QWs[1] is twofold. On one hand, it allows us to test the robustness of the quantum system in interaction with the environment, to measure the characteristic time of decoherence and to understand the underlying model of decoherence. This can be very useful for experimentalists. On the other, we can qualitatively and quantitatively characterize the transient dynamics between classical and quantum realms by a tunable toy model which is easily reproducible in physical experiences.

Theoretically speaking, there are two ways to model decoherence in QWs dynamics. One is to replace the unitary standard evolution by a nonunitary one, introducing projection operator that are responsible for the damping of the off-diagonal terms of the density matrix [21, 9,

[1] Note that a non-unitary version of QWs was introduced by Attal et al. [5][6]. These QWs, called Open Quantum Walks (OQWs), are formulated directly as quantum Markov chains. OQWs are very useful to model dissipative quantum systems dynamics.

36, 13]. The other way [2, 3, 19, 29], which is developed in the present chapter, consists in randomizing the parameters of the walks in coin or position state space, and then in averaging them (we will present this model in all the details in sec. (3.3)). In many cases both ways appear to be equivalent and in those cases we should be able to move from a formalism to the other. Before presenting both the methods, let us present some useful tools to describe qualitatively the QWs dynamics in presence of decoherence.

3.2.2 A qualitative picture

In modeling quantum decoherence, density matrices play an important role and they formally provide a method to represent the quantum statistics of the system. Let us recall that the *density matrix* is the matrix representation in a particular basis of the density operator $\hat{\rho}$, corresponding to the pure state $|\Psi\rangle$, defined as:

$$\hat{\rho} = |\Psi\rangle\langle\Psi|. \tag{3.1}$$

Suppose that $|\Psi\rangle = \sum_i c_i|\psi_i\rangle$, the density matrix written in basis $\{|\psi_i\rangle\}$ then transcribes in:

$$\hat{\rho} = |\Psi\rangle\langle\Psi| = \sum_{ij} c_i c_j^* |\psi_i\rangle\langle\psi_j|. \tag{3.2}$$

All the elements of the density matrices for which $i \neq j$ encode the coherence of the system between the different components $|\psi_i\rangle$ and are often called *interference terms* or *off-diagonal terms*. These elements tend to vanish when the system behaves classically, and can thus be considered as a measure of the quantumness of the system. In one-dimensional QWs, presented in this chapter, randomizing the coin state destroys the phase coherence - the interference terms - among the components of the state vector.

However, pure states are not sufficient to describe a quantum system in general, in particular when it is not a closed system anymore. In the interaction with the environment, the system looses (or disperses in the environment) information available to the observer. In such a situation we can describe the state as a *mixed state*, i.e. the set of all possible pure states ψ_i with associated classical probabilities p_i. This is therefore a classical ensemble.
The mixed state density matrix encodes the ignorance about the state of the system and reads:

$$\hat{\rho} = \sum_i p_i |\psi_i\rangle\langle\psi_i|. \tag{3.3}$$

The measure of purity of the system is important to characterize the transition from pure to mixed state and to denote the information loss. This measure of the system's "*mixedness*" can be computed as $Tr(\hat{\rho}^2)$ and is bounded from below by $1/d$, where d is the dimensionality of the Hilbert space and from above by 1, in case of pure state.

Another formal way to quantify the loss of information encoded in the initial pure quantum state is the *von Neumann entropy*, introduced by the mathematician in 1927. This measure can be seen as the classical notion of entropy in statistical mechanics and reads:

$$S(\hat{\rho}) = -Tr(\hat{\rho}\log_2\hat{\rho}) = -\sum_i \epsilon_i \log_2 \epsilon_i, \tag{3.4}$$

where ϵ_i denotes the ith eigenvalue of the density matrix. As in classical mechanics, the loss of information is necessarily associated with an increase of entropy.
Let us remark that in case of unitary QWs, we can measure the total entropy as well as the

entanglement entropy between coin state space and position state space. Therefore the entanglement entropy associated to one subsystem is derived from the total entropy tracing over the degree of freedom of the other subsystem:

$$S^r(\hat{\rho}^r) = -Tr(\hat{\rho}^r \log_2 \hat{\rho}^r). \tag{3.5}$$

In particular, as QWs are bipartite system consisting of *position-coin* states, for any Ψ of the system it is possible to find a new bi-orthonormal basis in which the reduced density operators $\hat{\rho}^r$ are both diagonal and share the same eigenvalues. This is possible thanks to the Schmidt decomposition[2] and the basis is called the Schmidt basis. As a consequence of the Schmidt decomposition theorem, the entanglement entropy of the two subsystems are equal. If we consider the entropy of one subsystem, we can use it as a measure of composite system's entanglement. Let us look at for example the trace on the position states:

$$S^r(\hat{\rho}^r_C) = -\sum_\alpha \epsilon^r_\alpha \log_2 \epsilon^r_\alpha, \qquad \alpha = \{c, c'\}, \tag{3.7}$$

where the reduced density matrix $\rho^r_C = \sum_{m=m'} \rho^{c,c'}_{m,m'}$. In an analogous way we can define ρ^r_P, tracing on the coin states. Let us remember that the entanglement entropy always reaches a limiting value depending on the initial state of the coin state. In Fig.3.1 we compute the entanglement entropy of a coherent QW, with a quantum coin B_θ, for different values of θ. We can observe that the entanglement entropy $S^r(\hat{\rho}^r_C)$ (or equivalently $S^r(\hat{\rho}^r_P)$) admits an absolute maximum for θ=$\pi/4$ when the largest part of the probability is uniformly spread. It admits a minimum for θ=$\pi/2$ and θ=0 when the particle propagates without interference.

If the system is subject to decoherence the entanglement entropies of the subsystems are in general no longer identical and the total entropy and the entropy of the subsystems increase.

An alternative way to investigate the breakdown of unitarity is represented by the Wigner function, introduced recently by Hinarejos et al. [18] and independently by Alberti et al. [4] for discrete time QWs. This formalism is advantageous in studying several quantum mechanical aspects of QWs and their dynamical behaviors in the quantum-to-classical transition. In contrast to the density matrix approach, this method permits to investigate various mechanisms underlying the loss of coherence, which are more understandable in phase space than in position space [26]. In order to define the Wigner function let us introduce a simple QW in a one dimensional lattice with two internal states represented by the density operator $\hat{\rho}$. The Wigner function $W^{c,c'}_m(k)$, as introduced in [4] reads :

$$W^{c,c'}_m(k) = \frac{1}{\pi} \int_{\frac{-\pi}{2}}^{\frac{\pi}{2}} dk' e^{-2ik'x} \langle k-k', c|\hat{\rho}|k+k', c'\rangle, \tag{3.8}$$

where the moments $k \in \mathbb{R}$. The standard probability in position and in momentum space is simply recovered by computing the marginals of the Wigner function:

$$|\Psi_m|^2 = \sum_{c,c'} \int_{-\infty}^{\infty} dk W^{c,c'}_m(k) \qquad |\Psi(k)|^2 = \sum_{c,c'} \sum_m W^{c,c'}_m(k). \tag{3.9}$$

[2]Theorem: (Schmidt decomposition) Suppose $|\Psi\rangle$ is a pure state a composite system AB. Then there exist orthonormal states $|i_A\rangle$ for system A, and orthonormal states $|i_B\rangle$ of system B such that:

$$|\psi\rangle = \sum_i \lambda_i |i_A\rangle |i_B\rangle \tag{3.6}$$

where the coefficients λ_i are non-negative real numbers satisfying $\sum_i \lambda_i^2 = 1$ known as Schmidt coefficients.

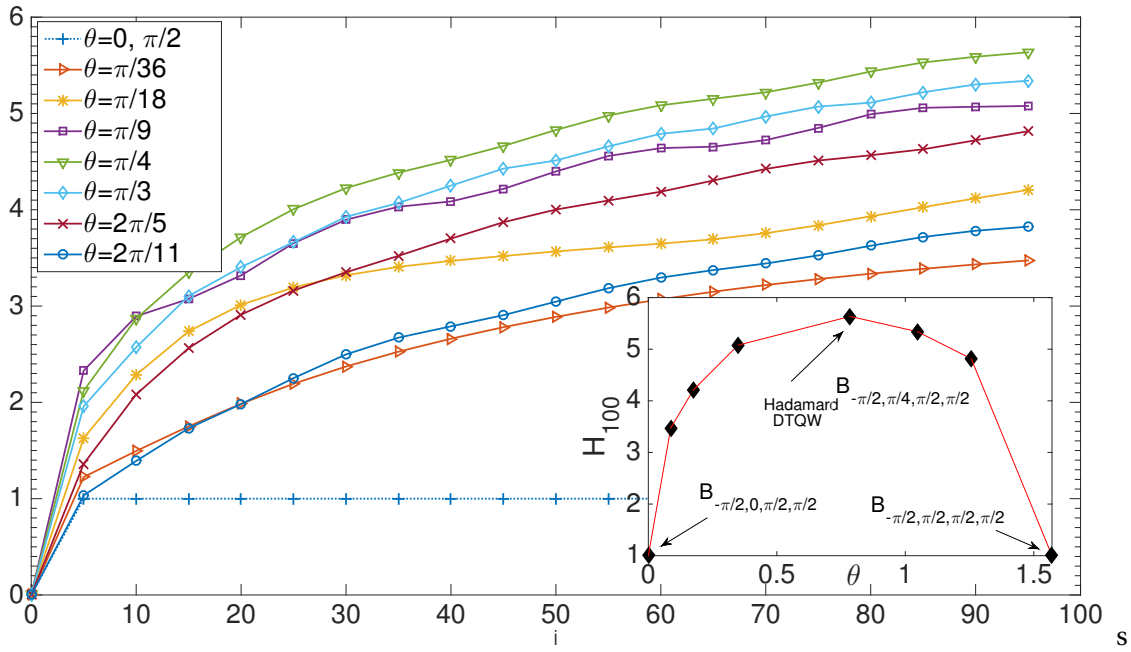

Figure 3.1: *Variation of entropy of measurement (or entanglement)* $(S_r)_j$ *VS time for different values of* θ*. Inside the figure: the variation of entropy VS* θ *for a given number of steps.*

The main difference between the Wigner function and the standard probability distribution is that it can take negative values, and we can interpret this non-positivity as a measure of non-classicality of the system. For instance in quantum optics, this is often interpreted as a signature of non-classical states of light, caused by a quantum interference phenomenon. More specifically in the study of QWs dynamics, the Wigner function, which permits to characterize position-momentum quantum correlation and quantum interference in phase space, leads to a clearer comprehension of the differences between spatial and spin loss of coherence and their short-time behaviors for the walk [4].

3.2.3 Projections cause spin and spatial decoherence

A recent approach to quantum decoherence, widely used in quantum information, has been introduced by Preskill [31] who generalized the von Neumann projective measurement. His formulation facilitated a general description of the evolution of the density matrix, including the evolution of pure states to mixed states, exactly as unitary transformations supported a description of coherent quantum evolution. This section will be devoted to introduce one of the main ways used to describe quantum decoherence in QWs.

Consider the initial state of the quantum walk represented by the density matrix $\rho_{j,m,m'}$ and $\mathbb{U}$ the one-step unitary operator (1.8), composed by a coin operator C followed by a translation operator T. The unitary evolution of $\rho_{j,m,m'}$ after M steps will be described by:

$$\rho_{j+M,m,m'} = U^M \rho_{j,m,m'} U^{\dagger M}. \tag{3.10}$$

The Eq. (3.10) is equivalent to the Eq. (1.8) in case of pure states and can more generally describe the time evolution of any quantum states, such as mixed states. If we now want to

describe decoherence, we should include in the evolution a discrete operation which violates the unitarity of the walk. In general this can be accomplished applying a projector operator to the evolution (3.10):

$$\rho_{j+M,m,m'} = (\mathbb{P}U)^M \rho_{j,m,m'} (U^\dagger \mathbb{P}^\dagger)^M. \tag{3.11}$$

Observe that here we can assume, for simplicity, that the operator $\mathbb{Q} = \mathbb{P}U$ is invariant under spatial translations. We should relax this assumption if we want to consider, for instance, inhomogeneous quantum coin operators. In addition to this, the nonunitary operator $\mathbb{Q}$ acts at each time step independently and following Kendon [22], it can be unpacked in a deterministic and reversible part and in a Markovian part. The latter contributes to the damping of the interference terms at constant rate p. For one time step the Eq. (3.11) reads in general:

$$\rho_{j+1,m,m'} = (1-p) U \rho_{j,m,m'} U^\dagger + p \sum_j \mathbb{Q}_j \rho_{j,m,m'} \mathbb{Q}^\dagger. \tag{3.12}$$

The above dynamical equation describes the decoherent evolution of a system that is projected by $\mathbb{Q}_j$ at each time step with probability p. Alberti et al. [4] consider more in detail different nonunitary operations separately acting on the spin space and position space with probability p_c and p_s respectively. Kendon and Tregenna [23] proved that the action of decoherence only in position space (p_c=0) or only in coin space ($p_s = 0$) is largely different if we consider the short time behavior of the evolution of spatial density probability. In particular they showed that if decoherence acts on coin state, it causes the formation of a cusp around $m = 0$ in the transition from quantum-to-classic behavior. In contrast, in the case of an initial loss of coherence in position space, the distribution takes the shape of a top-hat profile. Lopez and Paz [26] and Alberti et al. [4] proved respectively, on cycle and on one dimensional finite lattice, that these dynamics displayed qualitatively different behaviors by investigating systematically QW dynamics in Wigner representation.
Furthermore, the latter group of researchers demonstrated that spin decoherence acts on spatial coherences, suppressing with an exponential law the spatial correlation of the walk. Nevertheless, in some special cases, such as when the initial condition is not localized in momentum space, a spatial coherence can persist in a fully spin decoherent system.
On the other hand the spatial decoherence destroys directly the off-diagonal terms $\rho_{m,m'\neq m}$ with a rate $1-p_s$ per time step and the decoherence in position space implies decoherence in coin state because the position is conditioned by the state of the coin [23].
Let us note that the model of decoherence presented above can be analyzed in momentum space. Straightforward computations allow us to derive analytical properties of the walk, as in Brun et al. [9] who found the exact analytical expression of first and second order moments and computed the diffusion coefficient of the asymptotic transport.

3.3 Publication : "Discrete-time Quantum Walks in random artificial Gauge Fields."

As we have anticipated previously, another formal way to model decoherence in QWs can be randomizing the parameters of the step operator and then averaging the properties of the walk. Several authors have developed this technique in different specific frameworks, introducing random fluctuations in the coin operator [2, 3, 19, 29] or in the properties of the lattice [12]. In the model that we propose in the following publication, the parameters of the coin state

are random in time according to a uniform distribution. The asymptotic properties of the averaged transport are derived and we briefly discuss the formal continuous limit of the dynamical averaged evolution of the density matrix. However, even if similar results have been already found in the literature, here we introduce for the first time a formal connection with the fermion propagation in random synthetic gauge field and discuss the implications.

Discrete-time Quantum Walks in random artificial Gauge Fields

G. Di Molfetta* and F. Debbasch*
* *LERMA, Observatoire de Paris, PSL Research University, CNRS, Sorbonne Universités, UPMC Univ. Paris 6, UMR 8112, F-75014, Paris France*
(Dated: May 28, 2015)

Discrete-time quantum walks (DTQWs) in random artificial electric and gravitational fields are studied analytically and numerically. The analytical computations are carried by a new method which allows a direct exact analytical determination of the equations of motion obeyed by the average density operator. It is proven that randomness induces decoherence and that the quantum walks behave asymptotically like classical random walks. Asymptotic diffusion coefficients are computed exactly. The continuous limit is also obtained and discussed.

PACS numbers: 03.65.Pm, 05.60.Cg, 04.70.Bw, 73.21.Cd, 03.65.Pm, 03.67.-a, 02.50.Ey, 02.50.Fz, 02.50.Ga, 03.65.Yz, 04.62.+v

I. INTRODUCTION

Discrete time quantum walks (DTQWs) are simple formal analogues of classical random walks. They were first considered by Feynmann in [1], and then introduced in greater generality in [2] and [3]. They have been realized experimentally [4–10] and are important in many fields, ranging from fundamental quantum physics [10, 11] to quantum algorithmics [12, 13], solid state physics [14–17] and biophysics [18, 19].

It has been shown [20–22] recently that several DTQWs on the line admit a continuous limit identical to the propagation of a Dirac fermion in artificial electric and gravitational fields. These DTQWs are thus simple discrete models of quantum propagation in artificial gauge fields. Here, we consider artificial gauge fields which depend randomly on time and investigate analytically and numerically how this randomness influences quantum propagation. The analysis presented in this article is based on a direct analytical computation of the exact evolution equation obeyed by the average density operator. This presents several advantages. First, the average dynamics is thus known exactly, without the noise inherent in any numerical evaluation of averages. Second, knowing the exact average equations of motion makes it possible to study the average dynamics analytically. Finally, simulating directly the exact analytical equations of the average dynamics offers a significant gain in computation time over alternative methods where the average evolution is determined by simulating successively a large number of realizations of the random DTQWs.

Random DTQWs have already been studied by several authors (see for example [23–28]) , but the influence of random gauge fields has never been the object of specific analytical computations. In particular, exact expressions of the asymptotic density profiles as functions of the randomness caracteristics have never been computed. Our main results are (i) DTQWs interacting with artificial gauge fields which are random in time decohere and behave asymptotically like classical random walks (ii) the asymptotic density profiles of the DTQWs are Gaussian and we give exact analytical expressions of the asymptotic diffusion coefficients as functions of the noise amplitude which generates the randomness. We also support all results by direct numerical simulations of the average dynamics and finally discuss the continuous limits of the DTQWs interacting with random artificial gauge fields.

II. A FAMILY OF DTQWS COUPLED TO ARTIFICIAL ELECTRIC AND GRAVITATIONAL FIELDS

A. Wave-function evolution

1. *In physical space*

We consider discrete time quantum walks in one space dimension driven by a time-dependent quantum coin acting on a two-dimensional Hilbert space $\mathcal{H}$. The walks are defined by the following finite difference equations, valid for all $(j,m) \in \mathbb{N} \times \mathbb{Z}$:

$$\begin{bmatrix} \psi^L_{j+1,m} \\ \psi^R_{j+1,m} \end{bmatrix} = \mathcal{B}\left(\theta_j, \xi_j\right) \begin{bmatrix} \psi^L_{j,m+1} \\ \psi^R_{j,m-1} \end{bmatrix}, \tag{1}$$

where

$$\mathcal{B}(\theta,\xi) = \begin{bmatrix} e^{i\xi}\cos\theta & i\sin\theta \\ i\sin\theta & e^{-i\xi}\cos\theta \end{bmatrix}. \tag{2}$$

The operator represented by the matrix $\mathcal{B}$ is in $SU(2)$ and θ and ξ are two of the three Euler angles. The index j labels instants and takes all positive integer values. The index m labels spatial points. We choose to work on the circle and impose periodic boundary conditions. We thus introduce a strictly positive integer M and restrict m to all integer values between $-M$ and $+M$ *i.e.* $m \in \mathbb{Z}_M$. Results pertaining to DTQWs on the infinite line can be recovered by letting M tend to infinity.

For each instant j and each spatial point m, the wave function $\Psi_{jm} = \psi^L_{jm} b_L + \psi^R_{jm} b_R = \psi^a_{jm} b_a, a \in \{L, R\}$, has two components ψ^L_{jm} and ψ^R_{jm} on the spin basis (b_L, b_R) and these code for the probability amplitudes of the particle jumping towards the left or towards the right. Note that the spin basis is interpreted as being independent of j and m. For a given initial condition, the set of angles $\{\theta_j, \xi_j, j \in \mathbb{N}\}$ completely defines the walks and is arbitrary.

It has been proven in [20–22] that walks from this family are models of Dirac fermions coupled to artificial electric and gravitational fields. Details can be found in these references and in the first appendix to the present article.

2. *In Fourier space*

A practical tool to study quantum walks on the discrete circle is the discrete Fourier transform (DFT). Let $(A_m)_{m\in\mathbb{Z}_M}$ be an arbitray sequence of complex numbers defined on the discrete circle. The DFT of this sequence is the sequence $(\hat{A}_{k_n})_{n\in\mathbb{Z}_M}$ defined by

$$\hat{A}_{k_n} = \sum_{m=-M}^{+M} A_m \exp(ik_n m) \tag{3}$$

with $k_n = 2n\pi/(2M+1)$, $n \in \mathbb{Z}_M$. The original sequence can be recovered from its DFT by the relation:

$$A_m = \frac{1}{2M+1} \sum_{n=-M}^{+M} \hat{A}_{k_n} \exp(-ik_n m)\,. \tag{4}$$

For infinite M *i.e.* DTQWs on the infinite line, the DFT of an infinite sequence $(A_m)_{m\in\mathbb{Z}}$ becomes a function

$$\hat{A}(k) = \sum_{m\in\mathbb{Z}} A_m \exp(ikm) \tag{5}$$

defined for $k \in (-\pi, \pi)$ and the inverse relation reads:

$$A_m = \frac{1}{2\pi} \int_{-\pi}^{\pi} \hat{A}(k) \exp(-ikm)\, dk. \tag{6}$$

In Fourier space on the infinite line, the evolution equation (1) transcribes into

$$\begin{bmatrix} \hat{\psi}^L_{j+1}(k) \\ \hat{\psi}^R_{j+1}(k) \end{bmatrix} = \mathcal{C}(\theta_j, \xi_j, k) \begin{bmatrix} \hat{\psi}^L_j(k) \\ \hat{\psi}^R_j(k) \end{bmatrix} \tag{7}$$

where

$$\mathcal{C}(\theta_j, \xi_j, k) = \begin{bmatrix} e^{i\xi} \cos\theta e^{-ik} & i \sin\theta e^{+ik} \\ i \sin\theta e^{-ik} & e^{-i\xi} \cos\theta e^{+ik} \end{bmatrix} \tag{8}$$

for all $k \in (-\pi, \pi)$.

B. Density operator evolution

1. *In physical space*

The walks can also be described using the density operator $\rho = \Psi^* \otimes \Psi$. We introduce the basis $v_1 = b_L \otimes b_L$, $v_2 = b_L \otimes b_R$, $v_3 = b_R \otimes b_L$, $v_4 = b_R \otimes b_R$ and represent ρ by its components on this basis *i.e.* by the quantities $\rho^{ab}_{j,m,m'} = \psi^{b*}_{jm'} \psi^a_{jm}$, $\{a, b\} \in \{L, R\}^2$. Equation (1) delivers:

$$\begin{bmatrix} \rho^{LL}_{j+1,m,m'} \\ \rho^{LR}_{j+1,m,m'} \\ \rho^{RL}_{j+1,m,m'} \\ \rho^{RR}_{j+1,m,m'} \end{bmatrix} = \mathcal{Q}\left(\theta_j, \xi_j\right) \begin{bmatrix} \rho^{LL}_{j,m+1,m'+1} \\ \rho^{LR}_{j,m+1,m'-1} \\ \rho^{RL}_{j,m-1,m'+1} \\ \rho^{RR}_{j,m-1,m'-1} \end{bmatrix} \tag{9}$$

where

$$\mathcal{Q}(\theta,\xi) = \begin{bmatrix} c^2 & -ics\, e^{+i\xi} & +ics\, e^{-i\xi} & s^2 \\ -ics\, e^{+i\xi} & c^2 e^{+2i\xi} & s^2 & +ics\, e^{+i\xi} \\ +ics\, e^{-i\xi} & s^2 & c^2 e^{-2i\xi} & -ics\, e^{-i\xi} \\ s^2 & +ics\, e^{+i\xi} & -ics\, e^{-i\xi} & c^2 \end{bmatrix}, \tag{10}$$

with $c = \cos\theta$ and $s = \sin\theta$. The probability to find the walk at time j at point m is $N_{jm} = \rho^{LL}_{j,m,m} + \rho^{RR}_{j,m,m}$ and the sum $\sum_m N_{jm}$ is independent of j *i.e.* it is conserved by the walk. Contrary to equation (1), equation (9) can be used to describe walks with initial conditions which are not pure states. Equation (9) is thus more general than (1).

2. In Fourier space

Consider now, for any instant j, the double DFT of the density operator $\rho_{j,m,m'}$, which we denote by $\hat{\rho}_j(k,k')$ or, alternately, $\hat{\rho}_j(K,p)$ where $K = (k+k')/2$ is conjugate to $m+m'$ and $p = (k'-k)/2$ is conjugate to $m'-m$. For DTQWs on the infinite line, the range of both K and p is $(-\pi,+\pi)$. The DFT of the density operator obeys $\hat{\rho}_{j+1}(K,p) = \mathcal{R}\left(\theta_j,\xi_j,K,p\right)\hat{\rho}_j(K,p)$ with

$$\mathcal{R}(\theta,\xi,K,p) = \begin{bmatrix} c^2\, e^{2iK} & -ics\, e^{+i\xi}\, e^{-2ip} & +ics\, e^{-i\xi}\, e^{+2ip} & s^2\, e^{-2iK} \\ -ics\, e^{+i\xi}\, e^{2iK} & c^2 e^{+2i\xi}\, e^{-2ip} & s^2\, e^{+2ip} & +ics\, e^{+i\xi}\, e^{-2iK} \\ +ics\, e^{-i\xi}\, e^{2iK} & s^2\, e^{-2ip} & c^2 e^{-2i\xi}\, e^{+2ip} & -ics\, e^{-i\xi}\, e^{-2iK} \\ s^2\, e^{2iK} & +ics\, e^{+i\xi}\, e^{-2ip} & -ics\, e^{-i\xi}\, e^{+2ip} & c^2\, e^{-2iK} \end{bmatrix}. \tag{11}$$

Note that the operator $\mathcal{R}$ governing the evolution of $\bar{\rho}$ is unitary. This can be checked by a straightforward computation and it is a direct consequence of the unitarity of the operator $\mathcal{B}$.

III. RANDOMIZING THE FIELDS AND AVERAGING THE DYNAMICS

A. Randomizing the fields

The Hadamard walk corresponds to $\xi = \xi_H = \pi/2$ and $\theta = \theta_H = \pi/4$; since these angles are constant, the Hadamard walk describes propagation in the absence of electric and gravitational field [21, 22]. We now consider situations where one of the angles ξ and θ does depend on time and fluctuates around its Hadamard value. More precisely, we consider two cases. Case 1 corresponds to $\theta = \theta_H = \pi/4$ and ξ chosen randomly at each time-step with uniform probability law in the interval $(\pi/2 - \sigma/2, \pi/2 + \sigma/2)$, where $\sigma \in (0, 2\pi)$ is a fixed *i.e.* j-independent positive real number. As proven in [20–22] and detailed in the first appendix to the present article, a time-dependent θ is equivalent to a space-time metric whose purely spatial part depends on time, and such a metric represents a time-dependent relativistic gravitational field. Case 2 corresponds to $\xi = \xi_H = \pi/2$ and θ chosen randomly at each time-step with uniform probability law in the interval $(\pi/4 - \sigma/2, \pi/4 + \sigma/2)$. As proven in [22], a time-dependent ξ is equivalent to a time-dependent 'vector' potential, which represents a time-dependent electric feld.

Thus, in each case, a realization of the random gauge field is determined by a sequence $\omega = (\omega_1, \omega_2, ...)$ of independent random variables, where ω_j represents the value of the random angle θ or ξ at time j. If one follows the walk till time N, the relevant random sequence is the N-uple $\omega^N = (\omega_1, \omega_2, ..., \omega_N)$. For each value of σ and each instant j, ω_j is uniformly distributed in the interval $I_\sigma = (\omega_H - \sigma/2, \omega_H + \sigma/2)$ centered on the Hadamard value ω_H. The probability density of ω_j in this interval is thus simply $p_\sigma(\omega_j) = 1/\sigma$ and is independent of both ω_j and j. The probability density for $\omega^N = (\omega_1, \omega_2, ..., \omega_N)$ in I^N_σ is therefore $P_\sigma(\omega^N) = \Pi^N_{j=1} p_\sigma(\omega_j) = 1/\sigma^N$ and is independent of ω^N.

B. Averaging the dynamics

At fixed initial condition ρ_0 and for each time N, the density operator ρ_N at time N depends on the realization ω^N of the random angle up to time N. At fixed initial condition, the easiest way to compute statistical averages over

ω^N is to first compute the statistical average $\bar{\rho}_N$ of the density operator over ω^N:

$$\begin{aligned}\bar{\rho}_N &= \int_{I_\sigma^N} \rho_N(\omega^N) P_\sigma(\omega^N) d\omega^N \\ &= \int_{I_\sigma^N} \rho_N(\omega_1,...,\omega_N) p_\sigma(\omega_1)...p_\sigma(\omega_N) d\omega_1...d\omega_N \\ &= \int_{I_\sigma^N} \rho_N(\omega_1,...,\omega_N) \frac{1}{\sigma^N}\, d\omega_1...d\omega_N. \end{aligned} \tag{12}$$

Let us work in Fourier space. One can then write, for any realization $\omega^N = (\omega_1,...,\omega_N)$ of the random angle up to time N:

$$\begin{aligned}\hat{\rho}_N(\omega_1,...,\omega_N) &= \mathcal{R}(\omega_N)\hat{\rho}_{N-1}(\omega_1,...,\omega_{N-1}) \\ &= \mathcal{R}(\omega_N)...\mathcal{R}(\omega_1)\hat{\rho}_0, \end{aligned} \tag{13}$$

where the variables K and p have been omitted for clarity reasons. Since the ω_j's are statistically independent of each other and are identically distributed, one obtains:

$$\hat{\bar{\rho}}_N = \bar{\mathcal{R}}^N \hat{\bar{\rho}}_0 \tag{14}$$

where $\bar{\mathcal{R}}$ is the statistical average of the evolution operator $\mathcal{R}$ over the random angle $\omega = \theta$ or ξ (the other angle being fixed to its Hadamard value):

$$\begin{aligned}\bar{\mathcal{R}}(K,p,\sigma) &= \int_{I_\sigma} \mathcal{R}(\omega,K,p) p_\sigma(\omega) d\omega \\ \bar{\mathcal{R}}(K,p,\sigma) &= \int_{I_\sigma} \mathcal{R}(\omega,K,p) \frac{1}{\sigma}\, d\omega. \end{aligned} \tag{15}$$

The average evolution $\bar{\mathcal{R}}$ is thus a function of (K,p) and of the noise parameter σ and can be computed analytically from (11). It determines the evolution of the average density operator completely and, therefore, the average transport. Since everything that follows pertains only to the average transport, we simplify the notation by droping the bar on the letter ρ and the density operator of the averaged transport will now be designated simply by ρ.

A direct computation from (11) leads to the following exact expressions for the components of $\bar{\mathcal{R}}$ in the basis $\{v_1, v_2, v_3, v_4\}$ for case 1 (random electric field) and case 2 (random gravitational field):

$$\bar{\mathcal{R}}^e(K,p,\sigma) = \frac{1}{2}\begin{bmatrix} e^{2iK} & \mathrm{sinc}(\sigma/2)\, e^{-2ip} & \mathrm{sinc}(\sigma/2)\, e^{+2ip} & e^{-2iK} \\ \mathrm{sinc}(\sigma/2)\, e^{2iK} & -\mathrm{sinc}(\sigma)\, e^{-2ip} & e^{+2ip} & -\mathrm{sinc}(\sigma/2)\, e^{-2iK} \\ \mathrm{sinc}(\sigma/2)\, e^{2iK} & e^{-2ip} & -\mathrm{sinc}(\sigma)\, e^{+2ip} & -\mathrm{sinc}(\sigma/2)\, e^{-2iK} \\ e^{2iK} & -\mathrm{sinc}(\sigma/2)\, e^{-2ip} & -\mathrm{sinc}(\sigma/2)\, e^{+2ip} & e^{-2iK} \end{bmatrix}, \tag{16}$$

and

$$\bar{\mathcal{R}}^g(K,p,\sigma) = \frac{1}{2}\begin{bmatrix} e^{2iK} & \mathrm{sinc}(\sigma)\, e^{-2ip} & \mathrm{sinc}(\sigma)\, e^{+2ip} & e^{-2iK} \\ \mathrm{sinc}(\sigma)\, e^{2iK} & -e^{-2ip} & e^{+2ip} & -\mathrm{sinc}(\sigma)\, e^{-2iK} \\ \mathrm{sinc}(\sigma)\, e^{2iK} & e^{-2ip} & -e^{+2ip} & -\mathrm{sinc}(\sigma)\, e^{-2iK} \\ e^{2iK} & -\mathrm{sinc}(\sigma)\, e^{-2ip} & -\mathrm{sinc}(\sigma)\, e^{+2ip} & e^{-2iK} \end{bmatrix}, \tag{17}$$

It proves convenient for all subsequent computations to change basis in ρ space and introduce the new vectors $u_1 = v_1 + v_4$, $u_2 = v_1 - v_4$, $u_3 = v_2 + v_3$, $u_4 = v_2 - v_3$. In this new basis, the components of $\bar{\mathcal{R}}^e(K,p,\sigma)$ and $\bar{\mathcal{R}}^g(K,p,\sigma)$ read:

$$\bar{\mathcal{R}}^e(K,p,\sigma) = \begin{bmatrix} \cos(2K) & i\sin(2K) & 0 & 0 \\ 0 & 0 & \mathrm{sinc}(\sigma/2)\cos(2p) & -i\,\mathrm{sinc}(\sigma/2)\sin(2p) \\ i\,\mathrm{sinc}(\sigma/2)\sin(2K) & \mathrm{sinc}(\sigma/2)\cos(2K) & \frac{(1-\mathrm{sinc}(\sigma))}{2}\cos(2p) & i\frac{(\mathrm{sinc}(\sigma)-1)}{2}\sin(2p) \\ 0 & 0 & i\frac{(1+\mathrm{sinc}(\sigma))}{2}\sin(2p) & -\frac{(\mathrm{sinc}(\sigma)+1)}{2}\cos(2p) \end{bmatrix}, \tag{18}$$

$$\bar{\mathcal{R}}^g(K,p,\sigma) = \begin{bmatrix} \cos(2K) & i\sin(2K) & 0 & 0 \\ 0 & 0 & \mathrm{sinc}(\sigma)\cos(2p) & -i\,\mathrm{sinc}(\sigma)\sin(2p) \\ i\,\mathrm{sinc}(\sigma)\sin(2K) & \mathrm{sinc}(\sigma)\cos(2K) & 0 & 0 \\ 0 & 0 & i\sin(2p) & -\cos(2p) \end{bmatrix}, \tag{19}$$

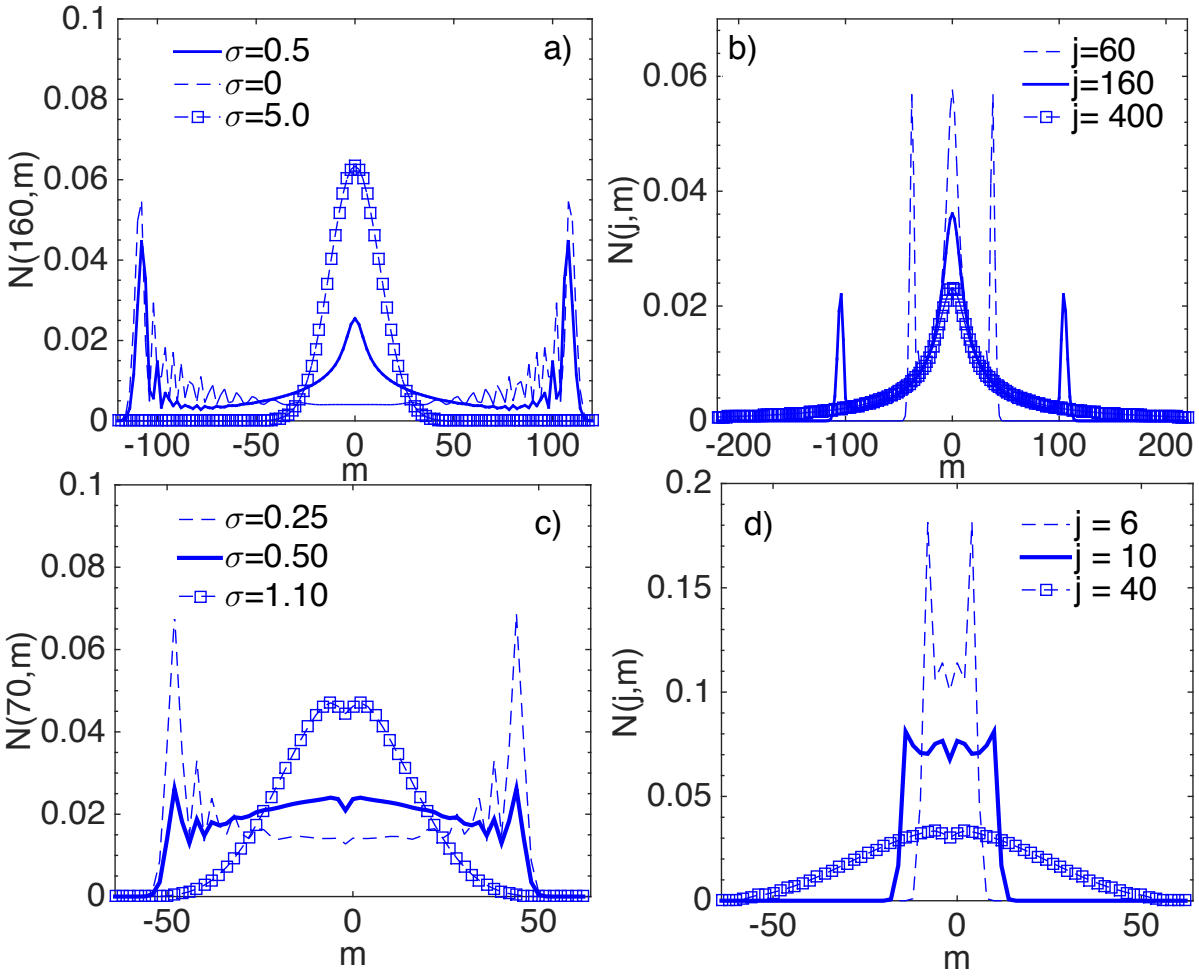

FIG. 1: (Color online) (left) Probability profile of the average transport in a random ξ-field (a) and θ-field (c) vs grid point m at $j = 160$ (a) and $j = 70$ (c) for different values of the noise parameter σ. (right) Probability profile of the average transport in a random ξ-field (b) and θ-field (d) vs grid point m for $\sigma = 0.5$ (d) and $\sigma = 0.8$ (d) at different time steps. Square marker represents fully decoherent regime, solid line the intermediate regime and dashed line indicates a fully coherent state.

We choose as initial condition the pure state defined by $\Psi_{j=0,m=0} = (b_L + ib_R)/\sqrt{2}$ and $\Psi_{j=0,m} = 0$ if $m \neq 0$. This state corresponds to the density operator $\rho_{j=0,m=0,m'=0} = (b_L \otimes b_L + b_R \otimes b_R + i(b_R \otimes b_L - b_L \otimes b_R))/2 = (u_1 - iu_4)/2$ and $\rho_{j=0,m,m'} = 0$ if $m \neq 0$ or $m' \neq 0$. In Fourier space, $\hat{\rho}_{j=0}(K,p) = (u_1 - iu_4)/2$ for all K and p.

For any realization of the noise *i.e.* for any given value of ω, the initial pure state evolves by the DTQW into a pure state. But the average evolutions descibed by $\bar{\mathcal{R}}^e$ and $\bar{\mathcal{R}}^g$ both transform the initial pure state into a superposition. However, the average transport is symmetrical around the origin, as is the classical Hadamard walk generated from the same initial condition.

Let us finally stress that, contrary to the operator $\mathcal{R}$ governing the unaveraged transport, the operators $\mathcal{R}^{e/g}$ governing the averaged transport are *not* unitary. This loss of unitarity generates qualitative differences between the unaveraged and the averaged transport. In particular, the averaged transport looses quantum coherence and is asymptotically diffusive. These two important consequences of the averaging process are analyzed in the remaining sections of this article.

IV. QUALITATIVE DESCRIPTION OF AVERAGE TRANSPORT

Typical density profiles of the average transport are shown in Figure 1 for random gravitational and random electric fields. For small enough values of the noise parameter σ, the average transport behaves at short times like the Hadamard walk and is ballistic. Ballistic behavior then gradually disappears and is replaced by diffusive behavior. For

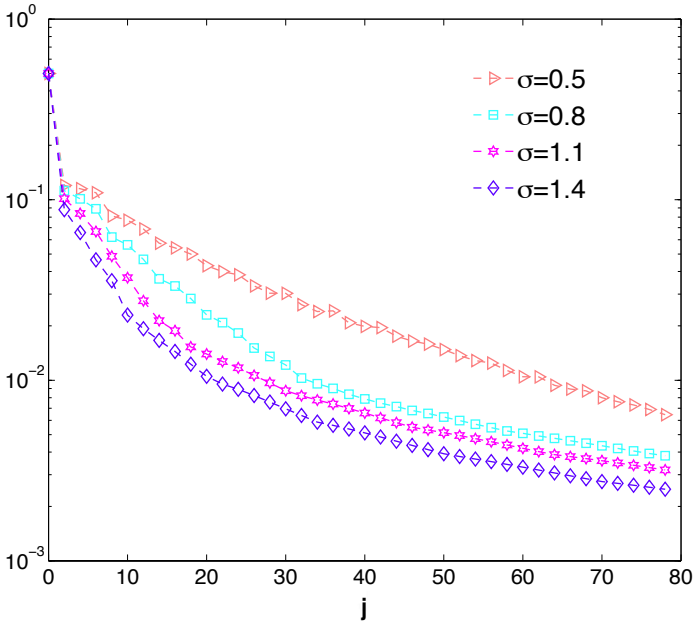

FIG. 2: Log-lin plot of time evolution of the spin coherence C_j in a random θ-field for various values of the noise parameter σ.

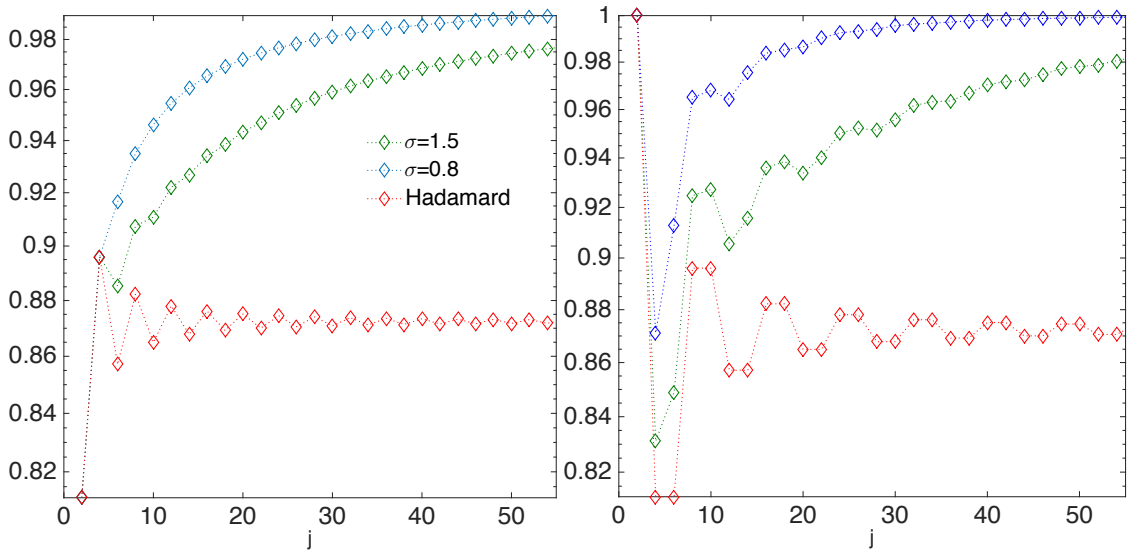

FIG. 3: Log-lin plot of time evolution of Shannon entanglement entropy S_r compared to the Shannon entanglement entropy of the average transport in a random θ-field (left) and ξ-field (right)

larger values of σ, ballistic behavior is replaced, even at short times, by diffusive behavior. Note that the Gaussian-like form of the asympotic density profiles presents a central dip when the DTQWs interact with random gravitational fields, but presents a central cusp when the DTQWs interact with random electric fields.

Asymptotically, DTQWs in electric and gravitational fields which are random in time thus behave like classical random walks. This means that the randomness in the fields prompts the DTQWs to loose coherence. This can be confirmed by considering the spin coherence defined by

$$C_j = \max_{m,m'} \mid \rho^{LR}_{j,m,m'} \mid . \tag{20}$$

Figure 2 displays the typical time-evolution of the spin coherence for various values of the noise parameter σ. These results confirm that the average transport loses spin coherence and that a higher value of σ leads to a quicker loss of spin coherence.

A brief comment on spatial coherence is in order. The retained initial condition vanishes everywhere except at $m = m' = 0$. If one prefers, the Fourier transform of the initial density operator is flat in both K and p space. There is thus initially no spatial coherence. As time increases, the Fourier transform $\hat{\rho}(K, p)$ of the density operator ρ becomes non flat in both K and p (see for example the asymptotic form (21) of $\hat{\rho}$). In other words, each K-mode acquires spatial coherence. But $\tilde{\rho}(p) = \sum_K \hat{\rho}(K, p)$ remains flat in p (data not shown) *i.e.* there is no *total* gain of spatial coherence.

The entanglement of the averaged dynamics can also be quantified by the Shannon entropy S_r of the reduced density operator ρ_r in spin space. To be precise [29–31], $\rho_r = \sum_m \rho_{m,m'=m}$ and the Shannon entropy $S_r = -\mathrm{tr}(\rho_r \log(\rho_r))$. The time-evolution of S_r is prensented is Figure 3, together with the entanglement entropy of the pure Hadamard walk with the same initial condition, which admits 0.872 as asymptotic value [32]. The increase in S_r signals the loss of coherence and the figure confirms that this decoherence by noise gets more effective as σ increases.

The scaling of the decoherence time for small values of σ can be evaluated by the following reasonning. As previously explained, the operator $\bar{\mathcal{R}}^{e/g}$ completely controls the average dynamics. For $\sigma = 0$, there is no noise and the DTQW never decoheres *i.e.* the decoherence time is infinite. The first non-vanishing terms in the expansion of $\bar{\mathcal{R}}^{e/g}$ around $\sigma = 0$ are of second order in σ. Thus, per time step, the effect of the noise on the DTQW is of order σ^2 for small enough values of σ. The typical decoherence time therefore scales as σ^{-2} for small values of σ.

The next section, together with the appendices, provides an analytical investigation of how coherence is lost. In particular, the asymptotic form of the density operator is computed exactly. The corresponding density is Gaussian, which confirms that the DTQW behaves asymptotically like a classical random walk. Also, the asymptotic density operator is proportionnal to $u_1 = v_1 + v_4 = b_L \otimes b_L + b_R \otimes b_R$. This proves that the spin coherence, which measures the amplitude of the $b_L \otimes b_R$ component, vanishes asymptotically, in accordance with Figure 2.

V. QUANTITATIVE DESCRIPTION OF THE ASYMPTOTIC REGIME

A. Central limit theorem

The average dynamics is entirely determined by the eigenvalues $\lambda_r^{e/g}$ and corresponding eigenvectors $w_r^{e/g}$, $r = 1, 2, 3, 4$, of the operators $\bar{\mathcal{R}}^{e/g}$. As evident from Figure 1, the density profiles of the average transport become larger and smoother with time. This suggest that the asymptotic dynamics can be understood by computing the eigenvalues and eigenvectors only for values of K much smaller than unity. The detailled analysis, though very instructive, is too involved to merit inclusion in the main body of this article and it is therefore presented in the Appendix. The main conclusion can be stated as follows.

Theorem. *Let $K_j = K_*/\sqrt{j}$ where K_* is an arbitrary but j-independent wave number. The average density operator in Fourier space admits as the time j tends to infinity the following approximate asymptotic expression:*

$$\hat{\rho}_j^{e/g}(K_j, p) \sim \frac{1}{2} \exp\left(-\alpha^{e/g}(p, \sigma) j K_j^2\right) u_1 \tag{21}$$

where

$$\alpha^e(p, \sigma) = 2\, \frac{3 + (sinc(\sigma))^2 + 2\,(sinc(\sigma/2))^2\,(1 + sinc(\sigma)) + 4\cos(2p)\left(sinc(\sigma) + (sinc(\sigma/2))^2\right)}{3 + (sinc(\sigma))^2 - 2\,(sinc(\sigma/2))^2\,(1 + sinc(\sigma)) + 4\cos(2p)\left(sinc(\sigma) - (sinc(\sigma/2))^2\right)} \tag{22}$$

and

$$\alpha^g(p, \sigma) = 2\, \frac{1 + (sinc(\sigma))^2}{1 - (sinc(\sigma))^2}. \tag{23}$$

This result is a central limit theorem which proves that the asymptotic density operator is approximately Gaussian in K-space, with a typical width (in K-space) which decreases as $j^{-1/2}$, as in classical random walks and non quantum diffusions. Note that α^g is actually independent of p.

One of the consequences of (21) is that the projection of $\hat{\rho}_{j=J}(K_J, p)$ on the subspace spanned by (u_2, u_3, u_4) tends to zero. Remembering the expressions of the u_i in termes of b_L and b_R, this means that $\hat{\rho}^{LR}$, $\hat{\rho}^{LR}$ and $\hat{\rho}^{LL} - \hat{\rho}^{RR}$ all tend to zero as J tends to infinity. The component along u_1 coincides with $\hat{\rho}^{LL} + \hat{\rho}^{RR}$ and determines the asymtotic density of the averaged walk after summation over p and Fourier transform over K.

B. Asymptotic mean-square displacement

Let us now explicitly compute the asymptotic expression of the mean-square displacement $\overline{m^2}^{e/g}$ in the special case of a random DTQW on the infinite line. Switching back the original spatial variables m and m' involves a double integration over K and p. The $2D$ measure to be used in this integration is $dkdk' = 2dKdp$. The density $N_{jm}^{e/g}$ at time j and point m is the trace over $m' = m$ of the component of the density operator along the basis vector u_1. Expression (C10) for $\hat{\rho}^{e/g}$ is only valid for $K \ll 1$ (see the Appendix). But the functions $\alpha^{e/g}(p,\sigma)$ are always non vanishing. The width $\Delta K(j,p)$ of $\hat{\rho}_j^{e/g}(K,p)$ in K thus scales as $1/\sqrt{j}$ and tends to zero as j tends to infinity. Thus, for large enough j, the density and mean square displacement are given by:

$$N_{jm}^{e/g} = \frac{1}{4\pi^2}\int_{p=-\pi}^{\pi} dp \int_{K=-\pi}^{\pi} dK \exp\left(-\alpha^{e/g}(p,\sigma) j K^2\right) \exp\left(-iKm\right) \tag{24}$$

and

$$\overline{m^2}^{e/g}(j,\sigma) = \frac{1}{4\pi^2}\sum_{m\in\mathbb{Z}} m^2 \int_{p=-\pi}^{\pi} dp \int_{K=-\pi}^{\pi} dK \exp\left(-\alpha^{e/g}(p,\sigma) j K^2\right) \exp\left(-iKm\right). \tag{25}$$

Since the width $\Delta K(j,p)$ of $\hat{\rho}_{j,K,p}$ scales as $1/\sqrt{j}$, one can also replace all discrete summations over m by integrals over the real line, because $\Delta K(j,p) \times \Delta x = 1/\sqrt{j} \times 1 \ll 1$ for large enough j. Indeed, a simple computation confirms that the integrated density $\int_{\mathbb{R}} dm N_{jm}^{e/g}$ (with $N_{jm}^{e/g}$ given by (24)) is equal to unity at all times j. Replacing in (25) the discrete summation over m by an integral delivers

$$\overline{m^2}^{e/g}(j,\sigma) = \frac{j}{\pi}\int_{-\pi}^{\pi} \alpha^{e/g}(p,\sigma) dp. \tag{26}$$

The computation of $\overline{m^2}^{g}(j,\sigma)$ is trivial because $\alpha^g(p,\sigma)$ does not depend on p. One finds

$$\overline{m^2}^{g}(j,\sigma) = 2D^g(\sigma) j \tag{27}$$

with

$$D^g(\sigma) = 2\,\frac{1+\left(\mathrm{sinc}(\sigma)\right)^2}{1-\left(\mathrm{sinc}(\sigma)\right)^2}. \tag{28}$$

The exact expression for $\overline{m^2}^{e}(j,\sigma)$ is more involved. A direct computation leads to:

$$\overline{m^2}^{e}(j,\sigma) = 2D^e(\sigma) j \tag{29}$$

with

$$D^e(\sigma) = \frac{2}{\mathrm{sinc}(\sigma) - \left(\mathrm{sinc}(\sigma/2)\right)^2}\left(\left(\mathrm{sinc}(\sigma) + \left(\mathrm{sinc}(\sigma/2)\right)^2\right) + \frac{2\left(\mathrm{sinc}(\sigma/2)\right)^2\left(\left(\mathrm{sinc}(\sigma)\right)^2 + 2\mathrm{sinc}(\sigma) - 3\right)}{s(\sigma)}\right) \tag{30}$$

with

$$s(\sigma) = \left[\left(3 + \left(\mathrm{sinc}(\sigma)\right)^2 - 2\left(\mathrm{sinc}(\sigma/2)\right)^2\left(1+\mathrm{sinc}(\sigma)\right)\right)^2 - 16\left(\mathrm{sinc}(\sigma) - \left(\mathrm{sinc}(\sigma/2)\right)^2\right)^2\right]^{1/2}. \tag{31}$$

In both electric and gravitational case, the asymptotic mean square displacement in physical space grows linearly in time, as for classical random walks and non quantum diffusions. The functions D^e and D^g are the asymptotic diffusion coefficients of the average transport. Both functions are strictly decreasing on $(0, 2\pi)$. Thus, decoherence occurs more rapidly as σ increases (see Section IV), but the asymptotic diffusion coefficients decrease with σ. We also note that $D^g(\sigma) < D^e(\sigma)$ for all $\sigma \in (0, 2\pi)$.

Figure 4 shows the time-evolution of the relative difference between the diffusion coefficients computed from (28), (28) and the mean square displacement computed from numerical simulations for various values of σ. This figures clearly supports the analytical computation presented in this Section.

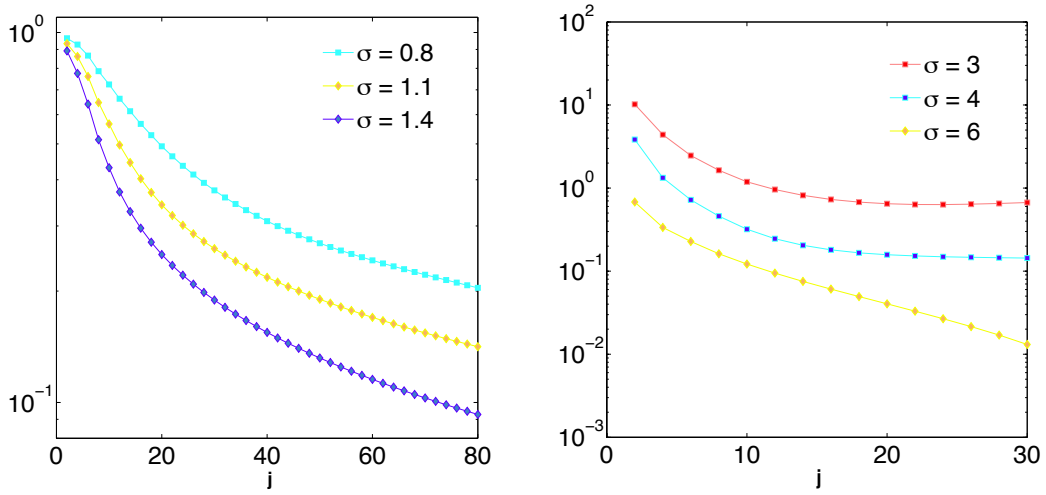

FIG. 4: Left (right) figure: time-evolution of the relative difference between the gravitational (eletric) diffusion coefficients computed from numerical simulations and the exact analytical expressions.

VI. CONTINUOUS LIMIT

The formal continuous limit of the original, unaveraged evolution equations (9) and (1) has already been considered in [21, 22] and coincides with the Dirac equation obeyed by a fermion minimally coupled to an electric field and/or a relativistic gravitational field. Let us now determine the formal continuous limit of the averaged evolution equations specified by the operators $\bar{\mathcal{R}}^e$ and $\bar{\mathcal{R}}^g$.

As shown and discussed in [21, 22] for the unaveraged evolution equations, the object which admits a continuous limit for $\theta = \theta_H$ or $\xi = \xi_H$ is not the original walk, but the walk derived from it by keeping only one time step out of two [**?**]. We thus search for the continuous limit of the following discrete equations:

$$\hat{\rho}_{j+2}(K,p) = \left(\bar{\mathcal{R}}^{e/g}(K,p,\sigma)\right)^2 \hat{\rho}_j(K,p). \tag{32}$$

To be specific, we restrain j to uneven positive integer values and decide to work on the inifinite line, so that K and p take all values in $(-\pi, +\pi)$.

We now supppose that, for all uneven $j = 2r+1$, $\rho_{j=2r+1,m,m'}$ (*resp.* $\hat{\rho}_{j=2r+1}(K,p)$) is the value taken by a certain function ρ (*resp.* $\hat{\rho}$) at 'time' $t_r = r$ and positions $x_m = m$ and $x_{m'} = m'$ (*resp.* momenta K and p). Roughly speaking, the continuous limit refers to situations where the function ρ (*resp.* $\hat{\rho}$) varies only little during one time step $t_{r+1} - t_r = 1$. A necessary and sufficient condition for this to be realized is that $\left(\bar{\mathcal{R}}^{e/g}(K,p,\sigma)\right)^2$ be close to unity. Direct inspection reveals that this transcribes into $\sigma \ll 1$, $K \ll 1$ and $p \ll 1$. The last two conditions mean that ρ has caracteristic spatial variation scales much larger than the distance $m+1-m = 1$ between adjacent grid points and the first condition states that the noise amplitude is small. Note that K, p and σ are *a priori* independent inifnitesimal quantities. In particular, there is no reason why K and p should be of the same order of magnitude.

The formal continuous limit is then obtained by expanding $\left(\bar{\mathcal{R}}^{e/g}(K,p,\sigma)\right)^2$ around $K = 0$, $p = 0$, $\sigma = 0$ and by replacing $\hat{\rho}_{j+2} - \hat{\rho}_j$ by $\partial_t \hat{\rho}$. One thus gets equations of the form :

$$\partial_t \hat{\rho}(t,K,p) = \left(\mathcal{S}^{e/g}(K,p,\sigma) - 1\right) \hat{\rho}(t,K,p) \tag{33}$$

where, for example,

$$\mathcal{S}^g(K,p,\sigma) = \begin{bmatrix} 1-4K^2 & 2iK & 2iK(1-\frac{p^2}{2})(1-\frac{\sigma^2}{6}) & 2Kp(1-\frac{\sigma^2}{6}) \\ 2iK(1-\frac{p^2}{2})(1-\frac{\sigma^2}{3}) & (1-4K^2)(1-\frac{p^2}{2})(1-\frac{\sigma^2}{3}) & p^2(1-\frac{\sigma^2}{6}) & 2ip(1-\frac{\sigma^2}{6}) \\ 2iK(1-\frac{\sigma^2}{6}) & -4K^2(1-\frac{\sigma^2}{6}) & (1-4K^2)(1-\frac{p^2}{2})(1-\frac{\sigma^2}{3}) & -ip(1-4K^2)(1-\frac{\sigma^2}{3}) \\ -2Kp(1-\frac{\sigma^2}{6}) & ip(1-4K^2)(1-\frac{\sigma^2}{6}) & -ip & 1-4p^2 \end{bmatrix} \tag{34}$$

at second order in all three independent infinitesimals K, p and σ. These equations can be translated into physical space by remembering that $-iK$ and $-ip$ are the Fourier representations of ∂_X and ∂_y where $X = (x + x')/2$ and $y = x' - x$.

The analysis presented in Sections III and IV above has been carried out with an initial condition which spreads over the whole K- and p-ranges. The resulting density operator does localize in time around $K = 0$, but it never localizes around $p = 0$ and remains spread in p-space. The continuous limit thus cannot be used to recover the results of Section IV. As can be checked directly from (34), the continuous limit equations nevertheless predict diffusive behavior if K is much lower than both p and σ. A systematic study of the continuous limit dynamics for various scaling laws obeyed by K, p and σ falls outside the scope of this article and will be presented elsewhere.

VII. CONCLUSION

We have studied two families of DTQWs which can be considered as simple models of quantum transport of a Dirac fermion in random electric or gravitational fields. We have proven analytically and confirmed numerically that randomness of the fields in time leads on average to decoherence of the walks. The asymptotic average transport is thus diffusive and we have computed exactly the diffusion coefficients. We have also obtained and discussed the continuous limit of the model.

A few words about the loss of coherence in DTQWs may prove useful at this point. Pure, deterministic DTQWs are standard quantum systems in the sense that their time-evolution is unitary. They thus never loose coherence nor do they exhibit diffusive behavior. As with any quantum system, the loss of coherence in DTQWs is induced by the so-called interaction with an environment. There are essentially two ways to model this interaction. The first one is to start from the unitary evolution of the density operator and to modify this unitary evolution into a non-unitary one by introducing so-called projector or measurement operators [23–25, 33]. The second way of introducing decoherence is the one followed in this article. It consists in introducing some randomness in the parameters of the DTQW and in averaging over this randomness [26–28, 34, 35]. Contrary to the unaveraged density operator, the averaged density operator then follows a non-unitary evolution and this breakdown of unitarity induces the loss of coherence and the asymptotic diffusive behavior displayed by the averaged transport.

The results of this article constitute/are an addition to the already extensive literature dealing with the asymptotic behavior of DTQWs and CTQWs. Standard deterministic QWs are famous for typically exhibiting asymptotic ballistic behavior. But diffusive and anomalous diffusive asymptotic behavior have also been observed [36, 37], as well as localization [35, 38, 39] and soliton-like structures [34].

Let us conclude by listing a few natural extensions of this work. The random artificial gauge fields considered in this article have two main characteristics: they depend only on time and the associated mean fields vanish [40]. One should therefore extend the analysis presented above to situations where the mean fields do not vanish and where the artificial gauge fields depend not only on time, but also on position. In particular, the continuous limit equation derived in Section VI is markedly different from both the Caldeira-Leggett [41, 42] and the relativistic Kolmogorov equation describing relativistic stochastic processes [43–45]. Indeed, because the random fields depend only on time, the dynamics considered in this article does not couple different (K, p)-modes, but these are coupled in both the Caldeira-Leggett and the relativistic Kolmogorov equation. Considering DTQWs coupled to artificial gauge fields which also depend randomly on position should therefore lead to master equations closer to the the Caldeira-Legget and the Kolmogorov models. Moreover, cases where both electric and gravitational fields vary randomly are certainly worth investigating.

Finally, at least some DTQWs in two spatial dimensions can be considered as models of quantum transport in electromagnetic fields [46]. The analysis presented in this article should therefore be repeated in higher dimensions to include random magnetic fields [47] and evaluate their effects on spintronics.

Appendix A: Interpretation in terms of artificial gauge fields

It has been proven in [20–22] that quantum walks in $(1 + 1)$ dimensional space-times can be viewed as modeling the transport of a Dirac fermion in artificial electric and gravitational fields generated by the time-dependance of the angles θ and ξ. We recall here some basic conclusions obtained in [20–22] and also offer new developments useful in interpreting the results of the present article.

The DTQWs defined by (1) are part of a larger family whose dynamics reads:

$$\begin{bmatrix} \psi^L_{j+1,m} \\ \psi^R_{j+1,m} \end{bmatrix} = \tilde{\mathcal{B}}\left(\theta_{j,m}, \xi_{j,m}, \zeta_{j,m}, \alpha_{j,m}\right) \begin{bmatrix} \psi^L_{j,m+1} \\ \psi^R_{j,m-1} \end{bmatrix}, \tag{A1}$$

where

$$\tilde{\mathcal{B}}(\theta,\xi,\zeta,\alpha) = e^{i\alpha}\begin{bmatrix} e^{i\xi}\cos\theta & e^{i\zeta}\sin\theta \\ -e^{i\zeta}\sin\theta & e^{-i\xi}\cos\theta \end{bmatrix}. \tag{A2}$$

The walks in this larger family are characterized by three time- and space-dependent Euler angles (θ,ξ,ζ) and by a global, also time- and space-dependent phase α. They have been shown to model the transport of Dirac fermions in artificial electric and relativistic gravitational fields generated by the time-dependence of the three Euler angles and of the global phase. In a $(1+1)$ dimensional space-time, an electric field derives from a 2-potential $A_{j,m} = (V_{j,m}, \mathcal{A}_{,mj})$ and a relativistic gravitational field is represented by $2D$ metrics $G_{j,m}$. The walks considered in this article correspond to

$$\begin{aligned} \xi &= \frac{\pi}{2} + \bar{\xi}_j \\ \theta &= \frac{\pi}{4} + \bar{\theta}_j \\ \alpha &= \frac{\pi}{2} + \bar{\alpha} \\ \zeta &= 0 \end{aligned} \tag{A3}$$

where $\bar{\xi}_j$ and $\bar{\theta}_j$ are random variables which depend on the time j and $\bar{\alpha} = 3\pi/2$. According to [22], these walks model the transport of a Dirac fermion in an electric field generated by the 2-potential

$$A_j = (V_j, \mathcal{A}_j) = \left(\bar{\alpha}_j, -\bar{\xi}_j\right) = \left(\pi/2, -\bar{\xi}_j\right) \tag{A4}$$

and in a gravitational field caracterized by the metric

$$G_j = \mathrm{diag}\left(1, -\cos^{-2}(\theta_j)\right). \tag{A5}$$

Since relativistic gravitational fields are represented by space-time metrics [48], making the angle θ a time-dependent random variable is equivalent to imposing a time-dependent random gravitational field. To better understand the electric aspects of the problem, let us recall that the DTQWs defined by (A1) exhibit the following exact discrete gauge invariance [22]:

$$\begin{aligned} \Psi'_{j,m} &= \Psi_{j,m} e^{-i\phi_{j,m}} \\ \xi'_{j,m} &= \xi_{j,m} + \delta_{j,m} \\ \theta'_{j,m} &= \theta_{j,m} \\ \alpha'_{j,m} &= \alpha_{j,m} + \frac{\sigma_{j,m}}{2} \\ \zeta'_{j,m} = &= \zeta_{j,m} - \delta_{j,m} \end{aligned} \tag{A6}$$

where

$$\begin{aligned} \sigma_{j,m} &= \phi_{j,m+1} + \phi_{j,m-1} - 2\phi_{j+1,m} \\ \delta_{j,m} &= \frac{\phi_{j,m+1} - \phi_{j,m-1}}{2} \end{aligned} \tag{A7}$$

and ϕ is an arbitrary time- and space-dependent phase shift. Let us now define a new quantity $E_{j,m}$ by

$$E_{j,m} = -\left(\mathcal{D}_s V\right)_{j,m} + \left(\mathcal{D}_t \mathcal{A}\right)_{j,m} \tag{A8}$$

where the actions of the operators $\mathcal{D}_s$ and $\mathcal{D}_s$ on an arbitrary time- and space-dependent quantity $u_{j,m}$ are

$$\left(\mathcal{D}_s u\right)_{j,m} = \frac{u_{j,m+1} - u_{j,m-1}}{2} \tag{A9}$$

and

$$\left(\mathcal{D}_t u\right)_{j,m} = \frac{2u_{j+1,m} - u_{j,m+1} - u_{j,m-1}}{2}. \tag{A10}$$

The operators $\mathcal{D}_s$ and $\mathcal{D}_t$ are discrete counterparts of space- and time-derivatives. It is straightforward to check that the quantity $E_{j,m}$ is gauge invariant and coincides, in the continuous limit, with the standard electric field $E(t,x)$, defined by $E(t,x) = -\partial_x V + \partial_t \mathcal{A}$. The quantity $E_{j.m}$ is thus a *bona fide* electric field in discrete space-time. For the DTQWs considered in this article, this electric field depends only on the time j and is related to the angle $\bar{\xi}$ by $E_j = -\left(\bar{\xi}_{j+1} - \bar{\xi}_j\right)$. Making this angle a time-dependent random variable is thus equivalent to imposing a random electric field.

Appendix B: Aymptotic computation of the eigenvalues and eigenvectors of the averaged transport operators

Let us here compute the eigenvalues $\lambda_r^{e/g}$ and eigenvectors $w_r^{e/g}$, $r = 1, 2, 3, 4$ only for values of K much smaller than unity. We do not perform an expansion in p because the initial condition is uniform in p and the average evolution does not localize the density operator around $p = 0$. Indeed, the initial condition is localized at $x' = x$ *i.e.* does not exhibit any spatial correlation and the dynamics does not create spatial correlations.

The second order expansions of the operators $\bar{\mathcal{R}}^e$ and $\bar{\mathcal{R}}^g$ in K read:

$$\bar{\mathcal{R}}_2^e(K,p,\sigma) = \begin{bmatrix} 1-2K^2 & 2iK & 0 & 0 \\ 0 & 0 & \mathrm{sinc}(\sigma/2)\cos(2p) & -i\,\mathrm{sinc}(\sigma/2)\sin(2p) \\ 2i\mathrm{sinc}(\sigma/2)K & \mathrm{sinc}(\sigma/2)\left(1-2K^2\right) & \frac{(1-\mathrm{sinc}(\sigma))}{2}\cos(2p) & i\frac{(\mathrm{sinc}(\sigma)-1)}{2}\sin(2p) \\ 0 & 0 & i\frac{(1+\mathrm{sinc}(\sigma))}{2}\sin(2p) & -\frac{(\mathrm{sinc}(\sigma)+1)}{2}\cos(2p) \end{bmatrix}, \tag{B1}$$

and

$$\bar{\mathcal{R}}_2^g(K,p,\sigma) = \begin{bmatrix} 1-2K^2 & 2iK & 0 & 0 \\ 0 & 0 & \mathrm{sinc}(\sigma)\cos(2p) & -i\,\mathrm{sinc}(\sigma)\sin(2p) \\ 2i\mathrm{sinc}(\sigma)K & \mathrm{sinc}(\sigma) & 0 & 0 \\ 0 & 0 & i\sin(2p) & -\cos(2p) \end{bmatrix}. \tag{B2}$$

For $K = 0$, these two matrices are both block diagonal and we write $\bar{\mathcal{R}}_2^{e/g}(K = 0, p, \sigma) = \mathrm{diag}(1, M^{e/g}(p,\sigma))$, where $M^{e/g}(p,\sigma)$ are 3×3 matrices acting in the space spanned by (u_2, u_3, u_4). The matrices $\bar{\mathcal{R}}_2^{e/g}(K = 0, p, \sigma)$ share u_1 as common eigenvector, which we identify as $w_1^{e/g}(K = 0, p, \sigma)$; the associated eigenvalue is $\lambda_1^{e/g}(K = 0, p, \sigma) = 1$. The other eigenvectors and eigenvalues, at zeroth order in K, are those of $M^{e/g}(p,\sigma)$. These eigenvalues can be computed analytically by solving the third-order characteristic polynomials associated to these matrices. The explicit expressions of these eignevalues are quite involved and need not be replicated here. What is important is how the moduli of these eigenvalues compares to unity. Direct inspection reveals that the moduli of all three $\lambda_r^e(0, p, \sigma)$, $r = 2, 3, 4$ are strictly inferior to unity if σ is not vanishing. The same goes for all three eigenvalues in the gravitational case, except for one of them which reaches ± 1 independantly of σ for $p = \pm\pi$ and is also equal to $+1$ for $p = 0$; the eigenspaces corresponding to $\lambda_4^g(\pm\pi, \sigma)$ and $\lambda_4^g(0, \sigma)$ are identical and generated by u_4, which we choose as $w_4^g(p = \pm\pi, \sigma) = w_4^g(0, \sigma)$. For other values of p, the eigenvalue $\lambda_4^g(p, \sigma)$ and the eigenvector $w_4^g(p, \sigma)$ are defined by continuity. All other eigenvectors need not be specified for what follows.

Let us now turn to non vanishing values of K. The characteristic polynomials of $\bar{\mathcal{R}}_2^{e/g}(K, p, \sigma)$ contain terms of order 2 and 4 in K; at lowest order in K, the corrections to the eigenvalues $\lambda_j^{e/g}(K = 0, p, \sigma)$ thus scale generically as K^2. Let λ be the variable of the characteristic polynomials. At second order in K, the K-dependent correction to each of the zeroth order eigenvalues $\lambda_r^{e/g}(K = 0, p, \sigma)$ can be found by expanding the characteristic polynomial of $\bar{\mathcal{R}}_2^{e/g}(K, p, \sigma)$ at first order in $\left(\lambda - \lambda_r^{e/g}(K = 0, p, \sigma)\right)$ and by keeping only the terms scaling as K^2. This gives rational expressions for the corrections to the eigenvalues; these rational expressions can be further simpified by a final expansion around $K = 0$ if p is treated as a finite, non infinitesimal quantity *i.e.* $\mid K \mid \ll \mid p \mid$. One then finds:

$$\lambda_1^{e/g}(K, p, \sigma) = 1 - \alpha^{e/g}(p,\sigma)K^2 + O(K^4) \tag{B3}$$

with

$$\alpha^e(p,\sigma) = 2\,\frac{3 + (\mathrm{sinc}(\sigma))^2 + 2\,(\mathrm{sinc}(\sigma/2))^2\,(1 + \mathrm{sinc}(\sigma)) + 4\cos(2p)\left(\mathrm{sinc}(\sigma) + (\mathrm{sinc}(\sigma/2))^2\right)}{3 + (\mathrm{sinc}(\sigma))^2 - 2\,(\mathrm{sinc}(\sigma/2))^2\,(1 + \mathrm{sinc}(\sigma)) + 4\cos(2p)\left(\mathrm{sinc}(\sigma) - (\mathrm{sinc}(\sigma/2))^2\right)} \tag{B4}$$

and

$$\alpha^g(p,\sigma) = 2\,\frac{1 + (\mathrm{sinc}(\sigma))^2}{1 - (\mathrm{sinc}(\sigma))^2}. \tag{B5}$$

Note that α^g is actually independent of p. Note also that the condition $\mid K \mid \ll \mid p \mid$ does not hinder asymptotic computations, at least on the infinite line. Indeed, as time increases, the density operator becomes more and more localized around $K = 0$, but it does not localize in p-space [**?**]. If one works on the infinite line, both K and p are continuous variables and the localization of the density operator around $K = 0$ implies that the size of the region in

p-space where the condition $\mid K \mid \ll \mid p \mid$ does not apply actually shrinks to zero with time. For dynamics taking place on a finite circle (finite value of M), computations are a little more involved but can nevertheless be carried out. We feel a detailled analysis of the problem for finite values of M does not bring any valuable insight on interesting physics or mathematics, and we thus restrict the analytical discussion of the asymptotic dunamics to DTQWs on the infinite line, where expressions (B4) and (B5) suffice.

A direct computation shows that the corrections to the eigenvectors are first order in K. By convention, we fix to unity the value of the first component of $w_1^{e/g}(K,p,\sigma)$ in the basis (u_1,u_2,u_3,u_4). One thus gets for example

$$w_1^g(K,p,\sigma) = \{1,\ \tfrac{2iK\mathrm{sinc}(\sigma)^2}{1-\mathrm{sinc}(\sigma)^2},\ \tfrac{2iK\mathrm{sinc}(\sigma)}{1-\mathrm{sinc}(\sigma)^2},\ \tfrac{-2K\mathrm{sinc}(\sigma)\tan(p)}{1-\mathrm{sinc}(\sigma)^2}\}. \tag{B6}$$

The expression of w_1^e is substantially more complicated and need not be reproduced here.

Appendix C: Asymptotic expression of the density operator in Fourier space

Let us now use the above results to determine the time evolution of the average density operator in both cases under consideration. The first step is to express the initial condition, $\hat{\rho}_{j=0}(K,p) = (u_1 - u_4)/2$ for all (K,p), as a linear combination of the eigenvectors $w_r^{e/g}(K,p,\sigma)$. We thus write, for $a = 1,2,3,4$

$$u_a = \sum_{r=1}^{4} u_{ar}^{e/g}(K,p,\sigma) w_r^{e/g}(K,p,\sigma) \tag{C1}$$

and, conversely,

$$w_r^{e/g}(K,p,\sigma) = \sum_{a=1}^{4} w_{ra}^{e/g}(K,p,\sigma) u_a. \tag{C2}$$

By the above discussion of the eigenvalues and eigenvectors of $\bar{\mathcal{R}}_2^{e/g}$, one has notably $u_{11}^{e/g}(K,p,\sigma) = 1$, $u_{1r}^{e/g}(K,p,\sigma) = O(K)$ for $r = 2,3,4$, $w_{11}^{e/g}(K,p,\sigma) = 1 + O(K)$.

One then writes', for all K and p:

$$\hat{\rho}_{j=0}(K,p) = \frac{1}{2}\sum_{r=1}^{4} \left(u_{1r}^{e/g}(K,p,\sigma) - u_{4r}^{e/g}(K,p,\sigma)\right) w_r^{e/g}(K,p,\sigma). \tag{C3}$$

which leads to

$$\hat{\rho}_{j=J}(K,p) = \frac{1}{2}\sum_{r=1}^{4} \left(\lambda_r^{e/g}(K,p,\sigma)\right)^J \left(u_{1r}^{e/g}(K,p,\sigma) - u_{4r}^{e/g}(K,p,\sigma)\right) w_r^{e/g}(K,p,\sigma) \tag{C4}$$

or, expressing the eigenvectors $w_r^{e/g}(K,p,\sigma)$ in terms of the original basis vectors (u_1,u_2,u_3,u_4):

$$\hat{\rho}_{j=J}(K,p) = \frac{1}{2}\sum_{r=1}^{4}\sum_{a=1}^{4} \left(\lambda_r^{e/g}(K,p,\sigma)\right)^J \left(u_{1r}^{e/g}(K,p,\sigma) - u_{4r}^{e/g}(K,p,\sigma)\right) w_{ra}^{e/g}(K,p,\sigma) u_a \tag{C5}$$

Now, for all r,

$$\lambda_r^{e/g}(K,p,\sigma)/\lambda_1^{e/g}(K,p,\sigma) = \lambda_r^{e/g}(K=0,p,\sigma)\left(1 + O(K^2)\right), \tag{C6}$$

since $\lambda_r^{e/g}(K=0,p,\sigma) = 1$. It follows that, for small enough K, the contributions to (C5) proportional to $\left(\lambda_r^{e/g}(K,p,\sigma)\right)^J$ are much smaller than the contribution proportionnal to $(\lambda_1^{e/g}(K,p,\sigma))^J$ for all values of p and σ such that $\mid \lambda_r^{e/g}(K=0,p,\sigma) \mid < 1$. According to the above discussion, this is realized for all $r \neq 1$ and for all values of p and σ, except in case 2 (random gravitational field) for $r = 4$, $p = \pm\pi$ or $p = 0$ and all values of σ. What happens at $p = \pm\pi$ has no incidence on the computation of the density operator in physical space. Indeed, for finite values of M, the maximum value $p_{\max}$ of $\mid p \mid$ is $p_{\max} = (2M/(2M+1))\pi < \pi$. Thus $\pm\pi$ is only reached in the limiting case of infinite M *i.e.* for quantum walks in the infinite line. However, $\pm p_{\max} = \pm\pi$ then only appear as upper and

lower bounds for integrals over p, and the values taken by $\hat{\rho}(J,K,p)$ at points $\pm\pi$ does not modify the values of the integrals. Moreover, all current computations are only valid for $\mid p \mid \ll \mid K \mid$ and are thus sl a priori invalid for $p=0$. What happens around $p=0$ has however no relevance to asymptotic computations on the infinite line because, as time increases, the density operator becomes more and more localized around $K=0$ (see discussion below (B5)).

For large enough J and small enough K, the double sum in (C5) thus simplifies into:

$$\hat{\rho}^{e/g}_{j=J}(K,p) = \frac{1}{2}\sum_{a=1}^{4}\left(\lambda_1^{e/g}(K,p,\sigma)\right)^J\left(u_{11}^{e/g}(K,p,\sigma) - u_{41}^{g/e}(K,p,\sigma)\right)w_{1a}^{e/g}(K,p,\sigma)u_a \tag{C7}$$

Now, $u_{11}^{e/g}(K,p,\sigma) = 1+O(K)$, $u_{41}^{e/g}(K,p,\sigma) = O(K)$, $w_{11}^{e/g}(K,p,\sigma) = 1+O(K)$ and $w_{1b}^{e/g}(K,p,\sigma) = O(K)$ for $b=2,3,4$. As far as orders of magnitude are concerned, equation (C7) gives:

$$\hat{\rho}^{e/g}_{j=J}(K,p) = \frac{1}{2}\left(1-\alpha^{e/g}(p,\sigma)K^2\right)^N\left(1+O(K)\right)u_1 + \sum_{b=2}^{4}O(K)u_b. \tag{C8}$$

At lowest order in K, $\left(1-\alpha^{e/g}(K,p,\sigma)K^2\right)^J = 1-\alpha^{e/g}(K,p,\sigma)JK^2$. We will now restrict the discussion to scales K and times J obeying $JK^2 \gg K$ i.e. $JK \gg 1$. Note that the maximum spatial spread of $\bar{\rho}$ at time J is $L_{\max}(J) = 2J$, so that the minimum value of K for which $\hat{\rho}$ takes non negligible values at time J is of order $K_{\min}(N) = 1/J$. The condition $JK \gg 1$ thus restricts the discussion to length scales much smaller than $L_{\max}(N)$. In particular, consider the time-dependent scale $K_J = K_*/\sqrt{J}$, where K_* is an arbitrary time-independent wave-vector. The wave-vector K_J obeys $JK_J^2 = K_*^2 \gg K_J$ for sufficiently large J. Thus, the possible diffusive behavior of the averaged transport is encompassed by the present discussion.

With the above assumption, equation (C7) implies the following approximate but very simple expression for the long time (large J) density operator in Fourier space:

$$\hat{\rho}^{e/g}_{j=J}(K,p) = \frac{1}{2}\left(1-\alpha^{e/g}(p,\sigma)K^2\right)^J u_1. \tag{C9}$$

In particular, for $K_J = K_*/\sqrt{J}$ (where K_* is an arbitrary but J-independent wave number) and large enough J,

$$\hat{\rho}^{e/g}_{j=J}(K_J,p) = \frac{1}{2}\left(1-\alpha^{e/g}(p,\sigma)\frac{K_*^2}{J}\right)^J u_1 \sim \frac{1}{2}\exp\left(-\alpha^{e/g}(p,\sigma)K_*^2\right)u_1 = \frac{1}{2}\exp\left(-\alpha^{e/g}(p,\sigma)JK_J^2\right)u_1. \tag{C10}$$

This is the approximate expression for the asymptotic density operator presented in the main body of this article.

[1] R.P. Feynman and A.R. Hibbs. Quantum mechanics and path integrals. *International Series in Pure and Applied Physics. McGraw-Hill Book Company*, 1965.

[2] Y. Aharonov, L. Davidovich, and N. Zagury. Quantum random walks. *Phys. Rev. A*, 48:1687, 1993.

[3] D.A. Meyer. From quantum cellular automata to quantum lattice gases. *J. Stat. Phys.*, 85, 1996.

[4] H. Schmitz, R. Matjeschk, Ch. Schneider, J. Glueckert, M. Enderlein, T. Huber, and T. Schaetz. Quantum walk of a trapped ion in phase space. *Phys. Rev. Lett.*, 103(090504):090504, August 2009.

[5] F. Zähringer, G. Kirchmair, R. Gerritsma, E. Solano, R. Blatt, and C.F. Roos. Realization of a quantum walk with one and two trapped ions. *Phys. Rev. Lett.*, 104:100503, 2010.

[6] A. Schreiber, K.N. Cassemiro, A. Gábris V. Potoček, P.J.Mosley, E. Andersson, I. Jex, and Ch. Silberhorn. Photons walking the line. *Phys. Rev. Lett.*, 104(050502):050502, 2010.

[7] Michal Karski, Leonid Förster, Jai-Min Cho, Andreas Steffen, Wolfgang Alt, Dieter Meschede, and Artur Widera. Quantum walk in position space with single optically trapped atoms. *Science*, 325(5937):174–177, 2009.

[8] Sansoni L, Sciarrino F, Vallone G, Mataloni P, Crespi A, Ramponi R, and Osellame R. Two-particle bosonic-fermionic quantum walk via 3d integrated photonics. *Phys. Rev. Lett.*, 108(010502):010502, 2012.

[9] B.C. Sanders, S.D. Bartlett, B. Tregenna, and P.L. Knight. Two-particle bosonic-fermionic quantum walk via 3d integrated photonics. *Phys. Rev. A*, 67:042305, 2003.

[10] B. Perets, Y. Lahini, F. Pozzi, M. Sorel, R. Morandotti, and Y. Silberberg. Realization of quantum walks with negligible decoherence in waveguide lattices. *Phys. Rev. Lett.*, 100:170506, 2008.

[11] D. Giulini, E. Joos, C. Kiefer, J. Kupsch, I.-O. Stamatescu, and H.D. Zeh. *Decoherence and the appearance of a Classical World in Quantum Theory.* Springer-Verlag, Berlin, 1996.

[12] A. Ambainis. Quantum walk algorithm for element distinctness. *SIAM Journal on Computing*, 37:210–239, 2007.

[13] F. Magniez, J. Roland A. Nayak, and M. Santha. Search via quantum walk. *SIAM Journal on Computing - Proceedings of the thirty-ninth annual ACM symposium on Theory of computing*, New York, 2007. ACM.

[14] C. Aslangul. Quantum dynamics of a particle with a spin-dependent velocity. *Journal of Physics A: Mathematical and Theoretical*, 38:1–16, 2005.

[15] S. Bose. Quantum communication through an unmodulated spin chain. *Phys. Rev. Lett.*, 91:207901, 2003.

[16] D. Burgarth. Quantum state transfer with spin chains. *University College London*, PhD thesis, 2006.

[17] S. Bose. Quantum communication through spin chain dynamics: an introductory overview. *Contemp. Phys.*, 48(Issue 1):13 – 30, January 2007.

[18] E. Collini, C.Y. Wong, K.E. Wilk, P.M.G. Curmi, P. Brumer, and G.D. Scholes. *Nature*, page 644.

[19] G.S. Engel, T.R. Calhoun, R.L. Read, T.-K. Ahn, T. Manal, Y.-C. Cheng, R.E. Blankenship, and G. R. Fleming. *Nature*, page 782.

[20] G. Di Molfetta and F. Debbasch. Discrete-time quantum walks: Continuous limit and symmetries. *J. Math. Phys.*, 53:123302, 2012.

[21] G. Di Molfetta, F. Debbasch, and M. Brachet. Quantum walks as massless dirac fermions in curved space. *Phys. Rev. A*, 88, 2013.

[22] G. Di Molfetta, F. Debbasch, and M. Brachet. Quantum walks in artificial electric and gravitational fields. *Phys. A*, 397, 2014.

[23] V. Kendon. Decoherence in quantum walks - a review. *Math. Struct. in Comp. Sc.*, 17(6):1169–1220, 2007.

[24] R. Vieira, E. P. M. Amorim, and G. Rigolin. Entangling power of disordered quantum walks. *Phys. Rev. A*, 89:042307, 2014.

[25] Todd A. Brun, Hilary A. Carteret, and Andris Ambainis. Quantum to classical transition for random walks. *Phys. Rev. Lett.*, 91:130602, Sep 2003.

[26] A. Ahlbrecht, H. Vogts, A. H. Werner, and R. F. Werner. Asymptotic evolution of quantum walks with random coin. *Journal of Mathematical Physics*, 52(4), 2011.

[27] Andre Ahlbrecht, Christopher Cedzich, Robert Matjeschk, VolkherB. Scholz, AlbertH. Werner, and ReinhardF. Werner. Asymptotic behavior of quantum walks with spatio-temporal coin fluctuations. *Quantum Information Processing*, 11(5):1219–1249, 2012.

[28] Alain Joye. Random time-dependent quantum walks. *Communications in Mathematical Physics*, 307(1):65–100, 2011.

[29] B. Kollar and M. Koniorczyk. Entropy rate of message sources driven by quantum walks. *Phys. Rev. A*, 89:022338, 2014.

[30] Chaobin Liu and Nelson Petulante. On the von neumann entropy of certain quantum walks subject to decoherence. *Mathematical Structures in Computer Science*, 20:1099–1115, 12 2010.

[31] C.M. Chandrasekhar, S. Banerjee, and R. Srikanth. Relationship between quantum walks and relativistic quantum mechanics. *Phys. Rev. A*, 81:062340, 2010.

[32] G. Abal, R. Siri, A. Romanelli, and R. Donangelo. Quantum walk on the line: Entanglement and nonlocal initial conditions. *Phys. Rev. A*, 73:042302, Apr 2006.

[33] Kota Chisaki, Norio Konno, Etsuo Segawa, and Yutaka Shikano. Crossovers induced by discrete-time quantum walks. *Quantum Information & Computation*, 11(9-10):741–760, 2011.

[34] C. Navarrete-Benlloch, A. Perez, and Eugenio Roldan. Nonlinear optical galton board. *Phys. Rev. A*, 75:062333, 2010.

[35] Hideaki Obuse and Norio Kawakami. Topological phases and delocalization of quantum walks in random environments. *Physical Review B*, 84(19):195139, 2011.

[36] Yutaka Shikano, Tatsuaki Wada, and Junsei Horikawa. Discrete-time quantum walk with feed-forward quantum coin. *Scientific reports*, 4, 2014.

[37] NV Prokof?ev and PCE Stamp. Decoherence and quantum walks: Anomalous diffusion and ballistic tails. *Physical Review A*, 74(2):020102, 2006.

[38] A Schreiber, KN Cassemiro, V Potoček, A Gábris, I Jex, and Ch Silberhorn. Decoherence and disorder in quantum walks: From ballistic spread to localization. *Physical review letters*, 106(18):180403, 2011.

[39] Norio Inui, Yoshinao Konishi, and Norio Konno. Localization of two-dimensional quantum walks. *Physical Review A*, 69(5):052323, 2004.

[40] F. Debbasch. What is a mean gravitational field? *Eur. Phys. J. B*, 37(2):257–270, 2004.

[41] A. J. Leggett, S. Chakravarty, A. T. Dorsey, Matthew P. A. Fisher, Anupam Garg, and W. Zwerger. Dynamics of the dissipative two-state system. *Rev. Mod. Phys.*, 59:1–85, Jan 1987.

[42] A.O. Caldeira and A.J. Leggett. Path integral approach to quantum brownian motion. *Physica A: Statistical Mechanics and its Applications*, 121(3):587 – 616, 1983.

[43] F. Debbasch, K. Mallick, and J.P. Rivet. Relativistic Ornstein-Uhlenbeck process. *J. Stat. Phys.*, 88:945, 1997.

[44] C. Chevalier and F. Debbasch. Relativistic diffusions: a unifying approach. *J. Math. Phys.*, 49:043303, 2008.

[45] F. Debbasch, D. Espaze, and V. Foulonneau. Can diffusions propagate? *J.Stat.Phys*, 149:37–49, 2012.

[46] G. Di Molfetta and F. Debbasch. Discrete-time quantum walks: Continuous limit in 1 + 1 and 1 + 2 dimension. *J.Comp.Th.Nanosc.*, 10,7:1621–1625, 2012.

[47] P. Arnault and F. Debbasch. Landau levels for discrete-time quantum walks in artificial magnetic fields. *arXiv preprint*, 1412.4337, 2014.

[48] R.M. Wald. *General Relativity*. The University of Chicago Press, Chicago, 1984.

[49] Note however that it is possible to keep all time steps if one is only interested in the continuous limit of the probability of the original walk

[50] A simple computation shows that the partly reduced density operator $\hat{\rho}_j^{pr}(p) = \sum_K \hat{\rho}_j(K,p)$ remains flat in p at all times,

as is the initial condition

Bibliography

[1] Y. Aharonov, L. Davidovich, and N. Zagury. Quantum random walks. *Phys. Rev. A*, 48:1687, 1993.

[2] A. Ahlbrecht, H. Vogts, A. H. Werner, and R. F. Werner. Asymptotic evolution of quantum walks with random coin. *Journal of Mathematical Physics*, 52(4), 2011. doi: http://dx.doi.org/10.1063/1.3575568. URL http://scitation.aip.org/content/aip/journal/jmp/52/4/10.1063/1.3575568.

[3] A. Ahlbrecht, C. Cedzich, R. Matjeschk, V. Scholz, A. Werner, and R. Werner. Asymptotic behavior of quantum walks with spatio-temporal coin fluctuations. *Quantum Information Processing*, 11 (5):1219–1249, 2012. ISSN 1570-0755. doi: 10.1007/s11128-012-0389-4. URL http://dx.doi.org/10.1007/s11128-012-0389-4.

[4] A. Alberti, W. Alt, R. Werner, and D. Meschede. Decoherence models for discrete-time quantum walks and their application to neutral atom experiments. *New Journal of Physics*, 16(12):123052–123080, 2014.

[5] S. Attal, F. Petruccione, C. Sabot, and I. Sinayskiy. Open quantum random walks. *Journal of Statistical Physics*, 147(4):832–852, 2012.

[6] S. Attal, F. Petruccione, and I. Sinayskiy. Open quantum walks on graphs. *Physics Letters A*, 376(18): 1545–1548, 2012.

[7] N. Bohr. Can quantum-mechanical description of physical reality be considered complete? *Physical review*, 48(8):696, 1935.

[8] M. A. Broome, A. Fedrizzi, B. P. Lanyon, I. Kassal, A. Aspuru-Guzik, and A. G. White. Discrete single-photon quantum walks with tunable decoherence. *Physical review letters*, 104(15):153602, 2010.

[9] T. A. Brun, H. A. Carteret, and A. Ambainis. Quantum to classical transition for random walks. *Phys. Rev. Lett.*, 91:130602, Sep 2003. doi: 10.1103/PhysRevLett.91.130602. URL http://link.aps.org/doi/10.1103/PhysRevLett.91.130602.

[10] M. Brune, E. Hagley, J. Dreyer, X. Maitre, A. Maali, C. Wunderlich, J. Raimond, and S. Haroche. Observing the progressive decoherence of the ?meter? in a quantum measurement. *Physical Review Letters*, 77(24):4887, 1996.

[11] A. Carvalho, P. Milman, R. de Matos Filho, and L. Davidovich. Decoherence, pointer engineering and quantum state protection. In *Modern Challenges in Quantum Optics*, pages 65–79. Springer, 2001.

[12] C. Chandrashekar and T. Busch. Quantum percolation and transition point of a directed discrete-time quantum walk. *Scientific reports*, 4, 2014.

[13] K. Chisaki, N. Konno, E. Segawa, and Y. Shikano. Crossovers induced by discrete-time quantum walks. *Quantum Information & Computation*, 11(9-10):741–760, 2011.

[14] D. G. Cory, M. Price, W. Maas, E. Knill, R. Laflamme, W. H. Zurek, T. F. Havel, and S. Somaroo. Experimental quantum error correction. *Physical Review Letters*, 81(10):2152, 1998.

[15] L. Davidovich, M. Brune, J. Raimond, and S. Haroche. Mesoscopic quantum coherences in cavity qed: Preparation and decoherence monitoring schemes. *Physical Review A*, 53(3):1295, 1996.

[16] W. Dür, R. Raussendorf, V. M. Kendon, and H.-J. Briegel. Quantum walks in optical lattices. *Physical Review A*, 66(5):052319, 2002.

[17] K. Gottfried. Quantum mechanics wa benjamin. *Inc., New York*, 1966.

[18] M. Hinarejos, M. C. Bañuls, and A. Pérez. Wigner formalism for a particle on an infinite lattice: dynamics and spin. *New Journal of Physics*, 17(1):013037, 2015.

[19] A. Joye. Random time-dependent quantum walks. *Communications in Mathematical Physics*, 307 (1):65–100, 2011. ISSN 0010-3616. doi: 10.1007/s00220-011-1297-7. URL http://dx.doi.org/10.1007/s00220-011-1297-7.

[20] M. Karski, L. Förster, J.-M. Choi, A. Steffen, W. Alt, D. Meschede, and A. Widera. Quantum walk in position space with single optically trapped atoms. *Science*, 325(5937):174–177, 2009.

[21] V. Kendon. Decoherence in quantum walks - a review. *Math. Struct. in Comp. Sc.*, 17(6):1169–1220, 2007.

[22] V. Kendon. Decoherence in quantum walks–a review. *Mathematical Structures in Computer Science*, 17(06):1169–1220, 2007.

[23] V. Kendon and B. Tregenna. Decoherence can be useful in quantum walks. *Physical Review A*, 67 (4):042315, 2003.

[24] E. Knill, R. Laflamme, and W. H. Zurek. Resilient quantum computation. *Science*, 279(5349):342–345, 1998.

[25] E. Knill, R. Laflamme, and L. Viola. Theory of quantum error correction for general noise. *Physical Review Letters*, 84(11):2525, 2000.

[26] C. C. Lopez and J. P. Paz. Phase-space approach to the study of decoherence in quantum walks. *Physical Review A*, 68(5):052305, 2003.

[27] C. Monroe, D. Meekhof, B. King, and D. Wineland. A ?schrödinger cat? superposition state of an atom. *Science*, 272(5265):1131–1136, 1996.

[28] J. Neumann. *Mathematische grundlagen der quantenmechanik*. Verlag von Julius Springer, 1932.

[29] H. Obuse and N. Kawakami. Topological phases and delocalization of quantum walks in random environments. *Physical Review B*, 84(19):195139, 2011.

[30] R. Omnes. *The interpretation of quantum mechanics*. Princeton University Press, 1994.

[31] J. Preskill. Lecture notes for physics 229: Quantum information and computation. *California Institute of Technology*, 1998.

[32] N. Prokof'ev and P. Stamp. Decoherence and quantum walks: Anomalous diffusion and ballistic tails. *Physical Review A*, 74(2):020102, 2006.

[33] C. Savage, S. L. Braunstein, and D. Walls. Macroscopic quantum superpositions by means of single-atom dispersion. *Optics letters*, 15(11):628–630, 1990.

[34] A. Schreiber, K. Cassemiro, V. Potoček, A. Gábris, I. Jex, and C. Silberhorn. Decoherence and disorder in quantum walks: From ballistic spread to localization. *Physical review letters*, 106(18):180403, 2011.

[35] E. Schrödinger. Die gegenwärtige situation in der quantenmechanik. *Naturwissenschaften*, 23(49): 823–828, 1935.

[36] R. Vieira, E. P. M. Amorim, and G. Rigolin. Entangling power of disordered quantum walks. *Phys. Rev. A*, 89:042307, 2014.

[37] L. Viola, E. Knill, and S. Lloyd. Dynamical decoupling of open quantum systems. *Physical Review Letters*, 82(12):2417, 1999.

[38] J. A. Wheeler and W. H. Zurek. *Quantum theory and measurement*. Princeton University Press, 2014.

[39] B. Yurke and D. Stoler. Generating quantum mechanical superpositions of macroscopically distinguishable states via amplitude dispersion. *Physical review letters*, 57(1):13, 1986.

[40] H.-D. Zeh. On the interpretation of measurement in quantum theory. *Foundations of Physics*, 1 (1):69–76, 1970.

[41] H. D. Zeh. Toward a quantum theory of observation. *Foundations of Physics*, 3(1):109–116, 1973.

[42] W. H. Zurek. Decoherence, einselection, and the quantum origins of the classical. *Rev. Mod. Phys.*, 75:715–775, May 2003. doi: 10.1103/RevModPhys.75.715. URL http://link.aps.org/doi/10.1103/RevModPhys.75.715.

Part II

... to spontaneous equilibration.

CHAPTER 4

THERMALIZATION AND QUANTUM WALKS

Summary

4.1 Absolute equilibrium in conservative systems 99

4.1.1 A general introduction 99

4.1.2 Thermalization and absolute equilibria in Galerkin truncated PDEs 100

4.1.3 From microcanonical to grand canonical ensemble 101

4.2 Nonlinear QW-like models and thermalization 102

4.2.1 Thermalization in closed quantum systems 102

4.2.2 QWs on N-cycle and limiting distribution 103

4.2.3 A Nonlinear Quantum Walk-like model on N-cycle 104

4.3 Publication: "Nonlinear Optical Galton Board: thermalization and continuous limit" 105

4.1 Absolute equilibrium in conservative systems

4.1.1 A general introduction

In classical statistical mechanics all dynamical systems in equilibrium or out of equilibrium can be described by a Liouville equation, a milestone in many-body theory. In the following we try to introduce the usual notation and definition that the reader can find in a standard textbook of statistical mechanics (e.g. *landau2013course*).

The Liouville equation describes the time evolution of the probability of finding the system in a given region of the phase space and expresses the conservation of the probability current in this space. Let us introduce a general dynamical system defined by:

$$\frac{\partial}{\partial_t}\mathbf{X} = V(X_1, ..., X_{2N}) \tag{4.1}$$

The $2N$-dimensional vector $\mathbf{X}$, which represents the coordinates of the system, evolves in the $2N$-dimensional phase space with a probability distribution $P(\mathbf{X}, t)$. The probability $P(\mathbf{X}, t)d^{2N}X$ obeys to the following PDE:

$$\frac{\partial}{\partial_t}P(\mathbf{X}, t) + \sum_{i=1}^{2N}\frac{\partial}{\partial_{X_i}}(V(X_1, ...X_{2N})P(X_1, ..., X_{2N}, t)) = 0, \tag{4.2}$$

which is called the *Liouville equation*, derived for the first time by the french mathematician Joseph Liouville in 1838. Now let us consider that the system is Hamiltonian and that $\mathbf{X}$ =

$\{q_1,...,q_N,p^1,...,p^N\} = \{\mathbf{q},\mathbf{p}\}$ is the vector of the conjugate real variable $\mathbf{q}$ and $\mathbf{p}$. The system is then described by the canonical equations:

$$\begin{aligned} \frac{\partial}{\partial_t}\mathbf{q} &= \frac{\partial \mathbf{H}}{\partial \mathbf{p}} \\ \frac{\partial}{\partial_t}\mathbf{p} &= -\frac{\partial \mathbf{H}}{\partial \mathbf{q}}, \end{aligned} \tag{4.3}$$

where $\mathbf{H}$ is the Hamiltonian of the system. For a such system the Eq. (4.2) can be simplified in the following form:

$$\frac{\partial}{\partial_t}P(\mathbf{X},t) + \mathbf{V}(\mathbf{X})\cdot\nabla P(\mathbf{X},t) = 0, \tag{4.4}$$

because the conjugate variables in $\mathbf{X}$ satisfy the divergence relation $\nabla\cdot\mathbf{V}(\mathbf{X}) = 0$.

Now let us suppose that Eq. (4.1) admits a set of integrals K_i. We can write for each integral:

$$\frac{dK_i}{dt} = \frac{\partial K_i}{\partial \mathbf{X}}\frac{\partial \mathbf{X}}{\partial t} = \nabla\mathbf{K}\cdot\mathbf{V}(\mathbf{X}) = 0 \tag{4.5}$$

The Eq. (4.4) with the Eq. (4.5) allows us to compute, if it exists, the stationary probability:

$$P_{st}(\mathbf{X}) = \frac{1}{\mathcal{Z}}e^{-\beta\sum_i K_i} \tag{4.6}$$

where $\mathcal{Z}$ is a normalization factor. The solution (4.6) is known as *absolute equilibrium*. In thermodynamics it represents a thermodynamic equilibrium, called Gibbs distribution, and β corresponds to the inverse of the thermodynamic temperature of the system. The evolution from the initial condition to the absolute equilibrium is called *equilibration*, or *thermalization* if it does not depend on the initial conditions.

4.1.2 Thermalization and absolute equilibria in Galerkin truncated PDEs

Absolute equilibria are typically observed, for instance, in real fluid at very high Reynolds numbers, where the energy transfers from macroscopic scales to molecular thermal energy [9]. In non-dissipative flow, artificial microscopic systems can cause an effective dissipation, leading to thermalization. This effective dissipative effect is a consequence of a Galerkin truncation that consists in taking the Fourier transform of the PDEs and retaining only a finite number of the Fourier coefficients as dynamical variables. This operation can be represented by a Galerkin projector which suppresses all the modes k greater than a given k_{max}, *i.e.* the truncation wavenumber. The truncated systems recover the original system only if the convergence of the numerical scheme is ensured. In other words the spectrum has to fall down rapidly at a wave number much smaller than the truncation wavenumber.

The thermalization phenomenon of the truncated system due to the effective viscosity was discovered by Lee [17] and studied in detail by Kraichnan [12] in 3D. Later Cichowlas et al. [7] analyzed an ideal non-dissipative flow obeying to the truncated Euler equations, grasping the underlying mechanism of thermalization in this system. Recently Krstulovic and Brachet [13][14] extended this analysis to the magneto-hydrodynamics (MHD) and the Gross-Pitaevskii (GP) equations. These equations together with the truncated compressible and incompressible Euler equations are all conservative truncated systems. The property that this

class of systems relaxes, with a very rich behavior, toward the statistical equilibrium is a very general fact.

4.1.3 From microcanonical to grand canonical ensemble

Let us examine the Eqs. (4.3), and suppose that the system admits the conserved quantities K_i and the equilibrium point (4.6). Following Landau and Lifshitz [16], we should be able to define the microcanonical ensemble by the probability dw of finding the system in states with $K_i = K_i^0$ (the overscript denotes the initial time $t = 0$):

$$dw \propto e^S \prod_i \delta(K_i - K_i^0), \tag{4.7}$$

where $S = log\Omega$ is the entropy with the number of accessible microstates. To obtain the microcanonical statistical states we integrate Eqs. (4.3) until the system reaches the thermodynamical equilibrium. However, the associated temperature β^{-1} is not always accessible. This is because, we cannot always obtain an explicit form for dw and S.
Following Krstulovic et al. [15], to control the temperature we should use the grand-canonical distribution probability given by the Boltzmann weight:

$$P_{st} = \frac{1}{Z} e^{-\beta F}, \tag{4.8}$$

where $F = \mathbf{H} - \sum_i \mu_i K_i$ and Z is a normalization function, β^{-1} is the temperature and μ_i are the Lagrange multiplier associated to each conserved quantities K_i. Let us mention that, as the microcanonical ensemble is controlled by the variables K_i^0, the grand canonical ensemble is characterized by the conjugate μ_i.

The key point that allows us to use the grand canonical ensemble, is a well known equivalence under very general circumstances between the microcanonical and grand canonical ensemble. In fact, in the thermodynamic limit, that is if the number of Fourier modes $N \to \infty$, both statistical ensembles are expected to be equivalent [16].

Let us now observe that computing the stationary distribution (4.8) is not a trivial problem, especially when the Hamiltonian in Eqs. (4.3) is not quadratic and therefore the statistical distribution is not Gaussian. Nonetheless Krstulovic et al. [15] have introduced an algorithm that generates absolute equilibrium for all Hamiltonian dynamics of the form (4.3) admitting a stable equilibrium point $\mathbf{X}^*$. The idea of this algorithm is to construct a stochastic process that converges to a stationary solution with the equilibrium distribution given by (4.8).

The stochastic process can be defined by the following Langevin equations:

$$\begin{aligned} \frac{\partial}{\partial_t}\mathbf{q} &= -\nu \frac{\partial \mathbf{H}}{\partial \mathbf{q}} + \sqrt{2\eta\nu}\xi^{\mathbf{1}}(\mathbf{t}) \\ \frac{\partial}{\partial_t}\mathbf{p} &= -\nu \frac{\partial \mathbf{H}}{\partial \mathbf{p}} + \sqrt{2\eta\nu}\xi^{\mathbf{2}}(\mathbf{t}), \end{aligned} \tag{4.9}$$

where $\langle \xi_i(t), \xi_j(t') \rangle = \delta_{ij}\delta(t - t')$ define a white Gaussian forcing term, with $\langle \xi_i(t) \rangle = 0$. The coefficients $(\eta, \nu) \in \mathbb{R}^+ \times \mathbb{R}^+$. The probability distribution P of the stochastic process, defined

by Eqs. (4.9), can be shown to obey the following Fokker-Planck equation:

$$\frac{\partial}{\partial_t}P = \nu\left[\frac{\partial}{\partial \mathbf{q}}(\frac{\partial}{\partial \mathbf{q}}HP) + \frac{\partial}{\partial \mathbf{p}}(\frac{\partial}{\partial \mathbf{p}}HP)\right] + \eta\nu\nabla^2 P, \tag{4.10}$$

where $\nabla^2 = \frac{\partial}{\partial \mathbf{p}}^2 + \frac{\partial}{\partial \mathbf{q}}^2$. The latter equation is the Fokker-Planck equation of the transition probability $P(\mathbf{p},\mathbf{q})$, a special case of the differential Chapman-Kolmogorov equation. It describes mathematically a diffusion process. The terms in square brackets are known as the drift terms and the Laplacian corresponds to the diffusion part. Let us comment that when the diffusion term is zero, the noise in (4.9) is zero. In this case the (4.10) reduces simply to the Liouville's equation, which describes a fully deterministic motion.

This Fokker-Planck equations shares the same stationary probability (4.8) [1] and we should now directly control the μ_i to fix the mean values $\langle K_i\rangle$ to K_i^0 and to reproduce the same absolute equilibrium reached by (4.3).

In conclusion we should briefly discuss the case of complex variables. Let us introduce $w = p + iq$ and $w^* = p - iq$, and the Hamiltonian is the same in Eqs. (4.3). The canonical equation for the complex variables w and w^* read:

$$\begin{aligned}\frac{\partial}{\partial_t}w &= -i\frac{\partial H}{\partial w^*}\\ \frac{\partial}{\partial_t}w^* &= i\frac{\partial H}{\partial w}.\end{aligned} \tag{4.11}$$

The Langevin process (4.9) transcribe in:

$$\begin{aligned}\frac{\partial}{\partial_t}w &= -\nu\frac{\partial H}{\partial w^*} + \sqrt{2\eta\nu}\Xi(t)\\ \frac{\partial}{\partial_t}w^* &= -\nu\frac{\partial H}{\partial w} + \sqrt{2\eta\nu}\Xi^*(t)\end{aligned} \tag{4.12}$$

where $\Xi(t) = \xi^1(t) + i\xi^2(t)$ is now a complex Gaussian white noise defined by $\langle \Xi_i(t)\Xi_j(t')\rangle = \delta_{ij}\delta(t-t')$ and $\langle \Xi_i(t)\rangle = 0$ The Fokker-Planck associated to latter stochastic process reads:

$$\frac{\partial}{\partial_t}P = -\frac{\partial}{\partial w}(\frac{\partial}{\partial w^*}P) - \frac{\partial}{\partial w^*}(\frac{\partial}{\partial w}P) + \eta\nu\frac{\partial^2}{\partial w\partial w^*}P \tag{4.13}$$

Let us just finally observe that in case the system is described by fields we have to replace derivative by functional derivative and delta Kronecker by a Dirac delta. Nevertheless, in this case we have to fix an ultraviolet cut-off, for instance Galerkin truncate the Fourier modes of the field, to prevent the infinite energy solutions.

4.2 Nonlinear QW-like models and thermalization

4.2.1 Thermalization in closed quantum systems

Thermalization in closed quantum systems is a very recent research topic and concerns mainly the understanding of complex quantum many-body systems (QMBs). When, in 1902, the sem-

[1] Let us notice that the Fokker-Planck presented here is different from the one Krstulovic et al. [15] found because the latter was associated with a different stochastic process. However, both shares the same stationary probability.

inal work "*Elementary principles in statical mechanics*" by Gibbs was published, quantum mechanics was not yet formalized. In contrast to classical statistical mechanics, it is not clear yet, in quantum theory, in what way interacting QMBs can equilibrate and thermalize.

Lately some results have been achieved on how thermal states of local systems emerge from complex quantum dynamics [20, 21, 22, 8]. Nonetheless, many questions are still open: how typical values emerge for macroscopic local observables with suppressed quantum fluctuation [21, 8]? How does the system behave close to phase transitions when the correlation length is comparable to the size of the system itself and thermalization is not expected? How does the macroscopic picture of thermodynamics and its second law arise from the microscopic description?

Discrete QCA are naturally good candidates to investigate thermalization because of the discrete structure of the matter. Meyer [18], for instance, was the first to introduce QCA to describe quantum many-body interactions, in particular quantum gas. Differently from QCA , DTQWs are one-particle presenting no interaction with other systems, and obey to reversible and linear dynamics.

Nonetheless, different Nonlinear QW-like (NQWs) models on the one-dimensional unrestricted line have been considered recently by Shikano et al. [25] and Navarrete-Benlloch et al. [19]. These models display complex behaviors in physical space and chaotic dynamics phases. The main aim of this chapter is to prove that at least one of them thermalizes. In particular preliminary works on several of these QW-like (but non linear) automaton on a cycle, showed that they mix and rich a limiting stationary distribution. Otherwise, usual QWs do not mix [2].

Let me mention an interesting line of research by Romanelli [23] who fist studied thermal equilibria in QW from a radically different point of view. In fact the QWs they study is perfectly linear. Yet, what they look at is coin degree of freedom versus position degree of freedom, and find that the position acts like a thermal bath on the coin. They have close forms Liouville equations for the coin states and in the thermodynamical limit they define a temperature to control the relaxation process. Their work started with the Hadamard Walk [23], but was extended to a generalized QW Romanelli and Segundo [24]. Let us notice that they compute the temperature as function of the initial condition. Usually in the literature this process is called equilibration and not thermalization, that in general does not depend on the initial condition, like in the model we introduce in sec. 4.3.

The section will be organized as follows: in sub-section (4.2.2) we define a QW on a N-cycle, recalling the concept of mixing time; in sub-section (4.2.3) we introduce two different examples of NQW-like model. Lastly, we present, in section (4.3), the publication where we proved that a Nonlinear Optical Galton Board on a cycle, a NQW-like model, converges in long-term to an absolute equilibrium (interpreted by a classical thermalization mechanism) and displays a final steady probability distribution independent of initial conditions.

4.2.2 QWs on N-cycle and limiting distribution

QWs on general graphs have been extensively investigated [26] and represent a cornerstone in contemporary quantum computing. They were first introduced by D. Aharonov et al. [1] and their limiting distribution have been then fully examined by Chisaki et al. [6] and Konno [11], respectively for the discrete time and continuous time quantum walks. Graphs can be very different, with their intrinsic topological properties, and the QWs behavior can depend

strongly on these properties. Here we specialize on a 2-regular graph.

Let us recall that a general connected graph G is defined by N connected vertices V and M edges E. The graph is undirected if the edges are not oriented. Classical random walks on graphs have been largely explored and their comprehension appears fundamental in the understanding of Markov chains in computational models. As in ergodic Markov chain, CRWs on graph tend to a limiting distribution and this distribution is unique. The number of steps, that the system performs before its distribution becomes infinitesimally close to its limiting distribution, is called *mixing time*. More formally, if $P(t)$ is the probability distribution of a CRW on a connected undirected graph, the mixing time τ_ϵ is defined as:

$$\tau_\epsilon = \min_t\{t|t \geq T \Rightarrow ||P_u(t) - \pi|| < \epsilon\} \tag{4.14}$$

In other words τ_ϵ represents the first time when the distance between the stationary distribution π and $P(t)$ is less than ϵ. Not surprisingly, quantum walks do not reach any stationary distribution because the unitarity prevents the walk to reach a steady state.

However, it is proved that the temporal average of the probability distribution does converge to a limiting distribution π^* under special assumptions[2]. The mixing time is therefore defined as follows:

$$M_\epsilon = \min\{T|\forall\, t \geq T \Rightarrow ||\overline{P_{QW}(t)} - \pi^*|| < \epsilon\} \tag{4.15}$$

In the particular case of N-cycle, with N *odd*, the characteristic mixing time of an homogeneous QW grows linearly, $N \log N$, in contrast to $O(N^2)$ in CRW.

4.2.3 A Nonlinear Quantum Walk-like model on N-cycle

In order to introduce a NQW-like model on N-cycle, let us maintain that the formal definition of QW, introduced in the first chapter, extends simply on cycle considering that now the canonical basis of position $|m\rangle \in \mathbb{Z}_N$.
Let us assume that the unitary step operator $\mathcal{U}$ depends, in some way to be defined, on the wave vector itself:

$$\mathcal{U}[\Psi] = \mathcal{T}\mathcal{B}[\Psi] \tag{4.16}$$

where $\mathcal{T}$ is the coin state dependent translation operator and $\mathcal{B}$ is the coin operator. The dependence of the coin operator on the state vector can take several forms. For instance in Shikano et al. [25] the quantum coin depends at each space time point of the lattice on a site-dependent rate function which includes the nearest-neighbor interactions:

$$g_{j,m} = |\psi^L_{j,m-1}| + i|\psi^R_{j,m+1}|, \tag{4.17}$$

and the quantum coin operator transcribes in:

$$\mathcal{B}[g_{j,m}] = \begin{pmatrix} g_{j,m} & -\sqrt{1-|g_{j,m}|^2} \\ \sqrt{1-|g_{j,m}|^2} & g^*_{j,m} \end{pmatrix}. \tag{4.18}$$

[2]The unitary operator of the QW on the Cayley graph of an Abelian group must have all distinct eigenvalues. See Theorem 3.5 in D. [1]. In particular in the non-degenerate case, verified only in the case of odd N, the distribution is uniform. For *even* N, the limiting distribution displays more interesting stationary profile distributions then in odd case and they have been investigated by Bednarska et al. [3].

This *feed-forward DTQW* leads, on an unrestricted line, to an anomalous diffusion behavior and a q-Gaussian limiting distribution. Analytical computations on the associated Markov model show a good agreement with numerical data. This model has been then generalized on the N-cycle by (Di Molfetta et al., 2014)[3] in the following way:

$$\mathcal{B}[g_{j,m}] = \begin{pmatrix} g^{\alpha,h}_{j,m} & -\sqrt{1-|g^{\alpha,h}_{j,m}|^2} \\ \sqrt{1-|g^{\alpha,h}_{j,m}|^2} & g^{\alpha,h^*}_{j,m} \end{pmatrix} \tag{4.19}$$

where the new rate function reads $g^{\alpha,h}_{j,m} = |\psi^L_{j,m-h}|^\alpha + i|\psi^R_{j,m+h}|^\alpha$.
The resulting behavior appears very complex and depends strongly on the parameter (α, h) (data not shown). Let us remark that the parameter h amplifies the nonlocal strength of the interaction. We have shown numerically that the behavior of these new walks, even in the case presented by Shikano et al. [25], but on the cycle, displays a chaotic dynamic and tends in long time to a uniform probability distribution (data not shown). Such a behavior is not typical for this model, but seems to share the main features with another NQW-like model introduced by Navarrete-Benlloch et al. [19]. The proposed scheme describes a classical light radiation that acquires intensity-dependent phase while traveling in a nonlinear medium as, for instance, in Kerr medium (like an optical fiber). In QWs formalism this can be represented by the following quantum coin:

$$\mathcal{B}[\psi^{L,R}_{j,m}] = \frac{1}{\sqrt{2}} \begin{pmatrix} \exp(ig|\psi^L|^2) & \exp(ig|\psi^R|^2) \\ \exp(ig|\psi^L|^2) & -\exp(ig|\psi^R|^2) \end{pmatrix} \tag{4.20}$$

The authors in Navarrete-Benlloch et al. [19] have found that the dynamics on a one-dimensional finite lattice appears very complex in the presence of formations of soliton-like structures, inelastic shocks and chaotic behaviors. In the next section we have reproduced exactly the same model but on N-cycle. We have shown numerically and analytically, at least in the continuous limit, that the walk tends to a limiting uniform distribution and thermalizes reaching the absolute equilibrium of the system.

4.3 Publication: "Nonlinear Optical Galton Board: thermalization and continuous limit"

One of the main ways to reproduce the QW dynamics is suggested by the seminal work of Sir Francis Galton in 1877 on random walks. In order to study the classical random walk he proposed a simple device stylized in Fig. 4.1, that is now called *Galton Board* or *Galton Quincunx*. As we can see in Fig. 4.1 balls roll down on a vertical board and are scattered in a regular grid by pins, reproducing a random walk and leading to a binomial distribution. In spite of its simplicity this model is still an inspiring source for researchers [5].

Now, let us imagine that waves replace balls: the main striking difference is that waves, in contrast to balls, do not run on a single path but traverse all possible paths simultaneously. Bouwmeester et al. [4] implement an optical version in a linear resonator, in which the frequency levels mimic the rolling balls, and the birefringent crystals play the same role of the scattering pins in the classical version of the quincunx. The main result of this experience,

[3] *Di Molfetta Giuseppe, Yutaka Shikano, Fabrice Debbasch, Marc Brachet*, Work in progress, project with the financial support of JSPS summer program (SP14203).

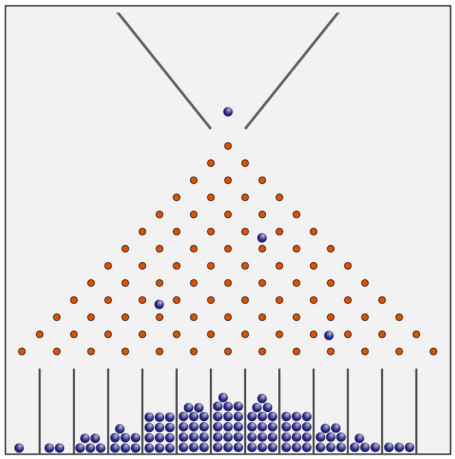

Figure 4.1: *Classical Galton Board.*

then realized by Knight et al. [10] in an optical bidirectional ring, was that the final probability distribution appeared very different from the Gaussian shape of the classical Galton board and presented the same features of standard QWs distribution. Indeed, QWs can be classically reproduced and optically implemented; in particular the Optical Galton Board (OGB) represents a natural way in which, the quantum probability amplitude for each component of the spinor, is replaced with the spectral intensities of the radiation.

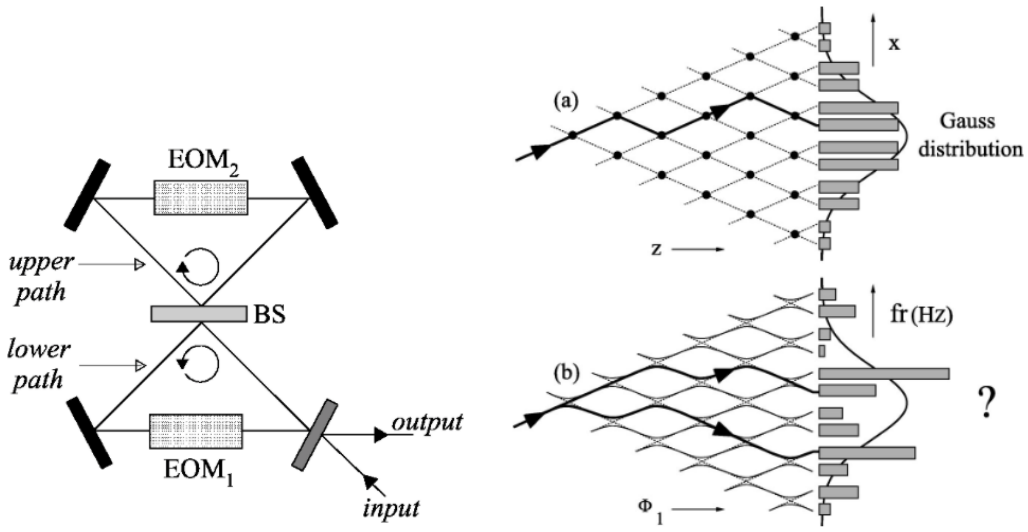

Figure 4.2: *(Left) The optical ring cavity for the implementation of the Optical Galton Board. The EOMs are the electro-optical modulators and the BS is the beam splitter. The solid gray rectangle is the partially reflecting mirror serving as input and output port and the black ones are the fully reflecting mirror of the cavity.(Adapted from Knight et al. [10]) (Right) On the top the probability distribution of a classical Galton board, and on the bottom the density profile of frequencies in the wave-mechanical case within the Landau-Zener crossings.* Φ_1 *is a control parameter proportional to time. (Adapted from Bouwmeester et al. [4])*

Fig. 4.2.a represents schematically how to implement OGB. The monochromatic radiation

passes through a beam splitter (BS) and it splits in two different paths, upper and lower. In the lower path the frequency of the light is increased of $\Delta\omega$ by a tuned electro-optical modulator. Then a system of mirrors in the cavity reflects back to the starting point both the components of radiation, and the OGB scheme is implemented again. Note that the BS here plays the role of the quantum coin $\mathcal{B}$ and the tuned electro-optical modulator shifts the frequency similarly to the shift operator and $\mathcal{T}$ translates the QWs on the physical lattice.

Nonlinear Optical Galton Board (NLOGB) was instead introduced by Navarrete-Benlloch et al. [19] and analyzed in QWs formalism. Differently from the linear case, in NLOGB the radiation acquires phase because of the nonlinearity of the medium. The scheme presented above remains exactly the same but it is possible to add optical fibers, for instance, before the modulators.

We present, in the next section, the NLOGB in long-term regime and we perform analytical computations to derive the formal continuous limit. We then provide numerical calculations to prove that the system thermalizes and demonstrate that the solution converges to a Gibbs distribution.

Nonlinear Optical Galton Board: thermalization and continuous limit

Giuseppe Di Molfetta and Fabrice Debbasch
LERMA, Observatoire de Paris, PSL Research University, CNRS, Sorbonne Universités, UPMC Univ. Paris 6, UMR 8112, F-75014, Paris France

Marc Brachet
Laboratoire de Physique Statistique de l'Ecole Normale Supérieure / PSL Research University, associé au CNRS et aux Universités Pierre-et-Marie-Curie Paris 06 et Paris Diderot, 24 Rue Lhomond, 75231 Paris, France

(Dated: June 13, 2015)

The nonlinear optical Galton board (NLOGB), a quantum walk like (but nonlinear) discrete time quantum automaton, is shown to admit a complex evolution leading to long time thermalized states. The continuous limit of the Galton Board is derived and shown to be a nonlinear Dirac equation (NLDE). The (Galerkin truncated) NLDE evolution is shown to thermalize toward states qualitatively similar to those of the NLOGB. The NLDE conserved quantities are derived and used to construct a stochastic differential equation converging to grand canonical distributions that are shown to reproduce the (micro canonical) NLDE thermalized statistics. Both the NLOGB and the Galerkin-truncated NLDE are thus demonstrated to exhibit spontaneous thermalization.

I. INTRODUCTION

At the fundamental level, quantum theory is linear. Yet, non linear models are often useful to take into account interaction in an effective manner. Two examples are the so-called nonlinear optical Galton board (NLOGB) [1] and the non-linear wave equations describing the dynamics of Bose-Einstein condensates (BEC). Though the NLOGB is discrete and wave equations are by definition continuous, these models have much in common. Indeed, the NLOGB is essentially a non-linear quantum walk (QW), and the formal continuous limits of linear QWs are wave equations [2–5]. Typical such wave equations are the Dirac or the Schrödinger equation which non-linear version, called the Gross-Pitaevskii equation (GPE), is used to model BEC [6]. Also, QW descriptions of BEC have been proposed in [7, 8].

Finally, numerical solutions of continuous wave equations are actually solutions of discrete systems approximating the continuous equations.

The NLOGB can be seen as a discrete model of nonlinear waves similar to those which propagate in BEC. One can therefore expect the NLOGB to display properties similar to those of the standard nonlinear model of BEC: the GPE. One such property which has until now never been explored on the NLOGB nor, more generally, in the context of QWs and quantum automata, is the so-called spontaneous thermalization.

In the context of (nonlinear) BEC, microcanonical equilibrium states are well-known to result from long-time integration of the so-called truncated (or Galerkin-projected) Gross-Pitaevskii equation (GPE) and involve a condensation mechanism [6, 9–11]. Furthermore, such thermalization is also known to happen in discretized (rather than spectrally-truncated) GPE [12]. Classical Galerkin-truncated systems have been studied since the early 50's in fluid mechanics. In this context, the (time reversible) Euler equation describing spatially-periodic classical ideal fluids is known to admit, when spectrally truncated at wavenumber $k_{\max}$, absolute equilibrium solutions with Gaussian statistics and equipartition of kinetic energy among all Fourier modes [13–16]. Furthermore, the dynamics of convergence toward equilibrium involves a direct energy cascade toward small-scales [17, 18].

The aim of the present work is to study thermalization phenomena in a spatially-periodic version of the NLOGB and relate it to the thermalization of its (Galerkin-truncated) continuous limit.

The paper is organized as follows. Section II is devoted to the definition of the NLOGB model and its numerical solution. The main result of this section is to display and characterize the complex behavior of the log-time regime. Section III is devoted to the behavior of the continuous limit (sect. III A), its conserved quantities (sect.III B) and the long-time behavior and thermalization of its Galerkin-truncated version (sect. III C). Finally section IV is our conclusion. Technical details are given in appendices.

II. NONLINEAR DISCRETE TIME QUANTUM WALK

A. Fundamentals

We consider discrete time spatially periodic quantum walks defined by the following equations:

$$\psi^-_{j+1,m} = \frac{1}{\sqrt{2}}[e^{ig|\psi^-_{j,m+1}|^2}\psi^-_{j,m+1} + e^{ig|\psi^+_{j,m+1}|^2}\psi^+_{j,m+1}] \quad (1)$$

$$\psi^+_{j+1,m} = \frac{1}{\sqrt{2}}[e^{ig|\psi^-_{j,m-1}|^2}\psi^-_{j,m-1} - e^{ig|\psi^+_{j,m-1}|^2}\psi^+_{j,m-1}]$$

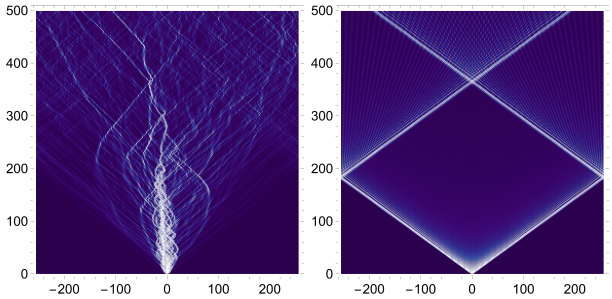

Figure 1. (Color online) Time evolution of the probability density $\Pi_{j,m}$ for (a) NLOGB (g=10 π) and (b) an Hadamard DTQW (g=0) with a symmetric initial condition $\Psi_{0,m} = \frac{\delta_{0,m}}{2}(b_- + ib_+)$. Resolution N = 256.

The index $m = 0, ..., N-1$ labels points on the circle and the index $j \in \mathbb{N}$ labels instants. The complex wave function or spinor $\Psi = \psi^- b_- + \psi^+ b_+$ is defined by its two components $\psi^\pm$ on a certain time- and space-independent basis (b_-, b_+). The parameter g fixes the importance of the non-linearity. For $g = 0$, equations (1) coincide with the evolution equations of the standard Hadamard walk. The probability $\Pi_j = \sum_m \left(|\psi^-_{j,m}|^2 + |\psi^+_{j,m}|^2\right) = \sum_m \Pi_{j,m}$ is independent of j *i.e.* it is conserved by the walk. We will henceforth denote it by Π.

B. Asymptotic behavior of the DTQWs

As displayed in Fig.1a, the family of DTQWs defined by equations (1) exhibits a very complex dynamics, much richer than the dynamics of the Hadamard walk shown for comparison in Fig.1b. Of particular interest is the asymptotic behavior of the family. Let $\Pi_{j,m}$ be the probability of finding the quantum walk at time j at point m and let $H_j(p)$ be the distribution of the the probability Π at time j *i.e.* $H_j(p)dp$ is the number of values of the space-coordinate m for which the probability $\Pi_{j,m}$ falls between p and $p+dp$. Direct numerical simulation (DNS) shows that $H_j(p)$ tends towards a stationary distribution $H^*(p)$ which depends only on the parameter g and not on the initial condition. Figure Fig. (2.a) displays how the probability $\Pi_{j,m}$ typically depends on m at fixed large values of j and Fig. (2.b) displays $H^*(p)$.

The existence of $H^*(p)$ is typical of non-linear chaotic systems. These systems also exhibit a great sensitivity towards initial conditions, and this sensitivity is confirmed by DNS of the NLOGB. Indeed, starting a DNS of the Hadamard walk with a symmetric initial condition delivers a numerical solution which is symmetrical at all times, whereas using the same initial condition in a DNS of the NLOGB delivers a numerical solution which is not symmetric (see Fig. 1.a). This symmetry breaking becomes greater with the time j (see Fig. (2.d) and depends on the resolution of the DNS and the strength of non linearities. In particular Fig.2.d show that the symmetry breaking starts from the round-off noise and we have verified that adding a non-symmetric noise to the initial condition produces a translation of the start point (data not shown) confirming that the symmetry breaking is due entirely to the round-off noise.

Note that this sensibility on initial conditions does not impact the determination of the stationary asymptotic distribution $H^*(p)$, since this distribution is the same for all initial conditions.

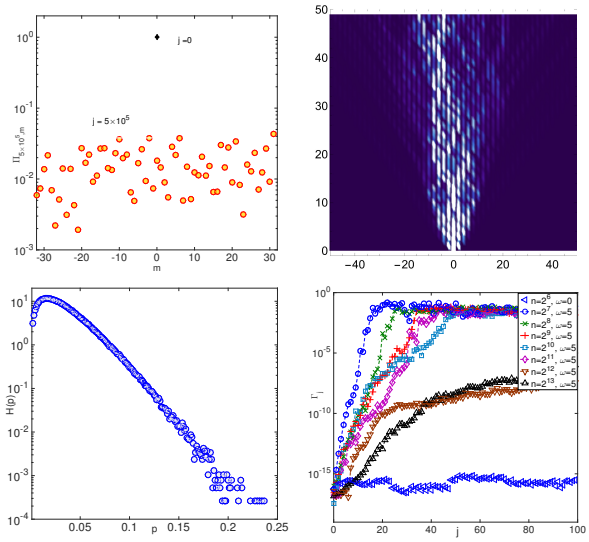

Figure 2. (a) Long time behavior. Log-Lin plot of the density $\Pi_{j,m}$ at time $j = 5 \times 10^5$ (yellow cercles) for the NLOGB with a symmetric initial condition $\Psi_{0,m} = \frac{\delta_{0,m}}{2}(b_- + ib_+)$ (black point) for g=10 π. Resolution $N = 64$. (b) Time evolution of the probability density $\Pi_{j,m}$ in same conditions that Fig. 1.b for short time behavior. (c) Log-Log histogram $H(p)$ of the density $\Pi_{j,m}$ at time $j = 5 \times 10^5$ for the NLOGB with a symmetric initial condition $\Psi_{0,m} = \frac{\delta_{0,m}}{2}(b_- + ib_+)$ and g=10 π. Resolution $N = 64$. (d) Asymmetry measure Γ_j versus time for different values of the resolution. $\Gamma_j = \sum_{m=0}^{N/2-1} \Pi_{j,m} - \sum_{m=N/2}^{N-1} \Pi_{j,m}$.

III. NONLINEAR DIRAC EQUATION

A. A non linear Dirac equation as continuous limit of the DTQWs

The asymptotic aspects of the NLOGB dynamics can be understood by investigating the continuous limit of these walks. The method employed is the same as in [2, 19, 20] and detailed computations are given

in Appendix A. The formal continuous limit of the NLQWs read:

$$\left(\mathbb{I}\partial_T - \sigma_3\partial_X - \frac{3ig}{4}\mathcal{M}(\Psi,\Psi^\dagger)\right)\Psi = 0 \qquad (2)$$

with

$$\mathcal{M}(\Psi,\Psi^\dagger) = \Psi^\dagger M \Psi, \qquad (3)$$

$$M = \mathbb{I} + \frac{\sigma_2}{3} \qquad (4)$$

where $\mathbb{I}$ is the identity,

$$\sigma_2 = \begin{pmatrix} 0 & -i \\ i & 0 \end{pmatrix}, \qquad \sigma_3 = \begin{pmatrix} 1 & 0 \\ 0 & -1 \end{pmatrix} \qquad (5)$$

are the second and third Pauli matrices. The continuous limit of the NLOGB is thus described by a non-linear Dirac equation (NLDE). The non-linearity is confined to the mass term, which depends quadratically on the spinor Ψ. Note that (spatially Two-dimensional) NLDE have also been used to describe experimental BEC on 2D hexagonal lattice [21–23].

The NLDE (2) is formally equivalent to Nambu-Jona-Lasinio-like equations (NJLE) (Nambu and Jona-Lasinio, [24]) in 1+1 dimension, which describe a non linear interaction between fermions with chiral symmetry. The constant g corresponds to a non linear coupling constant and if $g = 0$, (2) degenerates into the Weyl equation.

As detailed in Appendix B, the validity of the continuous limit is best confirmed by using Fourier pseudo-spectral methods [25], which are precise and rather easy to implement. In particular, Fig. (5) displays for different values of g the relative difference between the solution of equations (1) and (2) as a function of the ϵ parameter which controls the continuous limit.

Fig. (3) shows the typical profile of asymptotic probability density $\Pi(T,X)$ and the stationary distribution $H(p)$ of this density, as obtained form a Galerkin-truncated simulation of the NLDE, dealiased in a way that ensures conservation laws in the truncated system, see Appendix B. Both plots are strikingly similar to the corresponding plots presented in Fig. 2.a and 2.b obtained by numerically integrating the NLOGB. In other words, the NLOGB and the Galerkin-truncated NLDE seem to have very similar asymptotic behavior. We will now analyze in detail the asymptotic behavior of the Galerkin-truncated NLDE. We will first identify the conserved currents for the NLDE (Section III B) and then show that the asymptotic statistics Galerkin-truncated NLDE is identical to the so-called grand canonical statistics (III C).

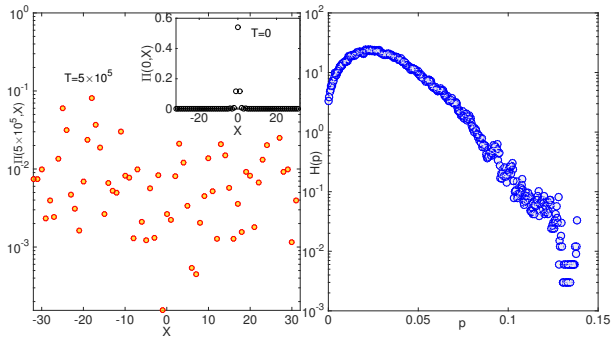

Figure 3. (Color online) (a) Log-Lin plot of the density $\Pi(T,X)$ at time $T = 5\times10^5$ (red square) obeying the Dirac equation with a symmetric gaussian initial condition $\Psi(0,X) = \frac{f(X)}{2}(b_- + ib_+)$ (black point) for g $=10\pi$. Resolution $N = 64$. The gaussian shape $f(X) = \frac{1}{2\pi\sigma}\exp\left(-X^2/\sqrt{2\sigma^2}\right)$ where σ $=10\Delta x$ (b) Histogram $H(p)$ of density Π.

B. Lagrangian formulation and conserved quantities

The NLDE derives from the following Lagrangian density:

$$\mathcal{L}(\Psi,\Psi^\dagger) = \frac{i}{2}\left[\overline{\Psi}\gamma^\mu(\partial_\mu\Psi) - (\partial_\mu\overline{\Psi})\gamma^\mu\Psi\right] - \frac{g}{2}\left(\overline{\Psi}N\Psi\right)^2 \qquad (6)$$

with

$$N = \gamma_0 + \frac{1}{\sqrt{3}}\gamma_5, \qquad (7)$$

$\gamma^0 = \sigma_1 = \begin{pmatrix} 0 & 1 \\ 1 & 0 \end{pmatrix}$, $\gamma^1 = \mathrm{i}\ \sigma_2$, $\gamma^5 = \mathrm{i}\ \gamma^0\gamma^1$, $\overline{\Psi} = \Psi^\dagger\gamma^0$ and $\partial_0 = \partial_T$, $\partial_1 = \partial_X$.

There are two conserved currents and these generate three integrals of motion (conserved quantities). The first current is simply the 2-current $J^\mu = \overline{\Psi}\gamma^\mu\Psi$ associated to the $U(1)$ invariance of the NLDE. The corresponding integral of motion is the total probability $\Pi = \int \Psi^\dagger\Psi dX$ of finding the fermion somewhere in space.

The other current is associated to the space-time translation invariance of the NLDE and is the stress-energy tensor

$$\mathcal{T}^{\mu\nu}(\Psi,\Psi^\dagger) = \frac{i}{2}[\overline{\Psi}\gamma^\mu(\partial^\nu\Psi) - (\partial^\nu\overline{\Psi})\gamma^\mu\Psi] - \eta^{\mu\nu}\mathcal{L} \quad (8)$$

where $\eta^{\mu\nu} = \mathrm{diag}(1,-1)$. The associated conserved quantities are the energy E and the momentum P, which are defined by

$$E[\Psi,\Psi^\dagger] = \int \mathcal{T}^{00}\left(\Psi(X),\Psi^\dagger(X)\right)dX \qquad (9)$$

and

$$P[\Psi,\Psi^\dagger]=\int \mathcal{T}^{01}\left(\Psi(X),\Psi^\dagger(X)\right)dX \qquad (10)$$

with

$$\mathcal{T}^{00}(\Psi,\Psi^\dagger)=-\frac{i}{2}\left[\overline{\Psi}\gamma^1(\partial_X\Psi)-(\partial_X\overline{\Psi})\gamma^1\Psi\right]-\frac{g}{2}\left(\overline{\Psi}N\Psi\right)^2 \qquad (11)$$

and

$$\mathcal{T}^{01}(\Psi,\Psi^\dagger)=-\frac{i}{2}\left[\overline{\Psi}\gamma^0(\partial_X\Psi)-(\partial_X\overline{\Psi})\gamma^0\Psi\right]. \qquad (12)$$

C. Thermalization in the Galerkin-truncated NLDE

If one studies the NLDE on the circle, it is natural to write at all times the spinor $\Psi(T,X)$ as a spatial Fourier series and to replace the NLDE by an evolution equation obeyed by the time-dependent Fourier coefficients $\hat{\Psi}(T,k)$. In performing a Galerkin truncation [26], one retains only a *finite* number of these coefficients as dynamical variables, say $\hat{\Psi}(T,k)$ with $k=-\frac{N}{2},...,\frac{N}{2}-1$, and replaces the exact NLDE dynamics by a new dynamics which, at small k, approximates at least formally the original NLDE dynamics. By Fourier transforming the $\hat{\Psi}(T,k)$, $k=-\frac{N}{2},...,\frac{N}{2}-1$, back to original physical space (*i.e.* the circle), one obtains a set of N spinors $\Psi_m(T)$, $m=0...,N-1$, which are to be interpreted as the values $\Psi(T,X_m)$ taken by the spinor field $\Psi(T,X)$ at point $X_m=\frac{2\pi m}{N}$ (see Appendix B). The spinors $\Psi(T,X_m)$ are on the same footing as the $\hat{\Psi}(T,k)$, $k=-\frac{N}{2},...,\frac{N}{2}-1$, and can be viewed as the dynamical variables of the Galerkin-truncated NLDE. We now denote by $\tilde{\Psi}(T)$ the collection $\{\Psi_m(T)=\Psi(T,X_m),m=0,...N-1\}$.

All integrals over space of quantities involving the Dirac field can be replaced by Riemann sums. Thus, the total probability, the energy and the momentum can now be viewed as functions of the collection $\left(\tilde{\Psi}(T),\tilde{\Psi}^*(T)\right)$. These functions will still be denoted by Π, P and E and are conserves by the Galerkin truncated dynamics, see Appendix B.

We now introduce two Lagrange multipliers μ and θ, define $H_{\theta\mu}=E-\theta P-\mu\Pi$ and consider the following stochastic differential equations:

$$\begin{aligned}\frac{d\Psi_m}{dT}&=-\frac{\partial H_{\theta\mu}}{\partial\Psi_m^*}+\eta\,\xi_m(T)\\ \frac{d\Psi_m^*}{dT}&=-\frac{\partial H_{\theta\mu}}{\partial\Psi_m}+\eta\,\xi_m^*(T)\end{aligned} \qquad (13)$$

where η is a real coefficient and the $\xi_m(T)$'s are complex independent Gaussian white noises [27] with correlation functions

$$<\xi_m(T)\xi_n^*(T')>=\delta_{mn}\,\delta(T-T'). \qquad (14)$$

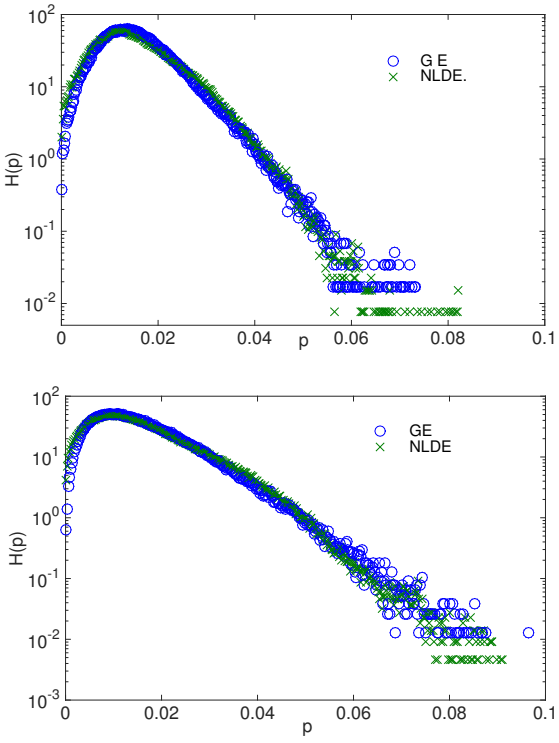

Figure 4. Histograms $H(p)$ of the thermalized state density $\Pi(X)$ for the NLDE and for the stochastic equations (13) for $g=10\pi$. The conserved quantities and the noise coefficient are: top E= -19.8, $P=0$, $\Pi=1$ and η =1; bottom E= -17.12, $P=0$, $\Pi=1$, T_0= 250, T_1=312 and η =1.6.

The density f of this stochastic process obeys the exact Fokker-Planck equation [10, 28, 29]

$$\partial_t f=\sum_m\left\{-\frac{\partial}{\partial\Psi_m}(\frac{\partial H}{\partial\Psi_m^*}f)-\frac{\partial}{\partial\Psi_m^*}(\frac{\partial H}{\partial\Psi_m}f)+\eta^2\frac{\partial^2 f}{\partial\Psi_m\Psi_m^*}\right\} \qquad (15)$$

The stationary solution $f_{\eta\theta\mu}$ of this equation is of the form

$$f_{\eta\theta\mu}=\frac{1}{Z_{\eta\theta\mu}}\exp\left(-\frac{2}{\eta^2}H_{\theta\mu}\right) \qquad (16)$$

which is the so-called grand canonical distribution with inverse temperature $2/\eta^2$.

We have simulated the stochastic equations (13) to obtain numerically the stationary distribution $f_{\eta\theta\mu}$ and compare it with the asymptotic long-time distribution of the Galerkin-truncated NLDE. Typical results are displayed in Fig. 4 and confirm that the Galerkin-truncated NLDE and the stochastic equations (13 are described by very similar distributions (see Appendix B).

IV. DISCUSSION

We have considered the NLOGB confined to the circle and we have shown that the continuous limit of this NLOGB is a NLDE identical to the NJLE-model. Pseudo-spectral numerical simulations reveal that the asymptotic behavior of the NLOGB is similar to the asymptotic behavior of the Galerkin-truncated NLDE and we have shown that the associated asymptotic statistics is identical to the grand-canonical statistics. Thus, both the NLOGB and the Galerkin-truncated NLDE exhibit spontaneous thermalization.

Previous work on other non-linear quantum walk [30] suggests that this observed spontaneous asymptotic thermalization is not a particular feature of the systems studied in this article, but will also be encountered in other non linear quantum walks, whatever the dimensions of the underlying physical space or of the coin space may be. It is obvious that quantum walks which thermalize will explore space in a very different manner from walks which do not thermalize, and their importance for quantum computing should certainly be explored in depth. In a different direction, it would be interesting to exhibit and analyze spontaneous thermalization in QWs couple to synthetic gauge fields [2, 20, 31].

Appendix A: Derivation of continuous limit

Consider for all $(n, j) \in \mathbb{N}^2$, the collection $W_j^n = (\Psi_{k,m})_{k=nj, m\in\mathbb{Z}}$. This collection represents the state of the NLOGB at 'time' $k = nj$. For any given n, the collection $S^n = (W_j^n)_{j\in\mathbb{N}}$ thus represents the entire history of the NLOGB observed through a stroboscope of 'period' n. The evolution equations for S^n are those linking W_{j+1}^n to W_j^n for all j. The method employed here to obtain the continuous limit of a generic S^n was introduced in [2, 20].

One first introduces a time-scale τ, a length-scale λ, an infinitesimal ϵ and interpret the space-index m as referring to position $x_m = m\epsilon\lambda = m\Delta x$ and the time index j as referring to the instant $t_j = j\epsilon\tau = j\Delta t$. The formal continuous limit is obtained expanding the equations defining S^n in Taylor series around $\epsilon = 0$ and by letting ϵ tend to zero. For the limit to exist, all zeroth order terms of the Taylor expansion must identically cancel each other and the differential equation describing the limit is then obtained by equating to zero the non identically vanishing, lowest order contribution.

The original NLOGB S^1 does not admit a continuous limit because the zeroth order terms do not cancel each other identically. The equations defining S^2 read:

$$\psi^-(t_j + 2\Delta t, x_m) = \frac{1}{2}[\mathcal{F}[\phi^-(t_j, x_m + \Delta x)] + \mathcal{F}[\phi^+(t_j, x_m - \Delta x)]$$

$$\psi^+(t_j + 2\Delta t, x_m) = \frac{1}{2}[\mathcal{F}[\phi^-(t_j, x_m - \Delta x)] - \mathcal{F}[\phi^+(t_j, x_m + \Delta x)]$$

where

$$\phi^{\mp}(t_j, x_m) = e^{ig|\psi^-(t_j, x_m+\Delta x)|^2}\psi^-(t_j, x_m + \Delta x)\pm e^{ig|\psi^-(t_j, x_m+\Delta x)|^2}\psi^+(t_j, x_m + \Delta x) \quad \text{(A1)}$$

and

$$\mathcal{F}[\phi(t_j, x_m)] = e^{ig|\phi(t_j, x_m)|^2}\phi(t_j, x_m). \quad \text{(A2)}$$

These equations admit a formal continuous limit, which reads:

$$(\mathbb{I}\partial_T - \mathcal{P}\partial_X - \frac{3ig}{4}\tilde{\mathcal{M}}(\Psi, \Psi^\dagger))\Psi = 0 \quad \text{(A3)}$$

where

$$\tilde{\mathcal{M}}(\Psi, \Psi^\dagger) = \Psi^\dagger \tilde{M}\Psi, \quad \text{(A4)}$$

$$\mathcal{P} = \frac{1}{2}\begin{pmatrix} 1 & 1 \\ 1 & -1 \end{pmatrix} \qquad \tilde{M} = \mathbb{I} - \frac{\sigma_2}{3} \quad \text{(A5)}$$

and $T = t/\tau$ and $X = x/\lambda$.

The operator P is self-adjoint and its eigenvalues are -1 and $+1$. Two eigenvectors associated to these eigenvalues are

$$\mathcal{B}_- = \left(\cos\frac{\theta}{8}\right) b_- + \left(\sin\frac{\theta}{8}\right) b_+ \quad \text{(A6)}$$

and

$$\mathcal{B}_+ = \left(\sin\frac{\theta}{8}\right) b_- - \left(\cos\frac{\theta}{8}\right) b_+. \quad \text{(A7)}$$

The family $(\mathcal{B}_-, \mathcal{B}_+)$ forms an orthonormal basis of the two dimensional spin Hilbert space. In this new basis, equation (A3) reads:

$$(\mathbb{I}\partial_T - \sigma_3\partial_X - \frac{3ig}{4}\mathcal{M}(\Psi, \Psi^\dagger))\Psi = 0 \quad \text{(A8)}$$

where

$$\mathcal{M}(\Psi, \Psi^\dagger) = \Psi^\dagger M\Psi, \quad \text{(A9)}$$

$$M = \mathbb{I} + \frac{\sigma_2}{3} \quad \text{(A10)}$$

Appendix B: Numerical Methods

We restrict ourself to 2π-periodic boundary conditions. A generic field $\Psi(X)$ is thus evaluated on the N collocation points $X_m = 2\pi m/N$, with $m = 0, N-1$ as $\Psi_m = \Psi(X_m)$. The discrete Fourier transforms are standardly defined as $\Psi(X_m) = \sum_{k=-N/2}^{N/2-1} \exp(ikX_m)\hat{\psi}_k$ and the inverse $\hat{\psi}_k = \frac{1}{N}\sum_{m=0}^{N-1}\psi(X_m)\exp(-ikX_m)$. These sums can

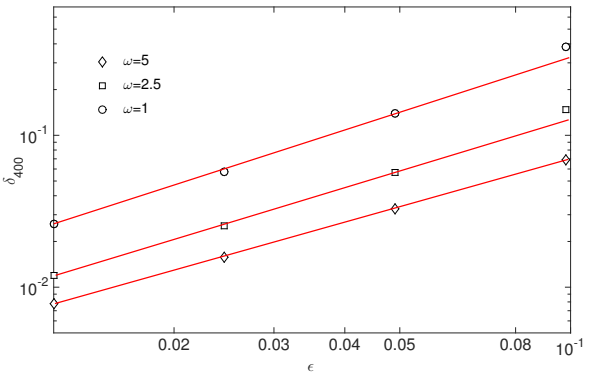

Figure 5. Log-Log plot of the relative difference δ_j at time $j = 400$, defined as $\frac{\sqrt{<(\rho_{QW}-\rho_D)^2>}}{<\rho_D>}$, for diffents ϵ=$2\pi/n$, (from right to left) n=2^6,2^7,2^8,2^9.

be evaluated in only $N\log(N)$ operations by using Fast Fourier Transforms (FFTs). Spatial derivatives of fields are evaluated in spectral space by multiplying by ik and products are evaluated in physical space. The original QW equations can also be simply cast in this setting, as the translation operator $\Psi_m \to \Psi_{m\pm1}$ is represented in Fourier space by $\hat{\Psi}_k \to \hat{\Psi}_k \exp(\pm ik2\pi/N)$. In this setting, the continuous limit is automatically taken when N is increased. As we can observe in Fig. (5) the relative difference scales as expected as ϵ for different values of ω.
However the pseudo-spectral code solving the NLPDEs generates a problem called aliasing [32]. In general the fields needs to be de-aliased by proper spectral truncation. Here, we used the so-called 2/3-rule in all our numerical schemes in the same way as done in reference [10]. De-aliasing is fundamentally important to preserve the conservation of the Galerkin truncated non linear dynamics as we can observe in Fig. (6). Indeed, although it is straightforward to show that Eq.(2) can be written

$$\partial_T \Psi_m = -i\frac{\partial E}{\partial \Psi_m^*} \tag{B1}$$

$$\partial_T \Psi_m^* = i\frac{\partial E}{\partial \Psi_m} \tag{B2}$$

and thus formally conserves the energy, it can be shown that exact conservation requires proper dealiasing (see appendix of ref. [10]).

As displayed in Fig.4, the statistical distributions generated by the NLDE dynamics Eq.(2) and by the stochastic equations (13) are really close and this can be justified on very general grounds.

First, by construction, the stochastic equations (13) generate the grand canonical distribution (16) that is controlled by the inverse temperature $2/\eta^2$ and the Lagrange multipliers μ and θ. On the other hand, as the spectrally-truncated dynamics (2) conserves Π, P and E, its long time behavior should be described by the so-called micro canonical distribution

$$f \sim \delta(E - E_{\rm in})\delta(\Pi - \Pi_{\rm in})\delta(P - P_{\rm in}). \tag{B3}$$

that is determined by the values ($E_{\rm in}$,$\Pi_{\rm in}$,$P_{\rm in}$) of the conserved quantities given by the initial condition $\Psi_{\rm in}$. As is well-known [33], under very general circumstances both grand canonical and micro canonical distribution yield similar statistical results (provided that the $2/\eta^2$ and the Lagrange multipliers μ and θ have values that correspond to $E_{\rm in}$,$\Pi_{\rm in}$,$P_{\rm in}$). Fig.4 indicates that, in this case, both distributions yield identical results for density fluctuations.

[1] C. Navarrete-Benlloch, A. Pérez, and Eugenio Roldán. Nonlinear optical Galton board. *Phys. Rev. A*, 75:062333, Jun 2007.

[2] G. DiMolfetta, F. Debbasch, and M. Brachet. Quantum walks in artificial electric and gravitational fields. *Phys. A*, 397, 2014.

[3] Pablo Arrighi and Stefano Facchini. Decoupled quantum walks, models of the klein-gordon and wave equations. *EPL (Europhysics Letters)*, 104(6):60004, 2013.

[4] Frederick W Strauch. Relativistic quantum walks. *Physical Review A*, 73(5):054302, 2006.

[5] CM Chandrashekar, Subhashish Banerjee, and R Srikanth. Relationship between quantum walks and relativistic quantum mechanics. *Physical Review A*, 81(6):062340, 2010.

[6] Natalia G. Berloff, Marc Brachet, and Nick P. Proukakis. Modeling quantum fluid dynamics at nonzero temperatures. *Proceedings of the National Academy of Sciences*, 111(Supplement 1):4675–4682, 2014.

[7] CM Chandrashekar. Disordered-quantum-walk-induced localization of a bose-einstein condensate. *Physical Review A*, 83(2):022320, 2011.

[8] CM Chandrashekar. Implementing the one-dimensional quantum (hadamard) walk using a bose-einstein condensate. *Physical Review A*, 74(3):032307, 2006.

[9] Giorgio Krstulovic and Marc Brachet. Dispersive bottleneck delaying thermalization of turbulent bose-einstein condensates. *Physical review letters*, 106(11):115303, 2011.

[10] Giorgio Krstulovic and Marc Brachet. Energy cascade with small-scale thermalization, counterflow metastability, and anomalous velocity of vortex rings in fourier-truncated gross-pitaevskii equation. *Physical Review E*, 83(6):066311, 2011.

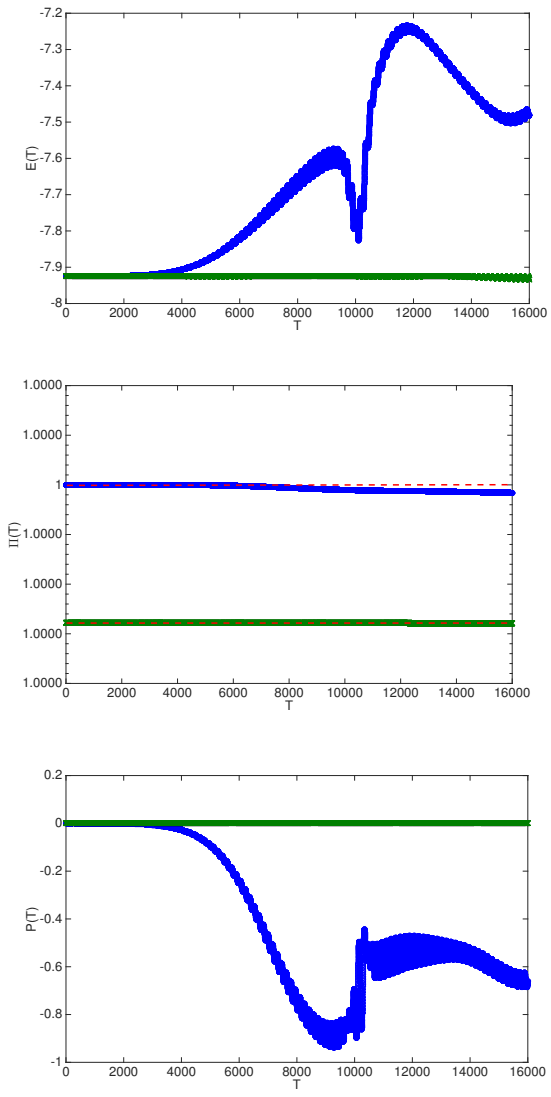

Figure 6. (Color On line) Time evolution of energy (top) $E(T)$, momentum (center) $P(T)$ and particle number $\Pi(T)$ simulated by a pseudo-spectral code for the spatial part and a 4th-order Runge Kutta for the time step. The resolution $N = 128$. The blue courbes represents the non dealiased code.

[11] Vishwanath Shukla, Marc Brachet, and Rahul Pandit. Turbulence in the two-dimensional fourier-truncated gross–pitaevskii equation. *New Journal of Physics*, 15(11):113025, 2013.

[12] Natalia G. Berloff and Anthony J. Youd. Dissipative dynamics of superfluid vortices at nonzero temperatures. *Phys. Rev. Lett.*, 99:145301, Oct 2007.

[13] Tsung-Dao Lee and Chen-Ning Yang. Statistical theory of equations of state and phase transitions. ii. lattice gas and ising model. *Physical Review*, 87(3):410, 1952.

[14] Robert H Kraichnan. On the statistical mechanics of an adiabatically compressible fluid. *The Journal of the Acoustical Society of America*, 27(3):438–441, 1955.

[15] Robert H Kraichnan. Helical turbulence and absolute equilibrium. *Journal of Fluid Mechanics*, 59(04):745–752, 1973.

[16] SA Orszag. Fluid dynamics, proceedings of the 1973 les houches summer school. 1977.

[17] C. Cichowlas, P. Bonaïti, F. Debbasch, and M. Brachet. Effective dissipation and turbulence in spectrally truncated euler flows. *Phys. Rev. Lett.*, 95:264502, 2005.

[18] G. Krstulovic, C. Cartes, M. Brachet, and E. Tirapegui. Generation and characterization of absolute equilibrium of compressible flows. *International Journal of Bifurcation and Chaos*, 19(10):3445–3459, 2009.

[19] G. DiMolfetta and F. Debbasch. Discrete-time quantum walks: Continuous limit and symmetries. *J. Math. Phys.*, 53:123302, 2012.

[20] G. DiMolfetta, F. Debbasch, and M. Brachet. Quantum walks as massless dirac fermions in curved space. *Phys. Rev. A*, 88, 2013.

[21] LH Haddad, KM O'Hara, and Lincoln D Carr. Nonlinear dirac equation in bose-einstein condensates: Preparation and stability of relativistic vortices. *Physical Review A*, 91(4):043609, 2015.

[22] LH Haddad and LD Carr. Relativistic linear stability equations for the nonlinear dirac equation in bose-einstein condensates. *EPL (Europhysics Letters)*, 94(5):56002, 2011.

[23] LH Haddad and LD Carr. The nonlinear dirac equation in bose–einstein condensates: Foundation and symmetries. *Physica D: Nonlinear Phenomena*, 238(15):1413–1421, 2009.

[24] Y. Nambu and G. Jona-Lasinio. Dynamical model of elementary particles based on an analogy with superconductivity. i. *Phys. Rev.*, 122:345–358, Apr 1961.

[25] David Gottlieb, Steven A Orszag, and Cambridge Hydrodynamics Inc MA. *Numerical analysis of spectral methods*. SIAM, 1977.

[26] Uriel Frisch, Susan Kurien, Rahul Pandit, Walter Pauls, Samriddhi Sankar Ray, Achim Wirth, and Jian-Zhou Zhu. Hyperviscosity, galerkin truncation, and bottlenecks in turbulence. *Physical Review Letters*, 101(14):144501, 2008.

[27] B. Oksendal. *Stochastic Differential Equations: An Introduction with Applications*. Universitext. Springer Berlin Heidelberg, 2013.

[28] N.G. Van Kampen. *Stochastic Processes in Physics and Chemistry*. North-Holland Personal Library. Elsevier Science, 2011.

[29] F. Langouche, D. Roekaerts, and E. Tirapegui. *Functional Integration and Semiclassical Expansions*. Mathematics and Its Applications. Springer Netherlands, 1982.

[30] Yutaka Shikano, Tatsuaki Wada, and Junsei Horikawa. Discrete-time quantum walk with feedforward quantum coin. *Scientific reports*, 4, 2014.

[31] Pablo Arrighi, Stefano Facchini, and Marcelo Forets. Quantum walks in curved spacetime. *arXiv preprint arXiv:1505.07023*, 2015.

[32] Steven A. Orszag. On the elimination of aliasing in finite-difference schemes by filtering high-wavenumber

components. *J. Atmos. Sci.*, 28:1074–1074, 1971.
[33] L.D. Landau and E.M. Lifshitz. *Statistical Physics*. Number Bd. 5. Elsevier Science, 2013.

Bibliography

[1] D. Aharonov, A. Ambainis, J. Kempe, and U. Vazirani. Quantum walks on graphs. In *Proceedings of the thirty-third annual ACM symposium on Theory of computing*, pages 50–59. ACM, 2001.

[2] A. Ambainis, E. Bach, A. Nayak, A. Vishwanath, and J. Watrous. One-dimensional quantum walks. In *Proceedings of the thirty-third annual ACM symposium on Theory of computing*, pages 37–49. ACM, 2001.

[3] M. Bednarska, A. Grudka, P. Kurzyński, T. Łuczak, and A. Wójcik. Quantum walks on cycles. *Physics Letters A*, 317(1):21–25, 2003.

[4] D. Bouwmeester, I. Marzoli, G. P. Karman, W. Schleich, and J. Woerdman. Optical galton board. *Physical Review A*, 61(1):013410, 1999.

[5] N. Chernov and D. Dolgopyat. Diffusive motion and recurrence on an idealized galton board. *Physical review letters*, 99(3):030601, 2007.

[6] K. Chisaki, M. Hamada, N. Konno, and E. Segawa. Limit theorems for discrete-time quantum walks on trees. *Interdisciplinary Information Sciences*, 15(3):423–429, 2009.

[7] C. Cichowlas, P. Bonaïti, F. Debbasch, and M. Brachet. Effective dissipation and turbulence in spectrally truncated euler flows. *Physical review letters*, 95(26):264502, 2005.

[8] J. Eisert, M. Friesdorf, and C. Gogolin. Quantum many-body systems out of equilibrium. *Nat. Phys.*, 11:124, 2015.

[9] U. Frisch, S. Kurien, R. Pandit, W. Pauls, S. S. Ray, A. Wirth, and J.-Z. Zhu. Hyperviscosity, galerkin truncation, and bottlenecks in turbulence. *Physical Review Letters*, 101(14):144501, 2008.

[10] P. L. Knight, E. Roldán, and J. E. Sipe. Optical cavity implementations of the quantum walk. *Optics Communications*, 227(1):147–157, 2003.

[11] N. Konno. Continuous-time quantum walks on trees in quantum probability theory. *Infinite Dimensional Analysis, Quantum Probability and Related Topics*, 9(02):287–297, 2006.

[12] R. H. Kraichnan. Helical turbulence and absolute equilibrium. *Journal of Fluid Mechanics*, 59(04): 745–752, 1973.

[13] G. Krstulovic and M. Brachet. Dispersive bottleneck delaying thermalization of turbulent bose-einstein condensates. *Physical review letters*, 106(11):115303, 2011.

[14] G. Krstulovic and M. Brachet. Energy cascade with small-scale thermalization, counterflow metastability, and anomalous velocity of vortex rings in fourier-truncated gross-pitaevskii equation. *Physical Review E*, 83(6):066311, 2011.

[15] G. Krstulovic, C. Cartes, M. Brachet, and E. Tirapegui. Generation and characterization of absolute equilibrium of compressible flows. *International Journal of Bifurcation and Chaos*, 19(10):3445–3459, 2009. doi: 10.1142/S021812740902489X. URL http://www.worldscientific.com/doi/abs/10.1142/S021812740902489X.

[16] L. D. Landau and E. M. Lifshitz. *Course of theoretical physics*. Elsevier, 2013.

[17] T.-D. Lee. On some statistical properties of hydrodynamical and magneto-hydrodynamical fields. *Quart Appl Math*, 1(10):69–74, 1952.

[18] D. A. Meyer. From quantum cellular automata to quantum lattice gases. *Journal of Statistical Physics*, 85(5-6):551–574, 1996.

[19] C. Navarrete-Benlloch, A. Perez, and E. Roldan. Nonlinear optical galton board. *Phys. Rev. A*, 75: 062333, 2010.

[20] S. Popescu, A. J. Short, and A. Winter. Entanglement and the foundations of statistical mechanics. *Nat. Phys.*, 2:754, 2006.

[21] P. Reimann. Foundation of statistical mechanics under experimentally realistic conditions. *Phys. Rev. Lett.*, 101:190403, 2008.

[22] M. Rigol, V. Dunjko, and M. Olshanii. Thermalization and its mechanism for generic isolated quantum systems. *Nature*, 452:854, 2008.

[23] A. Romanelli. Thermodynamic behavior of the quantum walk. *Physical Review A*, 85(1):012319, 2012.

[24] A. Romanelli and G. Segundo. The entanglement temperature of the generalized quantum walk. *Physica A: Statistical Mechanics and its Applications*, 393:646–654, 2014.

[25] Y. Shikano, T. Wada, and J. Horikawa. Discrete-time quantum walk with feed-forward quantum coin. *Scientific reports*, 4, 2014.

[26] S. E. Venegas-Andraca. Quantum walks: a comprehensive review. *Quantum Information Processing*, 11(5):1015–1106, 2012.

Part III

Conclusions and Perspectives

CHAPTER 5

CONCLUSIONS AND PERSPECTIVES

5.1 Conclusions

In this thesis we have studied several QWs in discrete space and discrete time with homogeneous and inhomogeneous quantum coin. In the first part, we proved that, under some conditions and employing the method presented for the first time in [5] and [6], these walks coincide with the propagation of a Dirac particle. In Chapter (1) we introduced the simplest case of the homogenous QW and formally derived its continuous limit, which recover the massless Dirac equation in flat (1+1)-spacetime.

In Chapter (2) we extended the previous analysis to the inhomogeneous QWs. In particular in [7] we proposed an explicit construction of DTQWs mimicking the propagation of a fermion in and around a (1+1)-dimensional black hole. This case has been validated by analytical calculation for the specific case of a 4D Schwarzschild non-charged black hole, in Lemaître coordinates, for a particle that starts its motion radially. By Direct Numerical Simulations (DNS) we proved that the agreement is surprisingly valid still when the initial condition is no longer smooth in respect to the lattice parameter. We have also proved (data not shown in this thesis) that the spacetime curvature, generated by the inhomogeneities of the QW, is still visible within a very small amount of time steps (for instance in 8 and 16 time steps).

The main goal obtained in [8] is that a large class of IDTQWs admit remarkably an exact discrete gauge invariance, which at the continuous limit coincides with the standard $U(1)$ Maxwell gauge invariance. In continuous limit these walks recover the Dirac equation of a fermion propagating in a gauge electric field. We validate this result with accurate pseudo-spectral numerical simulations in the specific case of a constant and static electric field.

In Chapter (3) we proposed two families of DTQWs as models mimicking quantum transport in time-dependent random electric and gravitational field. These systems, in long time behavior or large decoherence rate, loose spin and spatial coherence and the probability density tends to a limiting Gaussian distribution. However, in the transient regime, the QWs present two characteristic density profiles with a cusp in the case of the random electric field and a dip in the case of gravitational field. We should remark also that the loss of coherence is largely slower in the case of a random electric field (data not shown in this thesis). For both kinds of system we explicitly computed the diffusion coefficient and the analytical expression of the second moment in physical space. Let us finally regard that because of the spatial translation invariance of the random fields, the averaged transport operator does not couple the different Fourier modes.

We were the first to prove to the best of our knowledge (and we thus reported in Chapter (4)) that a nonlinear QW-like model thermalizes and reaches an absolute equilibrium in long time behavior. To prove this, we adopted the NLGOB introduced by Navarrete-Benlloch et al. [11]. Several new results have been presented at this stage: (i) the continuous limit of this discrete model corresponds to the NJL equations introduced as dynamical model of ele-

mentary particles based on analogy with superconductivity; (ii) this system relaxes toward the equilibrium with a rich and interesting transient. As in the Galerkin-truncated Euler-Voigt-α equation, (Di Molfetta et al. [9]), in the Galerkin truncated NJL, the thermalized small scales act as thermostats generating a pseudo-dissipation at large scales. (iii)The same asymptotic behavior is observed in the NLGOB.
Let us acknowledge that the algorithm introduced by Krstulovic et al. [10] to generate absolute equilibrium of spectrally truncated compressible flows in the hydrodynamics framework, has been adapted to the Galerkin truncated NJL. All these results are validated by precise numerical pseudo-spectral simulations for the spatial discretization and by a 4th order Runge-Kutta method for the time stepping.

5.2 Perspectives

All the works presented in this thesis should certainly be continued in several directions. One should first extend the main results of the first part of this thesis to QWs defined in physical space of higher dimension and/or defined in a higher-dimensional Hilbert space. Our group has started to work on the former direction, showing that certain QWs on 2D square lattices describe the transport of two-component spin 1/2 fermions coupled to arbitrary electromagnetic fields. In particular, Landau levels can be defined for these QWs (Arnault and Debbasch [1]). The next goal will be to exhibit families of 2D QWs on square lattices, that can be interpreted as the transport of two-component spin 1/2 fermions in arbitrary gravitational fields.

QWs defined in a higher-dimensional Hilbert space have been instead developed in a preliminary work carried out by Di Molfetta and Debbasch. We showed that several 1D QWs with more than two components (but still defined on square lattices) can be interpreted as quantum transport in non-abelian synthetic gauge fields. In particular we have proved[1] that QWs living in $SU(2) \otimes SU(n)$ can simulate $SU(n)$ Yang-Mills theory in flat and curved spacetime.

Another interesting perspective should be the extension of all the results above for QWs propagating on graph. In fact, on one hand graphs possess intrinsic geometrical properties, on the other QWs can be interpreted as fermions interacting with gauge fields, including gravitational fields. Now, gauge theories are based on geometry; for example, gravitational fields arise from the curvature of space-time. It is logical at this point to wonder what effects the interplay between the intrinsic geometry of a graph and the geometry of gauge fields has on coherent quantum transport.

Let us notice that a recent method of spacetime grouping introduced by Arrighi et al. [2] in the QWs framework may allow us to relate QWs to the interaction graph of a specific QCA . By changing the local interactions between the cells and the spatial distributions of the cells, we should obtain different emergent dynamics. Therefore, there could be two interesting extensions related to our works: (i) the former is to generally explore what possible QFTs can be described by different grouping operations; (ii) the latter, investigating the classical limit of these configurations by, for instance, a coarse graining procedure.

[1] G. Di Molfetta, F. Debbasch *Non-Abelian Quantum Walks*, preprint, 2015

Chapter (3) should be instead expanded considering other types of noises, such as position- and time-dependent noise, and investigating if they could permit a closer connection with some specific class of relativistic stochastic processes (Debbasch et al. [3]). Moreover, previous analysis carried out by G. Di Molfetta and F. Debbasch have related decoherent QWs dynamics to classical Bounded Velocity Stochastic Processes [4] and this subject clearly demands further analysis.

In Chapter (4) we have just presented some preliminary new results on a specific non-linear QW-like model and its continuous limit. We should first extend the same analysis to the model presented by Shikano et al. [12], notably in the generalized form proposed by Di Molfetta. Then, we have to move our analysis further by (i) proving that these quantum walks do thermalize and finally (ii) analyzing the thermalization in terms of gauge fields.

Let us recall, in the end, that we need to investigate all these QWs using some experimental setups in order to definitely validate our theoretical results.

Bibliography

[1] P. Arnault and F. Debbasch. Landau levels for discrete-time quantum walks in artificial magnetic fields. *arXiv preprint*, 1412.4337, 2014.

[2] P. Arrighi, S. Facchini, and M. Forets. Quantum walks in curved spacetime. *arXiv preprint*, 1505.07023, 2015.

[3] F. Debbasch, K. Mallick, and J. Rivet. Relativistic ornstein–uhlenbeck process. *Journal of statistical physics*, 88(3-4):945–966, 1997.

[4] F. Debbasch, G. Di Molfetta, D. Espaze, and V. Foulonneau. Propagation in quantum walks and relativistic diffusions. *Phys. Scr.*, 151:014044, 2012.

[5] G. Di Molfetta and F. Debbasch. Discrete-time quantum walks: Continuous limit and symmetries. *J. Math. Phys.*, 53:123302, 2012.

[6] G. Di Molfetta and F. Debbasch. Discrete-time quantum walks: Continuous limit in 1 + 1 and 1 + 2 dimension. *J.Comp.Th.Nanosc.*, 10,7:1621–1625, 2012.

[7] G. Di Molfetta, F. Debbasch, and F. Brachet. Quantum walks as massless dirac fermions in curved space. *Phys. Rev. A*, 88, 2013.

[8] G. Di Molfetta, F. Debbasch, and M. Brachet. Quantum walks in artificial electric and gravitational fields. *Phys. A*, 397, 2014.

[9] G. Di Molfetta, G. Krstlulovic, and M. Brachet. Self-truncation and scaling in euler-voigt-α and related fluid models. *arXiv preprint arXiv:1502.05544*, 2015.

[10] G. Krstulovic, C. Cartes, M. Brachet, and E. Tirapegui. Generation and characterization of absolute equilibrium of compressible flows. *International Journal of Bifurcation and Chaos*, 19(10):3445–3459, 2009. doi: 10.1142/S021812740902489X. URL http://www.worldscientific.com/doi/abs/10.1142/S021812740902489X.

[11] C. Navarrete-Benlloch, A. Perez, and E. Roldan. Nonlinear optical galton board. *Phys. Rev. A*, 75:062333, Jun 2007. doi: 10.1103/PhysRevA.75.062333. URL http://link.aps.org/doi/10.1103/PhysRevA.75.062333.

[12] Y. Shikano, T. Wada, and J. Horikawa. Discrete-time quantum walk with feed-forward quantum coin. *Scientific reports*, 4, 2014.

CHAPTER 6

ACADEMIC PUBLISHING AND SCIENTIFIC COMMUNICATIONS

6.1 Academic publishing

6.1.1 Submitted

- Nonlinear Optical Galton Board: thermalization and continuous limit, *G Di Molfetta, M.E. Brachet, F. Debbasch*, submitted to **Phys.Rev. E**

- Self-truncation and scaling in Euler-Voigt-α and related fluid models, *G Di Molfetta, M.E. Brachet, G. Krstulovic*, submitted to **Phys.Rev. E**, arXiv 1502.05544

- Discrete-time Quantum Walks in random artificial Gauge Fields, *G. Di Molfetta, F Debbasch*, submitted to **Physica A**, arXiv:1409.2122

6.1.2 Published

- Massless Dirac equation from Fibonacci discrete-time quantum walk, *G. Di Molfetta,L. Honter, B.B.Luo, Y. Shikano*, **Quantum Stud: Math. Found.**, 2196-5609, 1(10), 2015

- Quantum walks in artificial electric and gravitational Fields, *G Di Molfetta, F Debbasch, M E Brachet*, **Physica A**, Vol 397, 157-168, 2014

- Quantum walks as massless Dirac Fermions in curved Space-Time, *G Di Molfetta, F Debbasch, M E Brachet*, **Phys.Rev. A** 88, 042301, 2013

- Discrete-time quantum walks: Continuous limit and symmetries, *G di Molfetta, F. Debbasch*, **J. Math. Phys.** 53, 123302, 53 (123302), 2012

- Discrete Time Quantum walks, Continuous Limit in 1+1 and 1+2 dimensions, *G Di Molfetta, F Debbasch*, **Journal of Computational and theoretical Nanoscience**, Vol 10, 1-5, 2013

- Propagation in quantum walks and relativistic diffusions, *F Debbasch, G Di Molfetta, D Espaze, V Foulonneau* **Physica Scripta** (T151), 014044, 2012

6.1.3 Scientific Projects

IDRIS (Institute for Development and Resources in Intensive Scientific Computing), CNRS, Scientific Project, **"Auto-troncature et thermalisation à petite échelle dans le modele Euler-d'Hydrodynamique classique"**. *G Di Molfetta, M.E. Brachet, G. Krstulovic.*

6.2 Awards and Fellowship

Selected by CNRS for the JSPS Summer Program 2014, Fellowship "JSPS", CNRS - ENS Paris - Institute for Molecular Science Okazaki, *Supervisor: Yutaka Shikano.*

6.3 Workshop

- Workshop, **Quantum Dynamics and Quantum Walks**, Okazaki Conference Center, 24-26/11/12.
- Workshop, **Quantum Simulations and Quantum Walks**, Centro De Giorgi, SNS Pisa, 14-16/11/13
- Conference, **YITP Workshop on Quantum Information Physics**, Yukawa Institute for Theoretical Physics, Kyoto, 4-7/08/14
- Workshop, **Sapporo summer conference on dynamics of patterns in materials science**, Hokkaido University, 30/07/14

Appendices

APPENDIX A

NUMERICAL METHODS

Summary

A.1 Spectral Methods . . . 129
A.1.1 Fundamentals . . . 129
A.2 Convergence in spectral methods . . . 130
A.3 Approximate a PDE by spectral method . . . 130
A.3.1 Galerkin method . . . 131
A.3.2 Pseudo-spectral method . . . 131
A.3.3 De-aliasing . . . 132
A.3.4 Time-stepping . . . 132
A.4 Discrete Fourier Transform . . . 133

The equations simulated by our numerical code are the finite difference equations of the QWs, the linear and nonlinearDirac equations and the stochastic hyperbolic equations. In all these cases, except when the parameters of the DTQW are non-homogeneous in space, the discrete dynamical systems associated to those equations, have been simulated by the pseudo-spectral methods. In all other cases we have employed the Direct Numerical Simulations (DNS).

A.1 Spectral Methods

A.1.1 Fundamentals

Let us introduce the periodic fields f that verify: $f(x+L) = f(x)$ where L is the periodicity of the lattice. In order to simplify, let us choose $L = 2\pi$. Then the continuous function $f(x)$ can be expressed on the Fourier basis:

$$f(x) = \sum_{k=-\infty}^{\infty} \hat{f}_k e^{ikx}. \tag{A.1}$$

We define the scalar product as:

$$\langle g, h \rangle = \frac{1}{2\pi} \int_0^{2\pi} \overline{g}(x) h(x) dx, \tag{A.2}$$

where the Fourier coefficients read:

$$\hat{f}_k = \langle e^{ikx}, \psi(x) \rangle = \frac{1}{2\pi} \int_0^{2\pi} dx f(x) e^{-ikx}. \tag{A.3}$$

Generally, we can access to the knowledge of f through its value at the discrete finite set of points:

$$f_j = f(x_j) \tag{A.4}$$

with $x_j = j\Delta_x$ and $j = 0, 1, 2, ..., N-1$, so that the discrete space interval $\Delta x = \frac{2\pi}{N}$. This set is called "physical space". The Fourier coefficients are therefore approximated by:

$$\hat{f}_N(k) = \frac{1}{N}\sum_{n=0}^{N-1} f(x_n)e^{-ikx_n}, \tag{A.5}$$

with $x_n = \frac{2\pi n}{N}$, $n = 0, ..., N-1$. The latter equation define what we call the Discrete Fourier Transform (DFT). We then project f over a basis of N functions (*e.g.* the trigonometric function), and finally define f_N, the approximated function of f, just inverting the last DFT:

$$f_N(x_n) = \sum_{k=-N/2}^{N/2-1} \hat{f}_N(k)e^{ikx_n} \tag{A.6}$$

The points $k = -\frac{N}{2}, ..., \frac{N}{2} - 1$ represent the discrete "spectral space". Now let us observe that computing the DFT and its inverse requires $O(N^2)$ operations. This has represented a real problem, until Cooley and Tukey [1], introduced in 1965 the Fast Fourier Transform, FFT. This algorithm permits to reduce the number of operations to $O(N\log_2 N)$. Another advantage of the FFT, and in general of the Fourier transforms, concerns the factorization of the convolutions in 2 and 3 dimensions, but it will be not useful in this thesis where all physical systems are described in $(1+1)$ dimensions.

In conclusion, let us keep in mind that in this thesis, all the field vector $\Psi(x)$ and its Fourier transformed are approximated in 1-dimensional space by:

$$\begin{cases} \Psi_m = \sum_{k=-N/2}^{N/2-1} e^{2i\pi mk/N}\hat{\Psi}_k \\ \hat{\Psi}_k = \frac{1}{N}\sum_{m=0}^{N-1} e^{-2i\pi mk/N}\Psi_j \end{cases} \tag{A.7}$$

A.2 Convergence in spectral methods

In order to approximate a solution f of a PDE, we can employ finite difference methods of order p. In these methods the precision of the approximation depends on the order p of the Taylor development, and it is in general of $O(\Delta x^p)$. In spectral methods, instead, the coefficients $\hat{f}_N$ are computed over the N points fixed by our code resolution. In other words, we can increase the precision increasing the numerical resolution and notably it is not fixed *a priori*, such as in the finite difference methods. For example, for an interval $\Delta x \propto O(1/N)$, the error in the pseudo-spectral code is of order $O[(1/N)^N]$. The error decreases faster than any polynome of order N. This is what we call an *exponential convergence*.

A.3 Approximate a PDE by spectral method

Now, let us suppose that we need to solve a PDE in 1-dimensional space and that it takes the following form:

$$D(\Psi) = 0 \qquad \Psi(x,0) = \Psi^0(x) \tag{A.8}$$

where D is a linear differential operator, T is a positive number and Ψ is defined in $[0, 2\pi]\times]0, T]$. The approximation of Ψ is defined as the solution of the approximated PDE. We should find a function $\Psi_N(x,t)$ in $[0, 2\pi]\times]0, T]$, so that:

$$D(\Psi_N) = 0 \qquad \Psi_N(x,0) = \Psi^0_N(x) \tag{A.9}$$

where Ψ_N is defined in $[0,2\pi]\times]0,T]$.

In order to solve this problem we should compute the Fourier coefficient Ψ_N so that $D(\Psi_N)$ vanishes. In this thesis we have employed two important spectral methods: the Galerkin method and the pseudo-spectral method.

A.3.1 Galerkin method

In order to illustrate the idea of this method, let us introduce a simple example from fluido-dynamics and present the inviscid Burgers equation:

$$\frac{\partial}{\partial_t}\Psi(x)+\Psi(x)\frac{\partial}{\partial_x}\Psi(x)=0 \tag{A.10}$$

with the following periodic conditions:

$$\Psi(x+2\pi)=\Psi(x). \tag{A.11}$$

The DFT of Ψ, therefore, obeys to the following equation:

$$\frac{\partial}{\partial_t}(\sum_{n=-N/2}^{N/2-1} e^{inx}\hat{\Psi}_n)=-(\sum_{j=-N/2}^{N/2-1} e^{ijx}\hat{\Psi}_j)\frac{\partial}{\partial_x}(\sum_{k=-N/2}^{N/2-1} e^{ikx}\hat{\Psi}_k) \tag{A.12}$$

If the linear terms contain only wave number $|k|\leq N/2$, the nonlinear term of order 2 contains wave number $|k|\leq N$. The Galerkin method consists in retaining only the terms with wave number $|k|\leq N/2$. The above equation, after simplifications, reads:

$$\frac{\partial}{\partial_t}\hat{\Psi}_k=\sum_{j+k=n}\hat{\Psi}_j ik\hat{\Psi}_k \tag{A.13}$$

The sufficient number of operations to evaluate the convolution is of order $O(N^2)$, that represents a high computational cost. For this reason we compute the nonlinear term in physical space (by just N operation) and we translate the solution from the spectral to physical space and vice versa by FFT ($O(N\log N)$). We will see, in the next section, that the pseudo-spectral method is based on this idea.

A.3.2 Pseudo-spectral method

The pseudo-spectral methods consist in computing the approximation of a function over a determined basis, interpolating over a finite set of grid points (or collocation points). Therefore, the PDE will be exactly solved at the collocation points. We have employed this idea in computing the convolution in the physical space: we define as basis the DFT of the trigonometric functions (Dirac δ), which corresponds exactly to our collocation points. For the nonlinear term in A.12, we use two inverse FFT in order to compute Ψ and $\frac{\partial}{\partial_x}\Psi$ in the physical space. Then, we calculate the product and we use again a FFT in order to come back to the spectral

space:

$$DFT(\Psi\frac{\partial}{\partial_x}\Psi) = \frac{1}{N}\sum_{l=0}^{N-1}\Psi_l\frac{\partial}{\partial_x}\Psi_l e^{-i2\pi\frac{ln}{N}} \tag{A.14}$$

$$= \frac{1}{N}\sum_{l=0}^{N-1} e^{-i2\pi\frac{ln}{N}}\sum_{p=0}^{N-1} e^{i2\pi\frac{lp}{N}}\hat{\Psi}_p\sum_{q=0}^{N-1} e^{i2\pi\frac{lq}{N}}\frac{\partial\hat{\Psi}}{\partial_x}_q \tag{A.15}$$

$$= \frac{1}{N}\sum_{l=0}^{N-1}\sum_{p=0}^{N-1}\sum_{q=0}^{N-1} e^{-i2\pi\frac{l(n-p-q)}{N}}\hat{\Psi}_p\frac{\partial\hat{\Psi}}{\partial_x}_q \tag{A.16}$$

$$\frac{\partial}{\partial_t}(\hat{\Psi}_N)_n = \sum_{j+k=n[N]}(\hat{\Psi}_N)_j ik(\hat{\Psi}_N)_k \tag{A.17}$$

In other words, the approximated Fourier coefficients in the above equation are composed by all the exact coefficients along with other terms for which the function e^{inx} is indistinguishable from the $e^{inx}[N]$ (modulo N). This phenomenon is know as *aliasing*. Note, in conclusion, that extending these results to a generic nonlinear Dirac equation in $(1+1)$ is straightforward.

A.3.3 De-aliasing

Let us study a lattice of N grid points where the wave number k varies in the interval $[-N/2, N/2]$. Therefore the values $k_1 + k_2$ vary between $-N$ and N and, because of the aliasing problem, are replicated in the same interval. In order to solve this problem, we can truncate the spectrum by a cut-off $|k_{max}|$. For a nonlinearity of order 2, it is possible to prove that $2k_{max} - N < -k_{max}$ or equivalently $k_{max} < \frac{N}{3}$. In other words, we should eliminate all the values of k greater than $N/3$ and smaller than $-N/3$. In this way, all replicated values vanish at each time step. Let us remark that solving the aliasing problem is necessary to preserve correctly the integration by parts. In particular, the violation of this property leads to the non-conservation of the integrals, when they exist, in the considered EDP. More generally for a nonlinearity of order d we can de-aliase by the following rule:

$$k_{max} \leq \frac{M}{d+1} \tag{A.18}$$

A.3.4 Time-stepping

In the previous section we have introduced the pseudo-spectral methods to discretize the spatial part of the initial PDE and obtain an ODE system. Typically to discretize the PDE in an ODE, we should employ a method which is explicit for the nonlinear term and an implicit one for the linear part. In particular in this thesis we will use an Euler scheme (implicit or explicit) and a Runge-Kutta method of 4th order. Let us recall these three methods separately.
Consider the partial differential equations of the form:

$$\partial_t\Psi + G(\Psi) + L\Psi = 0 \tag{A.19}$$

where L is a linear operator and $G(\Psi)$ is a nonlinear operator. Suppose that the initial condition is known $\Psi(0,x) = \Psi_0(x)$. Discretization in time is given by all the $t_j \in \mathbb{R}^+ = jdt$ where $j \in \mathbb{N}$. The different schemes are:

- Explicit Euler (order $O(dt)$)

$$\Psi_{j+1} = \Psi_j + E[\Psi_j] \tag{A.20}$$
$$\mathcal{E}[\Psi_j] = dt(L\Psi + G[\Psi]) \tag{A.21}$$

- Implicit Euler (order $O(dt)$)

$$\Psi_{j+1} = \frac{\Psi_j + dtG[\Psi]}{1 - dtL} \tag{A.22}$$
$$\tag{A.23}$$

- Runge-Kutta (order $O(dt^4)$)

$$\Psi_{j+1} = \Psi_j + \frac{k_1}{6} + \frac{k_2}{3} + \frac{k_3}{3} + \frac{k_4}{6} + \frac{k_1}{6} \tag{A.24}$$
$$k_1 = E[\Psi_j] \tag{A.25}$$
$$k_2 = E[\Psi_j + \frac{k_1}{2}] \tag{A.26}$$
$$k_3 = E[\Psi_j + \frac{k_2}{2}] \tag{A.27}$$
$$k_4 = E[\Psi_j + k_3] \tag{A.28}$$

The RK-schemes is the more accurate and we will use it when we need to verify conserved quantities. Otherwise we use the following combined scheme:

$$\mathcal{I}[\Psi_n] = \frac{\Psi_j}{1 - dtL} \tag{A.29}$$
$$\Psi_{j+1} = \mathcal{I}[\Psi_j + dtG[\Psi_j]] \tag{A.30}$$

.

A.4 Discrete Fourier Transform

Let us now briefly describe the Fourier representation of the DTQWs. We know that QWs can be numerically implemented in two equivalent ways: in direct physical and in Fourier space. Generally the latter is preferable because the transformed unitary step operator becomes local and the translation operator is diagonal in Fourier basis. We therefore systematically prefer numerical simulation in Fourier space, when it is possible.

Consider the QWs, with the space homogeneous quantum coin, in physical space:

$$\begin{pmatrix} \psi^L(x_m, t_j + \Delta t) \\ \psi^R(x_m, t_j + \Delta t) \end{pmatrix} = C(\alpha(t_j), \theta(t_j), \xi(t_j), \zeta(t_j)) \begin{pmatrix} \psi^L(t_j, x_m - \Delta x) \\ \psi^R(t_j, x_m + \Delta x) \end{pmatrix} \tag{A.31}$$

Let us restrict the domain of $\Psi(x_m, t_j)$ to a 2π-periodic boundary conditions and for any integer N>0 consider the set of points:

$$x_m = \frac{2\pi m}{N} \tag{A.32}$$

where $m = 0,...,N-1$ referred to as nodes or grid points; now define the lattice parameter Δx, equal to $\frac{2\pi}{N}$. The discrete Fourier coefficients of the complex-valued function $\Psi(x_m, t_j)$ with

respects to the grids points are:

$$\tilde{\Psi}_k(t_j) = \frac{1}{N}\sum_{m=0}^{N-1}\Psi(x_m,t_j)e^{-ikx_m}, \tag{A.33}$$

where $-\frac{N}{2} \leq k \leq \frac{N}{2}-1$. Because of the orthogonality, over the interval $[0,2\pi]$, of the set of functions $\phi_k(x_m) = e^{-ikx_m}$, we can write the following inversion formula:

$$\Psi(t_j,x_m) = \sum_{k=-N/2}^{N/2-1}\tilde{\Psi}_k(t_j)e^{ikx_m}. \tag{A.34}$$

The above polynomial represents the Discrete Fourier transform (DFT) of $\Psi(t_j,x_m)$.

Let us mention that this DFT can be accomplished by the Fast Fourier Transform algorithm introduced by Cooley and Tukey [1]. In general FFT causes N to be a power of 2 and, if the data are fully complex, it requires $O(N\log_2 N)$ instead of $O(N^2)$ real operations required by straightforward sum. Moreover FFT incurs less errors, due to round-off, than the direct summation method Cooley et al. [2].
The way by which translation is accomplished in spectral space is given by the following operation:

$$\psi(t_j,x_m \pm \Delta x) = \sum_{m=-N/2}^{N/2-1} e^{\pm ik\Delta x}\tilde{\psi}_k(t_j)e^{ikx_m} \tag{A.35}$$

and therefore, the equations A.31 read:

$$\Psi(x_m,t_j+\Delta t) = C(\alpha(t_j),\theta(t_j),\xi(t_j),\zeta(t_j))\sum_{m=-N/2}^{N/2-1} T_k\tilde{\Psi}_k(t_j)e^{ikx_m}, \tag{A.36}$$

where the trasformed translation operator is diagonal and reads as:

$$T_k = \begin{pmatrix} e^{-ik\Delta x} & 0 \\ 0 & e^{ik\Delta x} \end{pmatrix} \tag{A.37}$$

Let us remark in conclusion that in this setting the continuous limit is automatically taken when N is increased. This allowed us to evaluate with high precision the discrepancy between the QW and the corresponding solution of the Dirac equation.

Bibliography

[1] J. W. Cooley and J. W. Tukey. An algorithm for the machine calculation of complex fourier series. *Mathematics of computation*, 19(90):297–301, 1965.

[2] J. W. Cooley, P. A. Lewis, and P. D. Welch. The fast fourier transform and its applications. *Education, IEEE Transactions on*, 12(1):27–34, 1969.

APPENDIX B

TRUNCATED EULER-VOIGT-α EQUATION AND THERMALIZATION

Summary

B.1 Absolute equilibria in truncated Euler equation 135

B.2 Eddy-damped quasi-normal Markovian theory (EDQNM) 136

B.3 Self-truncation 136

B.4 Publication A1: "Self-truncation and scaling in Euler-Voigt-α and related fluid models" 137

B.1 Absolute equilibria in truncated Euler equation

The incompressible 3D Euler equation are introduced to describe a nonviscous classic fluid by Euler in 1757 and appears for the first time in the *Principes généraux du mouvement des fluides*:

$$\partial_t \mathbf{u} + (\mathbf{u}\cdot\nabla)\mathbf{u} = -\frac{1}{\rho}\nabla p \qquad \nabla\cdot\mathbf{u} = 0. \tag{B.1}$$

The truncated version of these equation are then presented and investigated in [12, 5, 6, 13, 2, 2, 9, 10]. The truncation is obtained by a Galerkin truncation presented in sec. A.3.1 and the equations of motion read:

$$\partial_t \hat{u}_\alpha(\mathbf{k},t) = \mathcal{P}_G[-i\frac{i}{2}\mathcal{P}_{\alpha\beta\gamma}(\mathbf{k})\sum_p \hat{u}_\beta(\mathbf{p},t)\hat{u}_\gamma(\mathbf{k}-\mathbf{p},t)] \tag{B.2}$$

where the projector $\mathcal{P}_{\alpha\beta\gamma} = k_\beta P_{\alpha\gamma} + k_\gamma P_{\alpha\beta}$ with $P_{\alpha\beta} = \delta_{\alpha\beta} - k_\alpha k_\beta / k^2$. $P_{\alpha\beta}$ is the projector into divergence-less function ($\hat{u}(\mathbf{k})\cdot\mathbf{k}$=0) and P_G is the Galerkin projector that ensures the $\hat{u}(k) \equiv 0$, $\forall |k| > k_{max}$. Conservation of energy E and Helicity H was already shown by Lee [12] and Kraichnan [5]. Thermalization was proved by Orszag [13] and Cichowlas et al. [2] showed that B.2 displays a Kolmogorov spectrum.

Both conserved quantities, the energy and the helicity, help us to characterize the transition of the system to the fully relaxation. For instance, let us keep in mind the case of vanishing helicity, the only conserved quantity is the Energy and it reads:

$$E = \frac{1}{2}\sum_k |\hat{u}(\mathbf{k},t)|^2 \tag{B.3}$$

and the absolute equilibrium is simply described by the Boltzmann weight:

$$P_{st} = \frac{1}{Z}e^{-\beta E} \tag{B.4}$$

Note that eq. B.4 is a solution of the associated Liouville equation of the system B.2, therefore when is given by p.d.f. B.4, the velocity field remains in a statistically stationary state.
More in detail, Cichowlas et al. [2] found that in long time behavior a clear spontaneous scale separation appears in energy spectrum. Large and small scales display a different behavior: at small scales the thermalized modes of energy spectrum rise as k^2 and act by a pseudo-dissipative effect (as an effective thermal bath) on large scale. The progressive thermalization extends to larges scales till a fully repartition of the energy. Note that the large scales behavior, before fully equilibration, is compatible with a K41 scaling, that is the typical Kolmogorov spectrum in case of viscous turbulent hydrodynamics ([4, 3]). In this temporal evolution of spectrum the wave number k_{th}, defined as the mode triggering the process of thermalization plays an important role and quantifies the degree of thermalization of the whole system.

B.2 Eddy-damped quasi-normal Markovian theory (EDQNM)

The eddy-damped quasi-normal Markovian theory was introduced by Orszag [13] in order to treat analytically turbulence and in particular it has been used to study thermalization from Kolmogorov $k^{-5/3}$ scaling to absolute equilibria. It was also largely used in the past in numerical simulations as it allows a large scale separation with a relatively low computational cost.

This theory takes into account some important assumptions to determine the evolution of the energy spectrum: (i) the isotropy of the flow, (ii) the Gaussian statistical distribution of the Fourier modes in the statistics of the flow. Note that the definition of quasi-normality derived from the fact that this assumption is relaxed on the third moment that does not vanish (as they would be for zero mean Gaussian variable). The last assumption is (iii) Markovianity, that is reached dropping out the dependence of the past introducing an eddy-damped term η_k which takes into consideration the nonlinear interaction. The resulting equation is:

$$\left[\partial_t + 2\nu k^2\right] E(k,t) = \int\int_{\Delta} \Theta_{kpq}(xy+z^3)[k^2 pE(p,t)E(q,t)p^3 E(q,t)E(k,t)]\frac{dpdq}{pq} \tag{B.5}$$

where the characteristic time Θ_{kpq} is defined by:

$$\Theta_{kpq} = \frac{1-\exp(-(\eta_k+\eta_p+\eta_q)\,t)}{\eta_k+\eta_p+\eta_q} \tag{B.6}$$

In the EDQNM theory the eddy damped η_k is defined as:

$$\eta_k = \nu k^2 + \lambda\sqrt{\int_0^k s^2 E(s,t)\,ds} \tag{B.7}$$

This theory introduced by Orszag [13] has been then used by Bos and Bertoglio [1] in the inviscid case ($\nu = 0$) and introducing an effectivity viscosity, the eddy viscosity, used to explain the thermalization behavior and the dependence of E on the Fourier modes.

B.3 Self-truncation

As we have seen, the effect of Galerkin truncated Euler equation is responsible for the energy cascade toward small-scales and contains transient that mimics the irreversible viscous effects produced by the *microword* of small scale partially thermalized Fourier modes. Recently Krstulovic and Brachet [8] [7] have introduced in the case of superfluids the Galerkin-

truncated Gross Pitaevskii equation. In that case absolute equilibria exist and energy cascade is accompanied by an energy transfer to large scale. Furthemore it has been observed that partial thermalization is independent of the truncation wave number and that can be observed defining a self-truncation wave number k_{st}. This can be explained by the fact that an increase of dispersion (that is controlled by a physical parameter called "healing length") produces a slowdown of the energy transfer at small scales inducing a bottleneck and the emergence of a self-truncation.

B.4 Publication A1: "Self-truncation and scaling in Euler-Voigt-α and related fluid models"

In the following publication we proposed a generalization of the Euler-Voigt-α introduced by Larios et al. [11] in a different context. This model was characterized by a penalization of the small scales and recovered the standard Euler equation in the limit $\alpha = 0$. The main aim of the article was to show self-truncation in inviscid generalized Euler-Voigt-α model and investigated all the temporal regimes. We introduced Leith and EDQNM model to describe analytically the self-truncation and we showed that in long time behavior the spectrum is self-similar and $k_s t \propto t^{\eta}$. The exponent η was determined analytically.

Self-truncation and scaling in Euler-Voigt-α and related fluid models

Giuseppe Di Molfetta
LERMA, Observatoire de Paris, PSL Research University, CNRS, Sorbonne Universits, UPMC Univ. Paris 6, UMR 8112, F-75014, Paris France

Giorgio Krstlulovic
Laboratoire Lagrange, UMR7293, Université de Nice Sophia-Antipolis, CNRS, Observatoire de la Côte dAzur, BP 4229, 06304 Nice Cedex 4, France

Marc Brachet
Laboratoire de Physique Statistique de l'Ecole Normale Supérieure / PSL Research University, associé au CNRS et aux Universités Pierre-et-Marie-Curie Paris 06 et Paris Diderot, 24 Rue Lhomond, 75231 Paris, France

(Dated: April 13, 2015)

A generalization of the $3D$ Euler-Voigt-α model is obtained by introducing derivatives of arbitrary order β (instead of 2) in the Helmholtz operator. The $\beta \to \infty$ limit is shown to correspond to Galerkin truncation of the Euler equation. Direct numerical simulations (DNS) of the model are performed with resolutions up to 2048^3 and Taylor-Green initial data. DNS performed at large β demonstrate that this simple classical hydrodynamical model presents a self-truncation behavior, similar to that previously observed for the Gross-Pitaeveskii equation in Krstulovic and Brachet [Phys. Rev. Lett. 106, 115303 (2011)]. The self-truncation regime of the generalized model is shown to reproduce the behavior of the truncated Euler equation demonstrated in Cichowlas et al. [Phys. Rev. Lett. 95, 264502 (2005)]. The long-time growth of the self-truncation wavenumber $k_{\rm st}$ appears to be self-similar.

Two related α-Voigt versions of the EDQNM model and the Leith model are introduced. These simplified theoretical models are shown to reasonably reproduce intermediate time DNS results. The values of the self-similar exponents of these models are found analytically.

I. INTRODUCTION

Classical Galerkin-truncated systems have been studied since the early 50's in fluid mechanics. In this context, the (time reversible) Euler equation describing spatially-periodic classical ideal fluids is known to admit, when spectrally truncated at wavenumber $k_{\rm max}$, absolute equilibrium solutions with Gaussian statistics and equipartition of kinetic energy among all Fourier modes [1–4]. Furthermore, the dynamics of convergence toward equilibrium involves a direct energy cascade toward small-scales and contains (long-lasting) transient that mimic (irreversible) viscous effects that are produced by the "gas" of high-wavenumber partially-thermalized Fourier modes generating (pseudo) dissipative effects [5–7].

In the the case of superfluids, the relevent equation is the so-called truncated (or Galerkin-projected) Gross-Pitaevskii equation (TGPE). In the TGPE case, absolute equilibrium can also be obtained by a direct energy cascade, in a way similar to that of the truncated Euler case, with final thermalization accompanied by vortex annihilation. Furthermore, increasing the amount of dispersion produces a slowdown of the energy transfer at small-scales inducing a bottleneck and a partial thermalization that is independent of the truncation wavenumber and takes place below a 'self-truncation' wavenumber $k_{\rm st}(t)$ that is observed to slowly increase with time [8–10].

The purpose of the present paper is is to find and study such self-truncation phenomena in the simpler context of classical hydrodynamics of an ideal fluid. This is obtained by using equation of motion of the Euler type. To wit, we study here a simple generalization of the standard $3D$ Euler-Voigt-α model [11, 12]. Compared to the Euler equations, this conservative model penalizes the formation of small scales. We show that this penalization is enough to produce a self truncation regime. Our main findings are that the self-truncation regime of this generalized model reproduces the behavior of the truncated Euler equation [5]. The long-time behavior of the energy spectrum appears to be self-similar.

To understand this self-similarity we further introduce two different models that are α-Voigt versions of the Eddy-Damped Quasi-Normal Markovian (EDQNM) model and the Leith model, respectively. Both models are shown to present behaviors that are similar to that of the Euler-Voigt-α model. The relative simplicity of these models allows us to determine the analytical values of the self-similar exponents.

The paper is organized as follows. Section II is devoted to our generalized model. Basic definitions of the Euler-Voigt-α model are given in section II A. Numerical methods and performed computations are detailed in section II B. Our results on the self truncation regime are described in section II C. The long-time behavior is studied in section II D. Related theoretical models are presented in section III. Section III A is devoted to the αV-EDQNM model and section III B to the αV-Leith model. Finally, our main results are summarized in sec-

tion IV where we give our conclusions.

II. EULER-VOIGT-α MODEL

A. Definition of the model

The standard $3D$ Euler-Voigt-α model [11, 12] is a partial differential equation for the $3D$ velocity field $\mathbf{u}(\mathbf{x},\mathbf{y},\mathbf{z},\mathbf{t})$ that explicitly reads

$$\begin{aligned}(1-\alpha^2\nabla^2)\frac{\partial \mathbf{u}}{\partial t} &= -(\mathbf{u}\cdot\nabla)\mathbf{u} - \nabla p \\ \nabla\cdot\mathbf{u} &= 0. \end{aligned} \tag{1}$$

The operator $-\alpha^2\nabla^2\frac{\partial}{\partial t}$ (as we will see later) suppresses the formation of scales smaller than α. The associated wave number to this scales is denoted $k_\alpha = \alpha^{-1}$. We refer to the operator in Eq.1 as the α-term.

Let us define the generalized $3D$ Euler-Voigt-α model:

$$\begin{aligned}(1+(-\alpha^2\nabla^2)^{\frac{\beta}{2}})\frac{\partial \mathbf{u}}{\partial t} &= -(\mathbf{u}\cdot\nabla)\mathbf{u} - \nabla p \\ \nabla\cdot\mathbf{u} &= 0, \end{aligned} \tag{2}$$

where the power β is an even integer. We refer to β as the penalization exponent as its increase enhances the suppression of small scale generation. When $\alpha = 0$, the generalised model Eq. (2) reduces to the standard $3D$ incompressible Euler equations

$$\frac{\partial \mathbf{u}}{\partial t} + \mathbf{u}\cdot\nabla\mathbf{u} = -\nabla\mathbf{p}, \quad \nabla\cdot\mathbf{u} = \mathbf{0}. \tag{3}$$

We consider here spatially-periodic solutions defined in the domain $\Omega = [0, 2\pi]^3$. The kinetic energy spectrum $E(k,t)$ associated to (3) is defined as the sum over spherical shells

$$E_0(k,t) = \frac{1}{2}\sum_{\substack{\mathbf{k}\in\mathbb{Z}^3 \\ \mathbf{k-1/2}<|\mathbf{k}|<\mathbf{k+1/2}}} |\widehat{\mathbf{u}}(\mathbf{k},t)|^2, \tag{4}$$

and the energy

$$E_0 = \frac{1}{2(2\pi)^3}\int_\Omega |\mathbf{u}(\mathbf{x},t)|^2 d^3x = \frac{1}{2}\sum_{\mathbf{k}\in\mathbb{Z}^3}|\widehat{\mathbf{u}}(\mathbf{k},t)|^2,$$

is independent of time when $\mathbf{u}$ satisfies the 3D Euler equations (3). The conserved energy associated to the generalized Euler-Voigt-α model (2) is straightforward to obtain and reads in physical space

$$E_\alpha = \frac{1}{2(2\pi)^3}\int_\Omega \mathbf{u}\cdot[1+(-\alpha^2\nabla^2)^{\frac{\beta}{2}}]\mathbf{u}\, d^3x,$$

and in spectral space

$$E_\alpha = \frac{1}{2}\sum_{\mathbf{k}\in\mathbb{Z}^3}[1+(\alpha k)^\beta]|\widehat{\mathbf{u}}(\mathbf{k},t)|^2. \tag{5}$$

Consequently, the generalised energy spectrum is defined as

$$E_\alpha(k,t) = \frac{1}{2}\sum_{\substack{\mathbf{k}\in\mathbb{Z}^3 \\ \mathbf{k-1/2}<|\mathbf{k}|<\mathbf{k+1/2}}} [1+(\alpha k)^\beta]|\widehat{\mathbf{u}}(\mathbf{k},t)|^2. \tag{6}$$

In the following, we refer to $E_\alpha(k,t)$ as the energy spectrum and $E(k,t)$ as the kinetic energy spectrum. Equations (2) also conserve the generalised helicity

$$H_\alpha = \frac{1}{2}\sum[1+(\alpha k)^\beta]\,\widehat{\mathbf{u}}(\mathbf{k},t)\cdot\widehat{\omega}(-\mathbf{k},t). \tag{7}$$

In this work we only consider flows with $H_\alpha = 0$.

Let us remark that the differential operator multiplying the r.h.s. of our generalized $3D$ Euler-Voigt-α model (2) can be written in Fourier space as $1+(\alpha k)^\beta = 1+(k/k_\alpha)^\beta$. The formal limit $\beta\to\infty$ of Eq. (2) thus corresponds to a standard spherical Galerkin truncation ($\hat{\mathbf{u}}(\mathbf{k}) = 0$ for $|\mathbf{k}| > k_{\max}$) of the Euler equation (3) at $k_{\max} = k_\alpha$.

It is well known that the truncated Euler equation admits statistically stationary solutions given by the microcanonical distribution determined by the invariants [1, 3]. These solutions are the so called absolute equilibrium and lead to equipartition of energy among Fourier modes. The Euler-Voigt-α model considered as a truncated system, also admits absolute equilibrium solutions. When fully thermalized, Fourier modes can be described by the canonical Gibbs distribution $\hat{\mathbf{u}}(\mathbf{k}) \sim \mathcal{Z}^{-1}\exp\{-\beta E_\alpha[\hat{u}]\}$, where $\mathcal{Z}$ is the partition function [33]. As the invariant energy is quadratic, the absolute equilibrium is Gaussian and the Fourier modes are independent. This leads to the spectra

$$E_\alpha(k) = \frac{3E_\alpha k^2}{k_{\max}^3}, \text{ or } E(k) = \frac{3E_\alpha k^2}{k_{\max}^3(1+\alpha^\beta k^\beta)}. \tag{8}$$

The large scale behavior of the kinetic energy spectrum thus depends on the value of the penalization exponent β as $E(k)\sim k^{2-\beta}$. Therefore, in thermal equilibrium the small scales of $\mathbf{u}$ (i.e. $k \gg k_\alpha$) are penalized when $\beta > 0$.

Note that, in Fourier space, the differential operator in (2) can be defined for real values of $\beta \geq 0$. Choosing $\beta = 11/3$ yields an absolute equilibrium $E(k)\sim k^{-5/3}$ and thus a fully thermalized field following Kolmogorov scaling. In the same vein, choosing in two-dimensions $\beta = 2/3$ also yields Kolmogorov scaling, this time for the equipartition of enstrophy. This can represent an interesting alternative to the fractal decimation method that was used in reference [14].

B. Numerical method

The generalized $3D$ Euler-Voigt-α equations (2) are solved numerically using standard [15] pseudo-spectral methods with resolution N. Time marching is performed

using a second-order Runge-Kutta scheme and the solutions are spherically dealiased by suppressing, at each time step, the modes for which the wave-vector exceeds two-thirds of the maximum wave-number $N/2$ (thus a 2048^3 run is truncated at $|\mathbf{k}| > k_{\max} = 682$).

We consider here solutions of Eq. (2) that correspond to the so-called Taylor-Green (TG) [16] (2π-periodic) initial data $\mathbf{u}(\mathbf{x},\mathbf{y},\mathbf{z},\mathbf{0}) = \mathbf{u}^{\rm TG}(\mathbf{x},\mathbf{y},\mathbf{z})$, with

$$\mathbf{u}^{\rm TG} = (\sin(x)\cos(y)\cos(z), -\cos(x)\sin(y)\cos(z), 0). \tag{9}$$

The simulations reported in this paper were performed using a special purpose symmetric parallel code developed from that described in [17–20]. The code uses the symmetries of the Taylor-Green initial data to speed-up computations and optimize memory usage. The workload for a timestep is (roughly) twice that of a general periodic code running at a quarter of the resolution. Specifically, at a given computational cost, the ratio of the largest to the smallest scale available to a computation with enforced Taylor-Green symmetries is enhanced by a factor of 4 in linear resolution. This leads to a factor of 32 savings in total computational time and memory usage. The code is based on FFTW and a hybrid MPI-OpenMP scheme derived from that described in [21]. At resolution 2048^3 we used 512 MPI processes, each process spawning 8 OpenMP threads.

When compared with standard Euler equation (3) runs that were performed in reference [19], the only computational advantage of the the generalized $3D$ Euler-Voigt-α model (2) stems from the much weaker Courant-Friedrichs-Lewy (CFL) condition on the time step Δt which is conditioned by $k_\alpha = \alpha^{-1}$ rather than $k_{\max}$. We have performed a number of high-resolution runs that are summarised in Table I. The CFL condition $\Delta t\, k_\alpha \sim 0.1$ was enough to insure both stability and energy conservation up to 0.3% in the worst case.

Run	Res.	β	k_α	$t_{\max}$	Run	Res.	β	k_α	$t_{\max}$
Euler	1024	–	–	30	11	2048	2	100	15
1	1024	2	20	50	12	2048	2	200	15
2	1024	2	40	50	13	2048	4	50	15
3	1024	2	80	50	14	2048	4	100	15
4	1024	4	20	50	15	2048	4	200	15
5	1024	4	40	50	16	2048	6	50	15
6	1024	4	80	50	17	2048	6	100	15
7	1024	6	20	50	18	2048	6	200	15
8	1024	6	40	50	19	512	2	4	2300
9	1024	6	80	50	20	512	4	4	2300
10	2048	2	50	15	21	512	6	4	2300

TABLE I. List of runs of the generalized $3D$ Euler-Voigt-α model (2) with TaylorGreen initial data (9) and maximum integration time $t_{\max}$.

C. Self truncation

A first indication on the dynamics of the generalized Euler-Voigt-α model (2) with TaylorGreen initial data (9) is given by the behavior of the Energy spectra for a run at resolution 1024^3 with $\beta = 4$ and $k_\alpha = 80$ (run 6 Table I) that is displayed in Fig.1.

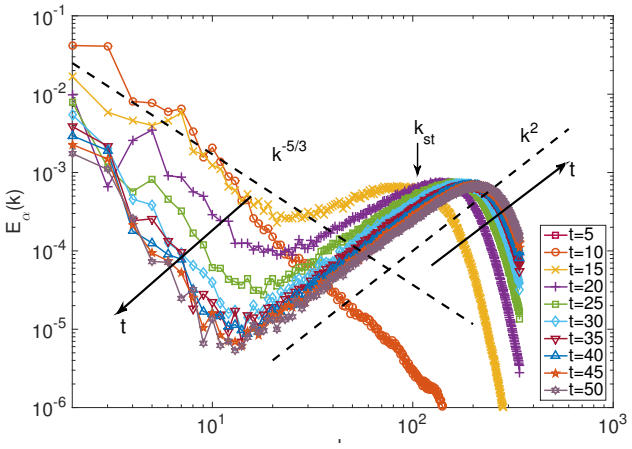

FIG. 1. (Color online) Temporal evolution (indicated by arrows) of the energy spectrum $E_\alpha(k)$ for $\beta = 4$ and $k_\alpha = 80$. Resolution 1024^3 ($k_{\max} = 342$). The dashed lines respectively display the Kolmogorov $k^{-5/3}$ and the equipartition k^2 scaling. The self-truncation wavenumber is indicated by the small vertical arrow.

Different regimes are clearly observed. First the energy is transferred toward small scales as in the standard Euler equation evolution ($t \leq 5$). Then the energy reaches the wavenumber $k_\alpha = 80$ and the α-term in (2) starts to suppress the energy transfer for $k > k_\alpha$. As a consequence, the energy piles up around this wavenumber, similarly to the truncated Euler case with a cut-off $\sim k_\alpha$. Note that a compatible Kolmogorov $k^{-5/3}$ scaling is observed at large scales ($t = 15$), followed by a partially thermalized zone in k^2 extending up to $k_{\rm st}$. The wavenumber $k_{\rm st}(t)$ then slowly growth from its initial value k_α until it eventually reaches the simulation cut-off $k_{\max}$. For $t \to \infty$ the system fully thermalises independently of the parameters (data not shown) and the spectrum is then described by the absolute equilibrium (8). Note that for $k > k_{\rm st}$ the energy quickly decays and the partial thermalization regime is thus independent of the simulation cut-off $k_{\max}$. We thus refer to $k_{\rm st}$ as the *self-truncation* wavenumber. A further discussion and justification for its name will be given later (see below, paragraph following Eq.10).

Figure 2 displays the spectra of simulations at resolution 2048^3 for different values of β and k_α taken at time $t = 10.2$. The self-truncation is apparent for the smaller k_α at all values of β and, for larger $\beta \geq 4$, at all values of k_α. The three ranges delimited by the *thermalization* wavenumber $k_{\rm th}$ and the *self-truncation* wavenumber $k_{\rm st}$ are clearly visible (see Fig.2.c) at this

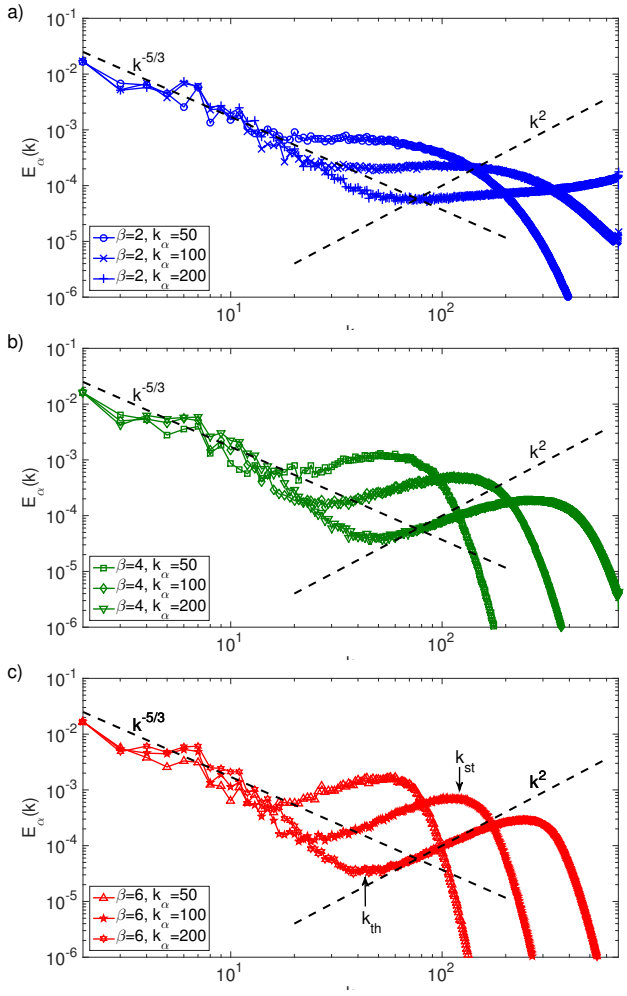

FIG. 2. (Color online) Energy spectrum $E_\alpha(k)$ versus k for $\beta = 2$ and $k_\alpha = 50$, 100 and 200 at $t = 10.2$. (b) Same conditions than in (a) but $\beta = 4$. c) Same conditions than in (a) but $\beta = 6$. The dashed-black lines corresponds to Kolmogorov scaling $E_\alpha(k) \sim k^{-5/3}$ and energy equipartition $E_\alpha(k) \sim k^2$. The thermalization wave number $k_{\rm th}$ and selftruncation $k_{\rm st}$ are indicated by arrows in (c).

high resolution. Formally, these zones correspond to the Kolomogorov regime ($k \ll k_{\rm th}$), the thermalization range ($k_{\rm th} \ll k \ll k_{\rm st}$) and the exponential energy decay ($k \gg k_{\rm st}$). Note that, at this intermediate time ($t = 10.2$), the $\beta = 6$ case appears to be already behaving somewhat like what is expected of the $\beta = \infty$ limit. Indeed, Fig. 2(c) is reminiscent of the previously studied truncated-Euler case (see Fig.1 of reference [5]). Of course, in the truncated Euler case no third decreasing zone exists as, when $\beta = \infty$, $E_\alpha(k) = 0$ for $k > k_\alpha$. In order to make the comparison with the $\beta = \infty$ limit more quantitative, following [5], we have computed the thermalized energy $E_{\rm th}(t) = \sum_{k_{\rm th}(t)<k} E(k,t)$ and the effective dissipation $\varepsilon(t) = \frac{{\rm d}E_{\rm th}(t)}{{\rm d}t}$. The time evolutions of $k_{\rm th}$, $E_{\rm th}$ and ε are presented on Fig.3. The agreement

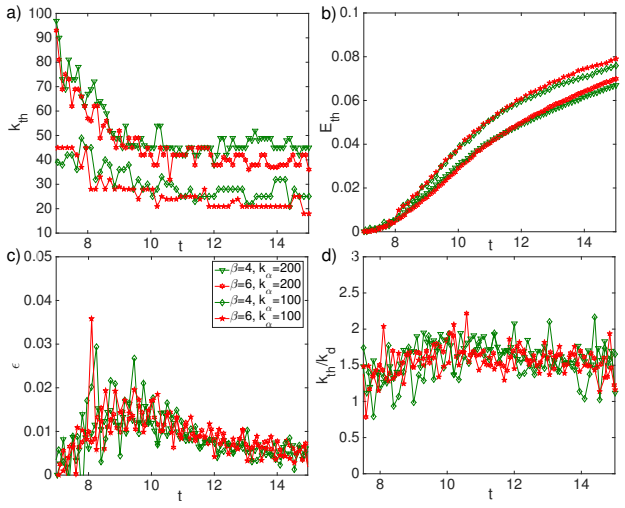

FIG. 3. (Color online) Temporal evolution of (a) $k_{\rm th}$, (b) $E_{\rm th}$, (d) $\epsilon = \frac{\partial E_{\rm th}}{\partial t}$, (e) $k_{\rm th}/k_{\rm d}$ with $k_{\rm d}$ estimated based on the self-truncation wavenumber $k_{\rm st}$, see Eq.(10).

with the truncated Euler data appears to be good (compare with Figs 2 and 4 in reference [5]). Note that these quantities do not appreciably depend on the value of β.

In references [5, 22], an effective generalized Navier-Stokes model for the dissipative dynamics of modes k close to $k_{\rm th}(t)$ was suggested for the original Euler case with fixed truncation at $k = k_{\rm max}$. In this case, the effective viscosity of the model was given by $\nu_{\rm eff} = \sqrt{E_{\rm th}}/k_{\rm max}$. If we assume that the generalized large-β case behaves similarly to the Euler case truncated at $k_{\rm st}$, we find that the dissipative wavenumber $k_{\rm d}$ should be given by

$$k_{\rm d} \sim \varepsilon^{1/4} (\sqrt{E_{\rm th}}/k_{\rm st})^{-3/4} \qquad (10)$$

The consistency of this estimation of the effective dissipation with the results displayed in Fig.3a-c requires that $k_{\rm d} \sim k_{\rm th}$. The ratio $k_{\rm th}/k_{\rm d}$ is displayed on figure Fig.3.d. It indeed seen to be of order unity and reasonably constant in time. Thus the large-β dynamics of Eq. (2) is seen to emulate the dynamics of the Euler equation, spectrally-truncated at $k_{\rm max} = k_{\rm st}$. For this reason, we call the regime where this behavior takes place the self-truncation regime.

In the self-truncation regime the energy spectrum $E_\alpha(k)$ sharply decreases for for $k > k_{\rm st}$ (see Fig.2). In order to quantify this behavior we have used the so-called analyticity strip (AS) method [23]. Let us recall that the idea is to monitor the 'width of the analyticity strip' $\delta(\geq 0)$ as a function of time, effectively measuring a 'distance to the singularity' [24]. Using spectral methods [15], $\delta(t)$ is obtained directly from the high-wavenumber exponential fall off of the spatial Fourier transform of the solution [25]. The AS method has been used to numerically study putative Euler singularities (see *e.g.* reference [19] for implementation details). The common procedure

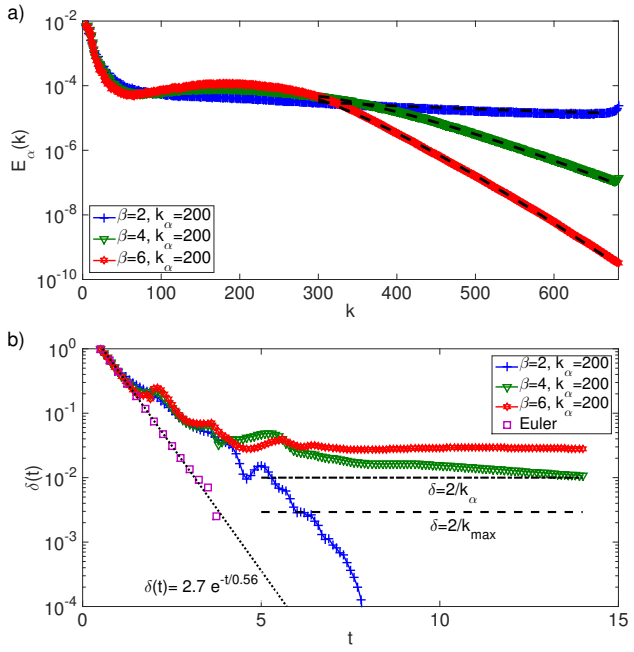

FIG. 4. (Color online) (a) Exponential decay of $E_\alpha(k)$ at $t = 7.8$. b) Time Evolution of energy spectrum fit parameter δ of Eq.(11): Horizontal lines correspond to $\delta k_{max} = 2$ (dashed black line) and $\delta k_\alpha = 2$ (dot-dashed black line). Exponential law (dot black line) $\delta = 2.7\exp(-t/0.56)$ from reference [19].

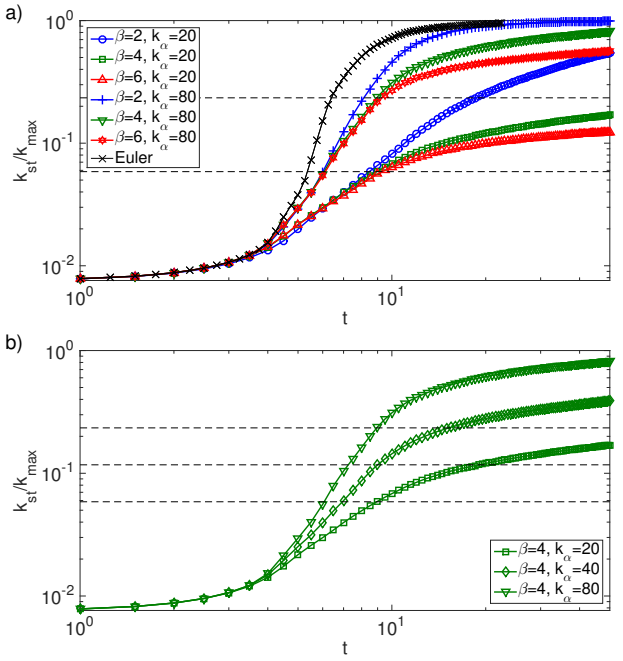

FIG. 5. (Color online) Time evolution of $k_{\rm st}(t)$ at resolution 1024^3 (see Table I) . a) Different values of β for $k_\alpha = 20$. The crosses show the Euler evolution of $k_{\rm st}$ ($\alpha = 0$). b) $\beta = 4$ and different values of k_α. The horizontal dashed lines represent the values of $k_\alpha/k_{\rm max}$.

is to perform a least-square fit at each time t on the logarithm of the energy spectrum $E_\alpha(k,t)$, using the functional form

$$\ln E_\alpha(k,t) = \ln C(t) - n(t)\,\ln k - 2k\,\delta(t). \qquad (11)$$

Energy spectra are fitted on the intervals $2 < k < k^*$ for $t < 2$ and on the interval $300 < k < \min(k^*, k_{\rm max})$ for $t > 2$, with $k^* = \inf\{k \,|\, E(k) < 10^{-32}\}$ denotes the beginning of round off noise. The fit presented in Fig.4.a in good agreement with the data. The time evolution of the fit parameter δ is displayed in Fig.4.b, where it is compared with the exponential in time law $\delta(t) = 2.7e^{-t/0.56}$ followed by the Euler equation (see reference [19]). The horizontal lines show the value of the length $2/k_{\rm max}$ (dashed) and $2/k_\alpha$ (dotted-dashed). It is apparent that the model follows the Euler dynamics as long as $\delta k_\alpha \gg 1$. The measure of the fit parameters is reliable as long as $\delta(t)$ remains larger than a few mesh sizes ($\delta k_{\rm max} \gg 1$), a condition required for the smallest scales to be accurately resolved and spectral convergence ensured. Thus the dimensionless quantity $\delta k_{\rm max}$ is a measure of spectral convergence. Therefore, the self-truncation solutions are solution of the full partial differential equation (2) and not of the spectrally truncated system.

From the mathematical point of view, Eq.(2) can be considered as ordinary differential equation as the right hand side can be shown to be a bounded continuos Lipschitz map between Banach spaces. In this case, existence and regularity can be proved using the same techniques than in (finite dimensional) ordinary differential equations [26].

D. Long-time behavior of $k_{\rm st}$

The self-truncation observed in Fig.2 is accompanied by a very slow growth of $k_{\rm st}$ until it reaches the simulation cut-off $k_{\rm max}$. Such a behavior was also observed in the dispersive self-truncation of the truncated Gross-Pitaevskii equation in two [10] and three [8, 9] dimensions. In the Gross-Pitaevski case, the self-truncation wavenumber $k_{\rm st}$ was shown to obey a power-law scaling

$$k_{\rm st}(t) \sim t^\eta, \qquad t \gg 1. \qquad (12)$$

Fig.5 displays the temporal evolution of $k_{\rm st}$ for different values of β and k_α. The wavenumber k_{st} is determined by the weighted average $k_{st} = \sqrt{(5/3)\sum_k E_\alpha(k,t)k^2/E_\alpha}$. With this definition, in the case of the absolute equilibrium (8) we obtain $k_{\rm st} = k_{\rm max}$. Note that $k_{\rm st}$ is defined for all times, even before the self-truncation starts to take place. It is in fact proportional to the inverse of the Taylor microscale [25].

Figure 5.a compares $k_{\rm st}(t)$ for different values of the penalization exponent β with $k_\alpha = 20$ (lower three curves) and $k_\alpha = 80$ (upper three curves). Note that for the short times when $k_{\rm st} < k_\alpha$ the temporal evolution of $k_{\rm st}$ is, as expected, independent of β. Furthermore, for the very

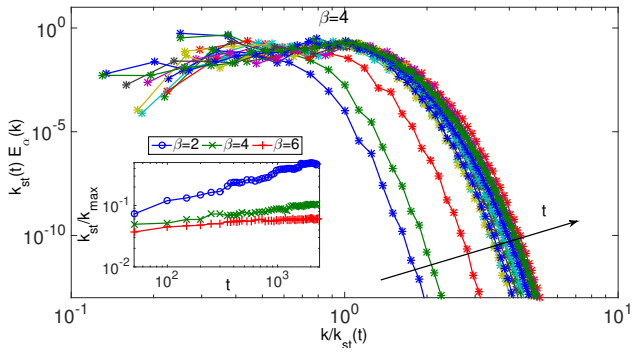

FIG. 6. (Color online) a) Temporal evolution of the self-similar function $\Psi(k/k_{\rm st}(t)) = E_\alpha(k,t)k_{\rm st}(t)$ (see Eq.13) for $\beta = 4$ and $k_\alpha = 4$. Data from direct numerical resolution of (2) at resolution 512^3. The inset shows the temporal evolution of $k_{\rm st}(t)/k_{\rm max}$ for different values of β.

short times, the penalization of small scales introduced by the α-term in the Euler-Voigt-α model is negligible and thus $k_{\rm st}$ is also independent of k_α as the dynamics is given by the (standard) Euler equation (black curve with crosses).

A behavior compatible with a power law is observed at long times. Note that the exponent seems to depend on the value of β thought the data do not allow a clear determination of the exponent η. The power-law behavior is contaminated by the initial dynamic as it is actually expected to have the form $k_{\rm st}(t) \sim (t - t_0)^\eta$, where t_0 is the time when self-truncation starts. Simulations where $t \gg t_0$ and $k_{\rm st} \ll k_{\rm max}$ are difficult to reach with the present choice of parameters and resolution.

In order to explore such power-law behavior a series of runs ($19-21$, see Table I) have been performed in resolution 512^3 and at small value of $k_\alpha = 4$. With this choice of parameter, self-truncation starts at low wavenumbers ($\sim k_\alpha$) and thus no Kolmogorov scaling can be observed. However such a choice allows very long temporal integrations (up to $t = 2300$) and to clearly observe the power-law behavior of $k_{\rm st}$, as apparent in the inset of Fig.5. The value of the exponent clearly depends on the penalization exponent β. The values measured for η are displayed in Table II. The power-law observed for $k_{\rm st}$ strongly suggests to look for self-similar behavior of the energy spectrum $E_\alpha(k,t)$, where the only temporal dependence of the spectrum is given by $k_{\rm st}(t)$. A self-similar form of the energy spectrum compatible with the conservation law (5) is given by

	$\beta = 2$	$\beta = 4$	$\beta = 6$
αV-Euler	$0.5 \pm 6 \times 10^{-3}$	$0.25 \pm 3 \times 10^{-3}$	$0.07 \pm 5 \times 10^{-3}$
αV-EDQNM	$0.33 \pm 5 \times 10^{-5}$	$0.11 \pm 9 \times 10^{-5}$	$0.085 \pm 1 \times 10^{-4}$
αV-Leith	0.33 ± 10^{-6}	$0.15 \pm 2 \times 10^{-4}$	$0.09 \pm 9 \times 10^{-6}$

TABLE II. Values of the exponent η of the self-truncation wavenumber $k_{\rm st}(t) \sim t^\eta$ (see (12)) obtained from direct numerical simulation of the Euler-Voigt-α model (2), αV-EDQNM (14-17) and αV-Leith model ($r = 2$).(24).

$$E_\alpha(k,t) = \frac{E_0}{k_{\rm st}(t)} \Psi\left(\frac{k}{k_{\rm st}(t)}\right) \tag{13}$$

Where E_0 is a constant with dimension of energy. The function $\Psi(z)$ is expected to behave as $\Psi(z) \sim z^2$ for $z \ll 1$ and exponentially decay for $z \gg 1$. Figure 6 displays $k_{\rm st}(t)E_\alpha(k,t)$ as a function of $k/k_{\rm st}(t)$ where the tendency to converge towards a self-similar distribution is confirmed for long times. The assumption of self-similarity implicitly supposes that the scale α is very small. Such hypothesis is valid only for long times such that $k_\alpha \ll k_{\rm st}(t) \ll k_{\rm max}$. Discrepancies with the full self-similar form are certainly due to the finite values of the infra-red and ultra-violet cut-off of the simulation. In order to develop further this idea, in the next sections we introduce two theoretical models that allow to obtain both a clear numerical support of self-similarity and an analytic expression for the self-truncation exponent η.

III. THEORETICAL MODELS

A. Eddy-damped Quasi-Markovian Euler-Voigt-α model

A popular model of turbulence is the so called Eddy-Damped Quasi-Markovian (EDQNM) closure [4]. It was derived in the 60-70's and is based on statistical closure of the velocity correlations in Fourier space plus some ad-hoc modeling of the dissipative time scales. It furnishes an integro-differential equation for the spectrum $E(k,t)$. EDQNM has been proved to be a powerful theoretical and numerical tool in the las 30 years as it allows to achieve a very large scale separation. It was also shown by Bos and Bertoglio [22] that EDQNM reproduces well the dynamics of the truncated Euler equation, including the $k^{-5/3}$ and k^2 scalings together with the relaxation to equilibrium. It was also used in [27] to give an analytic prediction of the effective viscosity acting on the large scales of truncated Euler flows.

The extension of EDQNM model to the Euler-Voigt-α case is straightforward. First, following Orszag derivation [4] but using equations (2), we directly find

$$\frac{\partial E(k,t)}{\partial t} = \frac{1}{1+\alpha^\beta k^\beta} T_{NL}(k,t) \tag{14}$$

where the nonlinear transfer T_{NL} is modeled as

$$T_{NL}(k,t) = \int\int_{\triangle} \Theta_{kpq}(xy + z^3) \left[\frac{k^2 p E(p,t) E(q,t)}{1+\alpha^\beta k^\beta} - \frac{p^3 E(q,t) E(k,t)}{1+\alpha^\beta p^\beta} \right] \frac{dp\,dq}{pq}. \tag{15}$$

In (15), $\triangle$ represents a strip in (p,q) space such that the three wavevectors $\mathbf{k}$, $\mathbf{p}$, $\mathbf{q}$ form a triangle. x, y, z, are

the cosine of the angles opposite to $\mathbf{k}$, $\mathbf{p}$, $\mathbf{q}$. Θ_{kpq} is a characteristic time defined as

$$\Theta_{kpq} = \frac{1 - \exp\left(-(\eta_k + \eta_p + \eta_q)t\right)}{\eta_k + \eta_p + \eta_q}. \qquad (16)$$

The standard EDQNM equations are recovered by setting $\alpha = 0$. Note that absolute equilibrium (8) is a stationary solution of (14) that satisfies detailed balance (no flux solution). The eddy damped inverse time η_k is defined as

$$\eta_k = \lambda' \sqrt{\int_0^k \frac{s^2 E(s,t)}{1 + \alpha^\beta s^\beta}\, ds}. \qquad (17)$$

In the limit $\alpha \to 0$ the standard eddy damped inverse time is recovered [28]. Note that for $\beta \to \infty$, the standard eddy time is also recovered for $k < k_\alpha = 1/\alpha$ whereas $\eta_k = 0$ for $k > k_\alpha$, consistently with the dynamics of the truncated Euler equation, as for $k > k_{\max}$ the dynamics is frozen. The constant λ defines a time scale and we use the standard value $\lambda = 0.36$. The truncation is imposed by omitting all interactions involving waves numbers larger than $k_{\max}$ in (15). We refer to (14-17) as αV-EDQNM model.

A number of simulations of the α-EDQNM equation has been performed and give a behavior that is similar to that of the DNS of the full Euler-Voigt-α model, including comparable time scales. Figure 7.a displays the energy spectrum for $\beta = 2, 4, 6$ and $k_\alpha = 10^4$ for a simulation with $k_{\max} = 43918$ (and 14.2 points per octave).

Fig. 7.a shows that the three zones observed in the Euler-Voigt-α model (see Fig.2), are also apparent in αV-EDQNM model spectra, with scaling laws extending for more than two decades. In the same spirit than in the Euler-Voigt-α DNS runs with a smaller value of $k_\alpha = 5$ have been performed, allowing a clear determination of the self truncation exponent η. The values are presented on Table II. Analogously to the Euler-Voigt-α DNS, we look for a self-similar behavior of the energy spectrum. The collapse is manifest in Fig. 7.b where the self-similar form (13) is displayed for $\beta = 4$. The αV-EDQNM model allows for directly looking for such self similar behavior and find the exponent η by counting powers. Indeed, introducing the self-similar form and the variable $z = k/k_{\rm st}(t)$ in (13) in the eddy damped inverse time (17) we find

$$\eta_z(t) = \lambda E_0^{1/2} k_{\rm st}(t) \sqrt{\int_0^z \frac{\Psi(z')\, z'^2}{(1 + \alpha^\beta k_{\rm st}(t)^\beta z'^\beta)^2}\, dz'}. \qquad (18)$$

The eddy damped inverse time can be thus expressed as $\eta_z = \lambda E_0^{1/2} k_{\rm st} I(z, \alpha k_{\rm st})$. Assuming that $I(z, \alpha k_{\rm st}) \sim (\alpha k_{\rm st})^\gamma$ we obtain for the characteristic time in the self-similar form $\Theta_{z_k z_p z_q} \sim k_{\rm st}^{-1-\gamma}$. In the same way, the non-linear transfer term (15) is found to scale with the self-truncation number as $T_{NL} \sim k_{\rm st}^{-1-\gamma+3-2-3\beta}$. Equating

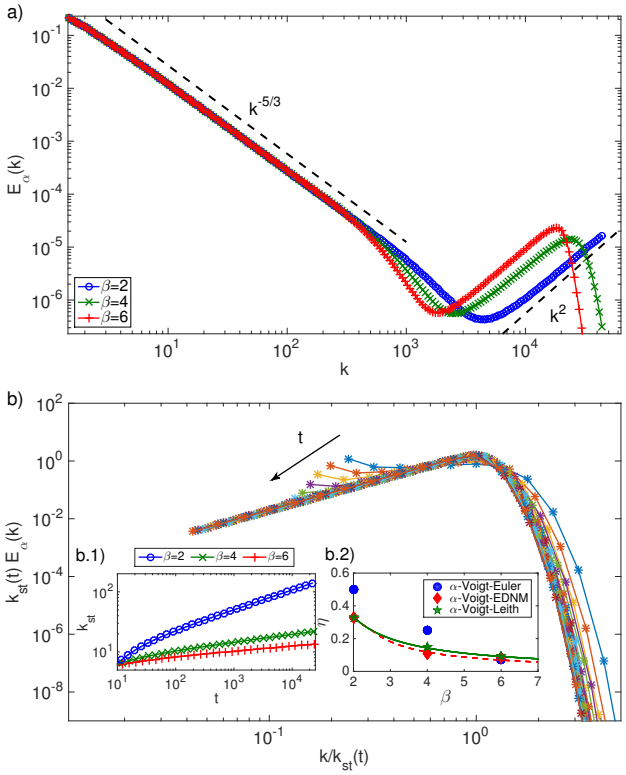

FIG. 7. (Color online) a) Energy spectra $E_\alpha(k)$ at $t = 3.5$ of the αV-EDQNM model, for different values of β, obtained with $k_\alpha = 10^4$ and $k_{max} = 43918$ (corresponding to resolution 131072, with 14.2 points per octave). b) Temporal evolution of the self-similar function $\Psi(k/k_{\rm st}(t)) = E_\alpha(k,t)k_{\rm st}(t)$ for $\beta = 4$ and $k_\alpha = 5$ and $k_{max} = 692$ (28.4 points par octave). The inset b.1 shows the temporal evolution of $k_{\rm st}(t)$ for different values of β. The inset b.2 shows the αV-EDQNM (red dashed line) and αV-Leith (solid green lines) theoretical predictions (19) and (25) for the self-truncation exponent η and numerical data from table II.

the left and right hand sides of (14) we obtain $\dot{k_{\rm st}} k_{\rm st}^{-2} \sim k_{\rm st}^{-\gamma-3\beta}$. Finally, the scaling $k_{\rm st}(t) \sim t^\eta$ leads to

$$\eta = \frac{1}{3\beta - 1 + \gamma} \qquad (19)$$

The exponent γ can be computed using the ansatz $\Psi(z) = z^2 \exp[-z]$ and it reads $\gamma = -\min[\beta, 5/2]$. The theoretical prediction confronted with the data are presented in good agreement in the inset b.2 of Fig.7.

B. α-Voight Leiht model.

Let us now introduce another model that shares the same dynamics properties than Euler-Voight-α. It is a spectral diffusion model that generalizes the so-called Leith model [29]. The original Leith model it is a phenomenological non-linear (local) spectral diffusion equation for the energy spectrum that admits the stationary

solutions corresponding to an absolute equilibrium and Kolmogorov scaling. When forcing and dissipation is added to the model, a steady state containing mixture of constant flux and thermal equilibrium was observed in [30]. It also known to posses self-similar solutions [31].

The simplest generalization of the Leith model to take into account the α-term that conserves the total energy $E_\alpha(k)$ is given by

$$\frac{\partial E}{\partial t} = -\frac{1}{(1+\alpha^\beta k^\beta)}\frac{\partial F}{\partial k}, \tag{20}$$

where $F(k)$ is a spectral (non-linear) flux. Following Leith's original derivation, we assume that the spectral flux is defined in terms of a diffusion coefficient $D(k)$ and a potential $Q(k)$ such that

$$F(k) = -\gamma k^2 D\frac{\partial Q}{\partial k} \tag{21}$$

Assuming locality in the flux, by dimensional analysis we obtain

$$D = k^{9/2-m}(E/k^2)^n(1+\alpha^\beta k^\beta)^p \tag{22}$$
$$Q = k^m(E/k^2)^{3/2-n}(1+\alpha^\beta k^\beta)^q \tag{23}$$

The dimensionless coefficient γ set the global time-scale and n, m, q, p are free parameters to be determined. The first contraint is given by the no-flux solution or the absolute equilibrium (8). Imposing that $F(k) = 0$ for the absolute equilibrium $E_\alpha(k) \sim k^2$ leads to $m = 0$ and $n = 3/2-q$. The second contraint is for the Kolmogorov-like solution $E_\alpha \sim k^{-5/3}$. Imposing that for such solutions the flux is given by $F = \epsilon/(1+\alpha^\beta k^\beta)^r$, we obtain $p = 3/2-q-r$, with r a free parameter. Such a flux can be easily interpreted in the limit of large β. Indeed, for $k \ll k_\alpha$ the α term is negligible, and the flux becomes constant. The Kolmogorov phenomenology is thus recovered. On the other hand for $k \gg k_\alpha$ the flux vanishes as expected. Taking into account the previous constraints, we obtain a family of a of diffusive αV-Leith models indexed by the parameter r:

$$\frac{\partial E_\alpha}{\partial t} = \frac{2q\gamma}{3}\frac{\partial}{\partial k}\left[\frac{k^{13/2}}{(1+\alpha^\beta k^\beta)^r}\frac{\partial}{\partial k}\left[E_\alpha^{3/2}k^{-3}\right]\right]. \tag{24}$$

The standard Leith model is recovered by setting $\beta = 0$ and rescaling the time.

The behavior of the Euler-Voight-α is indeed reproduced by the αV-Leith model (24). Figure 8.a displays the energy spectrum for different values of β and $r = 2$. The Kolmogorov $k^{-5/3}$, the equilibrium k^2 regimes and the fast decay for large k is manifest. The absence of a dissipative zone is apparent in Fig. 8.a, when compared both with the αV-EDQNM case (see Fig. 7.a) and the Euler Voigt-α model (see Fig.2). This is certainly due to the locality in Fourier space of the αV-Leith model.

As in the previous models, we look for self-similar solution of (24). Introducing (13) in to (24) we obtain in

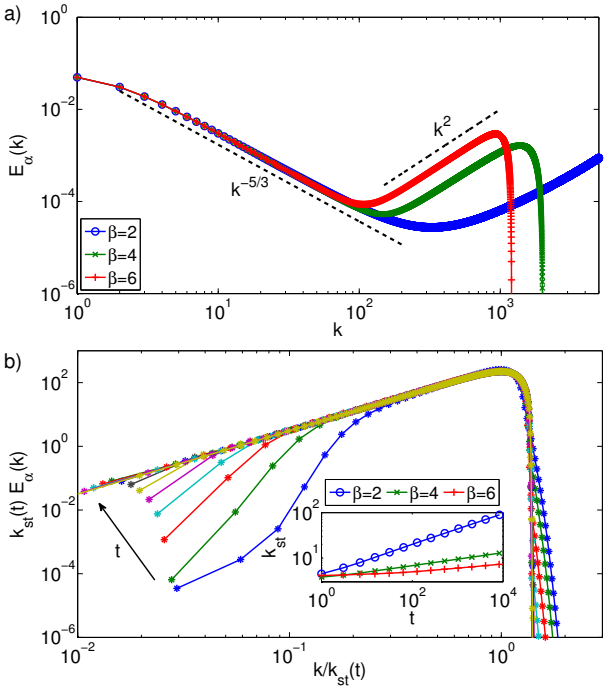

FIG. 8. (Color online) a) Energy spectra $E_\alpha(k)$ of the αV-Leith model (24) for different values of β obtained with $k_\alpha = 400$ and $k_{max} = 4000$. b) Temporal evolution of the self similar function $\Psi(k/k_{\rm st}(t)) = E_\alpha(k,t)k_{\rm st}(t)$ for $\beta = 4$ and $k_\alpha = 2$. The inset shows the temporal evolution of $k_{\rm st}(t)$ for different values of β.

the limit of $k \gg k_\alpha$ for the self-truncation exponent

$$\eta = \frac{1}{\beta r - 1}. \tag{25}$$

This prediction coincides with the one of EDQNM for $r = 2+\gamma/\beta$ (see Eq.(19)). The self-similarity behavior of $E_\alpha(k,t)$ is apparent in Fig.8.b, where the self-similar for is displayed for $\beta = 4$ and $r = 2$. The inset shows the temporal evolution of $k_{\rm st}(t)$ for different values of β. A power-law growth is manifest. The measured values of the exponent η are presented inTable II in good agreement with the prediction (25).

The self-similar analysis leads to a non-linear second-order ordinary differential equation for $\Psi(z)$ (see (13)). This equation cannot be solved analytically but an asymptotic analysis predicts $\Psi(z) \sim z^2$ for $z \ll 1$ and $\Psi(z) \sim (\text{cte} - z)^{3/2}$ for $z \gtrsim 1$. Data is compatible with this result (not shown). Note that, unlike the Euler-Voigt-α and αV-EDQNM models, the Leith model presents a sharp cut-off instead of an exponential decay.

IV. CONCLUSION

In summary the Euler-Voigt-α model allowed us to show that its self-truncation regime reproduces the behavior of the truncated Euler equation [5]. We also found

evidence for self-similarity in the long-time behavior of the energy spectrum. Introducing two different simplified models, the αV-EDQNM model and the αV-Leith model, we were able to show that they present behaviors similar to that of the Euler-Voigt-α model. We were able to determine the analytical values of the self-similar exponents of the simplified models.

In the present work we have used only integer values for β. As was noted in Sect.II A, choosing $\beta = 11/3$ yields an absolute equilibrium $E(k) \sim k^{-5/3}$ and, in two-dimensions, $\beta = 2/3$ also yields Kolmogorov scaling. This can represent an interesting alternative to the fractal decimation method that was used in reference [14].

The present work can be naturally extended to the $2D$ and $3D$ Ideal MHD equations. In this context, it was recently shown that dynamo action can be triggered by turbulence in absolute equilibrium [32]. Thermalization with $\beta = 11/3$ would allow for a more realistic velocity spectrum, mimicking the infinite Reynolds limit.

Acknowledgements: We acknowledge useful scientific discussions with Claude Bardos, Uriel Frisch, Annick Pouquet, Samriddhi S. Ray and Edriss Titi. The computations were carried out at IDRIS and the Mésocentre SIGAMM hosted at the Observatoire de la Côote d'Azur.

[1] T. Lee, Quart Appl Math **10**, 69 (1952).
[2] R. Kraichnan, J. Acoust. Soc. Am. **27**, 438 (1955).
[3] R. Kraichnan, J. Fluid Mech. **59**, 745 (1973).
[4] S. Orszag, *Statistical Theory of Turbulence* (in, Les Houches 1973: Fluid dynamics, R. Balian and J.L. Peube eds. Gordon and Breach, New York, 1977).
[5] C. Cichowlas, P. Bonaïti, F. Debbasch, and M. Brachet, Physical Review Letters **95**, 264502 (2005).
[6] G. Krstulovic, P. D. Mininni, M. E. Brachet, and A. Pouquet, Phys. Rev. E pp. 1–5 (2009).
[7] G. Krstulovic, C. Cartes, M. Brachet, and E. Tirapegui, International Journal of Bifurcation and Chaos **19**, 3445 (2009).
[8] G. Krstulovic and M. E. Brachet, Phys. Rev. Lett **106**, 115303 (2011).
[9] G. Krstulovic and M. E. Brachet, Phys. Rev. E **83**, 066311 (2011).
[10] V. Shukla, M. Brachet, and R. Pandit, New Journal of Physics **15**, 113025 (2013).
[11] Y. Cao, E. M. Lunasin, and E. S. Titi, Commun. Math. Sci **4**, 823 (2006).
[12] A. Larios and E. S. Titi, Discrete and Continuous Dynamical Systems - Series B **14**, 603 (2010).
[33] Note1, incompressibility must take into account when writing the Gibbs distribution, see [1].
[14] U. Frisch, A. Pomyalov, I. Procaccia, and S. S. Ray, Phys. Rev. Lett. **108**, 074501 (2012).
[15] D. Gottlieb and S. A. Orszag, *Numerical Analysis of Spectral Methods* (SIAM, Philadelphia, 1977).
[16] G. I. Taylor and A. E. Green, Proc. Roy. Soc. A **158**, 499 (1937).
[17] E. Lee, M. E. Brachet, A. Pouquet, P. D. Mininni, and D. Rosenberg, Phys. Rev. E **78**, 066401 (2008).
[18] A. Pouquet, E. Lee, M. E. Brachet, P. D. Mininni, and D. Rosenberg, Geophysical & Astrophysical Fluid Dynamics **104**, 115 (2010).
[19] M. D. Bustamante and M. Brachet, Phys. Rev. E **86**, 066302 (2012).
[20] M. E. Brachet, M. D. Bustamante, G. Krstulovic, P. D. Mininni, A. Pouquet, and D. Rosenberg, Phys. Rev. E **87**, 013110 (2013).
[21] P. D. Mininni, D. Rosenberg, R. Reddy, and A. Pouquet, Parallel Computing **37**, 316 (2011), ISSN 0167-8191.
[22] W. J. T. Bos and J.-P. Bertoglio, Physics of Fluids (1994-present) **18**, 071701 (2006).
[23] C. Sulem, P.-L. Sulem, and H. Frisch, Journal of Computational Physics **50**, 138 (1983).
[24] U. Frisch, T. Matsumoto, and J. Bec, Journal of Statistical Physics **113**, 761 (2003).
[25] U. Frisch, *Turbulence: The Legacy of A. N. Kolmogorov* (Cambridge University Press, 1995).
[26] E. Titi and C. Bardos, Private commmunication (2014).
[27] G. Krstulovic and M. Brachet, Physica D: Nonlinear Phenomena **237**, 2015 (2008).
[28] A. Fouquet, M. Lesieur, J. Andre, and C. Basdevant, Journal of Fluid Mechanics **72**, 305 (1975).
[29] C. E. Leith, Physics of Fluids (1958-1988) **10**, 1409 (1967).
[30] C. Connaughton and S. Nazarenko, Phys. Rev. Lett. **92**, 044501 (2004).
[31] V. N. Grebenev, S. V. Nazarenko, S. B. Medvedev, I. V. Schwab, and Y. A. Chirkunov, Journal of Physics A: Mathematical and Theoretical **47**, 025501 (2014).
[32] S. G. G. Prasath, S. Fauve, and M. Brachet, EPL (Europhysics Letters) **106**, 29002 (2014).
[33] Note1, incompressibility must take into account when writing the Gibbs distribution, see [1].

Bibliography

[1] W. J. Bos and J.-P. Bertoglio. Dynamics of spectrally truncated inviscid turbulence. *Physics of Fluids (1994-present)*, 18(7):071701, 2006.

[2] C. Cichowlas, P. Bonaïti, F. Debbasch, and M. Brachet. Effective dissipation and turbulence in spectrally truncated euler flows. *Physical review letters*, 95(26):264502, 2005.

[3] U. Frisch. *Turbulence: the legacy of AN Kolmogorov*. Cambridge university press, 1995.

[4] A. N. Kolmogorov. The local structure of turbulence in incompressible viscous fluid for very large reynolds numbers. In *Dokl. Akad. Nauk SSSR*, volume 30, pages 299–303, 1941.

[5] R. H. Kraichnan. Inertial ranges in two-dimensional turbulence. Technical report, DTIC Document, 1967.

[6] R. H. Kraichnan. Helical turbulence and absolute equilibrium. *Journal of Fluid Mechanics*, 59(04): 745–752, 1973.

[7] G. Krstulovic. Kelvin-wave cascade and dissipation in low-temperature superfluid vortices. *Physical Review E*, 86(5):055301, 2012.

[8] G. Krstulovic and M. Brachet. Dispersive bottleneck delaying thermalization of turbulent bose-einstein condensates. *Physical review letters*, 106(11):115303, 2011.

[9] G. Krstulovic and M. Brachet. Energy cascade with small-scale thermalization, counterflow metastability, and anomalous velocity of vortex rings in fourier-truncated gross-pitaevskii equation. *Physical Review E*, 83(6):066311, 2011.

[10] G. Krstulovic and M.-É. Brachet. Two-fluid model of the truncated euler equations. *Physica D: Nonlinear Phenomena*, 237(14):2015–2019, 2008.

[11] A. Larios, E. Titi, M. Petersen, and B. Wingate. Recent analytical and numerical results for the navier-stokes-voigt model and related models. In *APS Division of Fluid Dynamics Meeting Abstracts*, volume 1, 2010.

[12] T.-D. Lee. On some statistical properties of hydrodynamical and magneto-hydrodynamical fields. *Quart Appl Math*, 1(10):69–74, 1952.

[13] S. A. Orszag. Analytical theories of turbulence. *Journal of Fluid Mechanics*, 41(02):363–386, 1970.